USGS
science for a changing world

Prepared in cooperation with Northern Arizona University

Multi-Decadal Sandbar Response to Flow Management Downstream from a Large Dam—The Glen Canyon Dam on the Colorado River in Marble and Grand Canyons, Arizona

Professional Paper 1873

U.S. Department of the Interior
U.S. Geological Survey

Cover. Photograph of the sandbar at river mile 068R (river right) in eastern Grand Canyon, in the Colorado River by Tanner Canyon Rapids, taken on March 12, 2008. U.S. Geological Survey image was captured by a remote automated camera.

Multi-Decadal Sandbar Response to Flow Management Downstream from a Large Dam—The Glen Canyon Dam on the Colorado River in Marble and Grand Canyons, Arizona

By Joseph E. Hazel, Jr., Matthew A. Kaplinski, Daniel Hamill, Daniel Buscombe, Erich R. Mueller, Robert P. Ross, Keith Kohl, and Paul E. Grams

Prepared in cooperation with Northern Arizona University

Professional Paper 1873

U.S. Department of the Interior
U.S. Geological Survey

U.S. Geological Survey, Reston, Virginia: 2022

Suggested citation:
Hazel, J.E., Jr., Kaplinski, M.A., Hamill, D., Buscombe, D., Mueller, E.R., Ross, R.P., Kohl, K., and Grams, P.E., 2022, Multi-decadal sandbar response to flow management downstream from a large dam—The Glen Canyon Dam on the Colorado River in Marble and Grand Canyons, Arizona: U.S. Geological Survey Professional Paper 1873, 104 p., https://doi.org/10.3133/pp1873.

Associated data for this publication:
Grams, P.E., Hazel, J.E., Jr., Kaplinski, M.A., Ross, R.P., Hamill, D., Hensleigh, J., and Gushue, T., 2020, Long-term sandbar monitoring data along the Colorado River in Marble and Grand Canyons, Arizona: U.S. Geological Survey data release, https://doi.org/10.5066/P93F8JJK.

ISSN 2330-7102 (online)

Acknowledgments

This study was supported by funding from the Bureau of Reclamation through the U.S. Geological Survey (USGS) Grand Canyon Monitoring and Research Center (GCMRC) and was conducted in collaboration with the National Park Service (NPS; Grand Canyon National Park and Glen Canyon National Recreation Area). Scripts for automated data processing were written by Tim Andrews and revised by Philip Bailey and Matthew Reimer of North Arrow Research, Ltd. The web-based application for serving and interactively viewing the data at the GCMRC sandbar monitoring website was originally designed and programmed by Megan Hines and Kathryn Schoephoester of the USGS Center for Integrated Data Analytics (CIDA). The application was revised and integrated with the current sandbar database by North Arrow Research and James Hensleigh at the USGS Glen Canyon Dam Adaptive Management Program. We thank Terry Arundel and Tom Gushue at GCMRC for data archiving and geospatial data support, respectively. Dave Wegner (Bureau of Reclamation's Glen Canyon Environmental Studies), Larry Stevens (Grand Canyon National Park), Ted Melis (GCMRC), and Stan Beus (Northern Arizona University) were instrumental in the early stages of the project. The authors are grateful for the dedicated efforts of many field technicians, river guides, and volunteers who assisted in the fieldwork. Special thanks to Hilary Mayes, Jeff Bennet, Jeff Behan, Suzanne Rhodes, Meagan Polino, Eric Kellerup, Mark Manone, Karen Koestner, Laura Kennedy, Steve Bledsoe, Kenton Grua, Rod Parnell, Katie Chapman, Pete Weiss, and Brian Dierker for having spent hundreds of days on river trips while displaying the epitome of professional pride and commitment. Carol Fritzinger (GCMRC) is noted for her tireless logistical coordination. Bob Tusso (GCMRC) assisted with remote cameras and image analysis. Mark Gonzales designed the bathymetric systems used in this study and helped with data collection. Thanks to Emily Palmquist (GCMRC), Barbara Ralston (GCMRC), and Brad Butterfield (Northern Arizona University) for integrating vegetation surveys with the sandbar monitoring and for useful discussions of vegetation feedbacks on sedimentation patterns. Rod Parnell (Northern Arizona University), Jack Schmidt (Utah State University), and David Topping (USGS) contributed valuable discussions on geomorphic drivers. Reviews provided by Amy East (USGS), Daniel Hadley (University of Illinois), and Alan Kasprak (Fort Lewis College) resulted in substantial improvements to the manuscript and are gratefully acknowledged. We pay tribute to our colleagues who helped in the field and are now deceased—Greg Sponenburgh, Frank Protiva, and Ryan Seumptewa.

Contents

Figures

Tables

Conversion Factors

U.S. customary units to International System of Units

Multiply	By	To obtain
	Length	
inch (in.)	2.54	centimeter (cm)
foot (ft)	0.3048	meter (m)
mile (mi)	1.609	kilometer (km)
	Area	
square foot (ft^2)	0.09290	square meter (m^2)
square mile (mi^2)	2.590	square kilometer (km^2)
	Volume	
cubic foot (ft^3)	0.02832	cubic meter (m^3)
acre-foot (acre-ft)	1,233	cubic meter (m^3)
cubic mile (mi^3)	4.168	cubic kilometer (km^3)
	Flow rate	
cubic foot per second (ft^3/s)	0.02832	cubic meter per second (m^3/s)
	Mass	
ton, short (2,000 lb)	0.9072	megagram (Mg) or metric ton (t)
ton, long (2,240 lb)	1.016	metric ton (t)

International System of Units to U.S. customary units

Multiply	By	To obtain
	Length	
centimeter (cm)	0.3937	inch (in)
meter (m)	3.281	foot (ft)
kilometer (km)	0.6214	mile (mi)
	Area	
square meter (m^2)	10.76	square foot (ft^2)
square kilometer (km^2)	0.3861	square mile (mi^2)
	Volume	
cubic meter (m^3)	35.31	cubic foot (ft^3)
cubic meter (m^3)	0.0008107	acre-foot (acre-ft)
cubic kilometer (km^3)	0.2399	cubic mile (mi^3)
	Flow rate	
cubic meter per second (m^3/s)	35.31	cubic foot per second (ft^3/s)
	Mass	
megagram (Mg) or metric ton (t)	1.102	ton, short [2,000 lb]
metric ton (t)	0.9842	ton, short [2,000 lb]

Temperature in degrees Celsius (°C) may be converted to degrees Fahrenheit (°F) as °F = (1.8 × °C) + 32.

Temperature in degrees Fahrenheit (°F) may be converted to degrees Celsius (°C) as °C = (°F – 32) / 1.8.

Datum

Horizontal and vertical coordinate information is referenced to the 2007 realization of the National Spatial Reference System, North American Datum of 1983 (NSRS2007) and projected to 1983 State Plane Coordinates System, Arizona central zone, in meters.

Vertical positions (heights) are distances above the Geodetic Reference System 1980 (GRS 80) ellipse defined by NAD 83.

Elevation, as used in this report, refers to NAD 83/GRS 80 ellipsoid heights and not traditionally defined North American Vertical Datum of 1988 (NAVD 88) orthometric heights.

Abbreviations

BHBF	beach/habitat-building flows
DEM	digital elevation model
DOI	Department of the Interior
EIS	Environmental Impact Statement
FGDC	The Federal Geographic Data Committee
FIPS	Federal Information Processing Series
GCDAMP	Glen Canyon Dam Adaptive Management Program
GCES	Glen Canyon Environmental Studies
GCMRC	Grand Canyon Monitoring and Research Center
GPS	Global Positioning System
HFE	high-flow experiment
HMF	habitat maintenance flow
kHz	kilohertz
lidar	light detection and ranging
LTEMP	Long-Term Experimental Management Plan
LSSF	low summer steady flow experiment
MBES	multibeam echosounders
MLFF	modified low fluctuating flow alternative
NDEP	National Digital Elevation Program
NSRS	National Spatial Reference System
PCA	principal component analysis
RM	river mile (measured as distance downstream from Lees Ferry [RM 0], Ariz.)
ROD	Record of Decision
RTK-GPS	real-time kinematic Global Positioning Systems
SBES	singlebeam echosounders
SD	standard deviation
TIN	triangulated irregular network
TS	total station surveying
USGS	U.S. Geological Survey

Multi-Decadal Sandbar Response to Flow Management Downstream from a Large Dam—The Glen Canyon Dam on the Colorado River in Marble and Grand Canyons, Arizona

By Joseph E. Hazel, Jr.,[1] Matthew A. Kaplinski,[1] Daniel Hamill,[1] Daniel Buscombe,[1] Erich R. Mueller,[2] Robert P. Ross,[3] Keith Kohl,[3] and Paul E. Grams[3]

Abstract

Sandbars are an important resource in the Colorado River corridor in Marble and Grand Canyons, Arizona, downstream from Glen Canyon Dam. Sandbars provide aquatic and riparian habitat and are used as campsites by river runners and hikers. The study area is the Colorado River between Glen Canyon Dam and Diamond Creek, which is about 388 kilometers (241 miles) downstream from the dam. Closure of Glen Canyon Dam in 1963 and subsequent flow regulation reduced the sediment supply, limited the magnitude and frequency of floods, and increased the magnitude of baseflows. The result has been widespread erosion of sandbars and expansion of native and non-native vegetation on previously bare sand deposits in this debris-fan dominated canyon river. This study reports on the on-going long-term measurement program of Northern Arizona University, initiated in 1990 with the Bureau of Reclamation, and now also with the U.S. Geological Survey's Grand Canyon Monitoring and Research Center. We report on all sandbar measurements made between 1990 and 2020 to demonstrate the multi-decadal response of the sandbar monitoring sites resulting from flow regulation by Glen Canyon Dam. Because only one study site is located in Glen Canyon, the 25 kilometer (15.5 miles) reach just below Glen Canyon Dam, analyses of sandbar response are only made for the next two canyon segments in the down-river direction, Marble Canyon (388 kilometers [99 miles]) and Grand Canyon (265 kilometers [165 miles]), respectively, where the majority of study sites are located.

We show that a majority of monitoring sites increased in volume during a period of frequent controlled floods intended to rebuild sandbars. In the period from 2004 to 2020, which included seven controlled floods, a median discharge of 350 cubic meters per second (m^3/s), and greater than average tributary sand inputs in more than half of the years, net deposition occurred at 86 percent of long-term monitoring sites. This period was preceded by a period of net erosion (1990–2003) when there was one controlled flood greater than the nominal powerplant capacity of 940 m^3/s. During this period the median discharge from Glen Canyon Dam was 376 m^3/s and greater than average sand inputs occurred in only 36 percent of those years. At the end of the monitoring period in 2020, 61 percent of the study sites measured since 1990 underwent a net increase in sand volume. For the entire 31-year period, these trends were statistically significant for all six sandbar types studied, indicating that increased frequency of controlled flooding maintained sandbar volume at the majority of sites monitored. These floods, also referred to as high-flow experiments (HFEs), are part of a decision-making protocol approved in 2012 for coordinating dam releases timed to occur following large sand inputs to the Colorado River by a major tributary.

These findings are based on digital elevation models (DEMs) derived from approximately (~)1,800 repeat surveys of sandbar and channel bed topography made annually, or more frequently, at the 45 long-term monitoring sites, of which 31 have been monitored since 1990 and 14 were added between 1990 and 2008. This large collection of monitoring sites comprises just 7 to 9 percent of all sandbars in Marble and Grand Canyons, respectively. Nevertheless, when compared with measurements of a larger sample, these sites provide consistent characterization of average sandbar response, despite the local variability in channel and debris fan geometry. We use sand volume and normalized sand volume for tracking geomorphic changes of sandbars, because these metrics are sensitive to both changes in sandbar area and sandbar elevation. Based on checkpoint comparisons and repeat measurements, DEM elevation uncertainty was determined to be ±0.05 meter (m) and this uncertainty was used in a spatially uniform estimate of volume uncertainty. We find that the magnitudes of the topographic changes were substantially greater than the measurement uncertainty.

Sandbars of similar type throughout both Marble and Grand Canyons have responded similarly during the period of the HFE protocol, despite variations in sand supply and longitudinal extent of those inputs. It should be noted that tributary-supplied sand to Glen Canyon is negligible, much of the riverbed is now armored with cobbles, and the channel bed degradation is irreversible in the current flow and sediment supply regime. Because all these HFEs have been conducted during periods of sediment

[1]Northern Arizona University.

[2]Southern Utah University.

[3]U.S. Geological Survey.

enrichment, other factors such as vegetation and geomorphic setting are likely the primary causes of variation among the monitoring sites. A larger percentage of the sandbar population, predominantly located in narrow reaches where stage changes are greater, is composed of sandbar types that remain dynamic and consistently aggrade during HFEs. In contrast, wide reaches of the river corridor where stage change is not as great are characterized by sandbars that have been stabilized by vegetation and progressive aggradation during floods. In the former case, a majority of sandbars are likely to remain dynamic, requiring continued use of HFEs to achieve desired management goals. In the latter case, HFEs can do no better than replace the sediment eroded during normal dam operation between high-flow events, as they become less effective because of a diminishing amount of accommodation space available for deposition. Long-term sandbar trajectory and the continued effectiveness of HFEs are related to the differential vegetation establishment at each bar type. Future sandbar monitoring may need to consider the effects of riparian vegetation removal.

Introduction

Sand that is intermittently distributed along the banks of the Colorado River downstream from Glen Canyon Dam is an ongoing focus of scientific and management interest in Marble and Grand Canyons, Arizona (fig. 1). Sand deposits are considered an important resource in the Colorado River because they create habitat for endangered and native fish (Valdez and Ryel, 1995; Dodrill and others, 2015), provide substrate for riparian vegetation, marsh, and wetlands (Stevens and others, 1995), and are heavily used as recreational campsites (Phillips and others, 1986; Kaplinski and others, 2005; Hadley and others, 2018). Completion of Glen Canyon Dam in 1963 eliminated the supply of sand from the upper Colorado River Basin, resulting in a 95 percent reduction of the large, pre-dam seasonal flux of suspended sand to the modern Colorado River (Andrews, 1991; Topping and others, 2000). Tributaries in the lower Colorado River Basin, downstream from Glen Canyon Dam, are now the only source for replenishing sand deposits on the riverbed and banks in Glen Canyon National Recreation Area and in Grand Canyon National Park (fig. 1). These parks are managed for both resource preservation and recreation (fig. 2). Because the Colorado River in Grand Canyon National Park is dominated by bedrock cliffs and steep talus slopes, river-based recreation is dependent on the presence of sandbars as the primary locations of reliable, relatively flat, and accessible campsites (fig. 2). Approximately 25,000 river runners and hikers visit and camp along the corridor of the Colorado River in Grand Canyon National Park every year (National Park Service, 2006). Bare, open sand deposits were also distinctive features of the pre-dam river landscape (Rubin and others, 2002; Kasprak and others, 2018). Subaerially exposed sandbars are also a potential source of wind-blown sand for aeolian dune fields above the modern dam-controlled high-water line (Draut, 2012; East and others, 2016). Aeolian sediment in the river corridor downstream from Glen Canyon Dam is important as a cover that protects some archeological sites from gully erosion (Hereford and others, 1993; Pederson and others, 2006; Draut and others, 2008; Collins and others, 2009).

Sand deposits in Marble and Grand Canyons are located in zones of flow recirculation associated with channel constrictions where debris fans from tributary canyons impinge on the channel of the Colorado River (Howard and Dolan, 1981). In this and other debris-fan-affected canyons of the Colorado River Basin, the recirculating eddies are effective traps for sand that is otherwise transported in suspension (Howard and Dolan, 1981; Schmidt, 1990; Mueller and others, 2014a). Because most eddies are associated with debris fans that are fixed in location, sandbars formed in these eddies are persistent geomorphic features of the river corridor (Schmidt and Rubin, 1995). The adjustment of sandbars at decadal time scales to flow regulation in this debris-fan-dominated canyon river is the focus of this report. The study area is the Colorado River between Glen Canyon Dam and Diamond Creek, which is about 388 kilometers (km) (241 miles [mi]) downstream from the dam (fig. 1).

Channel adjustment (fine sediment evacuation or accumulation) resulting from changes in sediment supply and flow regime is a typical geomorphic response downstream from most dams in the western United States (Williams and Wolman, 1984; Grant and others, 2003; Schmidt and Wilcock, 2008). In Glen Canyon National Recreation Area, the bedrock-canyon reach just downstream from Glen Canyon Dam, resurveys of channel cross sections were first established by the U.S. Department of the Interior (DOI) Bureau of Reclamation (hereafter referred to as "Reclamation") starting in 1956. These surveys showed that the river channel was largely scoured of sand by a series of pulsed flows in 1965, which were released with the purpose of lowering the bed in the tailwater immediately below the Glen Canyon Dam outlet works (Pemberton, 1976). Because tributary-supplied sand to Glen Canyon is negligible, much of the riverbed is now armored with cobbles and the channel bed degradation is irreversible in the current flow and sediment supply regime (Grams and others, 2007).

In contrast to Glen Canyon, the effects of flow regulation and sand-supply limitation farther downstream in Grand Canyon National Park are more complex and exhibit a high degree of spatial and temporal variability owing to greater tributary sediment supply and differences in channel geomorphology caused by the abundant debris fans that create rapids and zones of recirculating flow where sand accumulates and forms sandbars (Schmidt and Grams, 2011a). Flow regulation by Glen Canyon Dam has resulted in a reduction of both the frequency and magnitude of high flows and an increase in the magnitude of low flows (fig. 3*A*). This flattening of the average annual hydrograph has altered the seasonality of discharge and increased the daily variation in discharge (Topping and others, 2003). Like most other power-producing dams, releases from Glen Canyon Dam fluctuate in response to daily, weekly, and seasonal variations in electrical demand and water delivery requirements. As a result, dam operations have increased the sand-transport capacity of the river during most months, and by removing annual spring

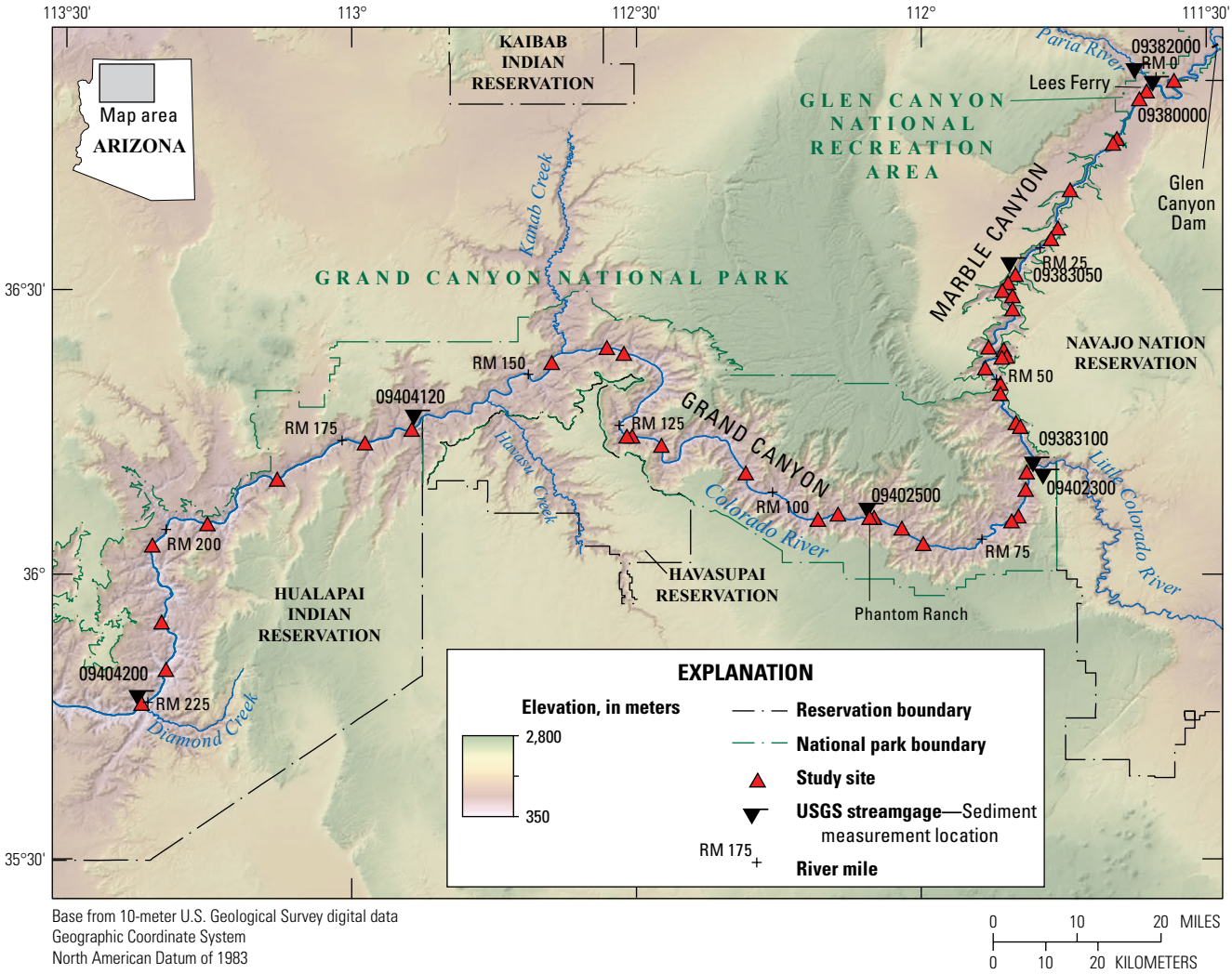

Figure 1. Regional map of the Colorado River in Glen, Marble, and Grand Canyons, Arizona, showing the locations of Lees Ferry, Glen Canyon Dam, and major tributaries. Also shown are the locations and station identifier of U.S. Geological Survey (USGS) streamgage stations used for sediment measurement and sandbar monitoring sites, referred to as study sites in this report (table 1). Glen Canyon Dam is approximately 15.5 river miles (RM) upstream from Lees Ferry, Ariz.

Figure 2. Photograph of the sandbar at river mile 068R (river right) in eastern Grand Canyon, in the Colorado River by Tanner Canyon Rapids, taken on March 12, 2008. This image was captured by a remote automated camera (Grams and others, 2018a). Flow in the main channel is from right to left. Discharge was approximately 320 cubic meters per second. Tents and camping equipment can be seen on the sandbar along with recreational rafts along the water's edge. For study sites, see table 1.

snowmelt floods, reduced the potential for deposition of sand at higher shoreline elevations. As measured at the U.S. Geological Survey streamgage station 09380000 at Lees Ferry, Arizona (fig. 1), the pre-dam 2-year flood magnitude was about 2,400 cubic meters per second (m^3/s), which is almost three times greater than the peak powerplant capacity of Glen Canyon Dam (Topping and others, 2003).

Collectively, these changes in hydrology and sediment supply caused erosion of sand from the bed and channel margins, such that sandbars and associated campsite areas are now considerably smaller in the present-day river compared to the pre-dam era (Dolan and others, 1974; Schmidt and Graf, 1990; Kearsley and others, 1994; Webb, 1996; Schmidt and others, 2004; Wright and others, 2005). Additionally, the

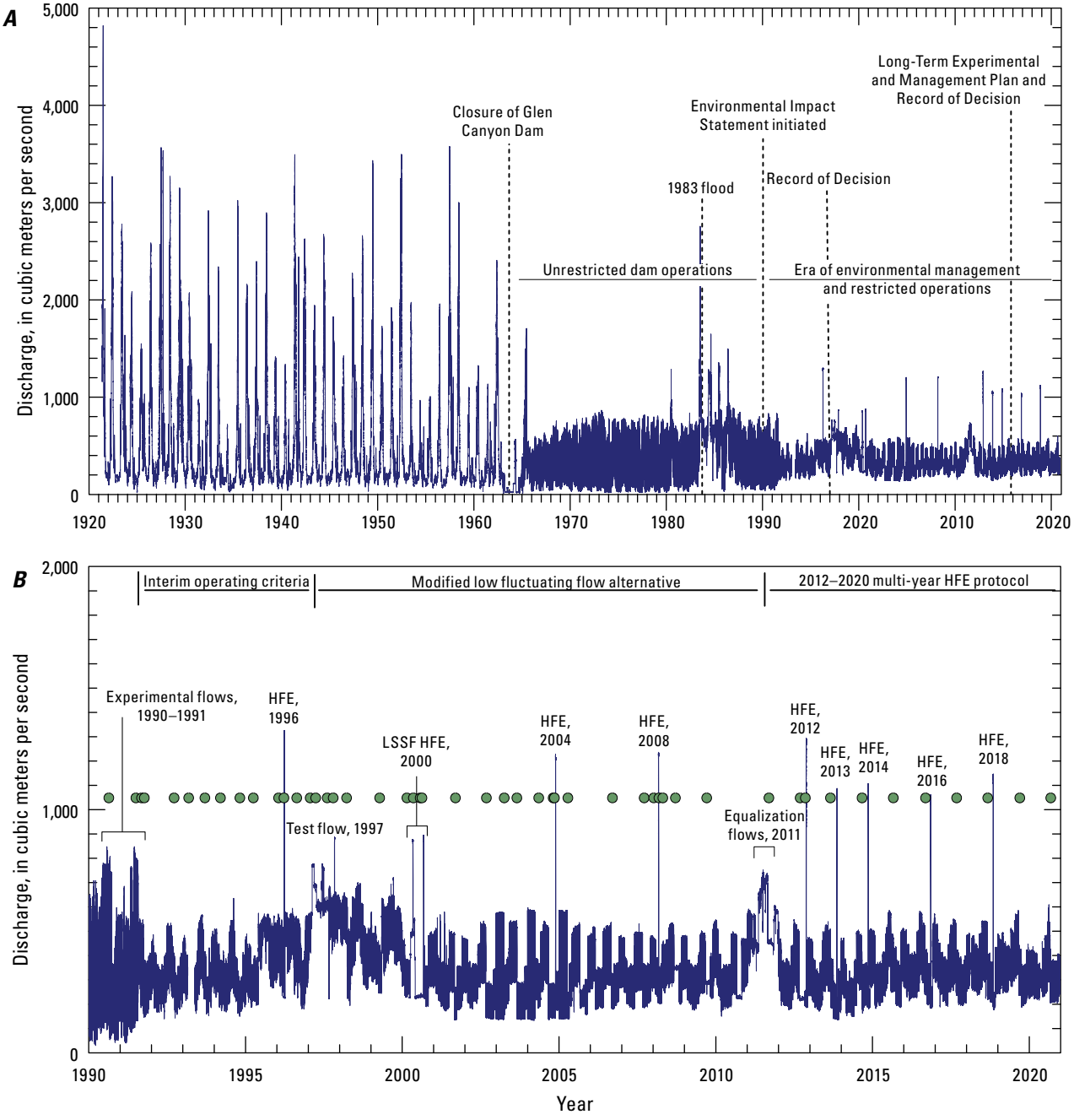

Figure 3. Plot of continuous discharge for the Colorado River at Lees Ferry, Arizona (U.S. Geological Survey streamgage station 09380000) (fig. 1). *A*, 1921 through 2020. Closure of Glen Canyon Dam in 1963 and changes in flow regime resulting from powerplant operations are shown. The timing of initiation of the 1996 Environmental Impact Statement, Record of Decision, and the subsequent 2016 Long-Term Experimental and Management Plan and Record of Decision for operations of Glen Canyon Dam are shown (U.S. Department of the Interior, 1996, 2016). *B*, 1990 through 2020. Management actions including high-flow experiments (HFEs) and the low summer steady flow experiment (LSSF) in 2000 are indicated. The green circles indicate timing of sandbar survey river trips made by Northern Arizona University (Hazel and others, 1999, 2010).

higher elevation parts of sandbars that have not been eroded have been transformed by vegetation encroachment. Lack of scour from annual floods has resulted in rapid colonization of native and non-native riparian vegetation on bar surfaces (Turner and Karpiscak, 1980; Sankey and others, 2015). The increase in riparian vegetation has created wildlife habitat, but as vegetation became denser and senescent, the reduction in open sand area along the river has resulted in a marked decrease in campsite areas available to river runners (Kaplinski and others, 2010; Hadley and others, 2017; 2018). Bare sand loss from hydrologic alteration and vegetation encroachment has also decreased sediment availability for aeolian transfer to upland landscapes, or locations above the stage of regularly occurring river floods (Kasprak and others, 2018), thus decreasing the ability of aeolian sediment to limit gully erosion and loss of irreplaceable archeological sites (Sankey and Draut, 2014).

Purpose and Scope

Field measurements of sandbar change in Grand Canyon National Park are conducted to support Reclamation's Glen Canyon Dam Adaptive Management Program (GCDAMP) and evaluate the effect of dam operations on sandbars and campsites. Although field-based monitoring of sandbars in Grand Canyon began in the early 1970s (Dolan and others, 1974; Howard, 1975), the focus of this report is the on-going long-term measurement program of Northern Arizona University initiated in 1990 (Beus and others, 1992; Hazel and others, 1999; 2010). Since 1990, the number of eddy sandbar study sites has expanded and methods have evolved from simple topographic profiles (that is, cross sections), to complete topographic mapping of exposed sandbars, and finally to comprehensive maps of both the exposed and submerged portions of sandbars (Kaplinski and others, 2009). The frequency of measurements has also varied in response to different policy and management activities and evolving scientific understanding of sandbar behavior (fig. 3*B*).

In this investigation we report on all sandbar measurements made between 1990 and 2020, including reanalysis of data reported by Beus and others (1992) and Hazel and others (1999, 2010). Our primary purposes are to (1) summarize the methods of sandbar data collection and processing, (2) describe the key monitoring metrics used to detect changes in sandbar size, (3) quantify the uncertainty in those monitoring metrics, and (4) demonstrate the multi-decadal response of the sandbar monitoring sites to flow management. The long-term loss or gain of sand is linked to longitudinal distribution of the study sites, depositional setting, and Glen Canyon Dam operations. We report on surveys made at 45 study sites on as many as 51 river trips (table 1.1 of appendix 1). The data presented in this report can be viewed in an interactive website (https://www.usgs.gov/apps/sandbar) and are also available from Grams and others (2020; https://doi.org/10.5066/P93F8JJK). New data are uploaded as they become available.

Physical Setting

Study Area, Place Names, and Units

The study area is the Colorado River between Glen Canyon Dam and Diamond Creek, about 388 km (241 miles) downstream from Glen Canyon Dam in northern Arizona (fig. 1). The study area encompasses parts of Glen Canyon National Recreation Area and Grand Canyon National Park in Glen, Marble, and Grand Canyons. Measurements are reported in the International System of Units (SI) system; however, study sites, locations, and place names are referred to by river mile (RM) location, with RM 0, in both the upstream and downstream directions, at Lees Ferry, Ariz. (table 1). The river mile convention has long been used as the standard reference system for locations along the Colorado River downstream from Glen Canyon Dam. The Colorado River Mile System was formalized in 2002 based on a river centerline (Gushue, 2019). This centerline was digitized using orthophotography and aerial light detection and ranging (lidar) elevation data collected in March 2000 at a discharge of 227 m^3/s and following the center of the river with the line equidistant from both shorelines. River miles and river kilometers were developed from measurements along this line. Lees Ferry is located 25 km downstream from Glen Canyon Dam, and 1.6 km upstream from the mouth of the Paria River and the northeastern boundary of Grand Canyon National Park (fig. 1).

We refer to Glen Canyon as the reach between Glen Canyon Dam (RM −15.5) and Lees Ferry, Arizona (RM 0), and Marble Canyon as the reach between Lees Ferry and the confluence of the Colorado River with the Little Colorado River, located at RM 61.5 (fig. 1). We refer to the Grand Canyon reach as the segment downstream from the Little Colorado River and extending to Diamond Creek (RM 226). Place names were derived from Stevens (1990) and Belknap and Belknap Evans (2001). The left (L) and right (R) sides of the river are determined as one faces downstream.

Geomorphic Framework

The Colorado River in Glen, Marble, and Grand Canyons flows through a deeply incised canyon confined by bedrock and talus. Channel width is controlled by the resistance to erosion of the bedrock exposed at river level (Howard and Dolan, 1981; Schmidt and Graf, 1990). The longitudinal profile includes shallow areas at rapids, riffles, and deep, low-velocity pools that typically occur upstream and downstream from rapids (Leopold, 1969). Rapids are located where tributary debris fans, and to a lesser extent talus deposits, constrict the river channel and steepen the gradient (Howard and Dolan, 1981). The accelerated flow through the channel constriction results in downstream flow separation as the channel cross-sectional area increases in width, leading to the formation of eddies with upstream-directed flow along the bank (fig. 4*A*). The lower flow velocities and shear stress in eddies promote deposition of sand from the suspended load, resulting in sandbars that persist in the same locations through time (Leopold, 1969).

Table 1. Sandbar study sites, Colorado River corridor, Glen Canyon Dam to Diamond Creek, Arizona.

[Site names are from Belknap and Belknap Evans (2001) and Stevens (1990) or are informally used. m^2, square meter]

Study site ID[1]	River mile (RM)[2]	Site name	Deposit type[3]	Site type[4]	Site size (m^2)[5]		Reach/relative width[6]
					Eddy	Channel	
−006R[7]	−0.6	Hidden Slough	U	—	11,113	13,910	0/W
003L[7]	2.5	Above Cathedral Wash	R	1b-Medium R	7,603	16,892	1/W
008L[7]	8.1	Jackass Creek	S	2-U	—	—	1/W
009L	8.9	9 Mile	R	1b-Medium R	—	—	1/W
016L[7]	16.6	Hot Na Na Wash	S	4-S	8,154	7,163	2/N
022R[7]	22.0	22 Mile	R	1a-Narrow R	7,290	6,797	2/N
024L	23.6	Lone Cedar	U	2-U	—	—	3/N
029L	29.5	Shinumo Wash	U	2-U	—	—	3/N
030R[7]	30.7	Sand Pile	R	1a-Narrow R	8,620	8,419	3/N
032R[7]	31.9	South Canyon	U	2-U	11,620	3,334	3/N
033L[7]	33.3	Redwall Cavern	R	4-S	—	—	3/N
035L	35.1	Nautiloid	S, R[8]	4-S	21,059	22,323	3/N
041R	41.4	Buck Farm	S, R	1b-Medium R	40,328	18,125	4/W
043L[7]	43.4	Anasazi Bridge	UP	3-UP	8,459	16,419	4/W
044L[7]	44.6	Eminence	S, R[8]	1b-Medium R	25,428	18,585	4/W
045L	45.0	Willie Taylor	S[8], R	1b-Medium R	22,541	13,279	4/W
047R[7]	47.6	Lower Saddle	R	1b-Medium R	28,486	18,936	4/W
050R[7]	50.2	Dinosaur	S, R	1b-Medium R	9,148	10,484	4/W
051L[7]	51.0	51 Mile	R	1c-Wide R	31,687	18,205	4/W
055R	55.9	Kwagunt Marsh	R	1c-Wide R	24,984	22,541	4/W
056R	56.6	Kwagunt Beach	U	2-U	—	—	4/W
062R	62.9	Crash Canyon	R	4-S	15,946	8,132	5/W
065R	65.2	Carbon Creek	S, R	1b-Medium R	16,220	27,448	5/W
068R[7]	68.8	Tanner	S, R	1c-Wide R	15,119	17,221	5/W
070R	70.1	Basalt	R	1c-Wide R	—	—	5/W
081L[7]	81.8	Grapevine	U	2-U	3,434	5,454	6/N
084R	84.6	Clear Creek	S, R	1a-Narrow R	—	—	6/N
087L[7]	87.6	Upper Cremation	UP	3-UP	1,153	8,525	6/N
091R[7]	91.8	91 Mile Creek	S	4-S	4,380	5,402	6/N
093L[7]	93.8	Granite	UP	3-UP	3,592	10,001	6/N
104R[7]	104.4	Emerald	UP	3-UP	1,021	3,997	6/N
119R[7]	119.4	Big Dune	R	1a-Narrow R	8,929	8,890	7/N
122R[7]	122.7	122 Mile Canyon	R	1a-Narrow R	8,241	8,724	7/N
123L[7]	123.3	Upper Forster	R	1b-Med. R	8,523	10,667	7/N
137L[7]	137.7	Football Field	R	1a-Narrow R	5,137	5,490	8/N
139R[7]	139.6	Fishtail	UP	3-UP	7,185	8,648	8/N
145L[7]	145.8	Above Olo	R	1a-Narrow R	1,276	5,930	9/N
167L[9]	167.2	Lower National	S	2-U	—	—	9/N
172L[7]	172.6	Below Mohawk	R	1b-Medium R	9,459	13,570	10/W
183R[7]	183.3	Below Chevron	R	1b-Medium R	5,081	12,409	10/W
194L[7]	194.6	Hualapai Acres	R	1c-Wide R	14,141	16,247	10/W
202R[7]	202.3	202 Mile	S, R[8]	4-S	13,937	7,084	10/W
213L[7]	213.3	Pumpkin Spring	U	1a-Narrow R	3,994	6,055	10/W
220R[7]	220.1	Middle 220 Mile	U	1b-Med. R	2,448	5,849	11/N
225R[7]	225.5	225 Mile	UP	3-UP	5,635	16,476	11/N

[1]The descriptor "L" denotes the location of the emergent sandbar at the study site on river-left and "R" for river-right, with the observer facing downstream. The number is the approximate location of the river mile marker based on the river mile (RM) centerline downstream from Lees Ferry (RM 0), Arizona.

[2]Approximate location based on the river mile (RM) centerline downstream from Lees Ferry (RM 0), Arizona.

[3]Deposit types surveyed: R, reattachment bar; S, separation bar; U, undifferentiated eddy bar; UP, upper pool reattachment bar. Note that some bar types have been recategorized and differ from those reported by Hazel and others (1999, 2010).

[4]Based on the metrics used for sandbar grouping in appendix table 1.2 as described by Mueller and others (2018); 1a, narrow reattachment bar; 1b, medium reattachment bar; 1c, wide reattachment bar; 2, undifferentiated eddy bar; 3, upper pool deposit; 4, separation bar. Where two deposit types are surveyed at one site the grouping reflects the dominant bar type.

[5]Eddy and channel size determined by a fixed boundary located at the base of the eddy sandbar.

[6]Geomorphic reach (0–11) and channel width (W, wide; N, narrow) from Schmidt and Graf (1990).

[7]Indicates the reference series of original long-term monitoring sites selected in 1990 by Beus and others (1992).

[8]Indicates sites where a deposit type was not surveyed in all years.

[9]On July 14, 2012, site 167L was partially buried by a debris flow in National Canyon and is therefore not included in analyses of temporal trends (appendix 3).

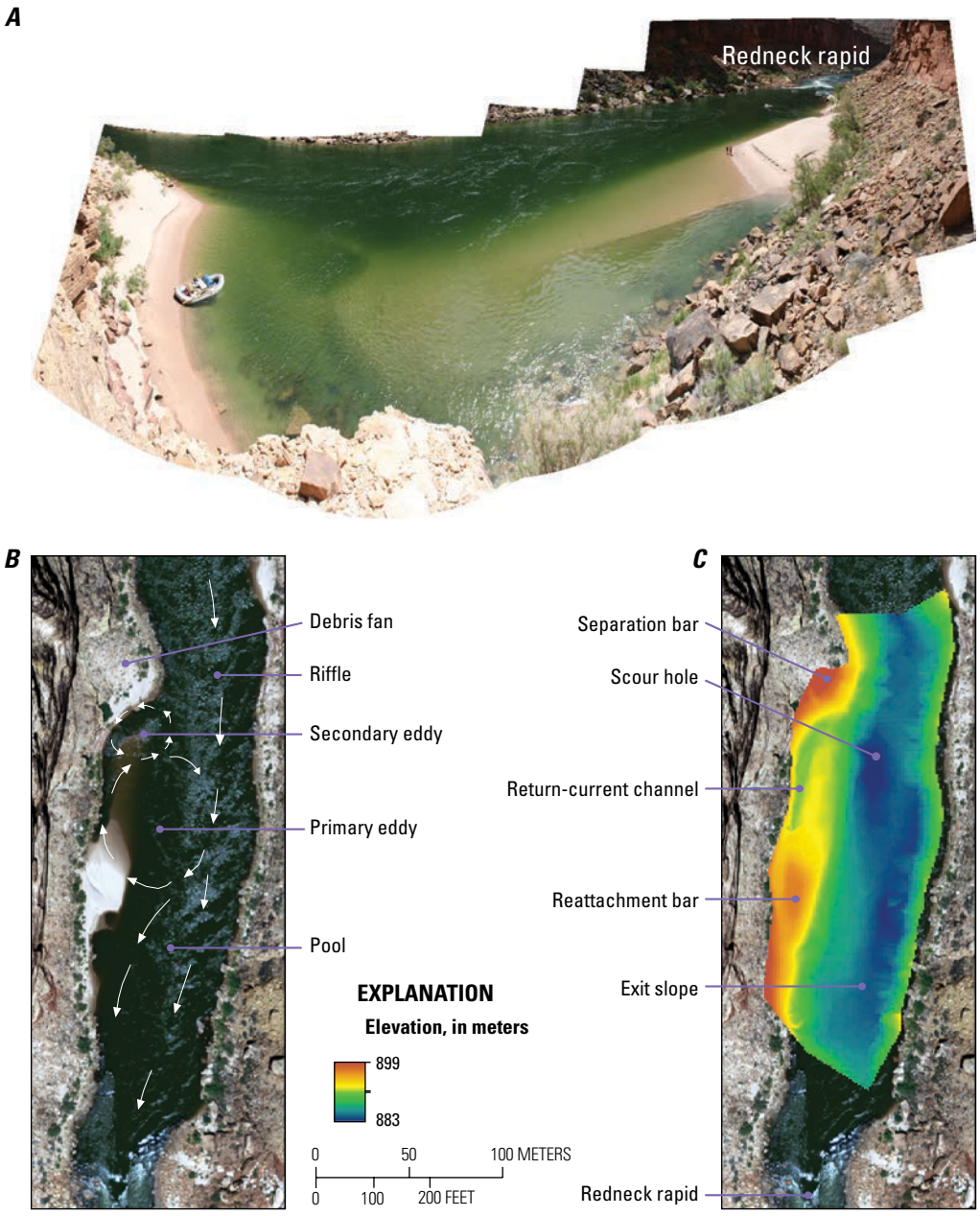

Figure 4. Images and a geomorphic description of the physical setting of sandbars in the Colorado River corridor, Marble Canyon. *A*, Mosaic of a typical fan-eddy complex at river mile (RM) 17.6. The view is oblique and downstream toward what is locally known as Redneck rapid. Channel width is relatively narrow here and confined by bedrock or steep talus banks. Flow in main channel of approximately (~) 251 cubic meters per second (m^3/s) is from left to right. The high-flow strandlines are from the previous day's peak release at Glen Canyon Dam of ~433 m^3/s. The raft is moored on a separation bar and the reattachment bar is being surveyed by two rodmen. Photograph by M. Kaplinski, Northern Arizona University, May 18, 2008. *B*, Aerial image of the same fan-eddy complex shows generalized hydraulics resulting from the debris-fan constriction of the river channel. Arrows indicate flow direction. Aerial image taken on May 29, 2009, at a discharge of 227 m^3/s (Davis, 2013). *C*, The aerial image in *B* overlaid with a digital elevation model (DEM) showing topography of the riverbed and sandbars as surveyed on May 8, 2013. Reattachment bars are deposited where flow reattaches to the bank and separation bars form in weak, unorganized flow or secondary eddies upstream from the primary eddy. Note the deep return-current channel that separates the two bar types and that much of the reattachment bar in the primary eddy is subaqueous. This example is from a study site not described in this report but is typical of the debris-fan eddy geomorphic setting in the study area (Grams and others, 2010). Data used to create the DEM in *C* is from Grams and others (2013).

Schmidt and Rubin (1995) termed this basic, repeating channel unit the "fan-eddy complex," composed of a channel-constricting debris fan, an upstream pool created by the backwater effect of the constriction, and a channel expansion with one or more eddies and plunge pool immediately downstream from the fan (fig. 4*B*). Downstream from the plunge pool, or scour hole, created by higher velocity flow through the constriction, the channel typically narrows and shallows, forming the pool exit slope (fig. 4*C*). A mid-channel or bank-attached cobble bar commonly occurs in these channel expansions. The coarse debris is the result of erosion of the upstream debris fan during pre-dam high flows (Webb and others, 1989). At lower discharges, flow typically passes around the margins of these cobble bars and creates a riffle.

The river corridor in Marble Canyon and Grand Canyon has been previously subdivided into 11 geomorphic reaches between Lees Ferry and Diamond Creek on the basis of bedrock lithology at river level and channel width (table 2). The frequency of fan-eddy complexes and the number and size of sandbars used as campsites also varies among the geomorphic reaches (Schmidt and Graf, 1990). Debris fans are less frequent in the steep and narrow upper Granite Gorge in eastern and central Grand Canyon between RM 75 and RM 115. Melis and others (1994) identified more than 500 tributaries that deliver coarse-grained sediment onto debris fans along the river, thus providing potential locations for the deposition of eddy sandbars. However, not all eddies contain persistent sandbars in the present-day river. Based on aerial photography collected in 2009, the frequency of eddies that contained sandbars varied from less than one per mile to nearly five per mile (table 2). In Marble Canyon, the mean frequency was three eddies containing a sandbar per river mile with frequency varying from 2.7 to 4.7 per river mile. In Grand Canyon, the mean frequency was two eddies per river mile with frequency varying from 0.9 to 3.5 per river mile. Thus, the distribution of sand deposits is controlled by the debris fans that create the fan-eddy complexes. There are more eddy sandbars in some narrower reaches; however, the size and extent are greatest in wider reaches where more space is available for deposition.

Although sandbars may contain minor amounts of silt and clay, primarily they are composed of sand. Thus, sand is the grain size of greatest interest to Grand Canyon researchers and managers (Schmidt and Grams, 2011a). Sand is defined as consisting of particles coarser than 0.625 millimeters (mm) in diameter and finer than 2 mm. Sand deposits in eddies have been described and classified by Schmidt (1990) as separation bars, which form near the upstream part of the eddy, and reattachment bars, which form where flow reattaches to the bank (fig. 4*C*). Where flow separates from the bank, separation bars are deposited in stagnating flow or secondary eddies associated with the primary eddy. The resulting deposits mantle the downstream surface of debris fans, but do not exist downstream from all debris fans. Generally, debris fans with steep, high slopes do not have separation deposits because no discharges occur at which a low-velocity area or secondary eddy exists (Schmidt, 1990). A ridge and runnel topography (fig. 5) is characteristic of many separation bars that are re-worked by surface waves emanating from the tail waves of rapids, building sand berms and pushing them onshore (Bauer and Schmidt, 1993). The resulting near-shore topography gives Grand Canyon sandbars their popular name, "beaches."

Reattachment bars have a distinctive morphology characterized by a platform projecting upstream into the center of the eddy and a return-current channel where upstream-directed flow is redirected along the bank (Rubin and others, 1990). This deep channel typically divides the subaerial separation bar

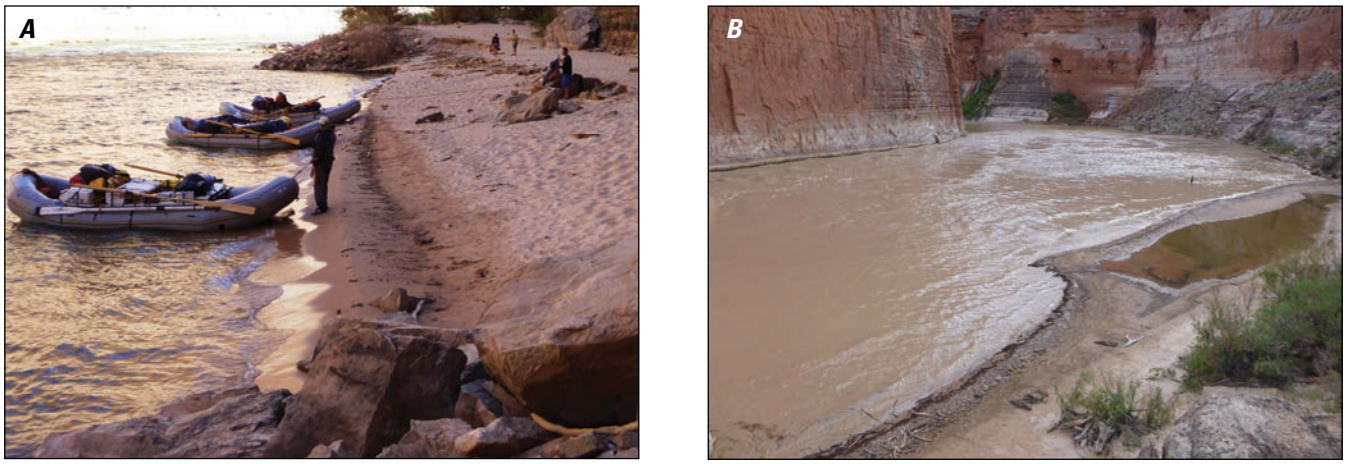

Figure 5. Photographs of accretionary berms that form at the water's edge and are a characteristic feature of separation and undifferentiated eddy bars, Colorado River corridor, Marble Canyon. *A*, At sites closer to the wave source in rapids, the foreshore slope may resemble a coastal, wave-dominated beach as the influence of waves and swash motion rework the bar topography. Photograph of study site 029L by J. Hazel, Northern Arizona University, October 5, 2012. *B*, Surging waves and a berm blocking the mouth of a poorly defined, abandoned return-current channel that had formed at a higher stage at study site 032R. Photograph by P. Grams, U.S. Geological Survey, October 7, 2011. Note that these sites are undifferentiated eddy bars where the topography and bar type cannot be distinguished between a separation bar and reattachment bar. For list of study sites, see table 1.

Table 2. Geomorphic reach characteristics along the Colorado River corridor in Marble and Grand Canyons.

[Reach designations are from Schmidt and Graf (1990), based on bedrock lithology at river level and related river channel morphology. The river miles (RM) number is the approximate location of the river mile marker based on the river mile centerline downstream from Lees Ferry (RM 0), Arizona. m^3/s, cubic meter per second; m^2, square meter]

Reach (RM)	Reach name	Geologic units at river level[1]	Reach description	Average channel width (m)[2]	Number of eddies containing sandbars per mile[3]	Percentage of eddies that have study sites	
						1990[4]	2008[5]
0–11.3[6]	Permian section	Kaibab Limestone, Toroweap Formation, Coconino Sandstone, Hermit Formation	Wide	99	2.7	6.7	10.0
11.4–22.5	Supai Gorge	Supai Group	Narrow	63	3.2	5.7	5.7
22.6–35.9	Redwall Gorge	Redwall Limestone	Narrow	71	4.7	3.2	9.7
36.0–61.5	Lower Marble Canyon	Muav Limestone, Bright Angel Shale, Tapeats Sandstone	Wide	96	3.2	6.2	9.9
61.6–77.4	Furnace Flats	Tapeats Sandstone, Unkar Group	Wide	102	2.4	2.6	10.5
77.5–117.8	Upper Granite Gorge	Zoroaster Complex, Trinity and Elves Chasm gneisses, Vishnu Schist	Narrow	61	0.9	14.3	17.1
117.9–125.5	Aisles	Tapeats Sandstone, Vishnu Schist	Narrow	76	3.6	11.1	11.1
125.6–139.9	Middle Granite Gorge	Tapeats Sandstone, Unkar Group, Vishnu Schist	Narrow	64	1.9	7.4	7.4
140–159.9	Muav Gorge	Muav Limestone	Narrow	51	1.4	3.6	3.6
160–213.8	Lower Canyon	Basalt, Muav Limestone, Bright Angel Shale	Wide	82	3.5	2.6	3.2
213.9–225.8	Lower Granite Gorge	Tapeats Sandstone, Vishnu Schist	Narrow	76	2.2	11.5	11.5

[1]Geologic units from Billingsley (2000).

[2]At 242 m^3/s, average based on cross sections every 0.1 river mile using modeled stage-elevation shorelines by Magirl and others (2008).

[3]Determined from a geomorphic base map constructed from aerial photographs (scale 1:4,800) taken in May 2009 at a constant river discharge of 226 m^3/s; constrained to debris-fan controlled eddies larger in size than 1,000 m^2 based on visible flow separation and channel geometry containing persistent sandbars.

[4]Based on the original study sites chosen by Beus and others (1992).

[5]Sandbar monitoring network utilized in this study after 2008.

[6]We adopt the definition of Marble Canyon and the Permian section geomorphic reach as beginning at the location of Lees Ferry (RM 0) as defined by Schmidt and Graf (1990), whereas some studies define this canyon reach as beginning at the mouth of the Paria River (RM 1) and the Grand Canyon National Park boundary. The first appearance of Kaibab Limestone at river level occurs 1 kilometer upstream from the Paria River (RM 0.6).

from the reattachment bar (fig. 4*A*). At lower flow levels, the return-current channel becomes stagnant as recirculating flow is partly blocked by an emergent reattachment bar (fig. 6). This low-velocity region can be suitable near-shore habitat for some species of native fish, including flannelmouth sucker (*Catostomus latipinnis*) and the endangered humpback chub (*Gila cypha*) (Korman and others, 2004; Schmidt and others, 2007; Dodrill and others, 2015). Reductions in high-magnitude discharges in the post-dam era have also promoted marsh development in return-current channels as they became less frequently inundated, thereby increasing diversity, production, and wildlife habitat availability (Stevens and others, 1995).

We use the term "undifferentiated eddy bar" at places where the unique topography of separation bars and reattachment bars cannot be distinguished because the deposits merge and lack a defined return channel (fig. 5). Reattachment bars also occur in eddies upstream from debris fans and are classified as "upper-pool deposits." Floodplain-like channel margin deposits are not directly associated with fan-eddy complex morphology and typically form along channel banks and minor flow obstructions (Schmidt and Graf, 1990). Because channel-margin deposits are typically smaller than eddy sandbars and are rarely used as campsites, they were not included in this study. This classification scheme for sandbar deposits has been applied to other rivers in the western United States, for example the Green and Yampa Rivers in Dinosaur National Monument and the Wild and Scenic River sections of the Salmon River and tributaries in Idaho, where expansions downstream from constrictions are the predominant

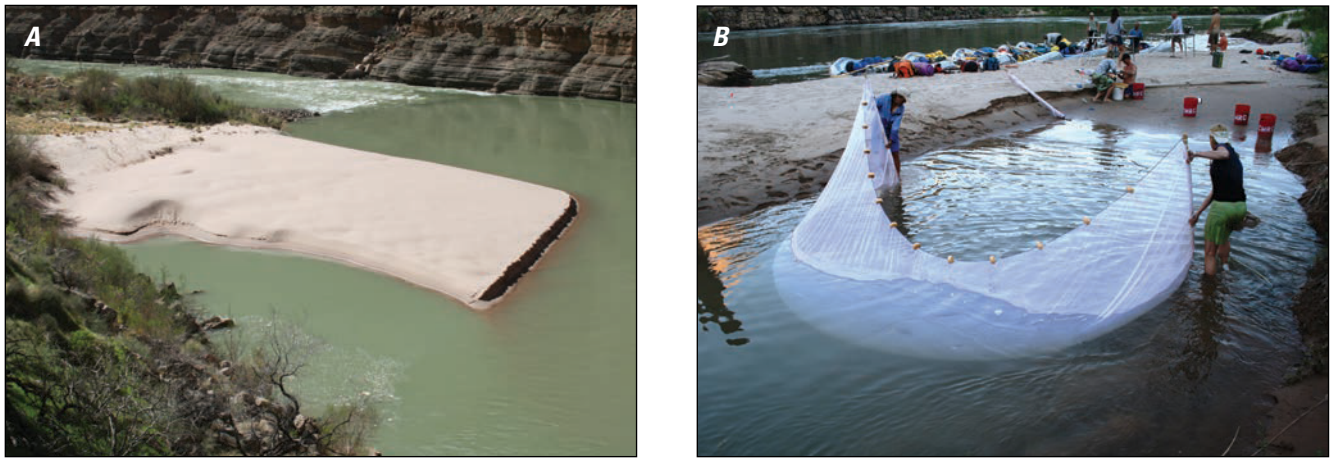

Figure 6. Photographs from the Colorado River corridor in Marble and Grand Canyons of reattachment bars that form under the primary eddy cell and have a distinctive morphology. *A*, At lower flow levels, the exposed reattachment bar platform extends upstream into the center of the eddy. Note the return-current channel where upstream-directed flow is redirected along the bank. Photograph of the study site 045L reattachment bar by J. Hazel, Northern Arizona University, March 31, 2008. *B*, Fish seining in a backwater created as recirculating flow to the return-current channel is blocked by an emergent reattachment bar. Photograph by M. Kaplinski, Northern Arizona University, near river mile 206.7, June 1, 2008. For list of study sites, see table 1.

depositional setting for sand (Schmidt and Rubin, 1995; Grams and Schmidt, 1999; Vincent and Andrews, 2008; Mueller and others, 2014b).

Recreational river runners utilize sandbars, bedrock ledges, and the higher parts of debris fans as campsites (Kearsley and others, 1994; Kaplinski and others, 2005) (fig. 2). Sandbars decrease in utility if they are too small or are covered with dense vegetation (fig. 7). Since closure of Glen Canyon Dam in 1963, the areal coverage of vegetation on otherwise bare sand surfaces has increased by nearly 50 percent (Kasprak and others, 2018). Other sandbars are not as preferred by river runners because of steep banks or exposed boulders that make boat mooring difficult. In a study of recreational use, Stewart and others (2003) found a strong preference for large size sandbars with shade from trees as important qualities of a raft trip and that the competition, or lack of camps in critical reaches of the canyon corridor, were sources of stress and anxiety during the high-use summer season. Critical reaches are segments of the river corridor where the number of available campsites are limited because of geomorphic setting, high demand for nearby attraction sites, or other logistical factors (Kearsley and Warren, 1993). These recreation reach designations closely parallel the geomorphic reach designations of Schmidt and

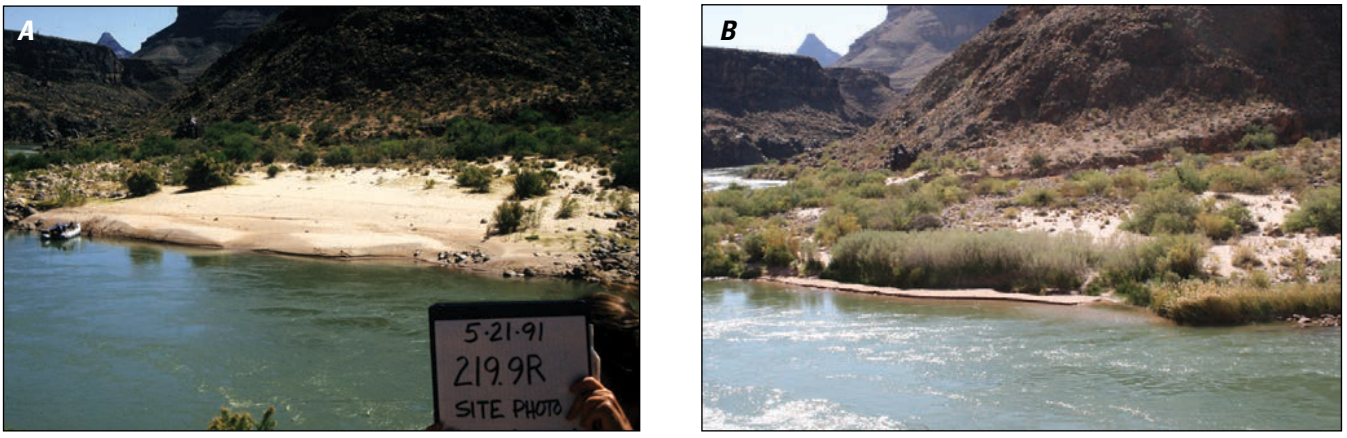

Figure 7. Photographs of repeat views of the study site 220R sandbar and campsite along the Colorado River corridor in the Grand Canyon. Flow in the main channel is right to left. Expansion of riparian vegetation, primarily tamarisk, or salt cedar (*Tamarix ramosissima x chinensis*), arrowweed (*Pluchea sericea*) and common reed (*Phragmites australis*), has greatly reduced the open sand area formerly available for camping on the previously unvegetated sandbar. *A*, Photograph taken May 21, 1991, by J. Hazel, Northern Arizona University, at a river discharge of approximately (~) 142 cubic meters per second (m^3/s). *B*, Photograph taken October 25, 2009, by M. Kaplinski, Northern Arizona University at a discharge of approximately (~) 330 m^3/s. For list of study sites, see table 1.

Graf (1990) (table 2); reaches designated as critical because of limited availability of campsites overlap with geomorphic reaches based on narrow channel width (Supai Gorge, RM 11.4–22.5; Redwall Gorge, RM 22.6–35.9; upper Granite Gorge, RM 77.5–117.8; and Muav Gorge, RM 140–155.9 [table 2]); whereas, noncritical reaches of the river in which campsites are plentiful overlap with the geomorphic reaches based on wide channel width (Permian Section; RM 0–11.3; Lower Marble Canyon, RM 36.0–61.5; Furnace Flats, RM 61.6–77.4; Lower Canyon, RM 160–213.8 [table 2]).

Background on Sandbar Monitoring

Sandbar Monitoring in the Context of River Management

Before the 1980s, little consideration was given to the effects of dam operation on rivers in the Western United States, even when the effects of flow regulation on the downstream environment included national parks established to preserve the natural environment (Ingram and others, 1991). The era of environmental management in Glen Canyon National Recreation Area and Grand Canyon National Park began in 1989 when the U.S. Department of the Interior (DOI) began the Environmental Impact Statement (EIS) process for operation of Glen Canyon Dam (DOI, 1995) (fig. 3*A*). As part of the Glen Canyon Dam EIS, Reclamation conducted a series of releases designed to help evaluate alternative flow scenarios that might reduce effects to downstream resources caused by flow regulation (Patten, 1991). Beginning in June 1990, twenty test flows with different flow patterns were released during the following 14-month period (fig. 3*B*). As part of this multidisciplinary research effort, Reclamation's Glen Canyon Environmental Studies, in cooperation with Northern Arizona University, initiated a sandbar monitoring project to measure the effect of the test flows on sandbar topography (Beus and others, 1992).

Following the 1990–91 experimental flows, restrictions on Glen Canyon Dam operations were imposed August 1, 1991, and the Colorado River was no longer managed solely for electrical power, reservoir storage, or water delivery (National Research Council, 1996). Current management now considers other natural and cultural resources, as well as the need to distribute water in accordance with the Law of the River under the 1922 Colorado River Compact (https://usbr.gov/lc/region/g1000/lawofrvr.html) and hydropower production. Interim Operating Criteria reduced maximum flows and the range of flow fluctuations (fig. 3*B*), with the intention of optimizing sandbar stability and sand storage in the river during preparation of the Glen Canyon Dam EIS (DOI, 1995). Glen Canyon Environmental Studies and Northern Arizona University continued sandbar monitoring in the early 1990s to evaluate the effects of the new flow regime (Patten, 1991).

The Record of Decision (ROD) for the "Operation of Glen Canyon Dam: Final Environmental Impact Statement" was signed by the Secretary of the Interior in October 1996 (DOI, 1996). The ROD formally established the GCDAMP (DOI, 1996). Under the auspices of GCDAMP, the Grand Canyon Monitoring and Research Center (GCMRC) succeeded Glen Canyon Environmental Studies in 1996 and continued the sandbar monitoring program established in 1990. One aspect of the GCDAMP is implementation of an experimental program that evaluates the environmental effects of dam releases on sandbars and other riverine resources (National Research Council, 1999; Patten and others, 2001; Wright and others, 2005). Scheduled high releases of short duration are implemented as part of this program to maintain existing camping beaches and wildlife habitat by modifying and creating sandbars, thus restoring some of the dynamics that result from flooding in an ecosystem. Termed "high-flow experiments" (HFEs), the magnitudes of these releases have ranged from slightly less than the nominal powerplant capacity of 940 m^3/s to 1,274 m^3/s (fig. 3*B*). Discharge greater than powerplant capacity requires use of the river outlet works, providing an additional 425 m^3/s to the HFE release, without having to use the spillways. There have now been 11 short-duration HFEs released between 1996 and 2018 (see "Flow Regimes and Tributary Sediment Supply" section).

On the basis of improved understanding of flood effects resulting from the first HFE released in 1996, and others in the early 2000s, Reclamation implemented a revised decision-making protocol for carrying out multiple HFEs over a 10-year period of experimentation, 2011–2020, known as the HFE Environmental Assessment Protocol (hereafter referred to as "HFE Protocol") (DOI, 2011). The management of water releases, and thus research and monitoring priorities, are now determined by the Long-Term Experimental and Management Plan (LTEMP) EIS (DOI, 2016). The LTEMP extended the HFE Protocol for another 20 years (through 2036). As described in the LTEMP ROD, the primary purpose of the HFE Protocol is to determine if sandbar building during HFEs exceeds sandbar erosion during periods between HFEs, such that sandbar size can be increased or maintained for several years.

Previous Measurements of Sandbars in Grand Canyon

Physical and ecological adjustments of the river corridor in the post-dam era were first recognized by Dolan and others (1974). Concerns for sandbar erosion, campsite loss, and vegetation encroachment led Grand Canyon National Park to initiate a study of sandbars using tape and transit to survey topographic profiles (Howard, 1975). Study site selection was not based on sandbar type, recreational use, or vegetation density, and was largely dictated by wherever the survey trip camped for the night. Howard and Dolan (1979) repeated the profile surveys and concluded that campsite loss because of sandbar erosion had stabilized by the late 1970s. This conclusion was based on 38 profile lines surveyed at 20 study sites (table 3). Continued monitoring of the profile lines in the 1980s by Beus and others (1985) and Schmidt and Graf (1990)

demonstrated that the largest system-wide geomorphic event in the post-dam era, until that time, was caused by the June 1983 snowmelt flood (fig. 8*A*). That year, watershed runoff in the upper Colorado River Basin was unusually high, filling the reservoir behind Glen Canyon Dam (Lake Powell) to capacity. This event required opening the Glen Canyon Dam spillways with discharge peaking at 2,756 m^3/s on June 29, 1983 (fig. 3*A*), about three times powerplant capacity (~940 m^3/s) (Topping and others, 2003). Discharge that spring and summer exceeded powerplant capacity for 68 consecutive days (see table 1 of Schmidt and Grams, 2011a). The 1983 flood created or enlarged many sandbars but eroded others. The effects of the 1983 flood were not well measured, however, and the effects on sandbars were largely inferred from campsite inventories (Brian and Thomas, 1984). Unusually large releases of long duration and daily discharge greater than powerplant capacity also occurred between 1984 and 1986 (fig. 3*A*), thus limiting topographic surveying and studies of sandbar change because the sandbars were submerged. Temporal changes in sandbar conditions were examined by Kearsley and others (1994) using aerial photographs taken in 1965, 1973, 1980, 1984, and 1990. They concluded that about 50 percent of the sandbars used as campsites were smaller in 1990 than in 1965 and only 2 percent were larger. It was generally agreed that any gains from sandbar rebuilding caused by the 1983 flood were temporary because of continued erosion during the floods of the mid-1980s (Schmidt and Grams, 2011a).

Despite the difficulty in obtaining topographic measurements of sandbars during the high flow years of the 1980s, progress in monitoring sandbar change was made when Glen Canyon Environmental Studies initiated mapping studies to increase the spatial scale over which sandbars could be measured (Patten, 1991). During two river trips in May and September 1985, Ferrari (1987) used traditional transit-stadia methods to add additional profiles and a plane table to make maps at 23 sandbars (fig. 8*B*), 8 of which were the same sites as those surveyed in 1974 and 1975 by Howard (1975) (table 3). However, this surveying technique was time consuming, the maps were drawn by hand, and there was important information lost between profiles. The surveys were not repeated, and the maps were never used to describe topographic changes, but new study sites were established, and control networks were created around each site that were used for future monitoring. During the same period (May 1984 to February 1986), the USGS launched an investigation to describe the hydraulic and sedimentologic characteristics of eddies and sandbars (see Rubin and others, 1990; Schmidt, 1990; Schmidt and Graf, 1990). As part of this effort, Schmidt and Graf (1990) made the first comprehensive maps of submerged and exposed sandbars by combining new technologies such as total station (TS) surveying with a boat-mounted echo-depth sounder equipped with a local microwave positioning system (fig. 9*A*; table 3). A TS is a theodolite (transit) integrated with an electronic distance meter. The slope distance, horizontal angle, and vertical angle between the instrument and a reflecting target are measured and later transformed to Cartesian coordinates. TS surveying dramatically decreased point collection time and reliance on the traditional profile-line method used by previous researchers. However, data collection was still limited by the amount of time required to enter the measurements into notebooks by hand and by manual production of topographic maps. In addition, there was considerable uncertainty in the bathymetric measurements because of uncertainty in raft

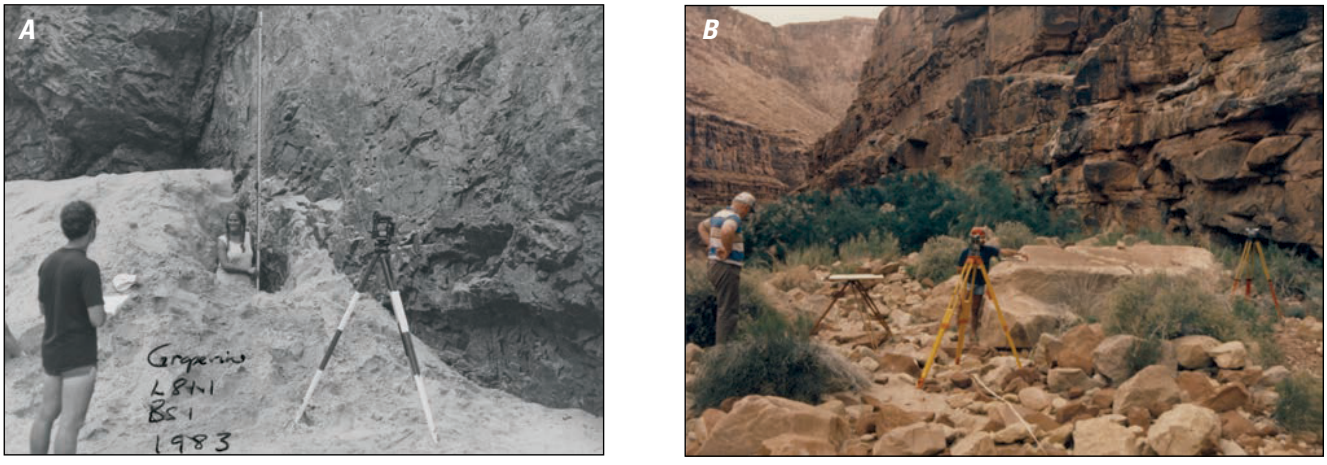

Figure 8. Photographs of early methods for topographic surveys of sandbars utilized in the study area, Colorado River corridor, Marble and Grand Canyons. *A*, Profile survey made in 1983 by transit, stadia rod, and tape at study site 081L "Grapevine Camp" (Beus and others, 1985). The rodman is standing over a nail established as a reference mark by Howard (1975) buried by sand deposited during the 1983 flood. Photograph by S. Beus, Northern Arizona University. *B*, Plane-table mapping by Ferrari (1987) at river mile (RM) 20 on May 8, 1985. The transit-stadia topography method was used to establish a baseline extending the length of the site of interest, with additional profiles oriented at right angles to the baseline. The plane table map was sketched in the field with the base line and benchmarks oriented to true north using a Brunton hand-held compass. View is toward the north and upstream. Photograph from Ferrari (1987). For list of study sites, see table 1.

Table 3. Description of previous direct measurements of sandbars in the study area, Colorado River corridor, Marble and Grand Canyons.

[TS, total station; SBES, singlebeam echosounder. For list of study sites, see table 1]

Author	Survey method	Type of data	Years	Common study sites[1, 2]
Howard (1975)	Tape and transit	38 profiles established at 20 sites; 7 profiles at 4 sites resurveyed in 1975	1974, 1975	035L, 081L, 087L, 093
Howard and Dolan (1979)	Tape and transit	Repeat of 13 profiles at 6 sites established by Howard (1975)	1976	035L
Dolan (1981)	Tape and transit	Repeat of 23 profiles at 15 of the Howard (1975) sites and 1 new site	1980	035L, 081L, 087L, 093L, 123L, 220R
Beus and others (1985)	Tape and transit	Repeat of 43 profiles at 19 of the Howard (1975) sites and 3 new sites	1982, 1983, 1984	035L, 081L, 093L, 123L
Ferrari (1987)	Tape, transit, and plane table	Hand drawn maps made at 8 of the Howard (1975) sites and 16 new sites	1985	035L, 047R, 056R, 087L, 220R
Schmidt and Graf (1990)	TS and SBES	Topographic surveys at 29 sites and bathymetric survey at 13 sites	1985, 1986	003L, 008L, 029L, 035L, 044L, 047R, 056R, 081L, 091R, 093L, 122R, 167L, 213L,
Andrews and others (1999)	TS and SBES	Topographic and bathymetric surveys at 5 sites	1996	044L, 047R, 062R, 065R

[1]The site descriptor "L" denotes the location at the study site on river-left and "R" for river-right, with the observer facing downstream. The number is the approximate location of the river mile marker based on the river mile (RM) centerline downstream from Lees Ferry (RM 0), Arizona.

[2]Study sites surveyed in common with previous studies.

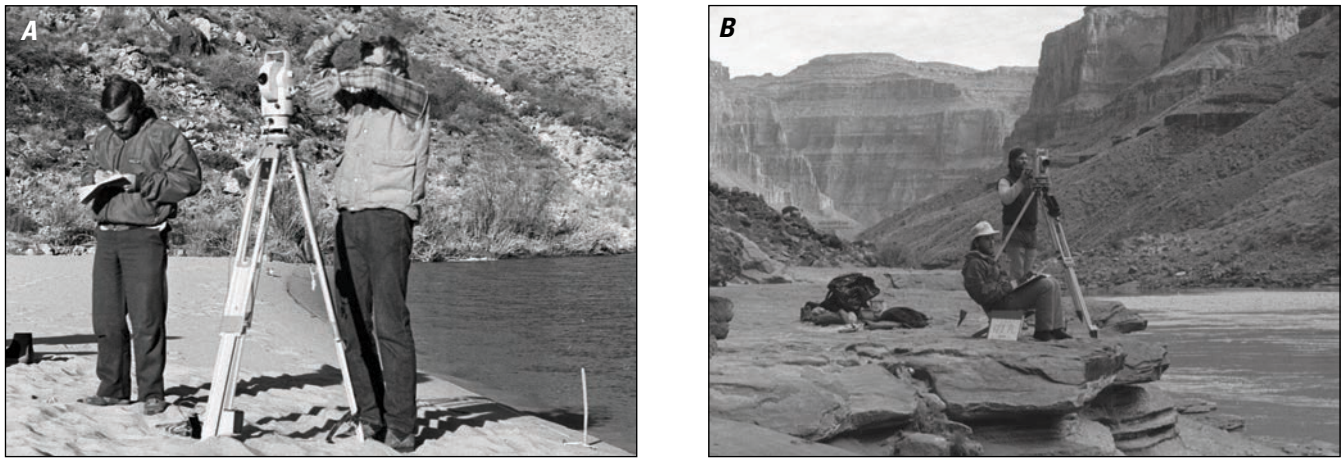

Figure 9. Photographs of sandbar surveys in 1986 and 1990. By the late 1980s, the total station (TS) had replaced the manual theodolite for topographic surveying. *A*, Sandbar survey at study site 047R on January 18, 1986. The instrument operator is Dr. John C. Schmidt of the U.S. Geological Survey. Utah State University photograph. *B*. Sandbar survey at study site 123L on November 12, 1990. Photograph by J. Hazel, Northern Arizona University. By 1991, the availability of electronic data loggers had reduced the need for paper field notes and the data transferred to a micro-computer in the field or desk-top computer upon completion of the river trip. For list of study sites, see table 1.

position and sparse distribution of data points. Consequently, some maps were omitted from analysis. Despite these limitations, Schmidt and Graf (1990) were the first to examine sandbar dynamics by extending their analysis into the third dimension to estimate changes in sand volume caused by erosion and deposition with repeat topographic surveys. They documented widespread erosion of sandbars during an experimental period of powerplant fluctuations between October 1985 and mid-January 1986. They also observed patterns of sand exchange between the main channel and eddies over a broad range of discharges, revealing processes by which fluctuating flows affect sandbar stability.

To quantify sandbar response to Reclamation's 1990–91 experimental flows (fig. 3*B*), Beus and others (1992) utilized TS surveying twice-monthly at as many as 32 study sites during periods of steady low discharge between each test flow. Low discharge enabled measurements to be made on otherwise inundated sandbars. Initially, the survey protocol included placement and recovery of 1-m-long scour wires to measure depths of scour and fill. The scour wires were hammered vertically into the sandbars at precise intervals along grid-based transects laid out by tape (fig. 10). The exposed (indicating erosion) or disturbed (indicating deposition) length was measured on the subsequent river

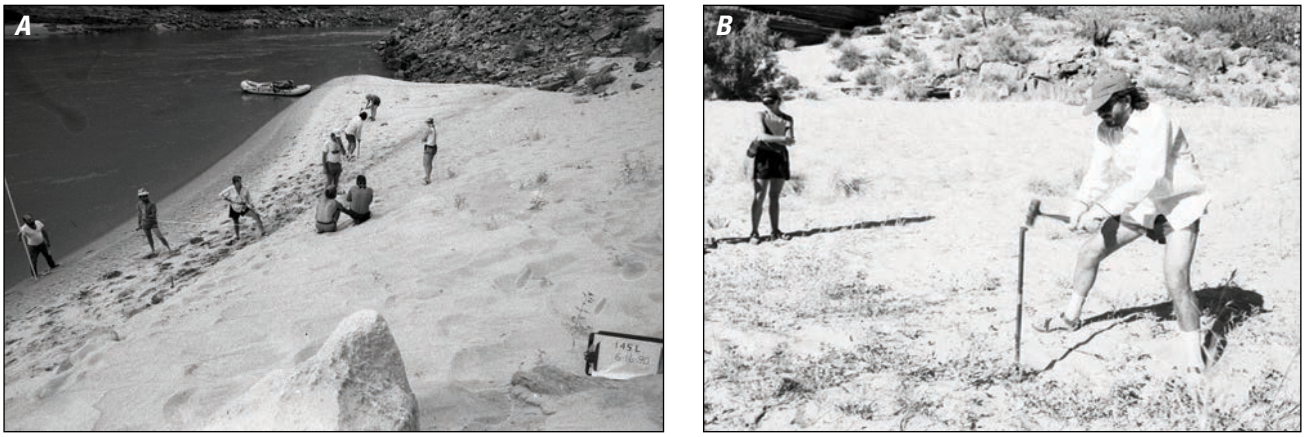

Figure 10. Photographs showing the scour wire method utilized by Beus and others (1992) early in the 1990–1991 Bureau of Reclamation experimental flow program involving the Glen Canyon Dam. *A*, Photograph of the tape and Brunton compass method used to orient transects between two known reference points, study site 145L, June 18, 1990. *B*, Each scour wire was pounded into the sandbar surface with a sledge hammer until the top of the wire was flush with the sandbar surface, study site 122R, June 15, 1990. The locations were surveyed by total station. After the subsequent test flow, the wires were relocated and the surface excavated until the wire was exposed. If scour had occurred, the length of the exposed wire lying horizontally indicated the depth of fill. If no scour had occurred, the amount of fill was the depth of sand above the top of the buried wire. Photographs by M. Kaplinski, Northern Arizona University. For list of study sites, see table 1.

trip. However, re-locating the wires using the stake-out method with a TS was time consuming and in many cases the wires were never found. Interpretation of scour or fill between surveys was uncertain because of undocumented changes between coarsely spaced wires owing to the three-dimensional nature of sandbar topography. It was discovered that sandbars can change dramatically in shape and size, yet change relatively little in their overall volume, because sand was simply redistributed within the same site with little net change. Thus, data collection protocol was reprioritized to spatially continuous TS surveying and terrain modeling early in the project (fig. 9*B*). Continued advancements in TS surveying technology, including automatic logging of measurements by digital data collectors, ensured the reliability and repeatability of the topographic mapping. In the field, data points could be collected and stored at a maximum rate of 240 points per hour and maps were made with computer-based topographic-surface modeling software, making it possible to detect potentially small changes (centimeter scale) in sandbar topography between each specific release. Data collection during the test flows was focused primarily on the zone between the levels of maximum and minimum inundation (termed the "hydrologically active zone"), with sparse point density elsewhere (time spent making field measurements was limited by the short 4-day periods of low flow between test flows). Bathymetric measurements were also made but the method was labor intensive, requiring five people to record the boat position and operate the echo-sounder (see "Data Collection" in the "Methods" section).

Despite changes in methodology and differences in sampling resolution, Beus and others (1992) were able to evaluate 16 of the 20 test flows based on ~500 surveys collected at 29 sites during the 14-month program. The repeat measurements of bar topography showed that sandbar responses were more variable than previous surveys, which had coarser spatial-temporal resolution, with some sandbars both eroding and gaining sand over the study period and others changing little. Erosion was prevalent during some steady flows and flows following depositional events were more likely to erode bars. Flows characterized by large daily fluctuations resulted in widespread deposition if associated with sediment contribution from tributaries. Although Beus and others (1992) did not demonstrate which specific flow alternative best maintained sandbars, the finding that bar behavior was correlated with tributary sediment inputs and antecedent condition (bar volume at the beginning of a given flow) provided a scientific basis for the HFEs included in the 1996 ROD on the EIS for operations of Glen Canyon Dam.

Stability of Eddy Sandbars

Sandbar erosion is caused by many processes such as wave action (Bauer and Schmidt, 1993), seepage erosion and slumping (Budhu and Gobin, 1994; Carpenter and others, 1995; Alvarez and Schmeeckle, 2013), wind deflation (East and others, 2016; Kasprak and others, 2018), side-canyon floods and hillslope runoff (Melis and others, 1994), and tractive force erosion from near-shore currents (Schmidt and Graf, 1990). The relative importance of these processes was not well understood until the mid-1990s, as initial studies were conducted during the 1980s high flow years, and because of the wide range of controlling factors that affect sandbar size besides changes in discharge. Even so, the research community generally agreed that erosion was a natural and expected process following closure of Glen Canyon Dam, one that was accelerated by low Colorado River sand concentrations and changes in flow regime

(Schmidt and Grams, 2011a). Generally, erosion rates increase when dam releases are increased to produce more hydroelectric power (see "Flow Regimes and Tributary Sediment Supply" section). However, erosion also occurs as discharge recedes and eddies contract in size, resulting in higher velocity downstream current in proximity to eddy sandbars. Under these conditions, sandbars are unstable and will slump and develop cutbanks that may extend the length of the sandbar during low discharges (fig. 11*A*, *B*). Rates of erosion are related to the amount of high-elevation deposition (Hazel and others, 1999; 2010), but those rates decrease as the availability of erodible sediment decreases (Schmidt and others 1995), or as a stable slope is

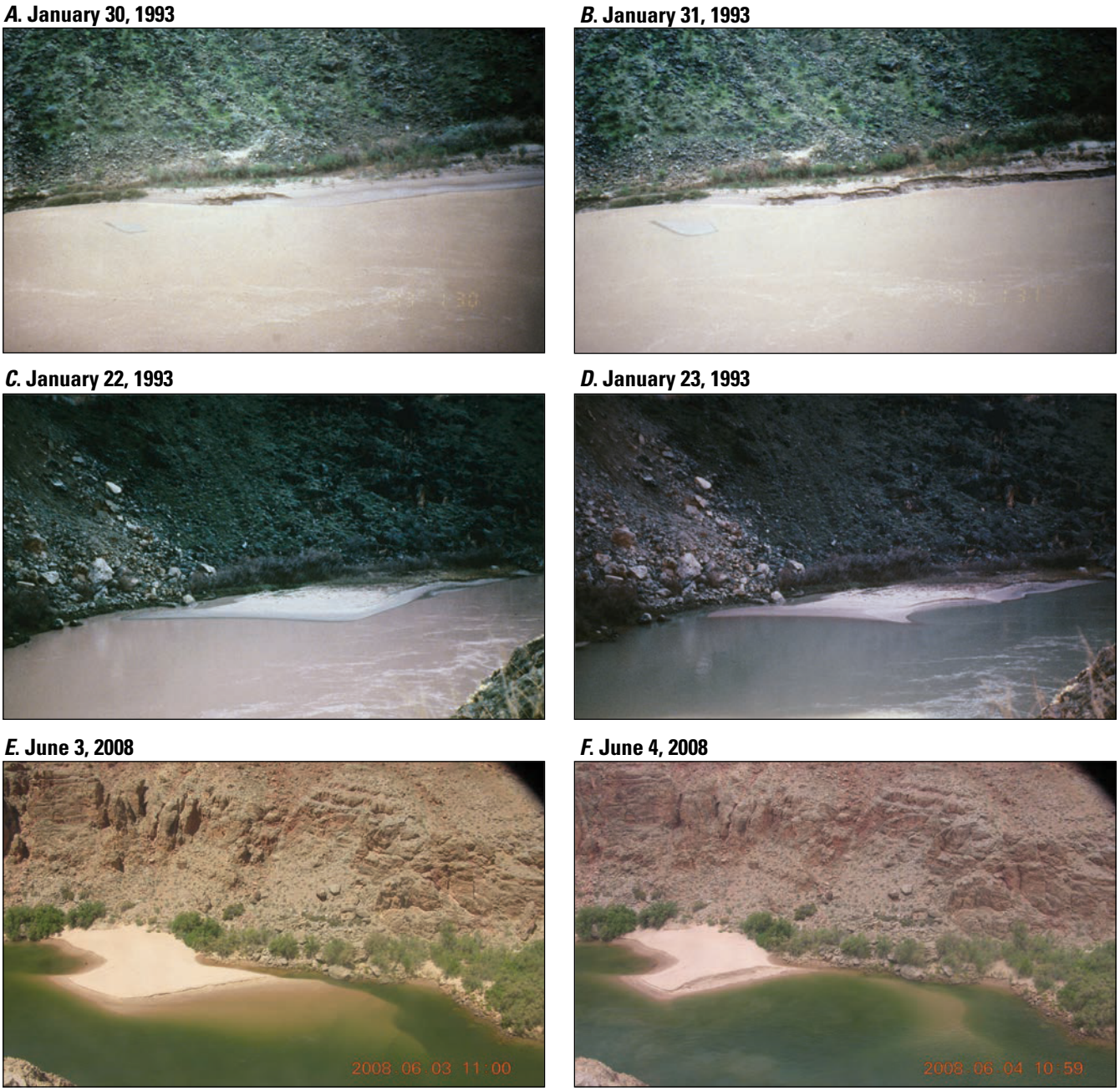

Figure 11. Photographs of examples of large bank failures in the study area, Colorado River corridor, Marble and Grand Canyons. Study site 172L shows bank collapse in *A* and *B*. Streamflow is from left to right. Note the newly formed cut-bank extending the length of the sandbar in *B*. Study site 044L shows erosion of the reattachment bar in *C* and *D*. Streamflow is from left to right. Note the circular-shaped erosional scar in *D*. Study site 030R shows large-scale mass failure in *E* and *F*. Streamflow is from right to left. Note the crescent-shaped area of scour similar in morphology to that in *D*. Bank failures have been observed on gently sloping sandbars as well as those with steep slope angles and can occur over time scales as short as a few minutes. Failure mechanisms are poorly understood but have been linked to changes in flow regime or sediment supply (Dexter and Cluer, 1999) and oversteepening of bar slopes during depositional events (Wright and Kaplinski, 2011). For study sites, see table 1. Images captured by remote automated cameras. Photographs *A*–*D*, Northern Arizona University; photographs *E*–*F*, U.S. Geological Survey (Grams and others, 2018a).

reached (Budhu and Gobin, 1994; Alvarez and Schmeeckle, 2013). Vegetation also increases sandbar stability and is effective at trapping sediment during floods by slowing flow velocities, causing sediment to drop out of suspension (Butterfield and others, 2020).

Computations of net topographic change from repeat surveys are known to underrepresent actual sediment flux because of the extended periods of bar reworking (spatial-temporal cycles in erosion and deposition) between surveys, where offsetting elevation changes can mask considerable sediment flux within a given site. In the early 1990s, time-lapse photography revealed that erosion and deposition could occur during a single event or on multiple occasions (Cluer, 1995; Dexter and Cluer, 1999), which could bias interpretation of sandbar change based on infrequent surveys. Referred to as "rapid-erosion events" by Cluer (1995), they include bank slumping as well as mass failures that happen instantaneously or on the order of minutes to hours (fig. 11*C*, *D*). Unlike erosion downstream of the reattachment point of the primary eddy at lower discharge (because of the decrease in eddy length and size), this pattern of erosion is characterized by a semicircular arc, consistent with the shape of upstream flow circulation, indicating that the erosion took place within the lower velocity eddy. This process has also been measured in detail during HFEs where deposition and oversteepening of the bar slope leads to mass failure (Andrews and others, 1999; Schmidt and others, 2004; Wright and Kaplinski, 2011). Thus, erosion can be progressive and can occur on long time scales or sand can be rapidly eroded from eddies. Depending on discharge patterns and sand supply, the eroded sand can be entirely replaced in a period of several days to a few weeks. This cyclic pattern of deposition and erosion was once thought to be an anomalous occurrence in the study area but is now recognized as common in a variety of fluvial and deltaic settings (Van Den Berg and others, 2002). For these reasons, our primary focus is on metrics of sandbar state at the time of each survey to evaluate annual- and decadal-scale trends in sandbar size. We compute differences of repeat topographic surveys to evaluate short-term response to discrete events, such as HFEs (for example, Hazel and others, 2010).

Flow Regimes and Tributary Sediment Supply

During a typical year of flow regulation by Glen Canyon Dam, the daily range of flows is large, seasonal variations in flow are minimal, and the typical magnitude of low flows has increased relative to pre-dam low flows (fig. 3). The 2-year recurrence peak flow of the post-dam period was 892 m^3/s, a 62 percent reduction from the magnitude of the 2-year recurrence peak flow of the pre-dam measurement period (Topping and others, 2003). Beginning in the early 1990s, releases from Glen Canyon Dam were scheduled according to the guidelines as described in the Modified Low Fluctuating Flow Alternative (MLFF) in the 1996 ROD (DOI, 1996). The MLFF restricted minimum and maximum flows to 141 m^3/s and 708 m^3/s, respectively, representing a strong departure from the unconstrained daily hydropower releases typical of the 1970s and 1980s (fig. 3*A*). In addition, normal operations that have continued as part of the MLFF are low-, medium-, and high-volume months, with low flows during the late spring and late fall, moderate flows in May and September, and high flows during mid-summer and mid-winter (fig. 3*B*). Normal operations also include reduced flows on weekends as electrical demand decreases. The daily fluctuation or range in flow was limited to 142 m^3/s during low-volume months, 170 m^3/s during medium-volume months, and 227 m^3/s during high-volume months. Dam releases now follow the guidelines established by the LTEMP EIS Record of Decision (DOI, 2016), which are similar to those of MLFF, with a few notable modifications. Among these are that monthly release volumes are more evenly distributed throughout the year to improve sediment conservation without affecting the annual release volume. The maximum daily fluctuation is now a continuous function of monthly volume, but still capped at 227 m^3/s, and to reduce sandbar erosion rates (Alvarez and Schmeeckle, 2013), ramping rates are now constrained to 113 m^3/s per hour when flows increase and 71 m^3/s per hour when flows decrease.

The median discharge from Glen Canyon Dam between 1991 and 2021 was 340 m^3/s, 58 percent greater than the pre-dam streamgage record from 1921–1963 (fig. 3). Thus, as the frequency of large floods greatly decreased following closure of Glen Canyon Dam, the magnitude of typical low flows has increased. Most annual dam releases since 1990 have been at the minimum-allowed volume of 10.15 cubic kilometers per year but there have been two periods of above-mean annual release volumes (1995–1999 and summer 2011) (fig. 12*A*). The 1995 through 1999 period (calendar years) was characterized by a mean discharge of 476 m^3/s, whereas equalization flows to Lake Mead in 2011 had a mean discharge of ~675 m^3/s from May 15 to September 1. Equalization flows are released under certain criteria by Reclamation to balance the amount of storage between Lake Powell and Lake Mead. A 5-year steady-flow experiment (intended to benefit native fish) was conducted in September and October of each year between 2008 and 2012. In sequence, the steady flows were 340, 283, 227, 453, and 227 m^3/s, respectively. Another departure from the LTEMP flow regime were non-native fish suppression flows with fluctuations of 142–566 m^3/s released January through March of 2003–2005.

The 1996 ROD recommended scheduled high releases of short duration be implemented for environmental purposes. This recommendation included habitat maintenance flows (HMFs), which are within powerplant capacity (~940 m^3/s), and beach-habitat-building flows (BHBFs), which exceed powerplant capacity. The former was intended to maintain existing camping beaches and wildlife habitat, and the latter to more extensively modify and create sandbars, thus restoring some of the dynamics that result from flooding in an ecosystem (DOI, 1995). More recently, "high-flow experiment" (HFE) has been used to describe all experimental flows from Glen Canyon Dam that have magnitudes ranging from powerplant capacity to 1,274 m^3/s (Schmidt and Grams, 2011a). Because powerplant capacity varies over time as a function of reservoir elevation and turbine

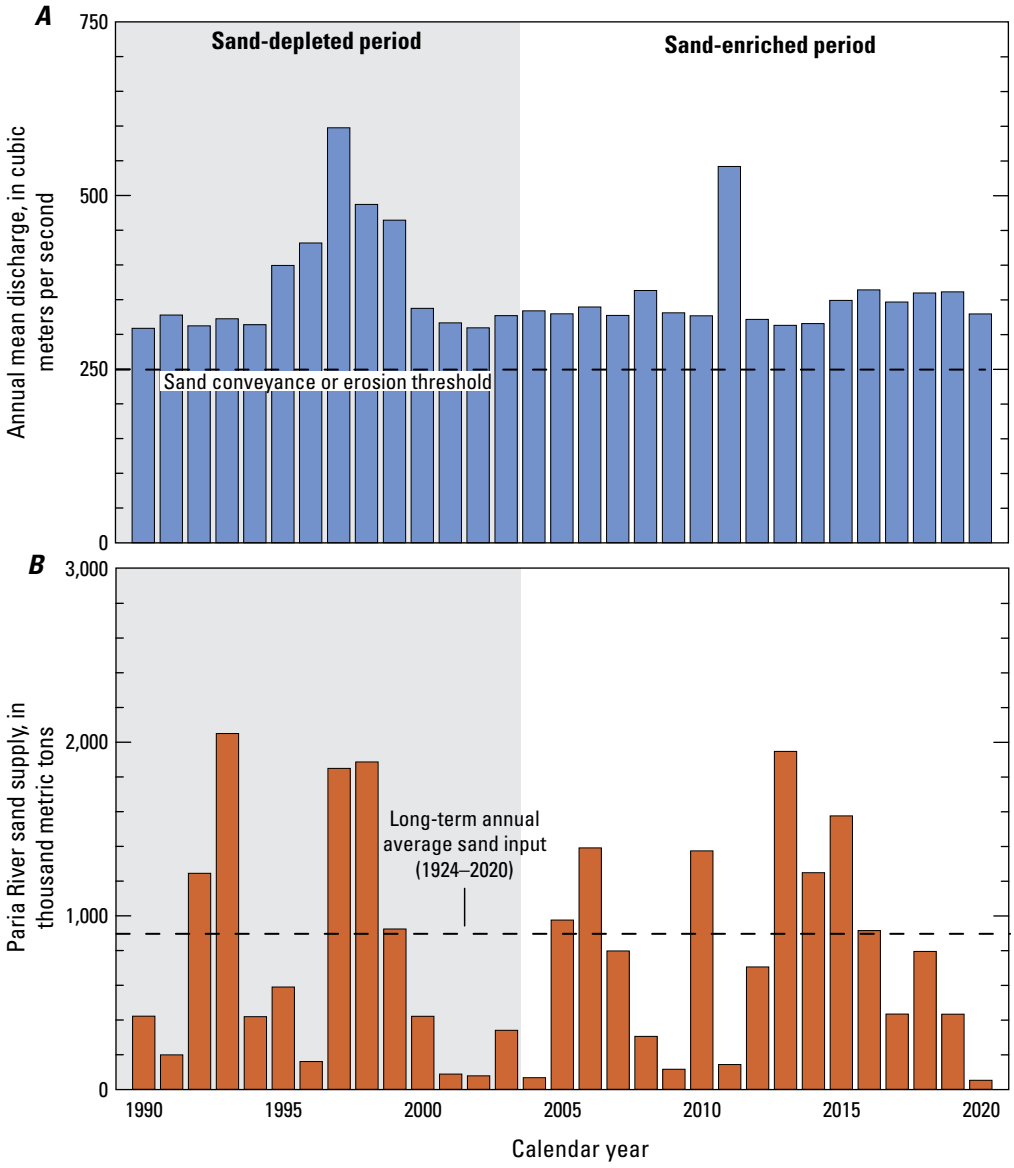

Figure 12. *A*, Bar graph of the annual mean discharge of the Glen Canyon Dam on the Colorado River measured at the U.S Geological Survey (USGS) Lees Ferry streamgage station (station 09380000), Arizona. *B*, Bar graph of Paria River sand supply between 1990 and 2020 at the USGS Paria River streamgage station (station 09382000), Lees Ferry, Arizona. The sand conveyance or erosion threshold of 250 cubic meters per second (m^3/s) was computed by Topping and others (2000). Paria River sand loads have a 20 percent uncertainty and were estimated by using modeled sand loads from Topping (1997) for the years prior to 1997 and using measured loads (Griffiths and others, 2014) from 1997 to 2020.

availability (one of the eight hydroelectric generating units was offline for maintenance), the amount of water released through the powerplant, combined with the river outlet works (425 m^3/s), has varied for each HFE. There have been 11 HFEs between 1996 and November 2018, including lower magnitude HMFs in 1997 and 2000 (fig. 3*B*; table 4). Each event was composed of a constant peak flow maintained for several days, ranging from about one-third to one-half of the pre-dam mean annual flood peak (2,400 m^3/s), and about one-fifth to one-sixth as large as the maximum historical pre-dam flood (5,940 m^3/s in 1884) (Topping and others, 2003). Despite substantially lower peak magnitudes than most pre-dam annual floods, HFEs occur infrequently and are geomorphically significant events in terms of ecosystem disturbance (Schmidt and Grams, 2011a).

In the post-dam period, the majority of sand inputs to the Colorado River downstream from Glen Canyon Dam are sourced from tributary streams. Among these, the Paria River is the primary source of sand to Marble Canyon. The Little Colorado River is the largest tributary to the Colorado River in Grand Canyon and the primary source of sand downstream from Marble Canyon. The average annual sand supply from the Paria River is variable but is substantially greater than the input from the Little Colorado River and from lesser, ungaged tributaries (Griffiths and others, 2014). Most of the sand input from the Paria River and the lesser tributaries is supplied to the Colorado River by short-duration floods. On a mean-annual basis, the Paria River supplies an amount of sediment equivalent to ~6 percent of the pre-dam sand loads of the Colorado River at the head of Marble Canyon at the upstream boundary of Grand Canyon National Park (Topping and others, 2000). The mean annual sand load (using a combination of modeled and measured sand loads) for the 98-year USGS Paria River streamgage record (at Lees Ferry, Ariz.) is 0.88±0.18 million megagrams (Mg) (fig. 12*B*). The Little Colorado River was also a major pre-dam supplier of sand to the Colorado River. However, reductions in flood magnitude and duration because of upstream water development, combined

Table 4. High-flow experiments (HFEs) released between 1996 and 2020 from Glen Canyon Dam as measured at the U.S. Geological Survey streamgage station on the Colorado River at Lees Ferry, Arizona (station 09380000).

[m^3/s, cubic meters per second; %, percent]

Year	HFE start date	HFE magnitude (m^3/s)	HFE duration (hours)	Percentage of maximum allowable magnitude[1] (%)
1996	March 26	1,274	168	100
1997	Nov. 3	872	48	68
2000	May 3	864	96	69
2000	Sept. 5	881	96	69
2004	Nov. 22	1,181	60	93
2008	March 6	1,212	60	95
2012	Nov. 19	1,260	24	99
2013	Nov. 11	1,048	96	82
2014	Nov. 10	1,076	96	84
2016	Nov. 7	1,034	96	81
2018	Nov. 5	1,079	65	85

[1]Defined as the maximum allowed discharge through the powerplant including the additional 425 m^3/s utilizing the river outlet works.

with the widespread establishment of dense riparian vegetation, reduced the total annual flow by the mid-1990s to nearly 50 percent of the mean-annual supply during the 1943–1995 period of record (Dean and Topping, 2019). Thus, the Paria River Basin is the dominant post-dam source of sand. In fact, deposits from the 2013 and 2014 HFEs suggest that 69–84 percent of the sand was derived from the Paria River (Chapman and others, 2020). In addition to the reduced sand supply, large tributary inputs remain in storage for only a few months before most of the introduced sediment is transported downstream, unless flows are below approximately 250 m^3/s (fig. 12*A*). Termed the "threshold for sand conveyance or erosion" (Topping and others, 2000), this discharge is exceeded during most releases from Glen Canyon Dam in the post-dam era and the river is now characterized by transport of sand in suspension through, or erosion of sand from, Marble and Grand Canyons.

We focused our analyses on two periods, defined by differences in Glen Canyon Dam flow regime, tributary sand supply, and HFE frequency. The first period is termed the "sand-depleted period," extending from 1990 through 2003 (calendar years), when both Marble and Grand Canyons were prone to sand export relative to sand input. Between 1990 and 2003, the mean Colorado River discharge at the Lees Ferry streamgage station was 376 m^3/s and the 250 m^3/s threshold (defined above) was exceeded 78 percent of the time. During the 1995–99 high-flow period, the discharge of the river was greater than 250 m^3/s 96 percent of the time (fig. 12*A*). Compared to the entire period of streamgage record, the sand supplied by the Paria River was average or above average in only 5 years during the 14-year period (fig. 12*B*). The mean annual sand load for this 14-year period, 0.76 ±0.15 million Mg, was substantially below average compared to the streamgage record. Because of below average tributary sand supply, discharges likely conveyed or eroded sand most of the time, and consequently the 1990–2003 period was one of sand deficit. In addition, because of the duration of discharges greater than 250 m^3/s, the 1990s were shown by Topping and others (2003) to be a decade of considerably more sand export than either the post-dam years of reservoir infilling, or the high flow years of the 1980s.

The second analysis period is termed the "sand-enriched period," extending from 2004 through 2020 and characterized by normal dam operations, HFEs in 2004 and 2008, and the period after implementation of the 10-year experimental HFE protocol in 2012. The mean Colorado River discharge at the Lees Ferry streamgage station during this 17-year period was 350 m^3/s and the 250 m^3/s threshold was exceeded 80 percent of the time (fig. 12*A*). Thus, this period was also biased toward either the conveyance of sand through, or the erosion of sand from, Marble and Grand Canyons. However, the duration of higher discharges more likely to erode sand from Marble and Grand Canyons occurred less frequently during the sand-enriched period. The discharge that was equaled or exceeded 10 percent of the time was 485 m^3/s in the sand-enriched period and 564 m^3/s in the sand-depleted period (a difference of 14 percent). In addition, tributary sand supply was greater than that delivered during the 1990–2003 sand-depleted period. There were 9 years where the amount of sand supplied by the Paria River was near average or above average (fig. 12*B*). The mean annual sand load computed from the Paria River streamgage station at Lees Ferry for the period was 0.77±0.15 million Mg, a sand delivery about 10 percent greater than the mean load input by the Paria River during the sand-depleted period. Furthermore, HFEs were coordinated to follow tributary inputs, and further timed so the HFE occurred before that sand was conveyed through the system and the river returned to a condition of sand deficit. Thus, sand was redistributed from low elevations in the channel to higher elevation sandbars and removed from downstream transport at least temporarily. Therefore, in this report we characterized the 2004–2020 period as a period of sand enrichment.

1993 Little Colorado River Floods

Floods from the Little Colorado River in January and February 1993 delivered a significant amount of sand to the mainstem Colorado River and contributed enough streamflow to elevate discharge downstream from the confluence by as much as 450 m^3/s. This event provided a natural test case for a sand-enriched bar-building flow. Three separate floods that winter, January 12–16, January 19–23, and February 23–26, raised flows that peaked at the USGS streamgage station at Grand Canyon (station 09402500; fig. 1) at approximately 966 m^3/s, 793 m^3/s, and 824 m^3/s, respectively. These floods delivered approximately 4.2 million Mg of sand to the mainstem river and the associated high sand concentrations led to the deposition of large eddy sandbars (Wiele and others, 1996). A surprising find was the large sandbar deposited in the "Crash Canyon" eddy at 062R in this study, a site that had been previously devoid of a subaerial sandbar (fig. 13*A*). Kaplinski and others (1995) showed that more than 100,000 m^3 of sand was deposited in both the eddy and adjacent main channel, an amount equivalent to a 7-m-thick layer of sand spread out over the measured area (24,000 square meters [m^2]; table 1). As a result, the site was added to the monitoring network to track the fate of the new deposit. The bar was largely removed

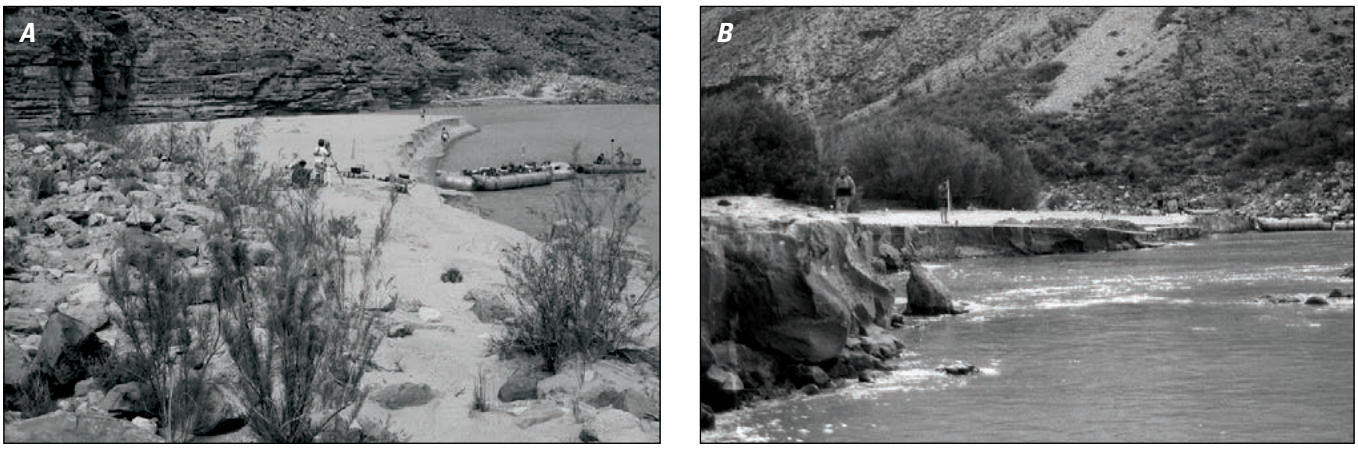

Figure 13. Photographs of deposition and erosion following the 1993 Little Colorado River floods, Grand Canyon. *A*, Photograph of the emergent reattachment bar at study site 062R on April 5, 1993. *B*, Photograph of study site 202R showing cutbank erosion following the 1993 Little Colorado River floods on April 13, 1993. Photographs by J. Hazel, Northern Arizona University. For list of study sites, see table 1.

when Glen Canyon Dam operations changed from low- to high-volume releases in July 1993 and completely eroded by 1995. At this site, and others aggraded by the 1993 floods, the new deposits were quickly eroded after the return to normal Glen Canyon Dam operations and large-scale cutbanks were observed at nearly every study site downstream of the Colorado River confluence with the Little Colorado River (fig. 13*B*).

1996 High-Flow Experiment

The first opportunity to comprehensively study physical processes during controlled flooding occurred in spring 1996 (fig. 3*B*; table 4), with a 7-day sustained discharge of 1,274 m^3/s (Webb and others, 1999). A major objective of the 1996 HFE was to determine if high releases from Glen Canyon Dam could effectively redistribute sand from the riverbed to the channel margins. However, the 1996 HFE was conducted following 2 years of below average sand inputs (fig. 12*B*). Suspended sediment during the test progressively coarsened over time (Topping and others, 1999; 2000) and the grain size of post-flood deposits vertically coarsened (Rubin and others, 1998), presumably because the sand supply was rapidly depleted. Modeling of depositional processes indicated that rates of bar deposition were proportional to the supply of sediment (Wiele and others, 1999). Repeat surveys showed that the majority of sandbar deposition occurred within the first 2 days of the test (Andrews and others, 1999). These physical process studies demonstrated that controlled flooding could be used in river management but that the design of future releases would benefit from considering the effect of decreasing main-channel sand concentrations on transport and deposition (Rubin and others, 1998; Schmidt, 1999).

1997 Test Flow

Observations during the 1996 HFE revealed the possibility that a shorter duration and lower magnitude flow could more effectively redistribute sand recently supplied by tributaries to the banks of the Colorado River. Tributary inputs from the Paria River in August and September 1997 significantly replenished sand in the Colorado River downstream from the confluence with the Colorado River (fig. 12*B*). This 2-month period of flooding resulted in sand inputs that were among the top 20 percent of mean annual sand load during the nearly 100 years of streamgage record on the Paria River (Topping and others, 2000). These sand inputs were also the first significant inputs from the Paria River since the winter of 1995, and the largest since 1980. Shortly after the inputs, GCDAMP recommended that a short-duration HMF be released from Glen Canyon Dam. Termed the 1997 Test Flow, the release occurred on November 3, 1997, and consisted of a constant flow of 872 m^3/s for 48 hours (fig. 3*B*; table 4). This was the first attempt by Reclamation to implement a flow release strategy for sediment redistribution following a tributary flood.

The 1997 Test Flow was conducted during a period of high releases (maximum daily flows for October to December exceeded ~500 m^3/s) in which there was high sediment transport that reduced the amount of available sediment; the 1997 Test Flow did not significantly aggrade sandbars. Hazel and others (2000) concluded that the magnitude of the release was not sufficient to distribute sand to open depositional locations at higher elevations. This concept of stage limitation was explored by Hazel and others (1999) who examined inundated areas where space was available for deposition during the 1996 HFE, termed "accommodation space." They directly correlated differences in depositional thickness with the magnitude of stage change in Marble Canyon.

The 2000 Low Summer Steady Flow Experiment

In 2000, the low summer steady flow experiment (LSSF) consisted of a 4-day flow of 864 m^3/s, followed by 3 months of constant 227 m^3/s discharge and then another 4-day release of 881 m^3/s (fig. 3*B*). The 4-day powerplant capacity flows are referred to as the May and September 2000 HMFs, respectively, and were intended to improve the quality of native fish spawning and rearing habitat (Hazel and others, 2006b; Schmidt and others, 2007; Ralston, 2011). However, the Paria River supplied very little

sediment to the Colorado River in the prior months, including the 3-month period when flows were kept below the 250 m^3/s sand conveyance threshold (fig. 12*B*). As a result, there was minimal sandbar building during either of the two HMFs released during this experiment (Schmidt and others, 2007). In addition, the reduced summer hydrograph resulted in proliferation of exotic tamarisk (*Tamarix ramosissima*) seedlings on bare open sand deposits, presumably transported by the May 2000 HMF. Scour by the September 2000 HMF resulted in some tamarisk seedling mortality but the 2000 LSSF demonstrated the rapid rate at which vegetation is established on bare shorelines not subject to frequent inundation (Ralston, 2011).

Sand-Enriched High-Flow Experiments

Improved understanding of flood effects resulting from the 1996 HFE and lower magnitude HMFs in 1997 and 2000 led to the decision to release HFEs in 2004 and 2008. In May 2012, the DOI implemented a new protocol for conducting multiple HFEs during sediment-enriched conditions for a 10-year period of experimentation (fig. 3*B*; table 4). These more recent HFEs were of shorter duration (60–96 hours) than the 1996 HFE (7 days), but all were released following substantial sand supply from the Paria River (Topping and others, 2010). The 2004, 2008, and 2012 HFE water releases increased from base to peak flows over 30-hour periods, a 50-percent slower rate of rise than the 1996 event. The 2004 HFE (November 22–24, 2004) was a 60-hour release of 1,181 m^3/s. The 2008 HFE (March 6–8, 2008) was a 60-hour release of 1,212 m^3/s.

On November 18–23, 2012, the first HFE under the multiyear flood protocol was released with duration of 120 hours, with 24 hours at peak release of 1,260 m^3/s. On November 11–14, 2013, the second HFE under the new protocol was released with a peak of 1,048 m^3/s for a total of 96 hours. The third HFE was also 96 hours, beginning on November 10, 2014, with a peak of 1,076 m^3/s. The fourth HFE conducted under the protocol occurred on November 7–12, 2016, with a peak of 1,034 m^3/s for a total of 96 hours. The most recent HFE to occur during the protocol was released November 5–7, 2018, with a peak of 1,079 m^3/s for a total of 60 hours. Pre- and post-HFE surveys were not made between 2012 and 2018 and sandbar response was largely determined from repeat photographs (Grams and others, 2018a) and sandbar monitoring data collected ~11 months after each event.

Methods

Data Collection

The topographic surveying protocol established by Beus and others (1992) was refined and continued between 1991 and 2020 (fig. 3*B*). The surveys were made annually or more frequently and were collected in a variety of environmental conditions, ranging in temperature from below 0 degrees Celsius (°C) to greater than 43 °C. Not all sites were surveyed on every river trip, and the number of study sites was gradually increased after 1991 (see "Study Site Selection and Distribution" section). Concurrent and coincident bathymetric measurements were only made during surveys conducted between 1990 and September 2000 and during surveys immediately before and after the 2004 and 2008 HFEs. As scientific insight and understanding of HFE sandbar response evolved, the monitoring strategy used to characterize sandbar conditions changed from direct evaluation of HFEs, and other flow experiments, to surveys made annually in the fall months at as many as 45 sites (table 1). Because many of the surveys from the 1990–91 experimental flow program are not comparable to the data collected after 1991, only the first survey of sufficient extent and data density, as well as the last survey bracketing the test flow period, are included herein. In total, we report on ~1,800 surveys collected between 1990 and 2020 in which individual study sites have as many as 51 repeat surveys (fig. 3*B*, table 1.1 of appendix 1).

Since the mid-1990s, there have been numerous technological advances in topographic and bathymetric surveying. Improvements in the hardware used for field surveys and the software used for post-processing greatly improved the rate at which data were collected and analyzed. Advances in sonar technologies, including navigation and positioning, addressed the difficulties in obtaining high-resolution bathymetric datasets. Other methods for topographic surveying that were evaluated, but ultimately not adopted, include aerial lidar photogrammetry (Davis, 2004), oblique laser scanning (ground-based lidar), oblique photogrammetry (Dexter and Cluer, 1999), multiview photogrammetry such as structure-from-motion (Rossi, 2018), and real-time kinematic Global Positioning Systems (RTK-GPS). Although TS surveying was a relatively new technological advancement in monitoring geomorphic change in 1990, more than two decades later, it still provides the best compromise of speed, accuracy, and coverage in the study area. The narrow river corridor is characterized by cliffs or steep slopes, and in places, dense vegetation; these factors limit visibility to the sky, making RTK-GPS surveying difficult (Hazel and others, 2008). Additionally, remote mapping technologies require substantial post-processing and are unable to survey submerged bed topography or topography underlying dense vegetation. Measurements in water as deep as 1.5 m (commonly in extremely turbid conditions) and in dense vegetation are required to ensure data consistency. When bathymetric measurements of bed topography were collected, both singlebeam echosounders (SBES) and multibeam echosounders (MBES) were used (Kaplinski and others, 1995; Kaplinski and others, 2009) (table 5).

Study Site Selection and Distribution

This study includes the 32 study sites established by Beus and others (1992), providing a 31-year record of sandbar change as of the writing of this report (table 1; table 1.1 of appendix 1). These sites are hereafter referred to as the "reference series." Sample size was increased by the addition of sites in 1993, 1996, 1999, 2002, and 2008. Beus and others (1992) reported on 29 sites but collected topographic measurements at a total of 32 sites.

Table 5. Summary of bathymetric survey equipment used in the study area in the Colorado River corridor, Marble and Grand Canyons.

Survey methodology (years of use)	Positioning system equipment	Operation of positioning equipment	Echo sounding equipment	Linking of position and depth data
1990–91	Cable/reel	Manual	Lowrance X–16	Manual
1992	Range azimuth	Manual	Lowrance X–16	Manual
1993–95	Range azimuth	Manual	Innerspace 448	Manual
1995	Range azimuth	Manual	Marimatech 206	Automated
1996–99	Range azimuth	Manual	Innerspace 448	Automated
2000	Range azimuth	Robotic	Innerspace 448	Automated
2000	Range azimuth	Robotic	Teledyne Reson 8124	Automated
2004–08	Range azimuth	Robotic	Teledyne Reson 8125	Automated

The missing sites (033L, 139R, and 225R) were later processed and reported on by Hazel and others (1999; 2010) who also added study sites 062R in 1993, 055R and 065R in 1996, and 035L in 1997. With the addition of seven sites in 2002 and two sites in 2008, the sample size was increased to the current total of 45 (table 1.2 of appendix 1). Hazel and others (2010) report on 57 sites; however, 12 of the sites were measured for a companion 2008 HFE study that focused on backwater habitat (Grams and others, 2010) and the sites have not been resurveyed. We include data for one site located in Glen Canyon (−006R) that is not included in analyses for Marble and Grand Canyons. Thus, there are 44 sites in Marble and Grand Canyons and 31 of those are the reference series that were established in 1990.

Beus and others (1992) listed the criteria used to select the reference series as (1) distribution of sites among the 11 geomorphic reaches (table 2), (2) distribution among bar types, (3) availability of historical topographic data, and (4) variation in recreational use intensity and vegetation cover. Some of these study sites were established by other researchers in the 1970s or 1980s (table 3). All were chosen before there was a general understanding of reach-scale variability in eddy bar sediment storage, and the sites were established based on the assumption that a study site was representative of nearby eddies, which was later shown to be incorrect (Grams and others, 2013). We therefore include in this report an evaluation of the sample size that is required to estimate average sandbar response (see "Sandbar Sample Size" section).

Averaged for the entire study area, there is one site every 8.4 km; however, the sites are not evenly distributed (fig. 1). Twenty sites are in the 100-km-long Marble Canyon segment and 24 sites are in the 264-km-long Grand Canyon segment. Thus, the density of sites in Marble Canyon is approximately double the density of sites in Grand Canyon. As new study sites were added to the monitoring network, a greater percentage were chosen from Marble Canyon than in Grand Canyon because the influence of the Glen Canyon Dam was thought to be greatest in the reach closest to Glen Canyon Dam. No sites were examined downstream from Diamond Creek (RM 226). Despite this uneven distribution of measurement sites, the Beus and others (1992) selection criteria are largely met because fan-eddy complexes occur less frequently in the Grand Canyon segment. At the beginning of the study in 1990, the reference series was composed of about 5 percent of the persistent, subaerially exposed sandbars in both Marble and Grand Canyons observed from 2009 aerial photography (table 2). The distribution of study sites in geomorphic reaches varied from 2.6 to 14.3 percent. By 2008, with the addition of more measurement sites, the population of eddies with monitored sandbars had increased to 9 percent and 7 percent in Marble and Grand Canyons, respectively. The distribution of study sites in geomorphic reaches varied from 3.2 to 17.1 percent.

Survey Control Network

The topographic surveys are referenced to at least three permanent control points for each study site. Where possible, control points established by previous researchers during tape and transit surveys were utilized if they provided good line-of-sight views. The control points are stable survey marks permanently monumented on rocks or bedrock ledges by a cross-cut X or other symbol, hardened masonry nail, carriage bolt, or aluminum and brass caps (table 2.1 of appendix 2). We refer to the control point over which a TS is placed as the benchmark. Because reference to a global datum was not available in 1990, each site was established on an independent, local datum referenced to an arbitrary elevation for the benchmark. At least two additional control points were established at each site for use as backsites to spatially orient the survey. Multiple points were established to ensure survey repeatability in case of point loss from deterioration, vandalism, sand burial, or rock fall.

Beginning in 2001, each local datum was referenced to positions published within the National Spatial Reference System (NSRS) with multiple static GPS vectors (Doyle, 1994). The inclusion of all control points in a high-accuracy geodetic-control network provided a common datum for all sites, critical

for quantitative accuracy assessments (The Federal Geographic Data Committee [FGDC], 1988). Adjusted geodetic positions were projected to 1983 Arizona State Plane central zone grid coordinates (Federal Information Processing Series [FIPS] zone 0202). Using the revised coordinate values, all data collected prior to 2001 were transformed to the 2007 realization (NSRS 2007) of the North American Datum of 1983 (NAD 83). Since 2007, all data have been collected in that datum. Horizontal positions and all triangulated irregular networks (TINs) and DEMs were projected onto the State Plane grid using the coordinates listed in table 2.1. Horizontal distortion of projected planimetric area is less than 0.05 percent at all sites.

Elevations were referenced to the NAD 83 mathematically derived ellipsoid from the Geodetic Reference System of 1980 (GRS 80) rather than the North American Vertical Datum of 1988 (NAVD 88). NAVD 88 uses the equipotential surface defined by a geoid model as its vertical origin (Milbert and Smith, 1996); however, with this vertical datum, orthometric heights (elevation above an equipotential surface that best represents sea level) change upon each revision of the geoid model because of refinements in modeling gravity anomalies (Saleh and others, 2003). Ellipsoid heights are not affected by improvements in geoid models and their use reduces the chance for vertical biases when merging datasets, thus providing a more consistent vertical datum for long-term sandbar monitoring.

Surveys and Instruments

Field work at each site was conducted with one to three ground-based TS survey crews and a bathymetry crew. The surveys were conducted with Lietz Set3c and Set4c, and Topcon GTS–313, GPT–2003, GTS233, and GTS243 total stations, all capable of 3 arc-second angle accuracy with automatic level compensators and 20× optical magnification. Ground surveys utilized 7.6-m Crain LR STD-series fiberglass collapsible levelling rods mounted with tilting, Sokkia reflective prisms. Radios were used to communicate between the instrument operator and rodmen to coordinate survey efforts (Hazel and others, 2008). After setup verification (appendix 4), data acquisition involved collecting ground points using a feature-based methodology. Points were initially surveyed along important changes or breaks of slope (referred to as breaklines), such as the top and bottom edges of bars and banks, water surface, and linear depressions (fig. 14*A*). The adjacent areas were infilled with points using transects spaced 2 to 3 m apart, extending from the back of the sandbar, at or near the interface with talus or bedrock, to 1.8 m or less below the water surface (fig. 14*B*). Points were collected on submerged areas to overlap with bathymetric data collection. The point collection goal on river trips without bathymetry was to reach the stage elevation of 227 m^3/s, the lowest discharge typical of normal hydropower plant operations that can be reached while wading. This important stage elevation separates the analysis of sandbar area and volume by elevation zone because sand below 227 m^3/s is almost always subaqueous, whereas the elevation zone above the maximum daily discharge of 708 m^3/s is only inundated by HFEs. Heavily vegetated areas above the elevation reached by a discharge of 708 m^3/s were not surveyed when field observations indicated the surfaces were stable. Surfaces were assumed stable only when they were not inundated between surveys, not affected by cutbank or gully erosion, and if the ground surface was covered by organic litter or soil crust. Data from earlier surveys were used to construct the topographic surfaces for these areas such that the site boundaries were constant. This practice was used primarily at study sites 051L, 055R, and 194L and occasionally at 065R, 093L, 119R and 202R to minimize trampling of sensitive soils and because the canopy height of woody riparian vegetation makes TS surveying difficult and time intensive. Comprehensive surveys were conducted at all sites in the early 1990s when vegetation was sparse and line-of-sight was not obstructed, and before and after the 1996, 2004, and 2008 HFEs.

When bathymetric data were collected, the surveyed area included the entire bed of the eddy in the channel expansion,

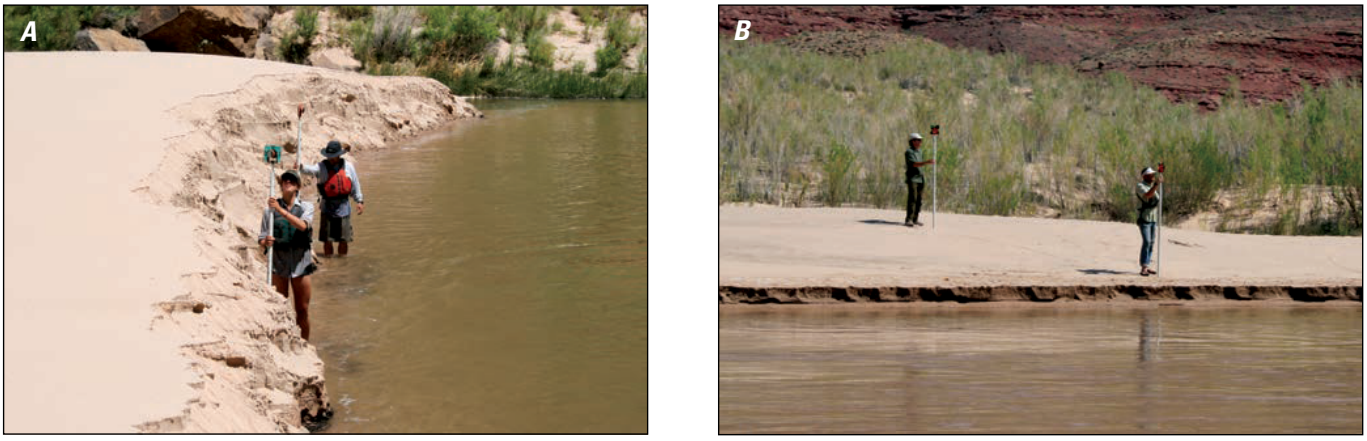

Figure 14. Photographs of feature-based topographic surveying in the Colorado River corridor in Grand Canyon. *A*, Two rodmen surveying a breakline (an important change or break of slope) at the base of a steep eroding cutbank following the 2008 high-flow experiment release from the Glen Canyon Dam. Photograph near river mile (RM) 206.7 by M. Kaplinski, Northern Arizona University, June 1, 2008. *B*, Infilling of adjacent areas between breaklines with transects spaced 2 to 3 meters apart. Photograph near RM 68 by J. Hazel, Northern Arizona University, April 5, 2008.

and the bed of the adjacent channel where the direction of flow is downstream. Where downstream eddy extent or pool length is not limited by an obvious hydraulic control (that is, a debris fan, gravel bar, or curving channel bank), the bathymetry coverage was terminated at approximately one to two channel widths downstream of the eddy.

The 1990–1991 surveys used a Lowrance X–16 echosounder mounted on a raft (table 5). On-shore personnel positioned over surveyed reference points visually guided a boat equipped with a cable-reel system to collect sonar profiles along 5-m transects. Distances along the cable were marked on the analog sonar recording. Subtracting the sonar depths from the surveyed water surface elevation determined the bottom elevations. The extent of areal coverage generated from this technique was limited to the region directly in front of the sandbar and to the 45 m length of the metered cable. The data had a high degree of horizontal positioning error (because the raft was subject to drift with increasing distance from shore). The October 1992 survey trip employed the same echosounder to expand coverage to include the entire eddy and adjacent channel area. Positioning was determined by targeting a reflective prism directly above the transducer with a TS. This method of data collection, though improved over the cable-reel system, was also subject to considerable uncertainty because of the difficulty in precisely coordinating measurements of boat position and depth.

In April 1993, Glen Canyon Environmental Studies developed a more sophisticated SBES with positions provided by a manually tracked range-azimuth navigation system (fig. 15*A*). Initially, the system used a 200 kilohertz (kHz) Innerspace model 448 echosounder with a 3-degree beamwidth and a manufacturer-reported depth-measurement specification of ±0.003 m. In 1994, a 3-degree beamwidth, 200 kHz Marimatech SMBB200 echosounder was configured to operate two transducers: one to transmit and the other to capture the return pulse, with a shoal capacity of 0.30 m. In 1996, the Innerspace echosounder was reconfigured with the same dual transducer capability and the Marimatech was then used infrequently as backup. Accurate depth soundings were ensured by lowering a plate at 1-m increments below the transducer with a steel cable and the echosounder calibrated to record the indicated depth. The measured depths were then subtracted from the height of the transducer to derive bottom elevations (Kaplinski and others, 2009). In addition, measured sound velocities were used to correct the basic time-of-travel data and provide a velocity-corrected distance between depth readings and the echosounder. Soundings were collected along preset transect lines oriented both parallel and perpendicular to the shoreline resulting in a 10×10 m grid spacing. The raw positioning information (slope distance, horizontal and vertical angles) were referenced to the benchmark coordinates and transmitted back to the raft by radio modem. The positions were measured using a hand-operated, optical range-azimuth instrument manufactured by Global Hydrographic called the "Super Hydro." This range-azimuth system was problematic and difficult to align vertically, requiring depth values to be adjusted by measured shoreline elevations. The Super Hydro was redesigned by the manufacturer in 1995 to fix alignment issues between the optical laser and theodolite scope, resulting in more reliable and precise positioning of the depth values. This eliminated the need for independent measurements of water surface elevation—a major source of uncertainty in river surveying because of water surface slope or changes in stage elevation (Byrnes and others, 2002). Beginning with the March 2000 surveys, positions and elevations were more precisely tracked with a Spectra Precision Geodimeter ATS–PT robotic TS (fig. 15*B*).

In August 2000, a MBES was deployed using a Teledyne Marine Reson Seabat 8124 transducer head projecting a 120-degree swath, and an array of 80 transducers operating at a frequency of 207 kHz (fig. 15*C*). The manufacturer depth-measurement specification for the Reson 8124 is a depth resolution of ±0.006 m. Heave, pitch, and roll corrections were provided using motion compensation measured with a TSS DMS–10 model sensor (Kaplinski and others, 2009). A KVH Industries, Inc., azimuth digital gyrocompass measured yaw or vessel attitude with a resolution of 0.5 degrees. MBES surveying also followed predetermined transects, but unlike SBES surveying, there are little or no gaps in bed coverage if swath overlap is maintained. The 2004 and 2008 surveys used a higher resolution Reson SeaBat 8125 echosounder. Both SBES and MBES soundings were collected and processed using HYPACK/HYSWEEP hydrographic software (Hypack, Inc., formerly Coastal Oceanographics, Inc.). Once the positioning and depths were edited and potential erroneous data points removed, the SBES data were filtered to include one coordinate value for every 1 to 2 m in horizontal distance. MBES soundings were also reduced to 2-m spacing to match that of SBES and to reduce computational cost. The coordinate values for MBES data were determined by using the median value of the range in elevations within a cell along with the northing and easting of the 2-m grid cell (Kaplinski and others, 2009). Filtered point densities ranged from 0.060/m^2 to 0.20/m^2 for the SBES data, whereas the MBES data reflect the higher point density of ~0.25/m^2 afforded by the more uniform 2×2 m grid.

Data collection also included repeat photography. Initially, site photographs were taken with hand-held cameras from the same general location. Beginning in 1991, a fixed camera system was employed at six sites to monitor sandbar stability (Cluer, 1992). By the mid-1990s, cameras were operating at as many as 43 sites as part of a separate photogrammetry project by Northern Arizona University (Cluer, 1995; Dexter and Cluer, 1999). The system consisted of an inexpensive Pentax IQZ 105 programmable camera installed in a .50 caliber military surplus ammunition can fitted with an acrylic window and attached to large boulders or to bedrock outcrops with silicon adhesive (fig. 16*A*). The boxes were camouflaged and typically located on the opposite side of the river to provide a high-oblique view of the sandbar. Each camera was loaded with 36-exposure color slide or negative film and the intervalometer set for repeat exposures once every 24 hours, ideally during local low river stage to capture maximum exposed sandbar area. Film was recovered and replaced on a monthly to bi-annual basis. Upon completion of the Northern Arizona University photogrammetry project in 1995, cameras at other sandbars were relocated to the study sites described in this report. Beginning in 2004, GCMRC began replacing the analog

Figure 15. Photographs of bathymetric surveying in the study area, Colorado River corridor, Marble and Grand Canyons. *A*, The 1990s Global Hydrographic "Super Hydro" singlebeam system consisting of a manual shore-based station, a boat-mounted transducer, and on-board computer controlling boat position and depth data collection. The survey vessel is a 5.2-meter (m)-long "mini-snout" boat with a 50 horsepower outboard motor. Photographs by M. Gonzales, U.S. Geological Survey. *B*, In 2000, a Geodimeter ATS–PT from Spectra Precision was used to robotically track and provide spatial coordinates for singlebeam echosounders (SBES) data collection. Photographs by J. Hazel, Northern Arizona University. *C*, Multibeam echosounder (MBES) (Teledyne Marine Reson Seabat 8124 sonar with TSS MAHRSS reference system for heave, pitch, roll, and heading) deployed from a 6.7-m full-sized snout boat. Left photograph by M. Kaplinski; right photograph by H. Chezar, U.S. Geological Survey.

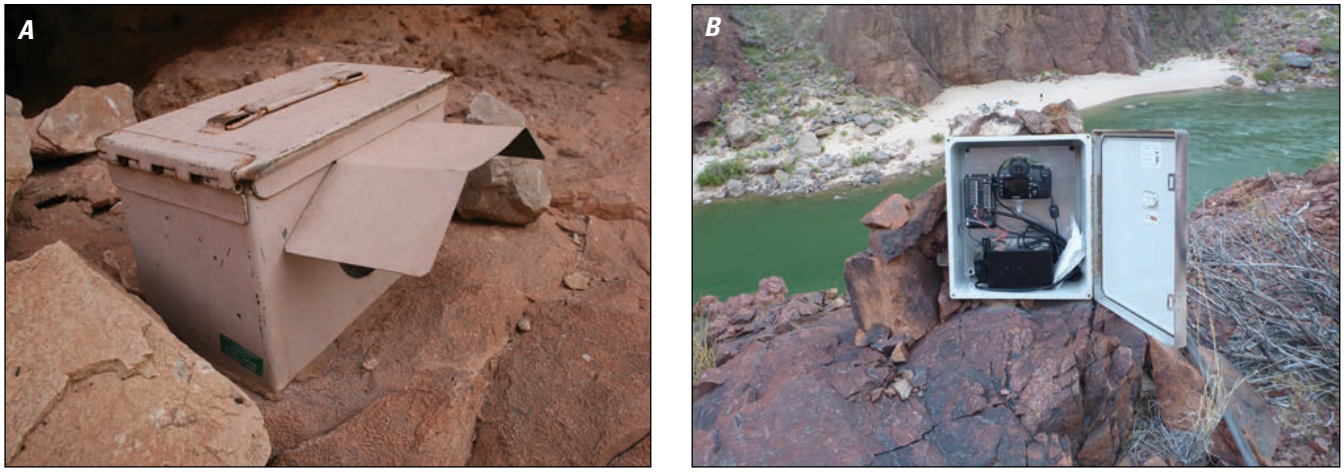

Figure 16. Photographs of one example of the remote camera system in the study area, Colorado River corridor, Marble and Grand Canyons. *A*, A Pentax IQZ 105 programmable camera was installed in a .50 caliber military surplus ammunition can with a plexiglass window. This camera was installed at study site 030R in January 1996 and 46 rolls of film (approximately [~] 1,600 images) were taken before removal in February 2010. Photograph by M. Kaplinski, Northern Arizona University, October 12, 2009. *B*, Beginning in 2004, the U.S Geological Survey's Grand Canyon Monitoring and Research Center (GCMRC) began replacing the analog cameras at the sites with digital cameras. Shown is a digital single-lens reflex (SLR) camera housed in a waterproof box at study site 081L. The system is powered by a solar panel and triggered by a Campbell Scientific CR200 datalogger to take five or more high-resolution images per day. Photograph taken by R. Tusso, U.S. Geological Survey, May 13, 2014. For list of study sites, see table 1.

cameras at the sites with digital cameras (fig. 16*B*). By 2014, all the analog cameras had been replaced, and additional cameras added to the monitoring network, for a total of 41 digital cameras (Tusso and others, 2015; Grams and others, 2018a). Because there are no suitable locations, study sites −006R, 029L, 035L, and 139R do not have cameras. Data from these camera systems are not included herein but are described because the images are used for context and discussion within this report. These sandbar time-series images can also be viewed at https://www.usgs.gov/apps/sandbar.

Digital Elevation Model Processing

Topographic Surface Modeling

Topographic surfaces were modeled using the TS and bathymetric point data to form triangulated irregular networks (TINs). TIN models are based on an irregular array of points to create non-overlapping, contiguous triangle facets with Delaunay triangulation (Peuker and others, 1978). The TINs were generated using software-defined radio (SDR) Mapping and Design software distributed by Sokkia Corporation (Datacom Software Research Limited, 1997). An example of survey point distribution and surface modeling is shown in figure 17. Because the format is vector based, a TIN can incorporate breaklines surveyed during the feature-based data collection by enforcing them as edges in the triangulation (fig. 17*A*). This key step in surface modeling interrupts the interpolation between individual points that do not lie on a continuous grade and a given triangle edge (Maune and others, 2007). Thus, morphological grade breaks and other features are accurately represented in the topographic surface (fig. 17*B*). Data errors and spurious breaklines (for example, crossing or miscoded breaklines) were edited, and additional breaklines added in areas of improper interpolation to ensure accurate model formation. MBES data rarely needed the addition of breaklines, but breaklines were inserted in SBES data where grade breaks were not represented properly in the surface (because the 10 m interval between transects can result in interpolation errors).

After the surveys were post-processed to represent accurate topographic surface models, the resulting TINs were linearly resampled and converted to concurrent grids of uniformly spaced 1-m points. A grid size of 1 m was determined to provide the most accurate surface representation given the input point density and surface complexity of the TINs (see "Digital Elevation Model (DEM) Grid Size" section in appendix 4). The grid of points was interpolated into raster DEMs where the center of each rectangular array of points (also referred to as a cell) reflects an elevation value (fig. 17*C*). For this report, we recomputed the entire data structure (1990–2020) using an automated processing script and database, described below. Computing volumes with DEMs rather than TINs allows faster computation, more consistent output, and is more efficient for analysis tools because of the concurrency of horizontally coincident points. The disadvantage of DEMs is that some terrain information is not captured by the grid surface representation of the original TIN surface (for example, points

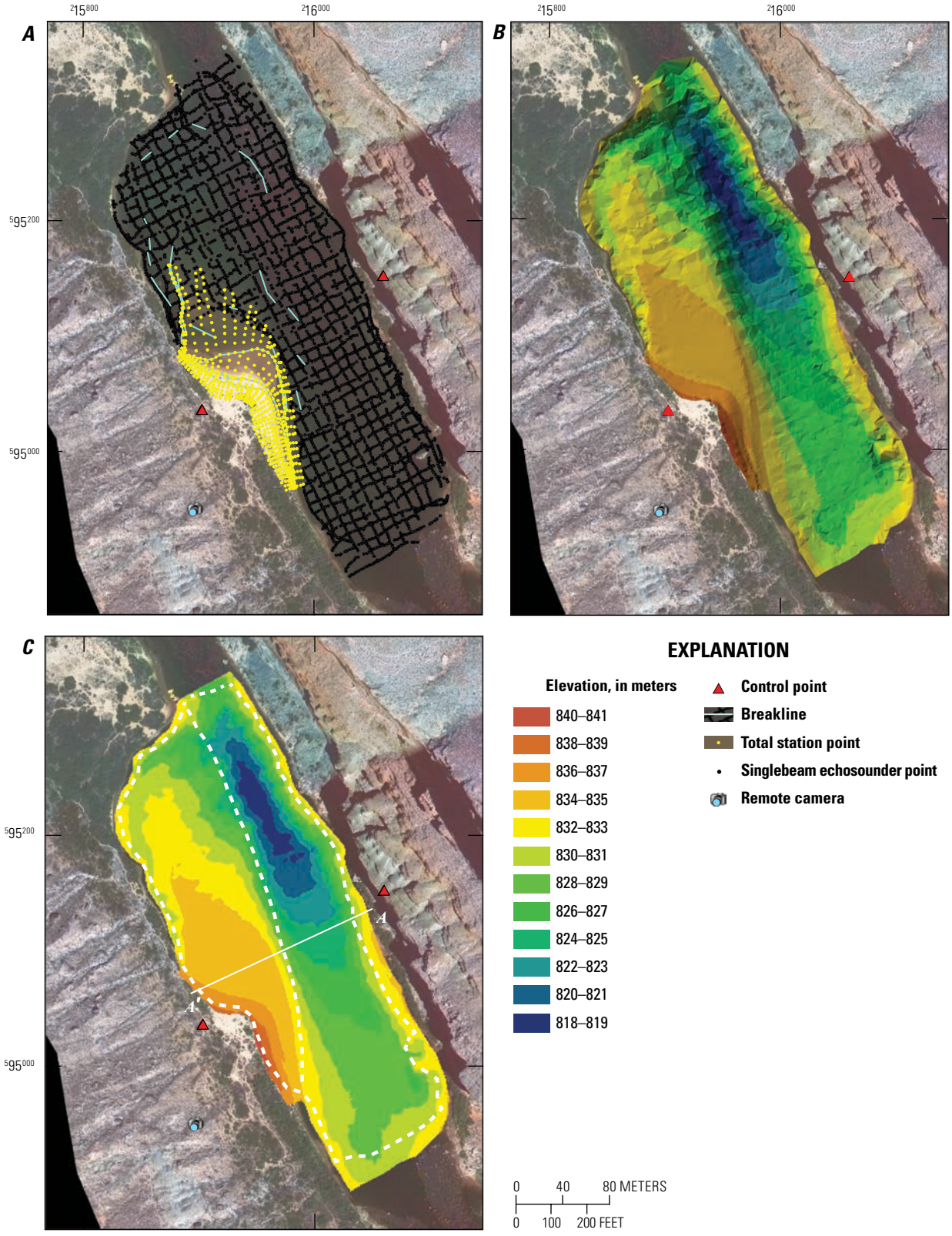

Figure 17. Maps showing an example of a point distribution and topographic surface model, Colorado River, Marble Canyon. *A*, Total station (TS) and singlebeam echosounder points (SBES) collected on the May 9, 1999, survey at study site 047R (see table 1). SBES data were collected along 10×10 meter (m) transects; the data were then filtered to points spaced 2 m apart. Shown are the breaklines (important changes or breaks of slope) used for accurate surface representation and control points used for data collection. *B*, Color-shaded triangulated irregular network (TIN) model created from the combined TS and SBES points in part *A*. *C*, Raster digital elevation model (DEM) derived from a grid size of 1 m points linearly resampled from the TIN. The solid white line is the approximate location of schematic cross section *A*–*A′* shown in figure 21. Dashed white lines show the eddy (left) and channel (right) computational boundaries. May 2009 aerial orthophotograph base from Davis (2013).

along the water surface elevation that define a linear feature). Additionally, creation of a DEM results in an edge condition (with a "stair-stepped" pattern) leading to discontinuous topography and errors in planimetric area, thus making areas enclosed by vector-based polygons (that is, the precisely delineated computational boundaries previously used for TIN volume and area computation by Hazel and others [1999, 2010]) difficult to analyze where there were few raster cells within the polygon (fig. 18*A*). Rather than use an irregular outer boundary along the survey edge in the 1-m DEMs (fig. 18*B*), the surfaces were linearly resampled to a raster grid size of 0.25 m, thus excluding grid cells where the center of the cell was outside the boundary and increasing cell count within the boundary (fig. 18*C*). To verify that area and volume estimates were not biased by conversion to raster DEMs, we compared volumes computed by each method (TIN and 0.25-m DEM) using a common computation area and above a common horizontal reference surface. For the TIN, the computational area was defined by a polygon and for the DEM the computational area was defined by a mask based on that polygon rasterized at 0.25-m resolution. For 30 different surfaces compared at three different study sites, the areas and volumes agreed to within 1 percent.

Automated Sandbar Area and Volume Computation

Sandbar areas and volumes were computed with a custom application that automates the workflow. The primary component of the processing workflow is the Sandbar Workbench (Grams and others, 2020), a desktop application developed in collaboration between GCMRC and North Arrow Research, Ltd., that performs the required analyses on the input data and stores the data in a database. It utilizes a program developed in the Python programming language with graphical frontends and geospatial analysis tools provided by Quantum Geographic Information System and Geospatial Data Abstraction Library open-source software. Once the database is populated with sandbar area and volume computations, the data may be visualized within the workbench or imported into another application for additional analyses. The analyses within the workbench are performed using an SQLite database that is local to each user but is also designed to synchronize to a master MySQL database hosted on a web server. That database is used to run a public website where the sandbar data can be visualized at the USGS Grand Canyon sandbar monitoring website at https://www.usgs.gov/apps/sandbar, and the data are available from the USGS as a data release (Grams and others, 2020).

The workbench requires four inputs in order to extract the area and volume information from a series of individual surveys: (1) comma-delineated text files of gridded points interpolated from the source TINs; (2) vector-based polygons representing the computational extent of the channel and eddy at each site, termed the computational boundary; (3) stage-discharge relations used to partition the computations into elevation zones defined by discharge range; and (4) two reference surfaces used to compute or normalize the area and volume values. The first reference surface, termed the "minimum surface" by Hazel and others (2006b), is used to derive a volume relative to, or above, a constant surface. Ideally, the reference surface would be the interface between sand and the underlying stable gravel or rock substrate. Because information on that contact is not available, for each site we computed a constant surface that represents the lowest observed sand elevations. This composite, synthetic surface was computed as the lowest observed elevation within each 1-m^2 grid cell from among all available surveys at each site (fig. 19). Thus, the "minimum surface" separates sand (or possibly gravel and coarser substrate) that is assumed to have never changed for the 31-year period of monitoring (below the minimum surface) from

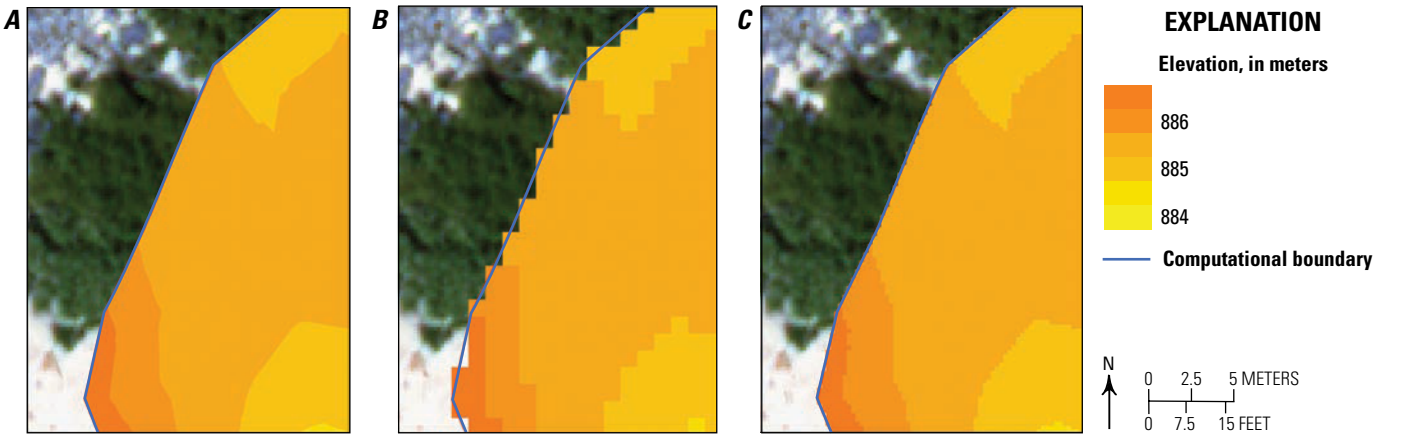

Figure 18. A triangulated irregular network (TIN) model and a digital elevation model (DEM) from a part of study site 022R showing an example of the edge-effect problem when calculating volumes using irregularly shaped polygons (computational boundaries) in the study area, Colorado River corridor in Marble and Grand Canyons. *A*, TIN model based on an irregular array of points. *B*, 1-meter (m) DEM interpolated from the TIN surface in part *A*. *C*, 0.25-m DEM. Note the smooth computational boundary in *A* and the edge-effect problem represented by the stair-stepped appearance in *B*. Because the grid cells do not lie exactly on the polygon boundary, areas outside the polygon are incorporated in the calculations and some areas inside the polygon are missed. The raster grid size of 0.25 m in *C* minimized the edge effect created by an irregular outer boundary by minimizing the number of cells overlapping the computation or polygon boundary to create a more uniform hard clip. Base images from Durning and others (2016).

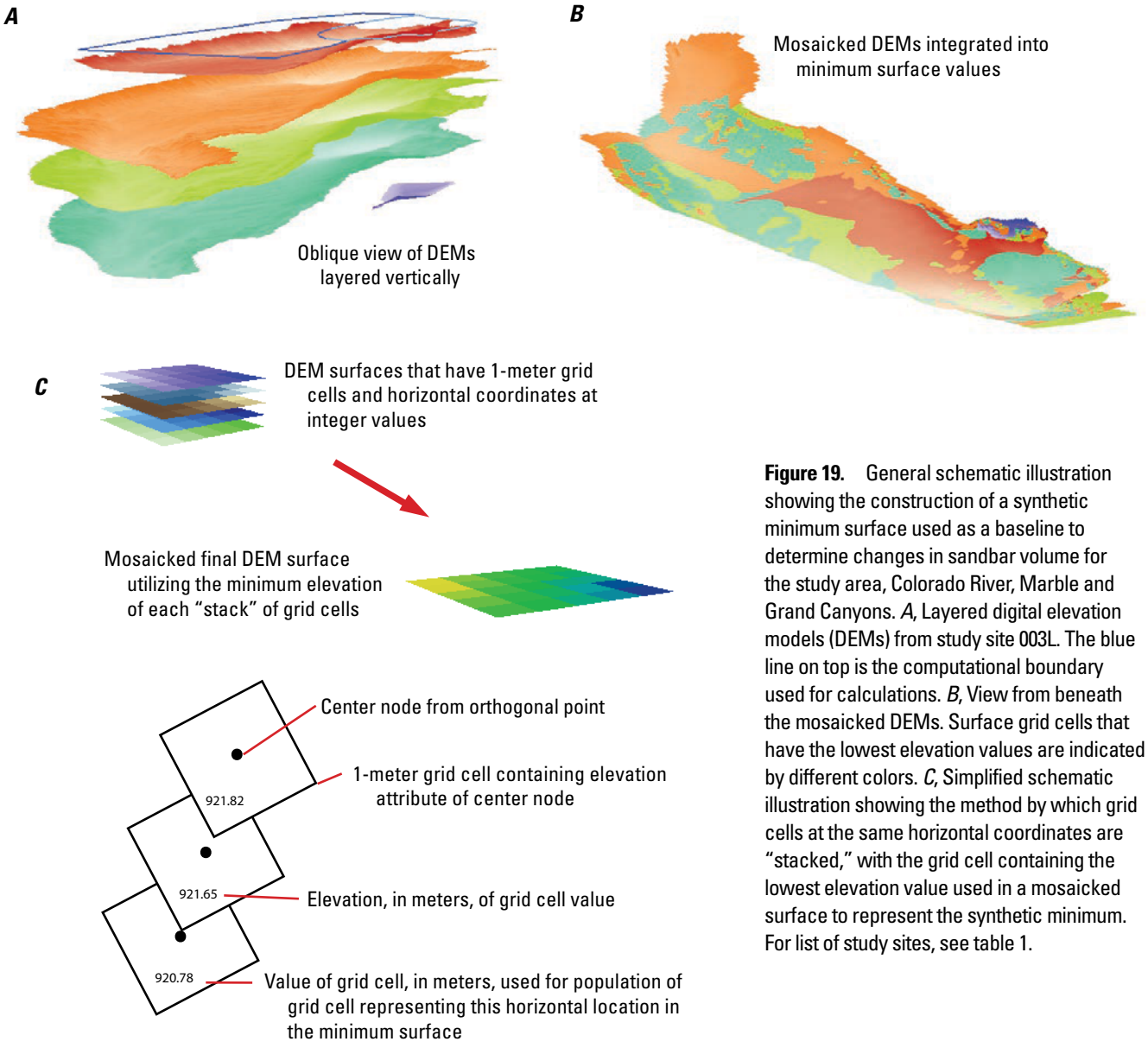

Figure 19. General schematic illustration showing the construction of a synthetic minimum surface used as a baseline to determine changes in sandbar volume for the study area, Colorado River, Marble and Grand Canyons. *A*, Layered digital elevation models (DEMs) from study site 003L. The blue line on top is the computational boundary used for calculations. *B*, View from beneath the mosaicked DEMs. Surface grid cells that have the lowest elevation values are indicated by different colors. *C*, Simplified schematic illustration showing the method by which grid cells at the same horizontal coordinates are "stacked," with the grid cell containing the lowest elevation value used in a mosaicked surface to represent the synthetic minimum. For list of study sites, see table 1.

sand that has been active during the monitoring period (fig. 20*A*). The second reference surface, termed the "maximum surface," was used to normalize the volume values. The maximum surface represents the maximum elevation measured and conceptually can be considered as the maximum depositional potential at a given site. Similar to the minimum surface, the maximum surface was derived by selecting the highest observed elevation within each 1-m^2 grid cell at each site (fig. 20*B*). The data reported herein and available from Grams and others (2020) are computed using the minimum and maximum reference surfaces derived from all surveys collected from 1990 through 2020.

Sandbar area and volume were computed separately for different elevation zones because deposition and erosion magnitudes vary at different elevations, and because the elevation of changes in sand storage affect the utility of the sandbar for camping. Furthermore, those elevation zones are defined by discharge range rather than fixed elevations because of the steep river gradient and large differences in stage-discharge relation between sites. We defined three elevation zones (fig. 21): (1) the low elevation zone represents the volume of sand between the minimum surface and the elevation reached by a 227 m^3/s flow; (2) the fluctuating zone is the region between 227 and 708 m^3/s (and also above the minimum surface); and (3) the controlled flood zone is the region above 708 m^3/s that is only inundated during HFEs. The latter two bins are collectively termed the high-elevation zone (that is, the region above the 227 m^3/s water-surface elevation). The sum of all three zones is referred to as the total site sandbar volume. Embedded within the workbench are

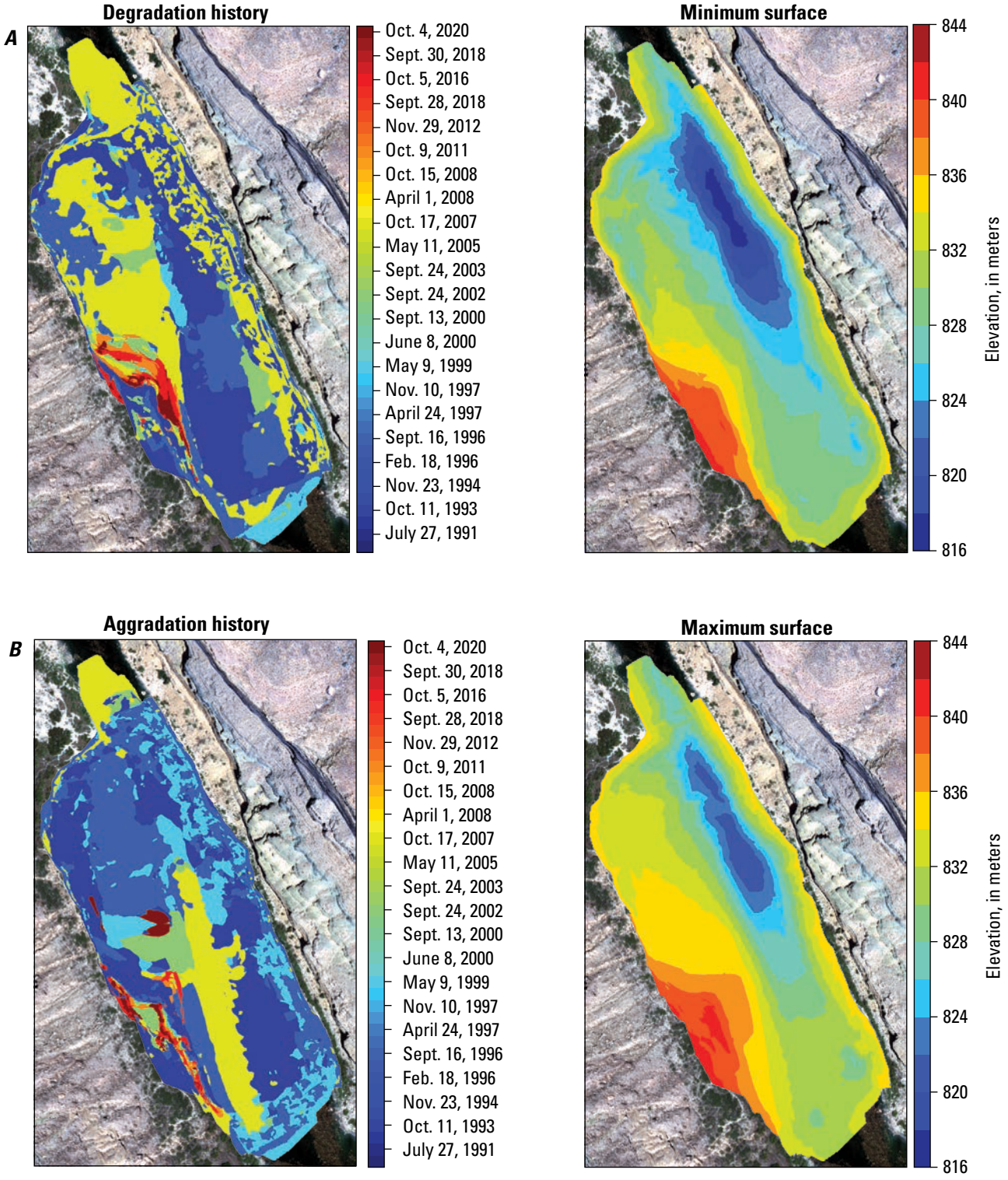

Figure 20. Maps from study site 047R showing sandbar and riverbed models in the study area, Colorado River, Marble and Grand Canyons. *A*, Degradation map and related minimum surface digital elevation model (DEM). *B*, Aggradation map and related maximum surface DEM. The surface grid cells with the lowest or highest elevation values derived from the stacked or mosaicked DEMs are independently used to generate both products. The aggradation and degradation surfaces indicate which surveys contribute spatially to the lowest or highest elevation values that constitute the minimum and maximum surfaces, respectively. Base images from Durning and others (2016).

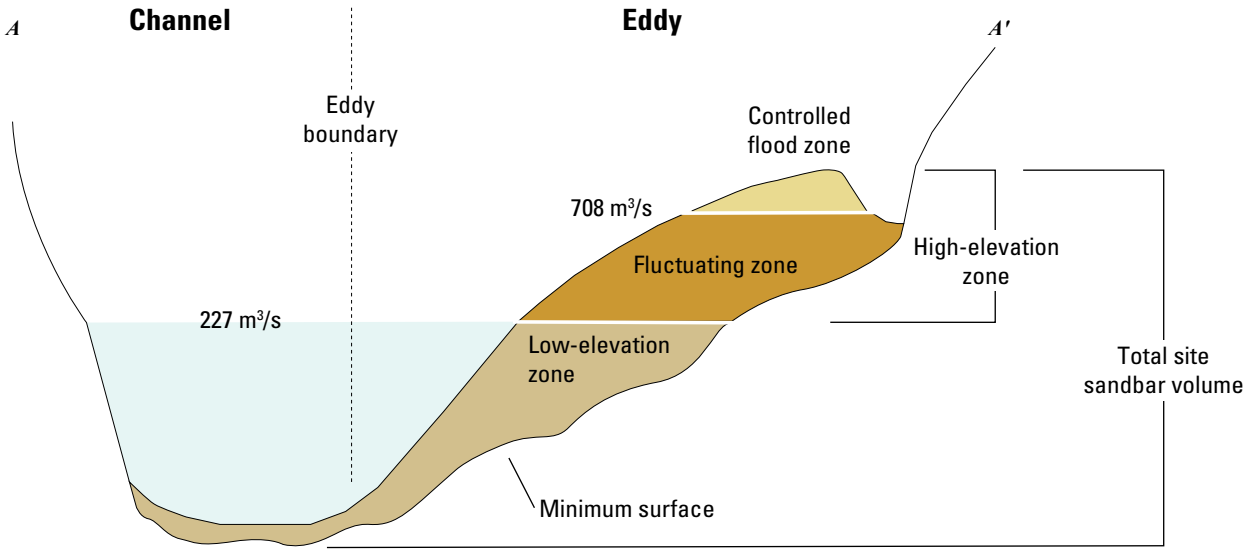

Figure 21. Schematic cross section of the eddy sandbar and channel. Three elevation zones are depicted within which deposit volume and area is calculated above the synthetic minimum surface. The low elevation zone represents the volume of sand between the minimum surface and the elevation reached by a 227 cubic meter per second (m^3/s) flow; The fluctuating zone is the region between 227 m^3/s and 708 m^3/s (and above the minimum surface); and the controlled flood zone is the region above 708 m^3/s that is only inundated during high-flow experiments (HFEs). The latter two bins are collectively termed the high-elevation zone (that is, the region above the 227 m^3/s water-surface elevation). The sum of all three zones is referred to as the total site sandbar volume. The zones are separated by two reference planes that correspond to the elevation reached by flows of 227 and 708 m^3/s, respectively. The schematic is derived from the cross section location *A*–*A′* shown in figure 17*C*. The cross section is viewed in a downstream direction. The inner dividing line between the eddy and main channel (eddy boundary) in the computational boundary is indicated by the dashed black line. The minimum surface is based on the lowest measured elevations of the bed and represents either bedrock or what we consider to be "non-erodible," stable sediment for the purposes of modelling.

lookup tables that contain stage-discharge relations developed by Hazel and others (2006a) and subsequently revised for this report (appendix 3). The stage-discharge relations are used to determine the elevations for discharges of 227 and 708 m^3/s at each site. The discharge of 227 m^3/s is a low discharge typical of normal Glen Canyon Dam operations that can be considered as "baseflow" (see "Flow Regimes and Tributary Sediment Supply" section) and, as shown by Wright and Kaplinski (2011), is a convenient and reasonable dividing line for evaluating sand volume transfer between low and high elevations. Below the 227 m^3/s elevation, sand is almost always subaqueous, whereas sand above this elevation is either within the fluctuating zone of dam releases or always subaerial. Furthermore, aerial photography is timed to be taken when there is a constant discharge of approximately 227 m^3/s, which aids in comparisons of sandbar area measured from remote sensing to those made in this study. Discharge is rarely greater than 708 m^3/s, and sand exposed above this elevation is the part of the sandbar most commonly used for camping.

In this report we restrict our analysis to data from the high-elevation zone. Measurements of the low-elevation zone have not been made since 2008, and those results were reported by Hazel and others (2010). We include measurements of planimetric sandbar area but focus on sandbar volume as the primary metric for evaluating changes in sandbar size. For calculations of area and volume, elevation zone boundaries at each site were represented by horizontal planes assigned with the elevation for discharges of 227 and 708 m^3/s, respectively. The area of a particular elevation zone was calculated by summing the 1-m grid cells that fall between the lines formed at the intersection of the topographic surface and the horizontal plane representing the elevation zone and the computational boundary:

$$A_{zone,t} = A_{within\_lower,t} - A_{within\_upper,t}, \quad (1)$$

where

t is a particular survey time,

$A_{zone,t}$ is the area within a specified elevation zone,

$A_{within\_upper,t}$ is the area of the survey within the upper elevation zone, and

$A_{within\_lower,t}$ is the area of the survey within the lower elevation zone.

The volume of sand for a specified elevation zone was calculated by subtracting the total volume of sand that is above the upper elevation zone plane from the total volume of sand that is above the lower elevation zone plane:

$$V_{zone,t} = V_{above\_lower,t} - V_{above\_upper,t} \quad (2)$$

where

$V_{zone,t}$ is a specified elevation zone,
$V_{above\_lower,t}$ is the lower elevation zone plane, and
$V_{above\_upper,t}$ is the upper elevation zone plane.

In the case of the controlled flood zone, $V_{above\_upper,t}$ is zero because the entire volume of sand above the elevation reached by 708 m^3/s is computed. The "corrected" volume of sand within each elevation zone relative to the minimum surface was then derived by subtracting the volume from the survey at time *t* from the volume from the minimum surface ($V_{min,zone}$) such that

$$V_{zone,t,corrected} = V_{zone,t} - V_{min,zone}, \quad (3)$$

Area calculations were not corrected relative to the minimum surface and are presented as described above.

Temporal patterns of volume change were evaluated by constructing time series using the results from two calculations. The first is a simple summation of sandbar area across all sites. The results from equation 3 are used in summation of corrected sandbar volume. This calculation requires that the sample size remain constant (which limits the analysis to the original long-term study sites) and is biased by dynamic sites with large temporal variations. However, in the case of volume it is a metric with well-constrained measurement uncertainty. The second is a normalization that was calculated by dividing the volume derived from equation 3 by the potential volume computed from the maximum surface ($V_{zone,max}$). The corrected volumes computed using equation 3 were normalized as follows:

$$V_{zone,norm,t} = \frac{V_{zone,t,corrected}}{V_{zone,max}}. \quad (4)$$

Sandbar planimetric area was also normalized by dividing the result of equation 1 by the maximum measured area in each zone:

$$A_{zone,norm,t} = \frac{A_{zone,t}}{A_{zone,max}}, \quad (5)$$

Normalization allows direct comparison of sites of differing size and complexity, and recognition of patterns of sandbar change that might be overwhelmed by small- or large-scale variability. In the case of volume, where the minimum surface does not contain elevations within a given elevation increment, the second term of equation 3 was set to zero. The normalized area and volume metrics do not generally approach the theoretical value of 1.0—a result that would only occur if deposition within every 1-m^2 grid cell was greater than that ever measured during the study period. This approach was used to examine temporal trends for high-elevation sand volume, but we also distinguished differences in response for the fluctuating zone and the controlled flood zone as well as between bar types.

To normalize for variability in the areal extent of sandbars, we converted changes in volume to changes in net thickness (*T*) at time *t* by dividing the change between specific surveys by the maximum measured area in each zone:

$$T_{zone,t} = \frac{V_{zone,t,corrected}}{A_{zone,max}}. \quad (6)$$

Errors (that is, sources of uncertainty) could be introduced into these calculations through the data used to construct the DEMs that are subject to measurement (random) and interpolation (systematic) error. Analyses of topographic surface quality and associated volume computations are described in appendix 4. The elevation uncertainty was determined to be ±0.05 m (table 4.7 of appendix 4). Because measurement errors were not biased in any one direction, we calculate the volume change at individual sites assuming no error when the individual metrics are normalized and then averaged as in equation 4. We also assume no error in area computations because the uncertainties are considerably smaller than those of volume computations. Uncertainty associated with time-series analyses using normalized volumes in equation 4 are represented by standard error. However, we report volumetric uncertainty when summing sandbar volume using equation 3. Because the minimum and maximum surfaces are held as fixed reference surfaces in equations 3 and 4, we consider these surfaces to have no error. Though accounting for measurement uncertainty is clearly important in general for determining differences between DEMs, for our study the magnitudes of the topographic changes were substantially greater than the measurement uncertainty.

Analytical Methods

Sandbar Site Type

Variation of sandbar response by geomorphic setting has been recognized since the classification scheme of Schmidt and Graf (1990) was first proposed. Based on this classification (referred to as deposit type in this report), the 45 monitoring sites include 25 reattachment bars, 12 separation bars, 10 undifferentiated eddy bars, and 6 upper pool deposits (table 1). Each monitoring site contains at least one sandbar, and some include more than one deposit type. A complementary approach is used here whereby the deposit types at individual sites were identified based on a consideration of the geomorphic setting as well as reach-scale metrics, using the principal component analysis (PCA) of Mueller and others (2018). In this approach, basic morphologic and hydraulic metrics such as channel width, stage-change with discharge, water surface slope, and vegetated area were assessed for each site to determine which were most similar (fig. 22; table 1.2 of appendix 1). Referred to as site type, this results in further subdivision that generally corresponds with the sandbar deposit types of Schmidt and Graf (1990) (fig. 23; table 1). Reattachment bars are subdivided into narrow, medium, and wide categories, reflecting increasing vegetation encroachment and channel width, and decreasing stage change

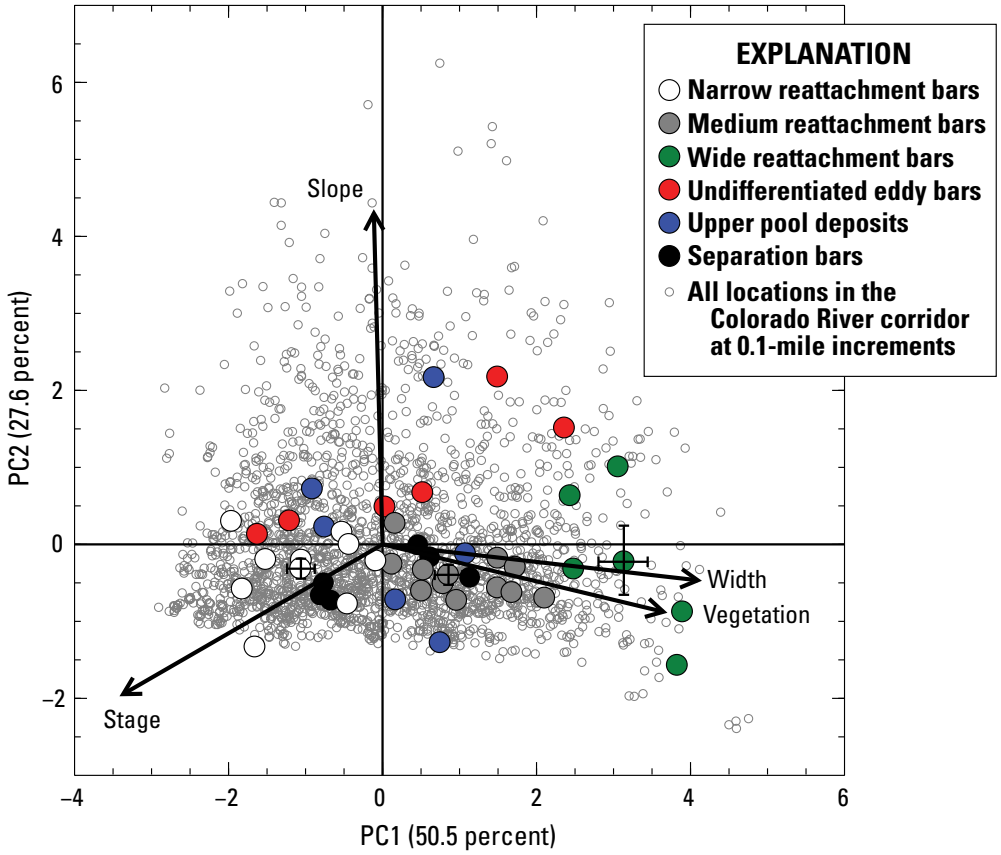

Figure 22. Plot of principal component analysis space (PCA) showing the long-term study sites (large solid circles) relative to all locations in the Colorado River corridor in Marble and Grand Canyons using the same sandbar response metrics at 0.1-mile increments (small open gray circles). The six different sandbar site types (fig. 23) are shown as different colors. Cross pattern shows the average PCA values for narrow, medium, and wide reattachment bar groups, respectively, with error bars showing standard error. Note that the individual hollow circles in the river corridor represents a continuous field of sites from the study area. Thus, the PCA is generalized for sites located elsewhere in the system and some locations are not captured in this analysis. However, the principal component (PC) attributes do explain differences in sandbar responses that agree with the geomorphic setting of individual sandbars in this study. From Mueller and others (2018); data from Mueller and others (2017). PC1, first principal component; PC2, second principal component

with discharge (increasing first principal component [PC1]). These are the group 1a, 1b, and 1c sites of Mueller and others (2018), respectively. Undifferentiated eddy bars are sites with reach-average channel gradient greater than approximately 0.002 (increasing second principal component [PC2]) and are narrow deposits formed just downstream from a debris fan with characteristics of both separation and reattachment bars (these are the group 2 sites of Mueller and others, 2018). Upper pool deposits (group 3 sites of Mueller and others, 2018) are in eddies upstream from debris fans. Separation bar deposits (group 4 sites of Mueller and others, 2018) are sites where the survey is of the separation bar and the reattachment bar, if present, is typically submerged (Mueller and others, 2018). The PCA analysis best discriminates the behavior of reattachment bars located at well-defined debris-fan eddy complexes. Upper pool deposits and separation deposits are not well discriminated by the PCA because the reach-scale geomorphic metrics are not well correlated with their hydraulic setting.

The reevaluation of sandbar deposits using the PCA analyses results in some differences from previous studies that are described below. Eight sites include both a separation and a reattachment bar. At study sites 041R, 044L, 045L, 050R, 065R, and 084R the PCA discriminates the sites as reattachment bars, thus the sum of the separation bar area or volume was included in the analysis of the site as a reattachment bar (table 1). At study sites 035L and 202R, the PCA discriminates the sites as separation bars, and low elevation reattachment bars (when measurable) were included in the analysis of the site as a separation bar. Two study sites, 033L and 062R, were previously classified by Hazel and others (2010) as reattachment bars. The PCA discriminates site type at these locations as separation bars and we kept that designation in the final analysis of the sites. Similarly, study site 167L was previously considered a separation bar by Schmidt and Graf (1990); however, the PCA places it as an undifferentiated eddy bar, and we kept that designation in the final analysis of sites. Other notable differences in sandbar classification from previous studies occur at study sites 068R and 070R. These sandbars were designated as undifferentiated eddy bars by Hazel and others (2010); however, these sites have larger PC1 values similar to those of wide reattachment bars (table 1.2 of appendix 1). Therefore, we adopt the reclassification of these sites as wide reattachment bars in this report. The lone exception to adoption of the Mueller and others (2018) site type classification is study site 081L. Based on bar morphology, we kept the undifferentiated eddy site type as described by Hazel and others (2010). Mueller and others (2018) did not include study site −006R (because it is in the tailwater reach of Glen Canyon); thus, they report on 44 sites and the same sample size is used in this report. Mueller and others (2018) considered study site 003L as an outlier because the bar behavior at this site is extremely variable (possibly because it is the closest site to the primary source of sand—the Paria River). However, since the PCA analysis classifies study site 003L as a 1b site we chose to include it in the analysis with other medium-sized reattachment bars. In the results and discussion that follow,

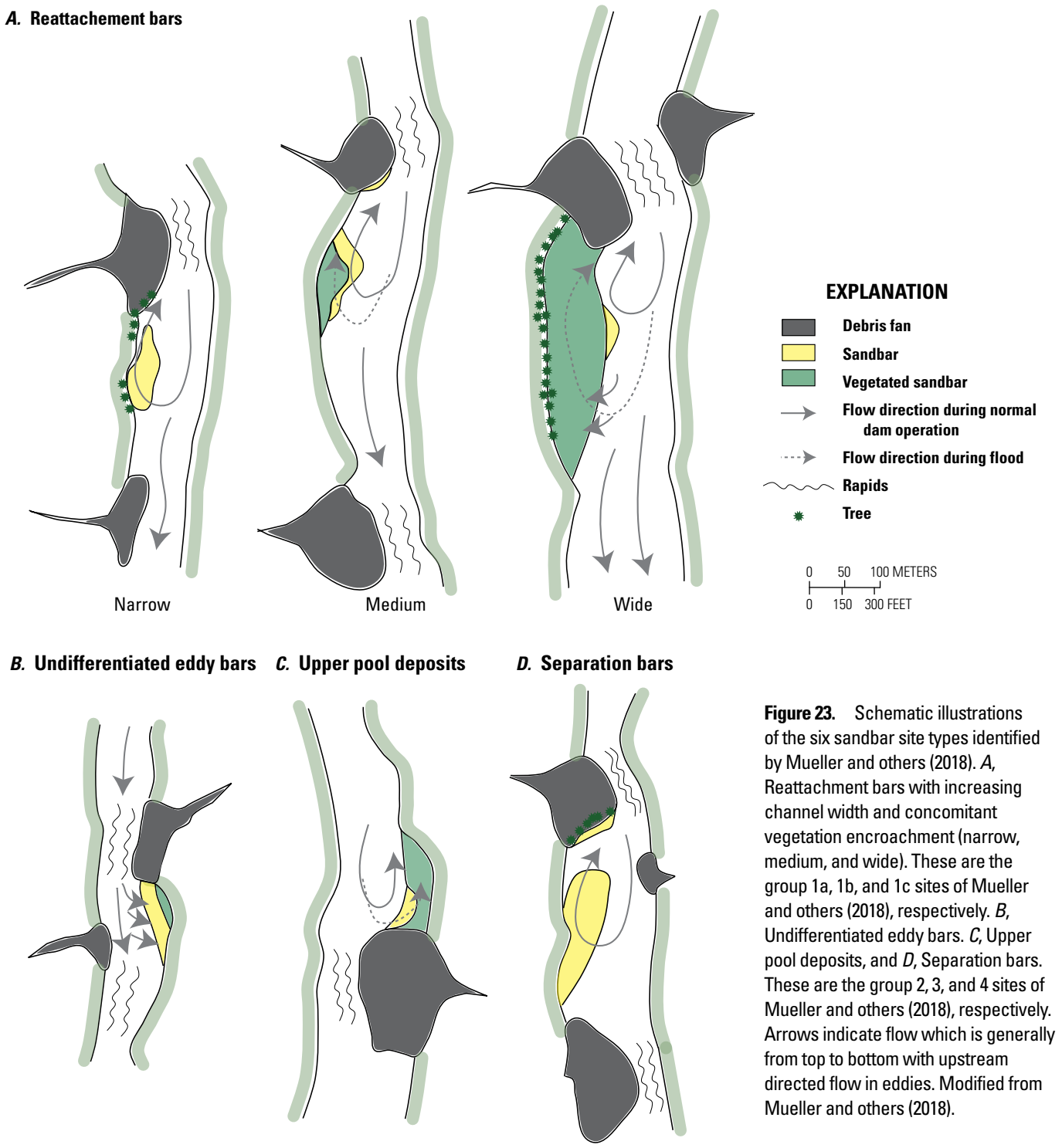

Figure 23. Schematic illustrations of the six sandbar site types identified by Mueller and others (2018). *A*, Reattachment bars with increasing channel width and concomitant vegetation encroachment (narrow, medium, and wide). These are the group 1a, 1b, and 1c sites of Mueller and others (2018), respectively. *B*, Undifferentiated eddy bars. *C*, Upper pool deposits, and *D*, Separation bars. These are the group 2, 3, and 4 sites of Mueller and others (2018), respectively. Arrows indicate flow which is generally from top to bottom with upstream directed flow in eddies. Modified from Mueller and others (2018).

the term sandbar refers to any of the deposit types of Schmidt and Graf (1990), whereas site type is used to describe the further subdivision of deposit types by Mueller and others (2018).

Segment-Scale Differences in Sandbar Behavior

The standard approach for evaluating spatial differences in sandbar response separates the monitoring sites into those occurring in Marble Canyon and those occurring in Grand Canyon (Hazel and others, 1999, 2010; Kaplinski and others, 2014; Mueller and others, 2018). Although the geomorphic characteristics of the sites support the classification into six site types, Mueller and others (2018) reported that bar response was similar among some of these types. Therefore, for several analyses, we grouped the six site types into three aggregated site types. The advantage is a greater sample size with which to examine segment-scale differences in bar response. Mueller and others (2018) showed that narrow and

medium reattachment bars are characterized by less vegetation cover and are subject to greater changes in stage discharge than other groupings because they occur where the channel is narrower (fig. 22). Most of the canyon corridor plots relatively low along the PC1 axis, associated with narrow (<0) and medium (<2) reattachment bars located in narrow parts of the canyon (fig. 24). Accordingly, we combined these two site types into one aggregation. Wide reattachment bars and upper pool deposits have dissimilar PC values but are in eddies upstream and downstream from debris fans, respectively, and are similar in that they are large reattachment bars in low energy hydraulic settings (wide pools) that have become stabilized by vegetation (fig. 23). Thus, these two bar types were combined into one aggregation. Undifferentiated eddy bars and separation bars are not as well correlated by hydraulic setting, but both are characterized by narrow sandbars that mantle debris fans or talus and these types were also combined into one sample size. The separation bar grouping does not contain persistent reattachment bars and the depositional locus is dominated by formation of bars at the point of flow separation. Undifferentiated eddy bars are characterized by having a steeper depositional environment (water surface slope averaged over 1 km) and tend to have a more elongate bar form, similar to separation bars, but without the morphology characteristic of reattachment bars.

The aggregated sandbar types in both Marble and Grand Canyons were evaluated for long-term trends in high-elevation volume computed from equation 3 using linear least-squares regressions. These regressions were used to analyze both shorter time periods corresponding to the 1990–2003 sand-depleted and 2004–2020 sand-enriched analysis periods, respectively, and for the entire 1990–2020 monitoring record. We tested the significance of the slope of the relations using a Student's t-test with a significance level of p=0.05 (Davis, 2002). The regressions were made only with data from surveys conducted at least 1 year following a depositional event, or any high-flow period with flows greater than those reached by normal dam operations (for example, the sustained high flows in 1997–1999, the 2011 equalization flows, and HFEs). We refer to this average volume as the "baseline sandbar volume;" thus, the temporal trends determined from the regressions reflect sandbar stability after a sustained period of bar adjustment and are a better indication of sandbar trajectory.

Sandbar Sample Size

We examined the effects of sample size on long-term trends in sandbar volume because the number of study sites increased during the monitoring period, and because not all sites were surveyed every year. As described above, when the study was implemented in 1990, the chosen study sites constituted about 5 percent of the total population of large eddy sandbars system-wide (see "Study Site Selection and Distribution" section). By 2008, the monitoring network had increased to about 9 and 7 percent of the sandbar population in Marble and Grand Canyons, respectively (table 2). This presents two major problems with sample size. The first issue is caused by progressively adding study sites and increasing the sample size. The larger sample size reduces the uncertainty in the estimate of average sandbar response; however, comparisons among unequal sample sizes may introduce bias. We evaluated the effect of changing sample size (n) by comparing two sample sizes in Marble Canyon using the trends in average normalized volume of the original reference series (n=10) to the final set of study sites for the

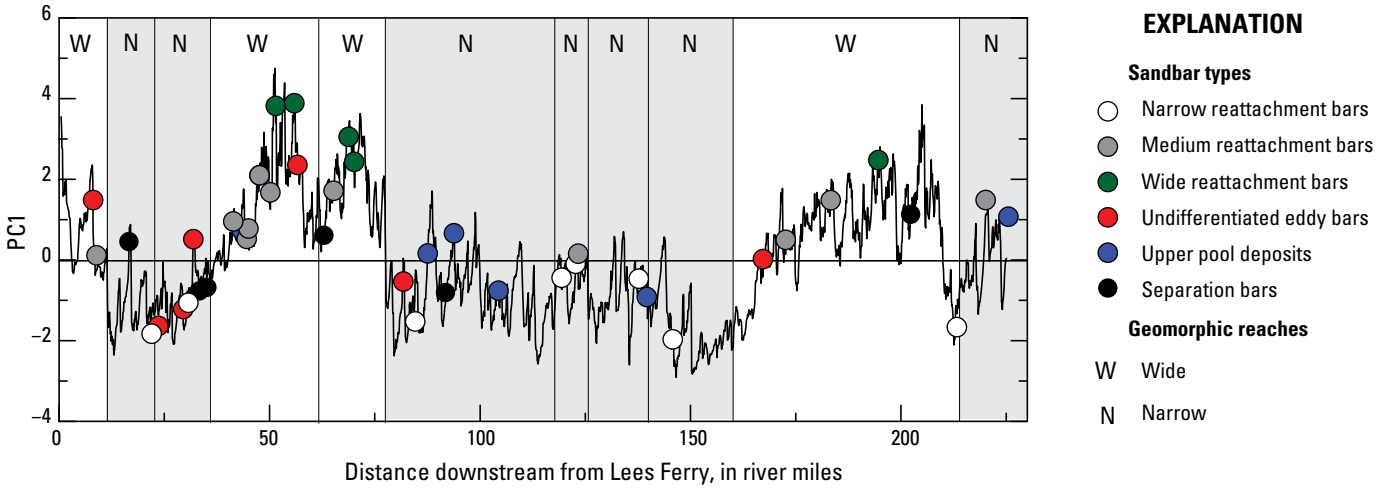

Figure 24. Graph of longitudinal trends in principal component 1 (PC1) space, Colorado River corridor, Marble and Grand Canyons. Colored dots represent the six sandbar types used in this report (from Mueller and others, 2018). Shown are the locations of the wide (W, no shading) and narrow (N, shaded gray) geomorphic reaches of Schmidt and Graf (1990). Note that the reaches generally coincide with the changes in PC1 space and that most of the canyon corridor plots relatively low in PC1 space, indicating the sandbar population is dominated by narrow and medium reattachment bars in narrow reaches of the canyon. Modified from Mueller and others (2018). River miles (RM) show the distance in miles, using the centerline of the Colorado River, downstream from Lees Ferry (RM 0), Arizona.

sand-enriched period (n=18). For each data point shown on the time series, the distributions used to calculate the normalized average volume were tested using a two-sided Student's t-test with p=0.05.

The second issue we address is undersampling. Whether we consider the reference series, or the full set of 44 sites, these sites still comprise less than 10 percent of sandbars in the study area. We evaluated the effect of undersampling by analyzing several datasets that included measurements of a much larger sample of sandbars in Marble Canyon and eastern Grand Canyon (table 6). The longer study reaches were examined as part of a reach-scale comprehensive mapping project designed to measure gross changes in sand storage (Kaplinski and others, 2017; Grams and others, 2018b). The first dataset we used was based on measurements of all sandbars made in as many as six study reaches in Marble Canyon that were 2.7 to 4.8 km in length and included 45 to 75 sandbars above the 227 m^3/s stage (table 7). Measurements were made in each of these reaches in May 2002, June 2004, November 2004, and December 2004. The second dataset included topographic measurements made at 84 sandbars throughout lower Marble Canyon and the lower part of Redwall Gorge geomorphic reach (RM 29.4 to 61.5) in 2009 and 2012, and 46 sandbars in eastern Grand Canyon (RM 61.6 to 88.3) in 2011 and 2014. We compared mean sandbar elevations rather than volume changes because the comprehensive mapping boundaries do not completely overlap with the computational boundaries used for the annual sandbar monitoring. Differences between the mean changes in sandbar elevation result only from inclusion of a different set of sandbars and not the use of different data or measurement methods. We further evaluated the number of sampling sites that would be required to estimate the mean change in sandbar elevation with a bootstrap analysis. In this analysis, we randomly selected from 1 to 83 of the 84 sandbars measured in lower Marble Canyon in 2009 and 2012. In 100 iterations for each sample size (1 to 83), we computed the mean change in sandbar elevation and the standard error of the mean. The same analysis was carried out on the 46 sandbars measured in eastern Grand Canyon in 2011 and 2014 (table 7).

Table 6. List of reaches in the Colorado River corridor, lower Marble Canyon and eastern Grand Canyon, where topographic measurements were collected at sandbars.

[RM, river mile; km, kilometer]

Reach	Extent (RM)[1]	Length (km)
Lower Marble Canyon	29.4–61.5[2]	51.7
Eastern Grand Canyon	61.6–88.3[3]	43.0
R2	1.1–2.8	2.7
R3	21.9–23.6	2.7
R4	29.4–32.0	4.2
R5	42.5–45.4	4.7
R6	54.4–56.1	2.7
R7	63.4–66.4	4.8

[1]Approximate location based on the river mile centerline downstream from Lees Ferry (RM 0), Arizona.

[2]In this case, lower Marble Canyon refers to the channel mapping reach of Kaplinski and others (2017) and Grams and others (2018b), including the lower part of the Redwall Gorge geomorphic reach (see table 3).

[3]In this case, eastern Grand Canyon refers to the channel mapping reach of Kaplinski and others (2017) and Grams and others (2018b), including the Furnace Flats and the upper part of the upper Granite Gorge geomorphic reaches (see table 3).

Table 7. List of comparisons in sand elevation between monitoring sites and all bars mapped in the encompassing reach, Colorado River corridor, lower Marble Canyon (LMC) and eastern Grand Canyon (EGC).

[km, kilometer; m, meters]

Comparison Interval	Reaches Mapped[1]	Mapped length (km)	Number of bars compared	Number of monitoring sites	Elevation change at monitoring sites (m)	Elevation change at all sites in reach (m)
Aug. 2000–Sept. 2000	R2, R4, R5, R7	16.4	45	14	0.13	0.16
Sept. 2000–May 2002	R2, R4, R5, R7	16.4	46	15	−0.09	−0.10
May 2002–May 2004	R2, R3, R4, R5, R7	19.1	64	20	−0.17	−0.27
May 2004–Nov. 2004	R2, R3, R4, R5, R6, R7	21.8	72	20	0.10	0.18
Nov. 2004–Dec. 2004	R2, R3, R4, R5, R6, R7	21.8	75	22	0.35	0.33
May 2002–Nov. 2004	R2, R3, R4, R5, R6, R7	21.8	75	22	−0.09	−0.10
May 2009–May 2012	LMC (includes R4, R5, and R6)	51.7	84	18	−0.10	−0.06
Apr. 2011–May 2014	EGC (includes R7)	43.0	46	6	0.14	0.02

[1]R, reaches (from table 6).

Results

Trends in Sandbar Volume

Overview of Changes, 1990–2020

Despite large annual and site-to-site variability in sandbar volume, several consistent patterns of erosion and deposition occurred during the study period. Erosion was most common during the sand-depleted period (1990–2003), and the high-elevation volume was the lowest measured at more than half of the study sites in the early 2000s (fig. 25). Among the narrow and medium reattachment bars, separation bars, and undifferentiated eddy bars, sand volume in the high-elevation zone decreased or did not change between July 1990 and February 1996, increased at nearly all study sites in response to the 1996 HFE, and decreased at nearly every site between April 1996 and October 2003. The sand volume at the end of the sand-depleted period in 2003 was less than that measured at the beginning (in 1990) at 19 of the 31 (61 percent) reference series sandbars (fig. 26*A*). Eleven of the 31 sites had a net decrease in sand thickness of 0.10 m or greater, whereas 8 sites had a net increase in sand thickness of 0.10 m or greater. The magnitude of decrease was very large (>0.20 m decrease in sand thickness) at study sites 003L, 016L, 030R, 047R, 081L, and 139R (fig. 25).

In contrast, increases in sand volume between 1990 and 2003 occurred at wide reattachment bars and upper pool deposits. Gains were primarily due to aggradation by the 1996 HFE. One study site (068R) had a large increase in volume (0.27 m) during this period because a debris flow in 1993 changed local hydraulics and sand storage dynamics at the site (appendix 3). The magnitude of increase in sand thickness was very large (>0.20 m) at study sites 044L, 093L, 183R, 194L, and 225R (based on the median post-HFE thickness change shown in table 1.2 of appendix 1). The 1993 Little Colorado River floods also caused aggradation, although at most sites the magnitude of deposition was smaller than occurred during the 1996 HFE. However, at study site 062R the volume increased by more than 1,000 percent. This gain was entirely eroded within 2 years (fig. 25). Thus, the pattern of change during the sand-depleted period was a decrease in volume at narrow and medium reattachment bars, separation bars, and undifferentiated eddy bars, whereas wide reattachment bars and upper pool deposits mostly aggraded.

During the sand-enriched period, more frequent HFEs generally resulted in aggradation in the high-elevation zone at a majority of the study sites (figs. 25 and 26*B*). Between 2004 and 2018, high-elevation zone sand thickness increased at 36 of the 42 (86 percent) sandbars (the two sites added in 2008 are not included in this comparison [009L and 070R; table 1.1 of appendix 1]). Twenty-three of the 42 sites had a net increase in sand thickness of 0.10 m or greater, whereas 6 sites had a net decrease in sand thickness. The magnitude of increase was very large (>0.20 m) at 29 percent of the sites. The net increase in sand thickness occurred at all site types but the sites with the greatest magnitude of increase were narrow and medium reattachment bars and upper pool deposits. Notable exceptions to the positive trend occurred at study sites 008L, 033L, 045L, 081L, and 091R, where erosion occurred. One site (167L) was partially buried by a debris flow from a side canyon in 2012 and is therefore not included in analyses of temporal trends (appendix 3).

At the reference series sites, the aggradation during the sand-enriched period offset much of the erosion that occurred during the sand-depleted period. At the end of the monitoring period in 2020, 19 of the 31 reference series sites (61 percent) had a net increase

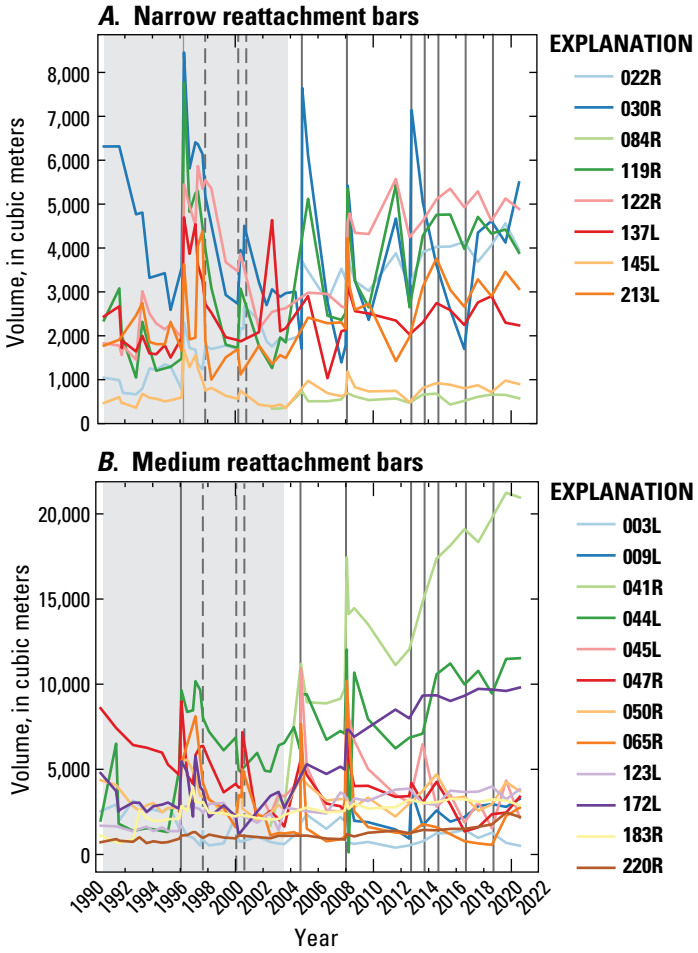

Figure 25. Graphs showing temporal trends in sandbar volume above the stage of 227 cubic meters per second (m^3/s) (high-elevation zone) at 44 sites in Marble and Grand Canyons. The six different types of sandbars defined for this study follow Mueller and others (2018) (fig. 23). *A*, Narrow reattachment bars. *B*, Medium reattachment bars. *C*, Wide reattachment bars. *D*, Undifferentiated eddy bars. *E*, Upper pool deposits. *F*, Separation bars. Uncertainties associated with the volume calculations are not shown for clarity. The outlier in the bottom right panel is a result of deposition at study site 062R (table 1) during the 1993 Little Colorado River floods. Gray areas indicate the sand-depleted period (1990–2003). Solid vertical lines indicate high-flow experiments (HFEs) and dashed vertical lines indicate smaller powerplant capacity flows (HMFs, habitat maintenance flows) from Glen Canyon Dam.

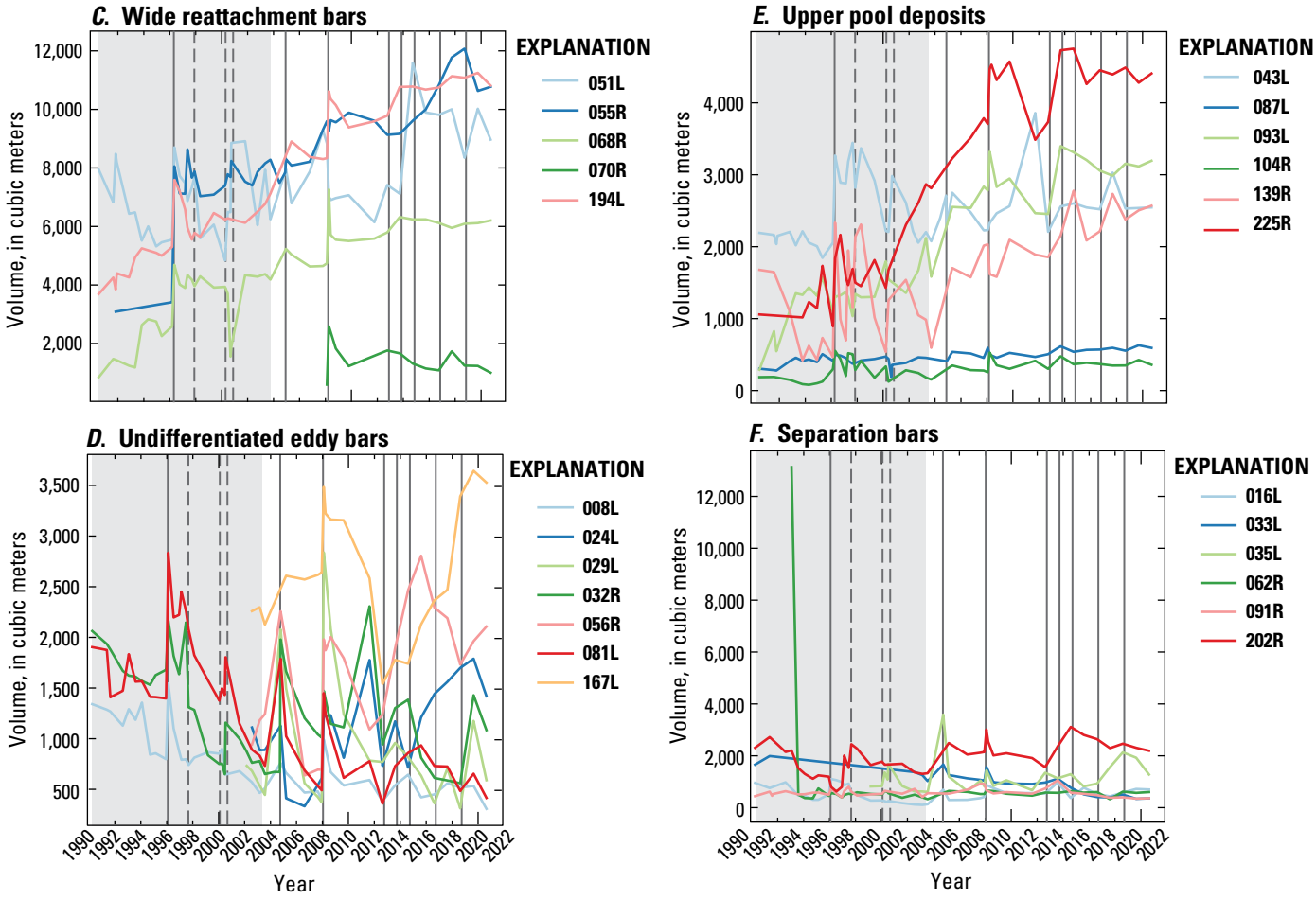

Figure 25.—Continued

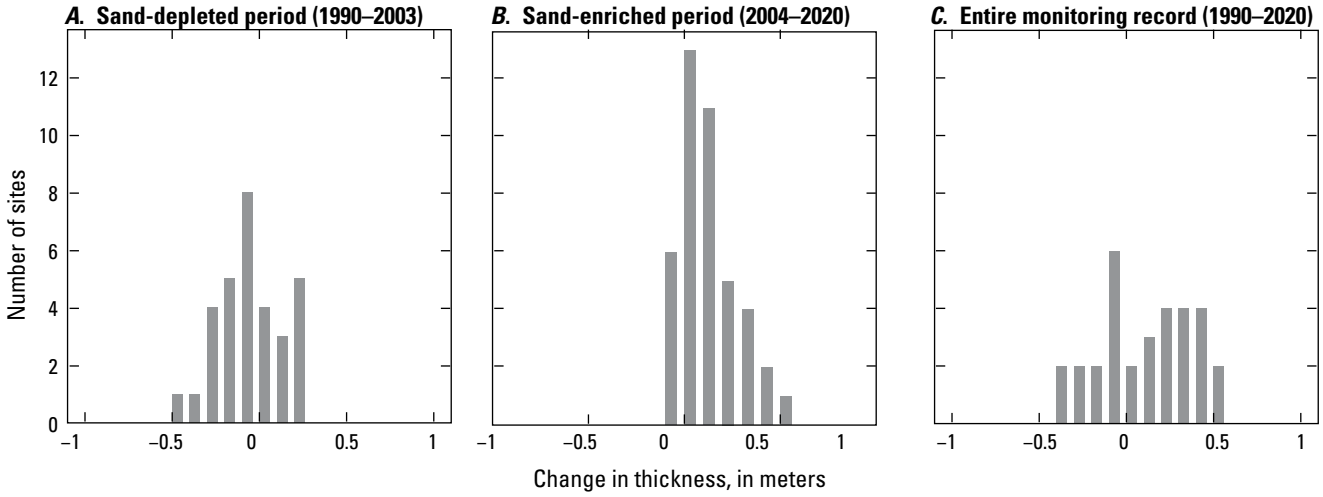

Figure 26. Histograms of changes in high-elevation sand thickness for three specific time periods in the Colorado River corridor, Marble and Grand Canyons. *A*, The sand-depleted period (1990–2003). *B*, The sand-enriched period (2004–2020). *C*, The entire monitoring record (1990–2020). The high-elevation zone is the region above the 227 cubic meters per second (m^3/s) water-surface elevation (see fig. 21).

in sand volume in the high-elevation zone compared to 1990. The magnitude of increase was very large (>0.20 m) at 55 percent of the sites (fig. 26*C*). However, some sites, primarily located in Marble Canyon, continued to decrease in sandbar volume despite periodic deposition during HFEs (for example, study sites 003L, 008L, 030R, 032R, 033L, 047R, and 081L). Although these sites of greatest erosion are clustered in the upstream part of the study area, this response is likely driven by site characteristics rather than location (discussed in the "Changes in Sandbar Volume by Site Type and Elevation Zone" section).

To assess the importance of site size and site-to-site variability, the two metrics for examining time series of average high-elevation bar response (that is, summation and normalization) are shown in figure 27 for each site type, respectively. Because uncertainty in the measurement of sand volume is small relative to the change in volume, summed volume for each site type (eq. 2) has low uncertainty. Net changes were greater than the uncertainty for all types of reattachment bars and for upper pool deposits. Because trends in summed volume are driven by the large sites with greatest sand volume, we also use the metric of normalized volume (eq. 3). In general, the long-term time series among all types of study sites was dominated by deposition during HFEs and erosion during normal dam operations following HFEs (fig. 27). Beyond this overall consistency, there were distinct differences in response among the six site types. Narrow reattachment bars underwent substantial deposition during HFEs followed by rapid erosion that resulted in little long-term net volume increase. Medium and wide reattachment bars also increased in volume during HFEs but eroded at slower rates, resulting in progressive increases in sand volume during the sand-enriched period. This increase was particularly evident following the implementation of the HFE protocol in 2012. Undifferentiated eddy bars demonstrated a negative trend. The long-term trend, however, was dominated by two reference series sites located in Marble Canyon (008L and 032R). In contrast, upper pool deposits show a response similar to that of wide reattachment bars, characterized by progressive aggradation through time. Some separation bars increased in volume following HFEs; however, deposition, when it occurred, was followed by high erosion rates. Generally, separation bars were smaller in 2020 than they were at the beginning of the monitoring period in 1990. In contrast to the other sandbar types, separation bars have continued to erode during the HFE protocol.

In summary, the plot of summed volume shows how sand volume changed for each bar type and the plot of normalized volume shows whether those changes were significant among bars

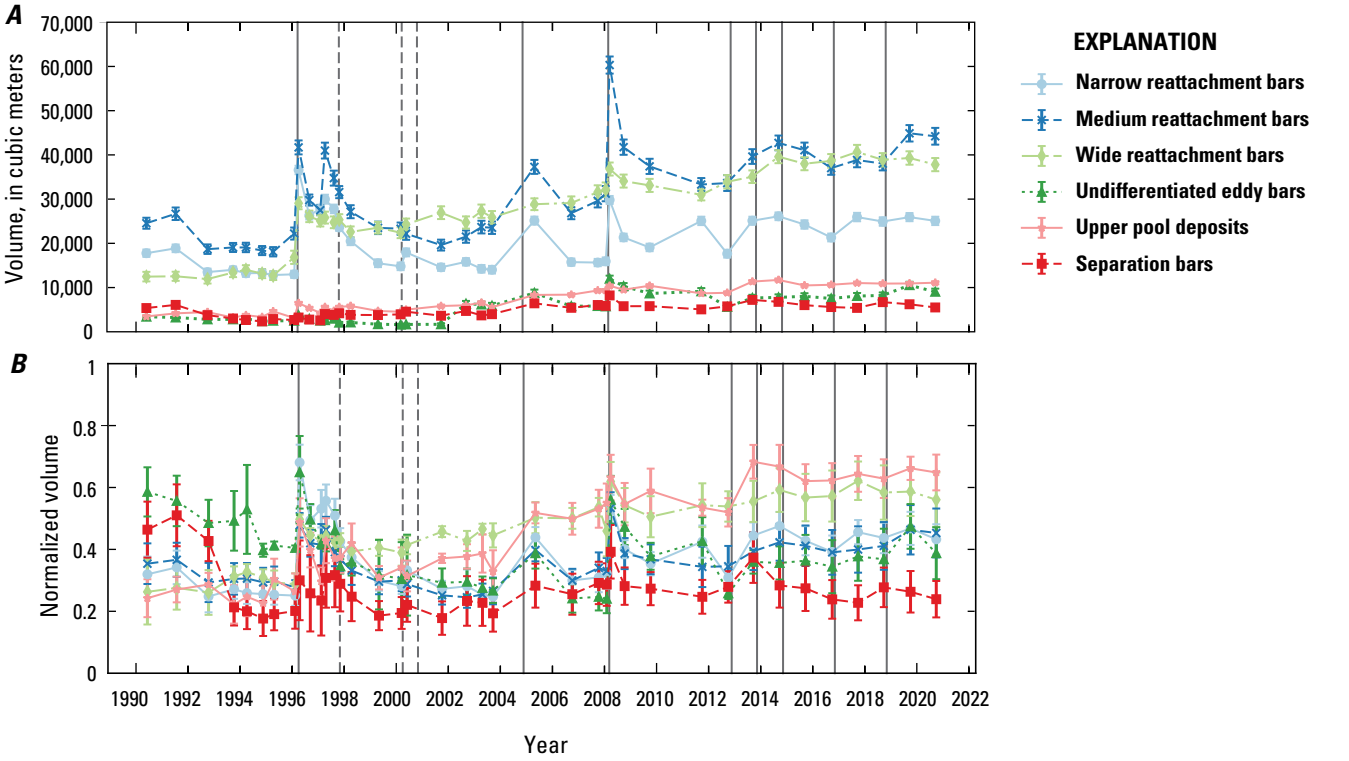

Figure 27. Graphs showing temporal trends in high-elevation sandbar volume at the six different types of sandbars (see fig. 23) in the study area, Colorado River corridor, Marble and Grand Canyons. *A*, Total volume (summation approach). *B*, Normalized volume. Uncertainties associated with the surface computations are shown in *A* and standard error is shown in *B*. Solid vertical lines are high-flow experiments (HFEs) and dashed lines are lesser magnitude, power-plant capacity flows (HMFs, habitat maintenance flows) from Glen Canyon Dam. The plot of summed volume (*A*) shows how sand volume changed for each bar type and the plot of normalized volume (*B*) shows whether those changes were significant among bars of all sizes within each site type. Note the sample population is based on the reference series sandbars and thus is the same for each metric.

of all sizes within each site type (fig. 27). For all reattachment bars and upper pool deposits, both summed volume and normalized volume increased significantly during HFEs, indicating that total site volume increased and that deposition was the average response among all bars of those types. There was no trend in summed volume for undifferentiated eddy bars and separation bars, but there was a significant decrease in normalized volumes. This lack of sensitivity in the summed volume metric occurs because the few large sites in these categories were stable while many smaller sites eroded.

Changes in Sandbar Volume by Site Type and Elevation Zone

Sandbar response to controlled floods and normal dam operations varies by elevation zone and by site type. Across all site types, HFEs deposit sand in the controlled flood zone and normal dam operations result in erosion of this sand, which is then either redeposited in one of the lower elevation zones, or advected out of the eddy and transported downstream. However, this basic sand redistribution process is different in its relative magnitude and timing for each site type. Narrow reattachment bars are the most dynamic and substantially erode following floods (fig. 28). Nonetheless, the increases in volume in the controlled flood zone during the HFE protocol (2012–2020) offset erosion in the fluctuating zone as shown by a progressive increase in the total volume of sand (high-elevation zone) between 1990 and 2020. In contrast, wide reattachment bars increased significantly in volume in the controlled flood zone following the 1996 HFE and continued to increase during subsequent floods (fig. 28). Changes in the fluctuating zone were variable whereas the increases at higher elevation were persistent, resulting in a long-term increase in volume of sandbars in this end of the reattachment bar spectrum. Undifferentiated eddy bars in the 1990s were characterized by a progressive decrease in volume in both the controlled flood and fluctuating zones (fig. 29). However, because there were only two sites of this type (008L and 032R) in the reference series, there is not sufficient sample size to estimate mean response. With the addition of four sites of this type to the monitoring network in 2002 (024L, 029L, 056R, and 167L; table 1.1 of appendix 1), the time series for undifferentiated eddy bars indicates a neutral to positive response during the sand-enriched period (fig. 29), which is similar to the average trend demonstrated by narrow reattachment bars. Upper pool deposits show a response similar to that of the wide reattachment bars (that is, progressive aggradation through time at all elevations). Upper pool deposits and wide reattachment bars are both characterized by lower stage change and increasing vegetated area (table 1.2 of appendix 1).

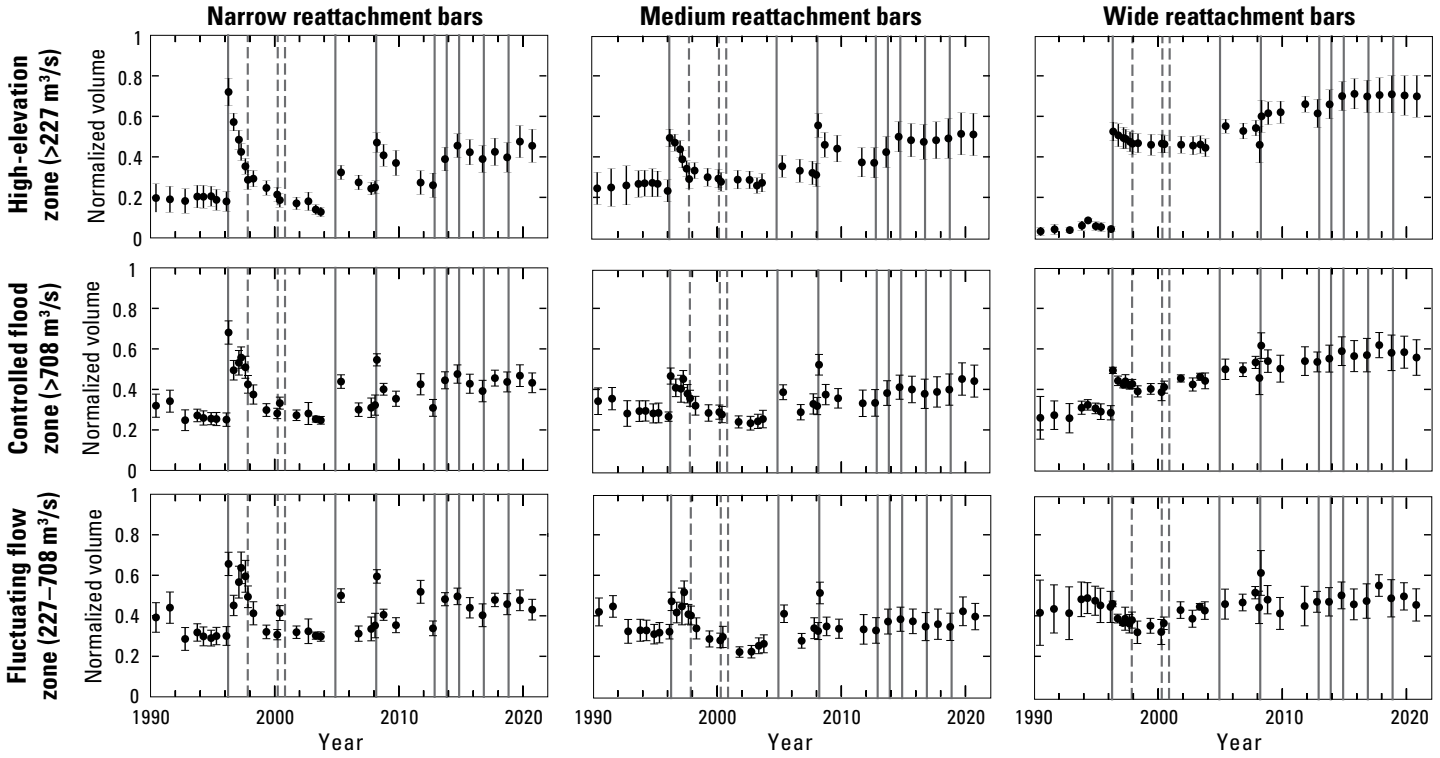

Figure 28. Plots of normalized volume time series for different elevation zones for reattachment sandbars in the study area, Colorado River corridor, Marble and Grand Canyons. Shown are narrow (left column), medium (middle column), and wide (right column) reattachment bars (see fig. 23). Error bars indicate the standard error. Solid vertical lines indicate high-flow experiments (HFEs) and dashed vertical lines indicate lesser magnitude habitat maintenance flows (HMFs) from Glen Canyon Dam. Note that these time series are constructed from all data available from any given survey run. Modified from Mueller and others (2018). >, greater than; m^3/s, cubic meters per second.

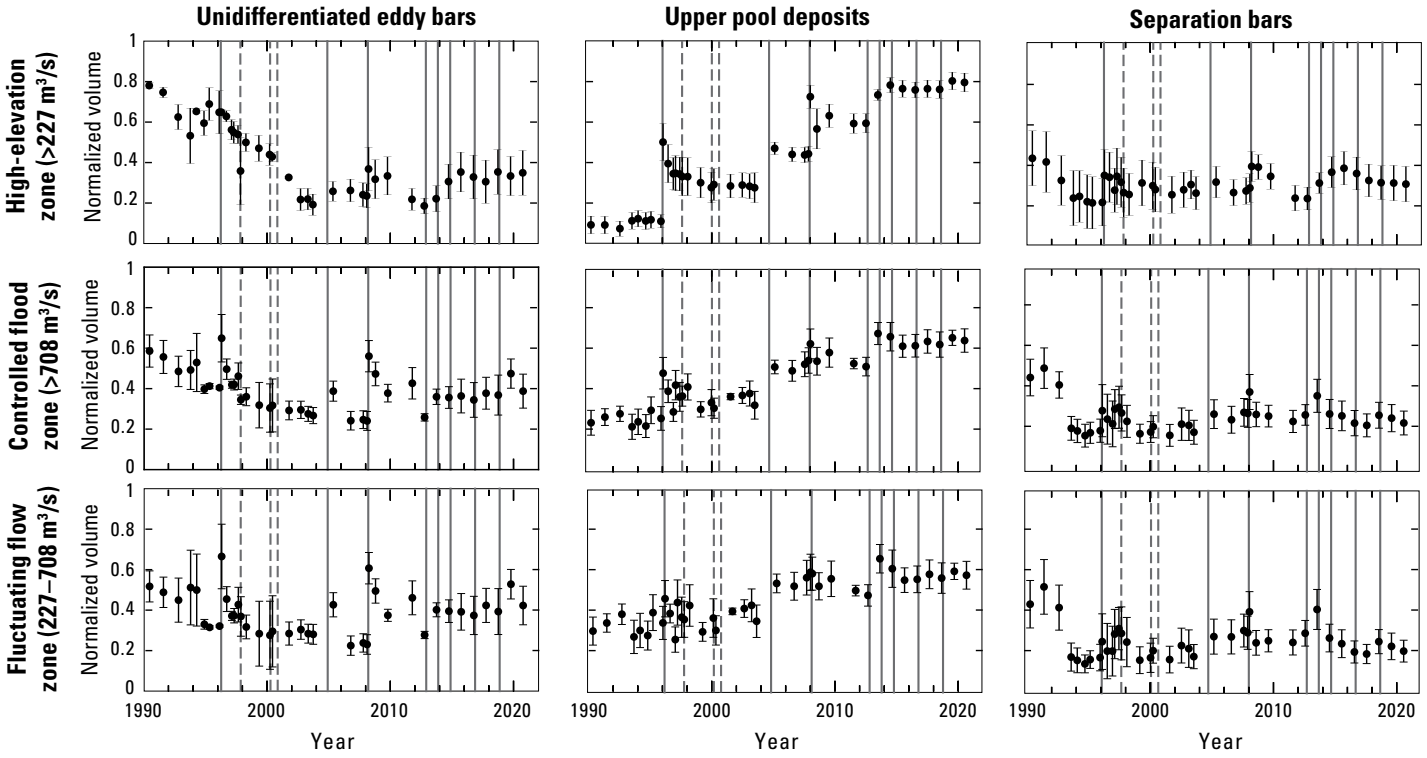

Figure 29. Plots of normalized volume time series for different elevation zones for sandbars in the study area, Colorado River corridor, Marble and Grand Canyons. Shown are undifferentiated eddy bars (left column), upper pool deposits (middle column), and separation bars (right column) (see fig. 23). Error bars indicate the standard error. Solid vertical lines indicate high-flow experiments (HFEs) and dashed vertical lines indicate lesser magnitude habitat maintenance flows (HMFs) from Glen Canyon Dam. Note that these time series are constructed from all data available from any given survey run. Modified from Mueller and others (2018). >, greater than; m^3/s, cubic meters per second.

Similar to the response demonstrated by undifferentiated eddy bars, separation bars were also characterized by erosion during the 1990s. This group tended to increase in volume in the controlled flood zone following HFEs but were generally smaller during the 2000s than they were at the beginning of the monitoring period. Except for upper pool sites in eddies just upstream from debris fans, the fluctuating flow zone shows little long-term trend for any group, suggesting that the dominant control on trends in sandbar volume is related to sand storage in the controlled flood zone.

Photographic comparisons indicate that temporal trends for different site types are at least partly controlled by the extent to which they have been colonized by vegetation, and, to a certain extent, the degree of vegetation encroachment is related to the magnitude of stage change (Mueller and others, 2018). Where there has been little vegetation establishment at narrow and medium reattachment bars, cyclic deposition and erosion dominate bar behavior with little to no long-term trend at many of the sites (fig. 30). In contrast, bars that eroded less during normal dam operations were more rapidly colonized by vegetation following HFEs. For example, wide reattachment bars, upper pool deposits, and some medium reattachment bars show this style of vegetation encroachment. With time, these site types became terraced by erosion, with topographic benches corresponding to the elevation zones of floodplain development described by Palmquist and others (2018) and Butterfield and others (2020) (fig. 31). Wide reattachment bars and upper pool deposits located in wide reaches, where the stage change during floods is less than at other site types, are not as distinctly terraced. Rather, these sites are more likely to be stabilized by vegetation, and floods have vertically aggraded large parts of the sandbar surfaces. These sites have increased substantially in volume as the elevation of sandbar surfaces increased with successive floods, particularly in the controlled flood zone, with relatively little post-flood erosion (fig. 32). Return channels that formed at these sites during the high flow years of the 1980s are now perched above the active part of the bar and primary eddy. After 1986, reduction of flooding led to widespread marsh development in return channels with stagnant flow (Stevens and others, 1995). When regulated flows were further restricted in the early 1990s as part of new operating criteria for Glen Canyon Dam (fig. 3), areal expansion of marshes continued until new deposition and burial of plants by the 1996 HFE. This aggradational event, as well as those of subsequent HFEs, raised plants further from base flows, which resulted in drying. The fluvial marshes prevalent in the early 1990s gradually disappeared in the following decade (Kearsley and Ayers, 1996). As the common

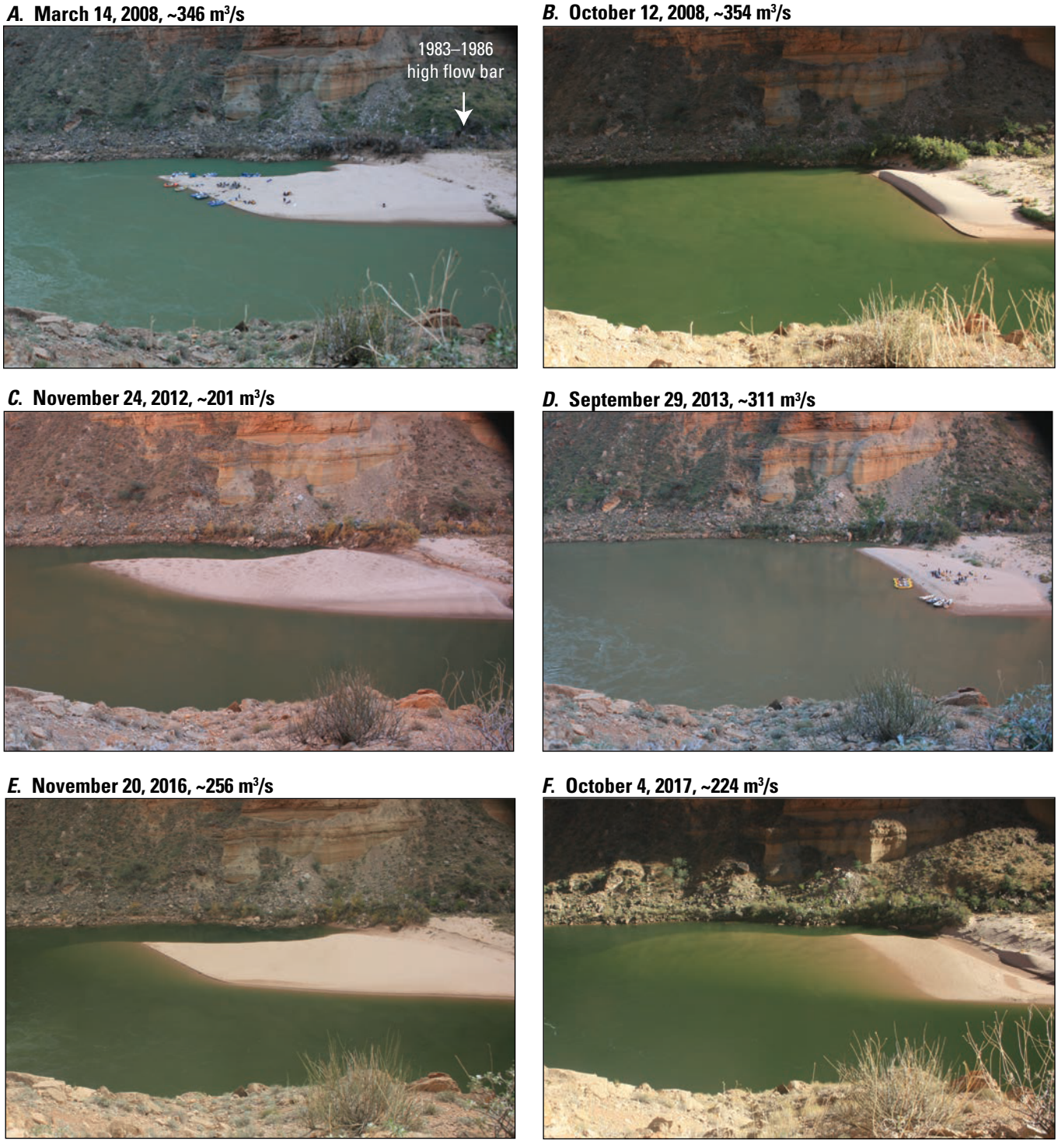

Figure 30. Photographs illustrating the cyclic pattern of deposition and erosion associated with study sites located in narrow reaches where sandbars are less vegetated and stage changes markedly with discharge. This example is the medium reattachment bar at study site 045L (table 1), Colorado River, Marble Canyon. The date and estimated discharge are given for each. Flow in the main channel is left to right. *A*, Post-2008 high-flow experiment (HFE) bar. *B*, Bar condition near the time of the topographic survey after 6 months of erosion during normal Glen Canyon Dam operations. *C*, Post-2012 HFE bar. *D*, Bar condition near the time of the topographic survey after 10 months of erosion during normal Glen Canyon Dam operations. *E*, Post-2016 HFE bar. *F*, Bar condition near the time of the topographic survey after 10 months of erosion during normal Glen Canyon Dam operations. Photographs by remote automated camera (Grams and others, 2018a). ~, approximately; m^3/s, cubic meters per second.

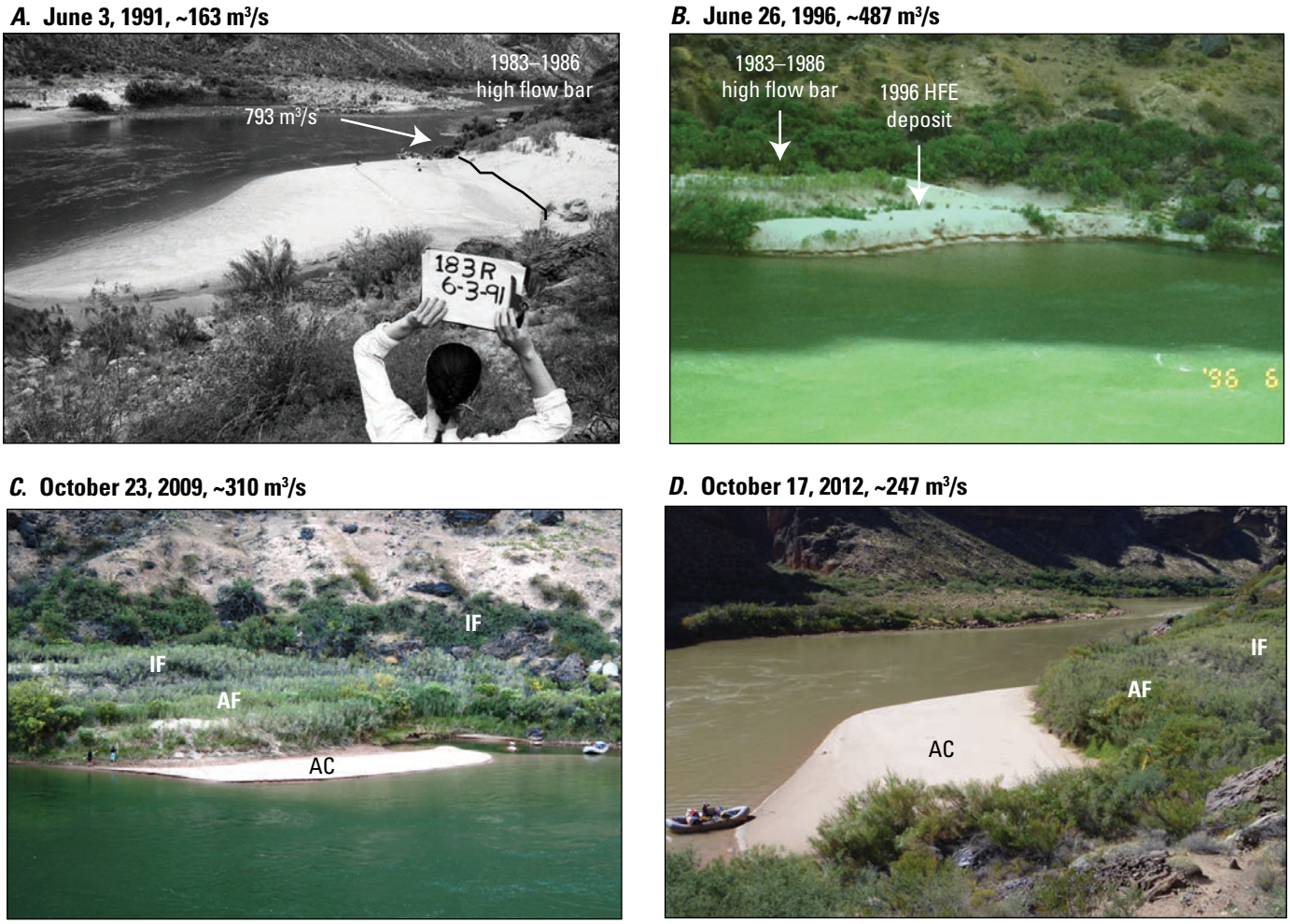

Figure 31. Photographs of a medium reattachment bar at study site 183R (table 1) in the Colorado River corridor, Grand Canyon. The date and estimated discharge from Glen Canyon Dam are given for each. *A*, Bare sandbar platform adjusted to inundation by fluctuating flows as high as 800 cubic meters per second (m^3/s) characteristic of the late 1980s flow regime. *B*, Deposition on the bar platform by the 1996 high-flow experiment (HFE). *C*, Successive HFEs and erosion led to terracing with distinct elevation zones in 2009. *D*, By 2012, topographic change at this site type became dominated by a smaller eddy and sandbar adjusted to reduced flow in front of the higher, vegetated deposit. Clonal riparian vegetation, such as arrowweed (*Pluchea sericea*), quickly colonized new deposits following each HFE. The benches generally correspond to the three hydrological zones described by Palmquist and others (2018). These are the active channel (AC), active floodplain (AF), and inactive floodplain (IF), respectively. The AC is the region between 227 m^3/s and 708 m^3/s (referred to as the fluctuating zone in this report [see fig. 21]). The AF overlaps with the controlled flood zone. The IF is within the zone inundated by pre-dam floods as well as the 1983–1986 high-flow period and is now largely decoupled from post-dam river hydrology. Flow in main channel is bottom to top in *A* and *D*, and from right to left in *B* and *C*. Photograph *A* and *D* by J. Hazel, Northern Arizona University; photographs *B* and *C* by remote automated camera (Grams and others, 2018a). ~, approximately; m^3/s, cubic meters per second.

herbaceous marsh species declined, riparian vegetation shifted to plants dominated by deeply rooted, and more drought tolerant, woody phreatophyte species (fig. 32). This vegetation feedback on sedimentation dynamics, combined with increased flood frequency during the HFE protocol has increased sandbar stability, resistance to erosion, and resulted in the transition from active sandbar to floodplain (Palmquist and others, 2018; Butterfield and others, 2020).

Undifferentiated eddy bars occur in higher gradient settings than other bar types where stage changes are greater (Mueller and others, 2018). Deposition typically occurs as a continuous strip from the separation point downstream toward the reattachment point, with the greatest flood deposition in the fluctuating flow zone (fig. 23). Both undifferentiated bars and separation bars are characterized by cyclic deposition and erosion, but the amount of erodible sediment in the fluctuating

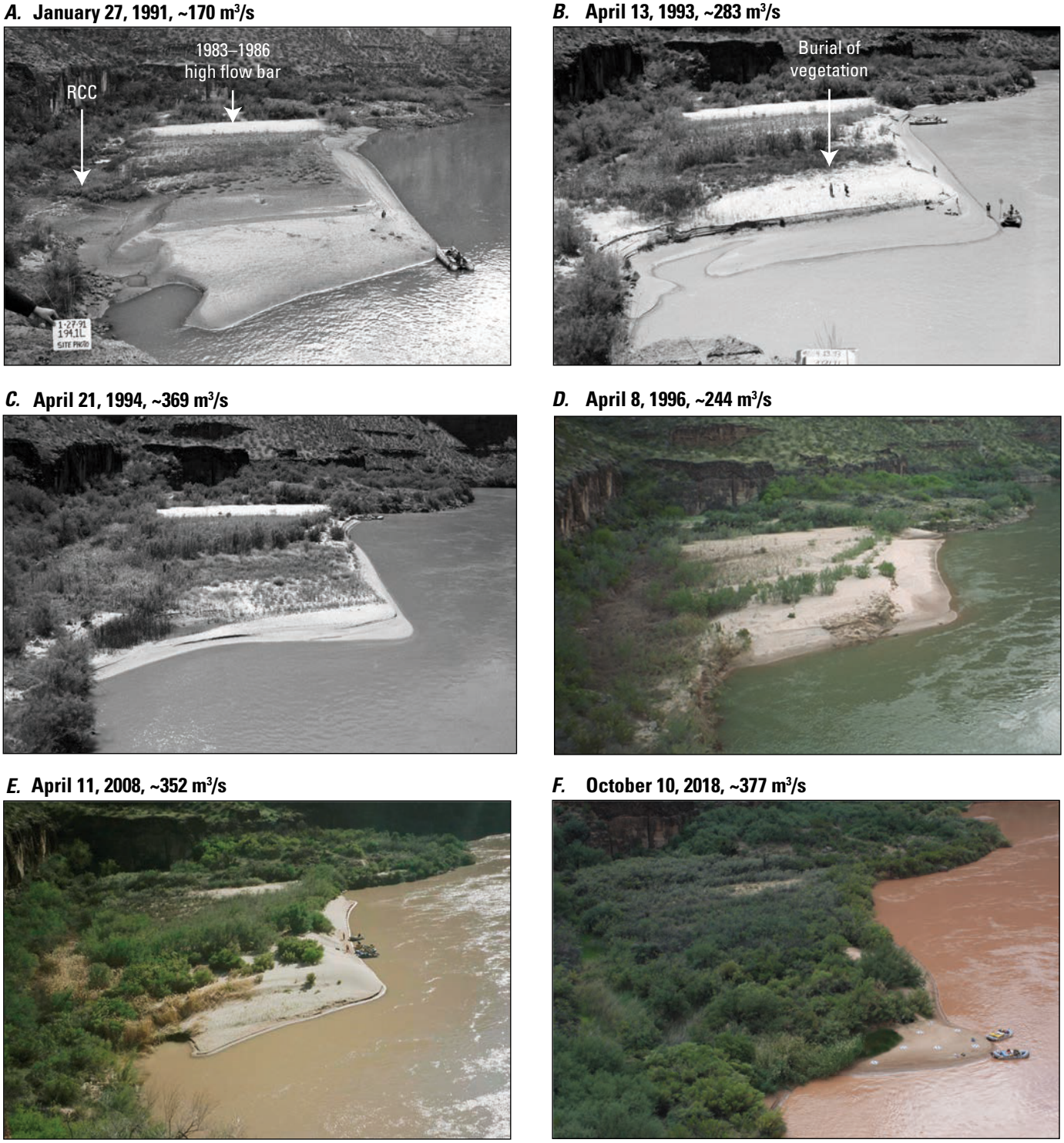

Figure 32. Photographs of a wide reattachment bar at study site 194L (table 1) in the Colorado River corridor, Grand Canyon. The date and estimated discharge from Glen Canyon Dam are given for each. Flow in main channel is bottom to top. *A*, Low-elevation bar platform separated from the bank by a return-current channel (RCC) formed during the high flow years of the 1980s. Marsh development is evident but much of the RCC is still bare sand. *B*, Deposition on the bar platform and infilling of the RCC by suspended fine sand and silt derived from the 1993 Little Colorado River floods. *C*, Marsh colonization accelerated after the sediment-rich floods in 1993, primarily by southern cattails (*Typha domingensis*) and common reed (*Phragmites australis*). In contrast, the bar platform was colonized by woody riparian species, primarily tamarisk (*Tamarix ramosissima* × *chinensis*), arrowweed (*Pluchea sericea*), Emory's baccharis (*Baccharis emoryi*), seep willow (*Baccharis salicifolia*) and coyote willow (*Salix exigua*). *D*, Deposition and burial of vegetation by the 1996 high-flow experiment (HFE). *E*, Vertical aggradation of the bar surface and vegetation burial by the 2008 HFE. *F*, Plant mortality was low following burial and by 2018 the bar surface was nearly completely covered with riparian vegetation dominated by woody phreatophytes. Photographs *A*–*C* by J. Hazel, Northern Arizona University; photographs *D*–*F* by remote automated camera (Grams and others, 2018a). ~, approximately; m^3/s, cubic meters per second.

zone is limited by armoring in the near-shore regions, which are underlain by debris fan deposits or talus (fig. 33). The deposits that remain after near-shore erosion may be protected by this armoring (Schmidt, 1990), but the highest elevations lack vegetation stabilization and may also be subject to considerable wind deflation and lowering of topographic surfaces (Sankey and others, 2015; East and others, 2016).

Trends in Sandbar Area

There was substantial site-to-site variability in high-elevation bar areas, both among bar types and within bars of the same type (fig. 34). The plot of summed high-elevation area for each site type shows clear trends in the medium and wide reattachment bars and weak trends for the other site types (fig. 35*A*). The changes in the plot of normalized area shows that those changes were not significant among bars of all sizes within each site type, nor was there a statistical difference in bar area between the sand-depleted and sand-enriched periods (fig. 35*B*). Trends for area in the fluctuating zone or controlled flood zone were examined and determined to be similar.

Because many of the changes in sand volume are caused by changes in sand thickness over a relatively stable bar area, changes in high-elevation sandbar area are poorly correlated with changes in high-elevation sandbar volume (fig. 36). Narrow reattachment bars, upper pool deposits, and separation bars have a moderate positive correlation whereas other bar types are weakly correlated or have no linear relation. This is at least partly a result of the variance among study sites but also indicates that volume is more sensitive to changes in bar morphology. For example, sites that are characterized by bar platforms gently sloping toward the deeper part of the eddy are subject to large-scale area changes as laterally migrating cutbanks erode into post-flood deposits (fig. 30). In

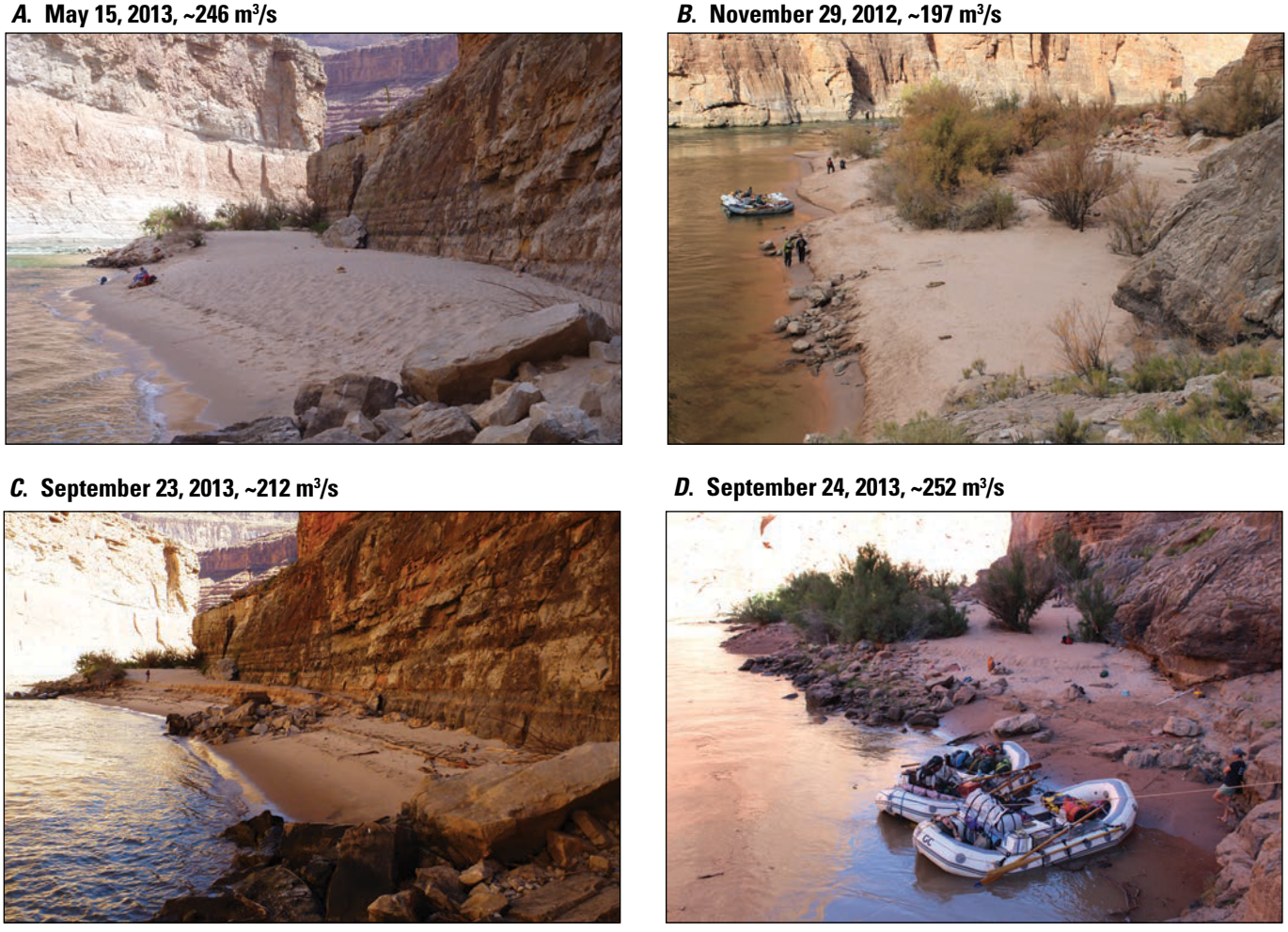

Figure 33. Photographs of undifferentiated eddy bars and separation bars showing high-flow experiment (HFE) deposition and post-flood erosion. *A*, Undifferentiated eddy bar at study site 029L. *B*, Separation bar at study site 035L. The date and estimated discharge from Glen Canyon Dam are given for each. Flow in main channel is top to bottom. The photographs in *A* and *B* show newly aggraded sandbars following the 2012 HFE. Note the near-shore erosion and exposure of talus and boulders in the fluctuating zone in both *C* and *D*. Photographs *C* and *D* were taken 5 and 10 months after the photographs of the 2012 HFE deposits in *A* and *B*, respectively. Photographs by J. Hazel, Northern Arizona University. For list of study sites, see table 1. ~, approximately; m^3/s, cubic meters per second.

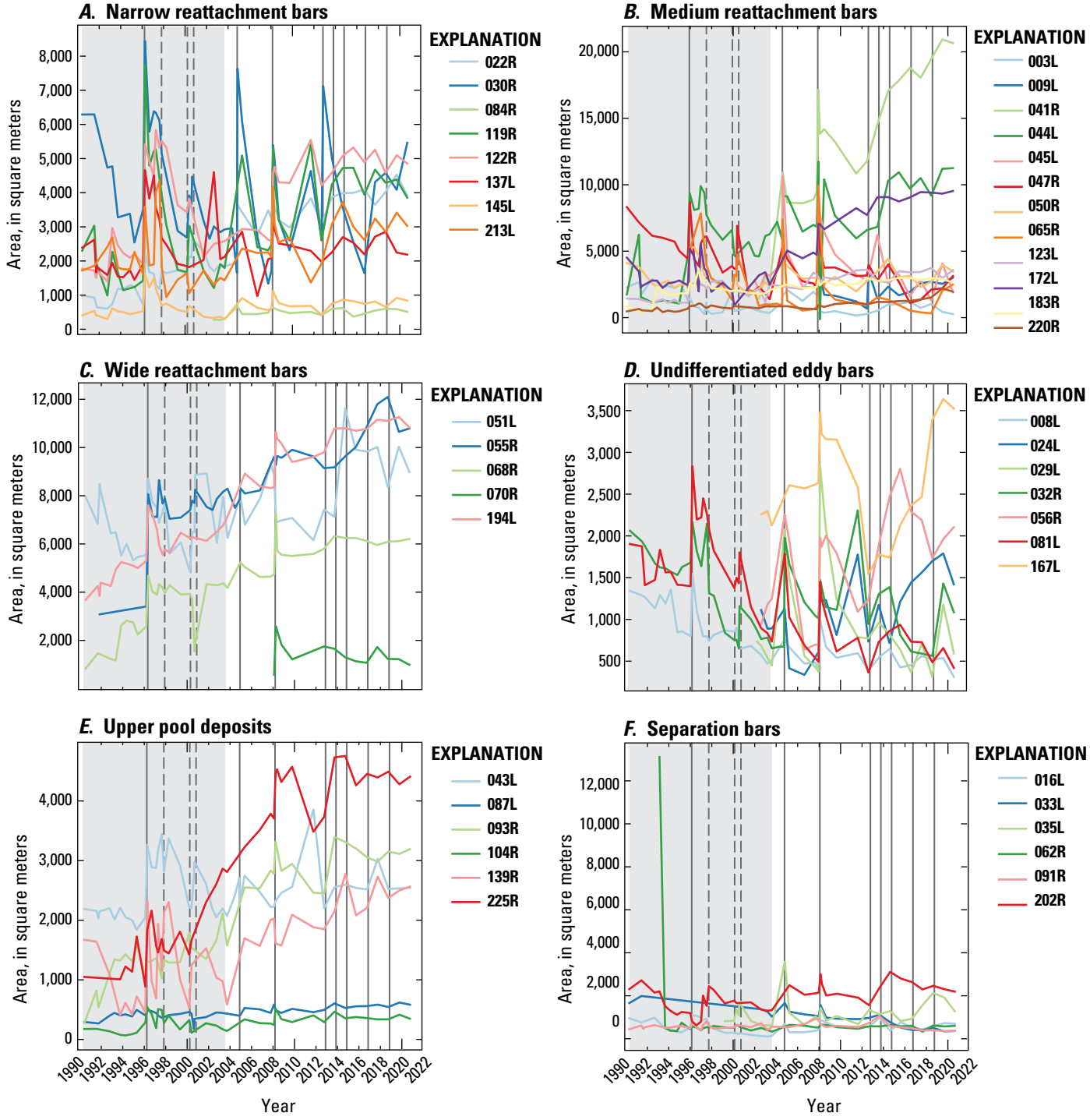

Figure 34. Graphs showing temporal trends in sandbar area above the stage of 227 cubic meters per second (m^3/s) (high-elevation zone; see fig. 21) at 44 study sites in the Colorado River corridor, Marble and Grand Canyons. The six different types of sandbars discussed follow Mueller and others (2018) (fig. 23). *A*, Narrow reattachment bars. *B*, Medium reattachment bars. *C*, Wide reattachment bars. *D*, Undifferentiated eddy bars. *E*, Upper pool deposits. *F*, Separation bars. Uncertainties associated with the area calculations are not shown for clarity. Gray areas indicate the sand-depleted period (1990–2003). Solid vertical lines indicate high-flow experiments (HFEs) and dashed vertical lines indicate smaller powerplant capacity flows (HMFs, habitat maintenance flows). The outlier in part *F* is a result of deposition at study site 062R during the 1993 Little Colorado River floods. For list of study sites, see table 1.

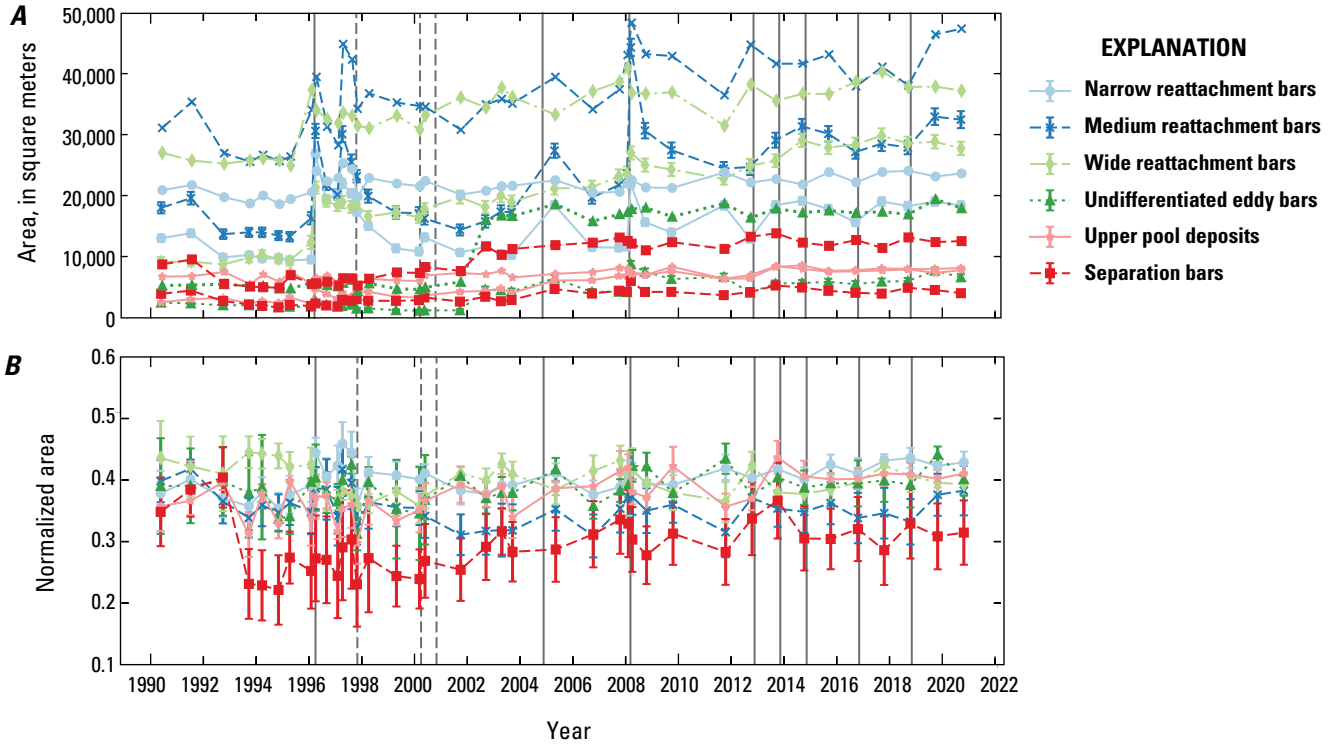

Figure 35. Graphs showing temporal trends in high-elevation sandbar areas (see fig. 21) in the Colorado River corridor, Marble and Grand Canyons. The six different types of sandbars discussed in this report follow Mueller and others (2018; fig. 23). *A*, Total area (summation approach). *B*, Normalized area. Note that there are no uncertainties associated with the area computations shown in *A*. Standard error bars are shown in *B*. Solid vertical lines are high-flow experiments (HFEs) released from Glen Canyon Dam, and dashed lines are lesser magnitude, power-plant capacity flows (HMFs, habitat maintenance flows). Note the sample population is based on the reference series of sandbars and thus is the same for each metric. For list of study sites, see table 1.

contrast, sandbar types characterized by more steeply sloping faces, such as upper pool deposits and undifferentiated eddy bars, tend to vertically aggrade during HFEs, resulting in an increase in bar thickness but little change in areal extent (fig. 33). This pattern of change is revealed by linear regressions of area and volume in both the fluctuating and controlled flood zones (fig. 37). There is little to no correlation of area changes between the two elevation zones for the overall population of sandbars, although the data in the scatter plot indicate a moderate negative correlation for reattachment bars, where R^2 is the coefficient of determination (R^2=0.35; not shown), but otherwise is not significant for other site types and the combined site types have an R^2=0.0158. In contrast, there is a moderately positive correlation of bar volume of all site types (R^2=0.42), significant at the 95 percent confidence level. This pattern of bar response occurs during HFEs whereby controlled flood zone area increases, thus decreasing fluctuating zone area (the bars are not increasing in areal extent they are simply changing in morphology). During the erosion that follows, fluctuating zone area increases via deposition at lower elevations and as cutbank erosion reduces the newly aggraded controlled flood zone area. This process in effect cancels out and, as a result, the high-elevation trend in bar area through time is mostly flat (fig. 35). The opposite is true for volume as evidenced by both elevation zones increasing in volume during HFEs, followed by decreases in volume during the intervening periods (although not at the same rates for different bar types). Thus, volume is emphasized in this report because it captures areal response to a significant event, as well as changes in bar elevation when there is no areal change.

Variations in Sandbar Behavior Between Marble and Grand Canyons

The 31-year time series for high-elevation zone volume by aggregated site type shows similar temporal trends for Marble and Grand Canyons (fig. 38). Regardless of sandbar type, the bars had reached a relative minimum by the mid-1990s, prior to the 1996 HFE, or by the early 2000s, approximately 5 to 7 years after the 1996 HFE increased high-elevation volume at most sites. After 2003, more frequent HFEs as part of the HFE protocol generally resulted in increased bar volumes. However, the data illustrate systematic differences between the sandbar types identified by Mueller and others (2018). These differences in average response make an assessment of overall long-term sandbar trajectory difficult. Identification of long-term average sandbar response

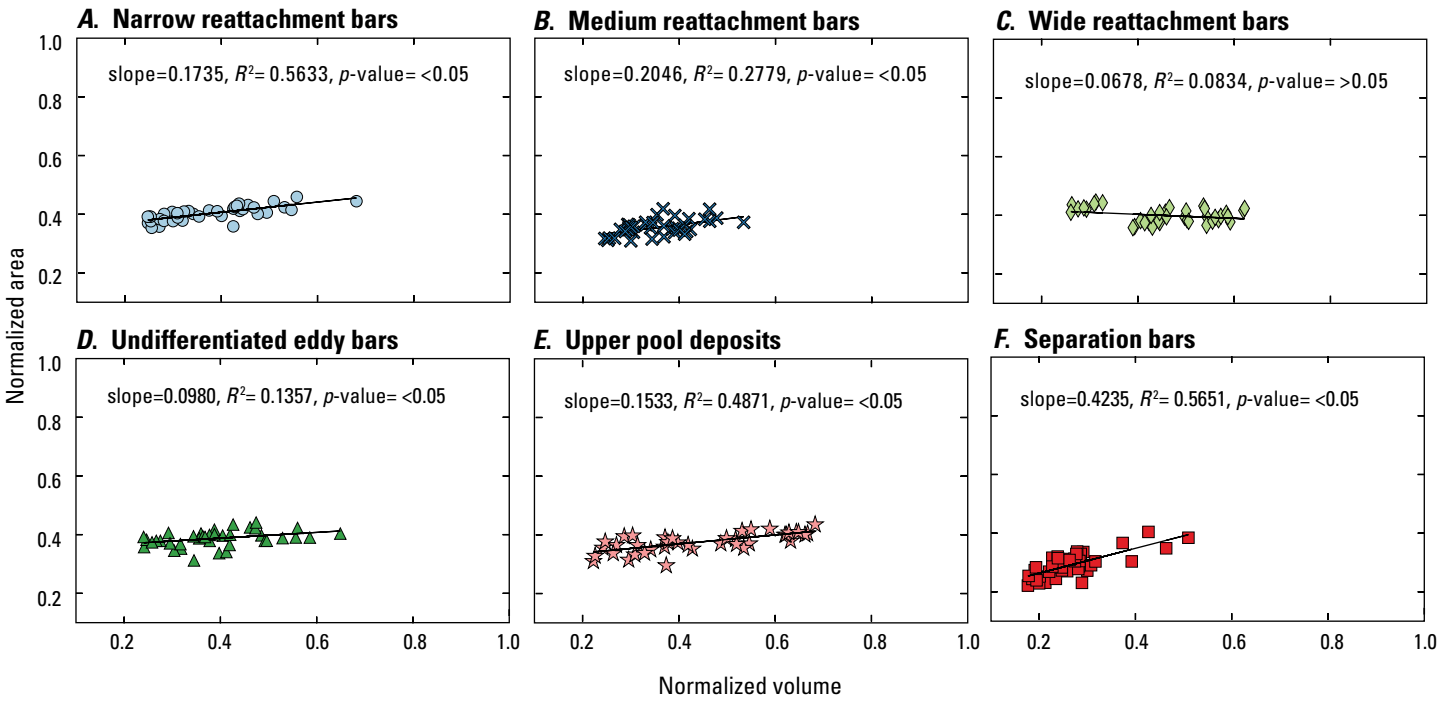

Figure 36. Graphs showing high-elevation area to volume relations for each sandbar type in the Colorado River corridor, Marble and Grand Canyons. *A*, Narrow reattachment bars. *B*, Medium reattachment bars. *C*, Wide reattachment bars. *D*, Undifferentiated eddy bars. *E*, Upper pool deposits. *F*, Separation bars. Plotted are the mean values for each survey run between 1990 and 2020. The solid black line is a least squares linear regression. R^2, coefficient of determination. High-elevation sandbar area is the area above the stage of 227 cubic meters per second (m^3/s).

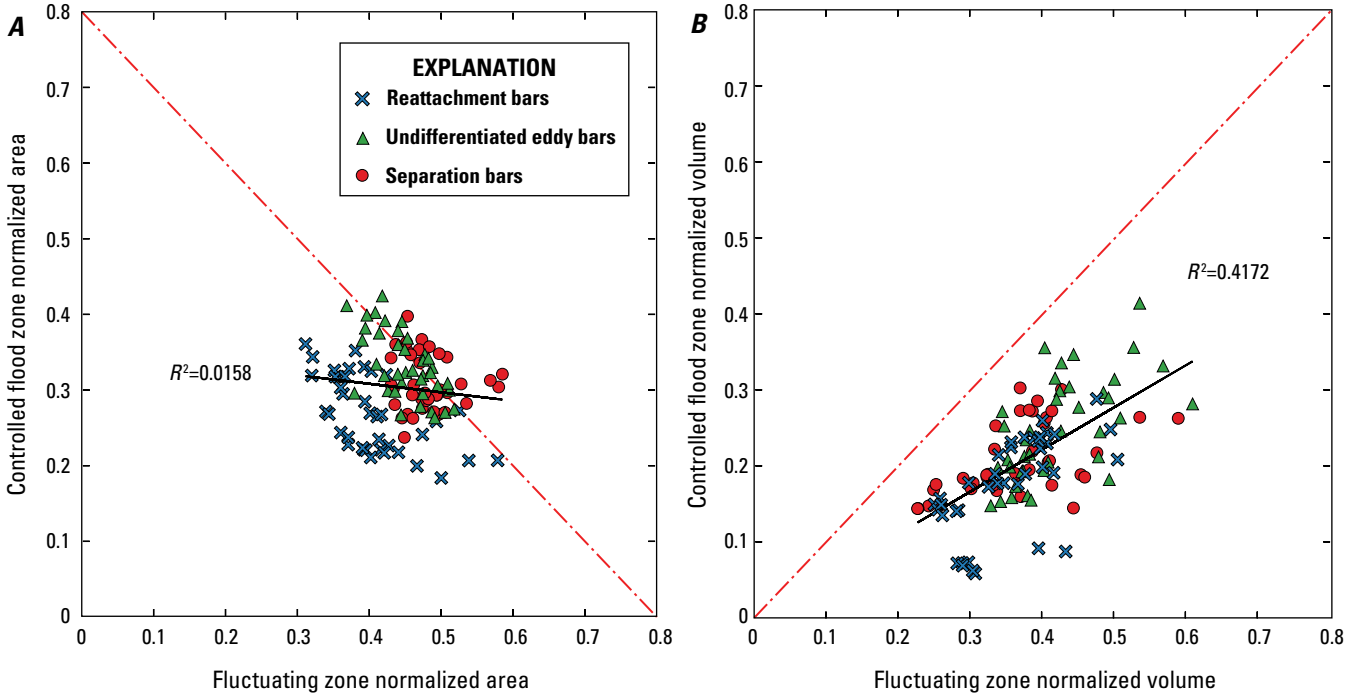

Figure 37. Graphs of area (*A*) and volume (*B*) relations between fluctuating zone and controlled flood zone in the Colorado River corridor, Marble and Grand Canyons. Plotted are the mean values for each survey run between 1990 and 2020. The "x" symbols for reattachment bars include four bar types: narrow, medium, and wide reattachment bars and upper pool deposits. The line of perfect agreement is shown in red. The solid black line is a least squares linear regression. R^2, coefficient of determination.

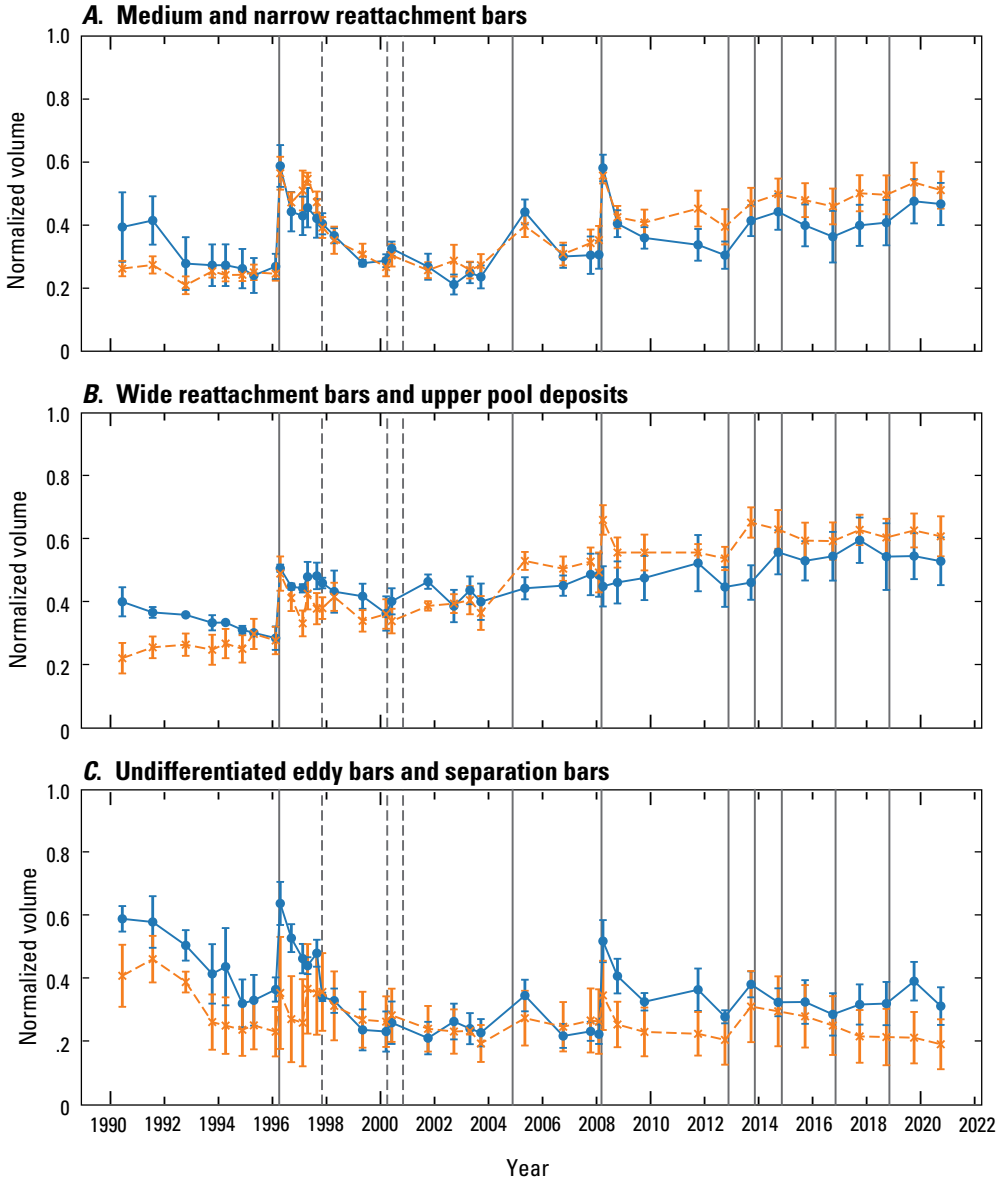

Figure 38. Graphs of variations in temporal sandbar response in the Colorado River corridor for Marble and Grand Canyons. Shown are normalized volumes for combined sandbar types in the high-elevation zone. *A*, Medium and narrow reattachment bars. *B*, Wide reattachment bars and upper pool deposits. *C*, Undifferentiated eddy bars and separation bars. Error bars indicate the standard error. Solid vertical lines indicate high-flow experiments (HFEs) and dashed vertical lines indicate smaller habitat maintenance flows (HMF) released from Glen Canyon Dam. Note that data from after the HFEs in 2012, 2013, 2014, 2016, and 2018 were collected approximately (~) 11 months after each high flow.

is further confounded by the fact that the time series includes measurements made just after depositional events such as HFEs, when sandbars are at their largest, and measurements made several years after depositional events, when the sandbars tend to be most eroded. A more complete representation of the temporal variability in long-term sandbar trajectory throughout Marble and Grand Canyons is possible by examination of only the "baseline sandbar volume," defined as the sandbar volume measured at least 12 months after a depositional event (HFE) or any other high flows greater than normal dam operations (for example, the 2011 equalization flows). Thus, surveys made about 11 months after each HFE conducted between 2012 and 2020 were not included because the sites were potentially still eroding.

Trends in baseline sandbar volume vary substantially among site types and monitoring periods (fig. 39). A positive trend line indicates net sand gain, and a negative trend indicates net sand loss (table 8). For the entire study period (1990–2020), trends were strongly positive for medium and wide reattachment bars and upper pool deposits in both Marble and Grand Canyons, whereas the trend for separation bars and undifferentiated eddy bars have a weak negative correlation with time. Trends were not significant for narrow and medium reattachment bars in Marble Canyon, indicating the average baseline volume of these sandbar types in this canyon segment was about equal to the average baseline sandbar volume measured in 1990.

The similarity in goodness-of-fit between the canyon segments at the end of the monitoring period in 2020 can be explained by the strong response of the sandbars to repeated HFEs during the sand-enriched period (fig. 39). The trends for the 2004–2020 data were strongly significant for narrow and medium reattachment bars (table 8) and have R^2 values of 0.88 and 0.96 for Marble and Grand Canyons, respectively. Similarly, regressions fit to data for the same period for wide reattachment bars and upper pool deposits are nearly equal (table 8), and have R^2 values of 0.77 and 0.83, respectively. In contrast, trends for separation bars and undifferentiated eddy deposits were weakly significant in Marble Canyon and not significant in Grand Canyon (table 8), and have R^2 values of 0.52 and 0.09, respectively.

Table 8. Slope and coefficient of determination for linear regressions fit to the aggregated time series for different sandbar types in the study area, Colorado River corridor, Marble and Grand Canyons.

[Bold numbers indicate relations significant at p=0.05; negative slope indicates net loss of sand during the analysis period. R^2, coefficient of determination; <, less than; E, exponent; p, from Student's t-test. For sandbar types, see fig. 23]

Reach[1]	Sand-depleted period (1990–2003)			Sand-enriched period (2004–2020)			Entire monitoring period (1990–2020)		
	R^2	Slope	p-value	R^2	Slope	p-value	R^2	Slope	p-value
Narrow and medium reattachment bars									
Marble Canyon	**0.49**	**−1.11E-01**	**0.05**	**0.88**	**2.03E-01**	**<0.01**	**0.34**	**1.30E-01**	**0.01**
Grand Canyon	0.34	3.72E-02	0.13	**0.96**	**2.49E-01**	**<0.01**	**0.88**	**2.91E-01**	**<0.01**
Wide reattachment bars and upper pool deposits									
Marble Canyon	0.15	6.83E-02	0.33	**0.77**	**1.34E-01**	**<0.01**	**0.76**	**2.36E-01**	**<0.01**
Grand Canyon	**0.94**	**1.80E-01**	**<0.01**	**0.83**	**2.23E-01**	**<0.01**	**0.95**	**4.35E-01**	**<0.01**
Undifferentiated eddy bars and separation bars									
Marble Canyon	**0.80**	**−3.28E-01**	**<0.01**	**0.52**	**8.40E-02**	**0.01**	**0.29**	**−1.85E-01**	**0.02**
Grand Canyon	0.48	−1.49E-01	0.06	0.09	−2.22E-02	0.37	**0.35**	**−1.11E-01**	**0.01**

[1]Marble Canyon is the reach from river mile 0 (RM 0) to the confluence with the Colorado River (RM 61.5) and Grand Canyon is the reach from RM 61.6 to RM 226, respectively. Location based on the river mile (RM) centerline downstream from Lees Ferry (RM 0), Arizona.

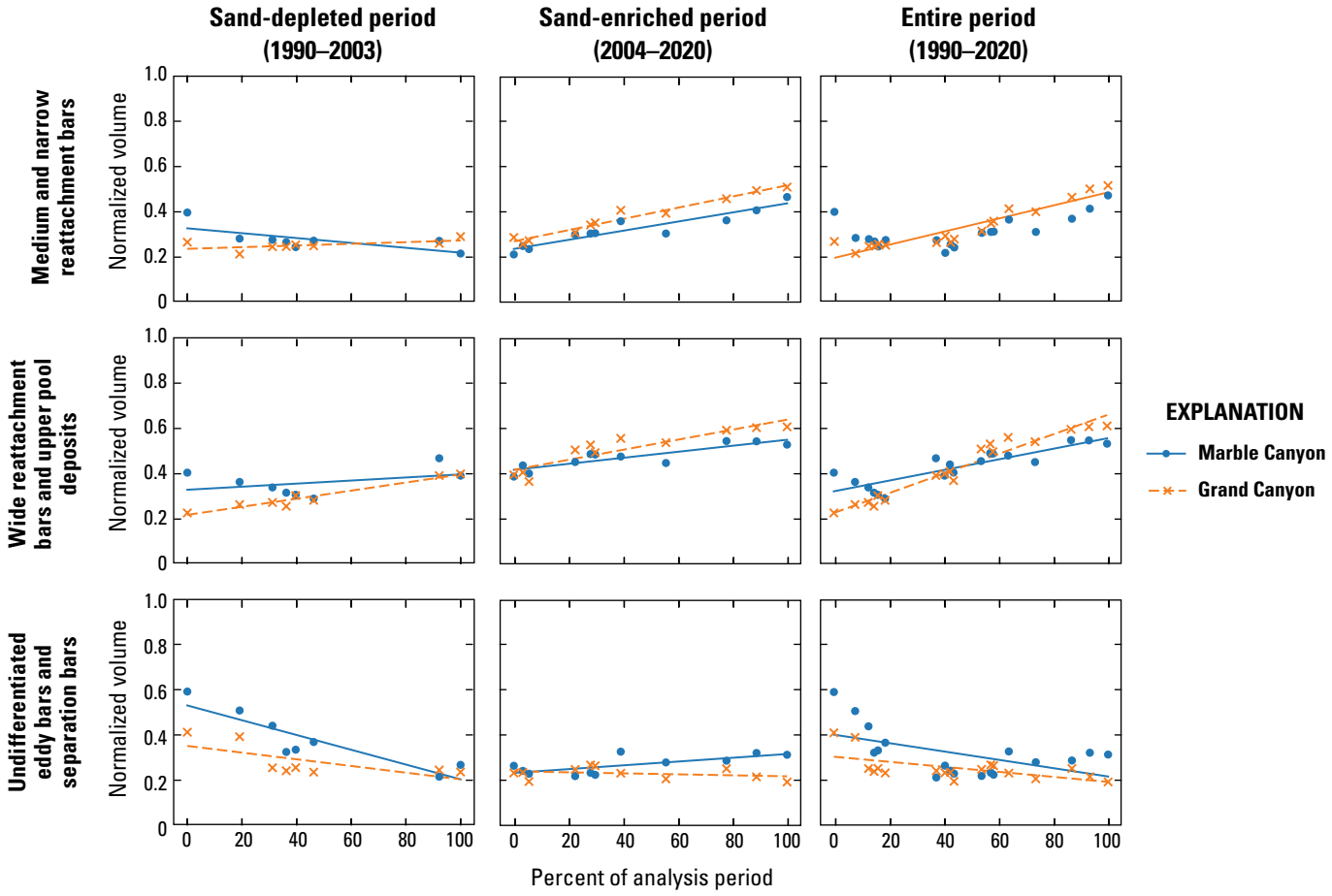

Figure 39. Graphs of linear regressions for baseline sandbar volume in the high-elevation zone comparing trends for Marble and Grand Canyons. The aggregated site types in the graphs use the same data as the average normalized time series in figure 38. However, the data points are limited to only those surveys made at least 1 year after a depositional event or other periods of sustained high flow. Coefficient of determination (R^2) and significance of the slope of the relations are shown in table 8. Error bars indicate the standard error. For each period, sand depleted (1990–2003), sand enriched (2004–2020), and the entire period (1990–2020), values were normalized by the maximum duration of the respective time span and scaled to values between 0 and 1.

As mentioned above, narrow and medium reattachment bars increase in size during HFEs and then decrease in subsequent years. The average normalized volume in 2020 was about the same as that measured in 1990 in Marble Canyon but in Grand Canyon the average normalized volume was substantially greater compared to the early 1990s (fig. 38). Nonetheless, the correlation for the baseline sandbar volume in Marble Canyon is nearly significant for the 1990 to 2020 comparison and the slope of the regression line is similar to that for Grand Canyon (fig. 39; table 8). This lack of a significant trend is partly attributed to large site-to-site variability in post-HFE erosion (flood-formed deposits erode rapidly but the rates decrease with time and those rates vary between sites). Nonetheless, the data indicate that narrow and medium reattachment bars were being maintained in size by the HFE protocol in both canyon segments. In contrast, wide reattachment bars and upper pool deposits show a positive slope with a net gain in sand volume through time in both canyon segments (fig. 39). The similarity of the regressions fit to the 2003–2020 data indicates that these sandbar types were stable over time as bar surfaces were vertically aggraded by HFEs with very little post-flood erosion.

Separation bars and undifferentiated eddy bars were generally smaller in 2020 than they were at the beginning of monitoring period in 1990 (fig. 38). The similar goodness-of-fit values for the linear regressions in Marble and Grand Canyon for the entire monitoring period suggests that these bar types were characterized by a gradual decline in volume during most years with no difference in bar response between these two canyon segments. Differences in significant linear relations between the two segments for the sand-depleted period (1990–2003) for this bar aggregation, as well as the others, were likely a result of deposition by the 1993 Little Colorado River floods. As already mentioned, the negative trend in Marble Canyon can also be attributed to two sites characterized by a progressive decrease in high-elevation volume over time (study sites 008L and 032R; fig. 25). After the addition of four study sites (024L, 029L, 056R, and 167L) to the monitoring network in 2002, the trends for the entire monitoring period (1990–2020) are nearly identical (fig. 39), and have R^2 values of 0.29 and 0.35, respectively (table 8). Collectively, the regressions for the aggregated time series of sandbar types illustrate the difficulty in identifying average sandbar response for a given segment (that is, Marble versus Grand Canyons) without taking into consideration the systematic differences in response over time among the different types of sandbars. Furthermore, these results indicate that not all site types were on the same long-term trajectory at the end of the monitoring period, yet the response of individual site types was markedly similar in both canyon segments.

Evaluation of Sample Size

The effect of increasing the sample size during the study period (1990 to 2020) was evaluated by comparing the mean normalized bar volumes estimated from the 1990 sample (10 sites in the reference series) to the volumes estimated using the present sample (18 sites) for Marble Canyon (fig. 40). The normalized volumes are slightly different, but the trends are similar, suggesting that the smaller set of study sites, represented by the reference series, characterized the response of the larger set of study sites reasonably well. Marble Canyon was chosen for this analysis because the study sites added in the late 1990s and early 2000s nearly doubled the sample size, whereas fewer sites were added in Grand Canyon (table 1.1 of appendix 1). The t-statistics for each data point on the times series were greater than the critical value at the 95 percent confidence level, indicating the means for the two sample sets were not significantly different. The greatest difference in mean normalized volumes of the two sample sizes occurred following the 2008 HFE when newly aggraded sandbars were eroding at different rates (see fig. 20 of Hazel and others, 2010). These results indicate that differences in sample size did not significantly change the central tendency in the style of change despite different site types being lumped together.

We also evaluated the degree to which our sample set of as many as 44 study sites represents the population of all sandbars

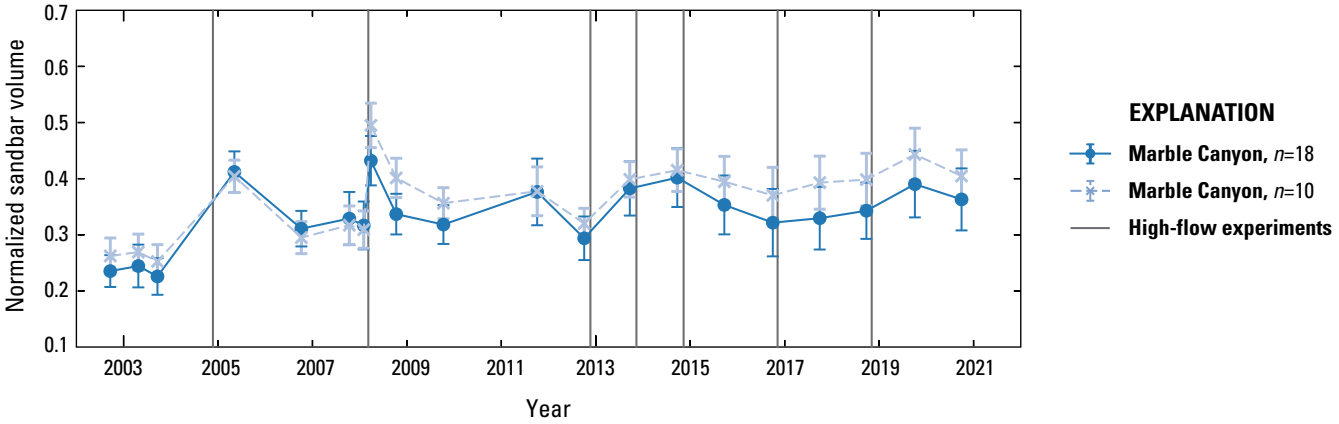

Figure 40. Graph of average normalized time series of high-elevation volume for monitoring sites in Marble Canyon, Arizona, comparing the effects of sample size (*n*). Solid vertical lines indicate high-flow experiments (HFEs). Error bars indicate the standard error. The variance of the larger sample size is less than that of the smaller sample; however, the long-term average trend is not substantially different. Two study sites are not included (009L and 045L) because they do not have monitoring records that span the period of interest (2002–2020). For list of study sites, see table 1.

by comparing the mean change in sandbar elevation among the monitoring sites with mean change in sandbar elevation among all deposit types measured in longer study reaches (table 7). The mean change in sandbar elevation for every deposit type mapped for each of eight different measurement intervals indicate a strong positive correlation (R^2=0.87) between changes in sand thickness at the long-term monitoring sites and changes at a larger selection of deposits in a given reach (fig. 41). For example, the mean change in sandbar thickness (volume divided by area) between 2009 and 2012 for the 14 monitoring sites in lower Marble Canyon (−0.06 m ±0.06 m standard error) was consistent with the mean change among the much larger set of 84 deposits mapped throughout that reach (−0.10±0.06 m [standard error]) (table 7). The largest proportional difference between changes at the collection of monitoring sites and reach-average changes occurred in eastern Grand Canyon. Between 2011 and 2014, there was a reach-average change in sandbar elevation of 0.02 m and a change of 0.14 m at the eight deposits located at six long-term monitoring sites in the same reach. This result indicates that the monitoring sites likely provide an accurate estimate of the direction of the sandbar response, but undersampling could potentially result in inaccurate estimates of change over shorter segments and may not accurately estimate the magnitude of erosion or deposition for the population of all sandbars.

We used repeat measurements taken at 84 sandbars throughout lower Marble Canyon (Kaplinski and others, 2017; Grams and others, 2018b) in a bootstrap analysis to estimate the relation between the number of monitoring sites and expected uncertainty (fig. 42*A*). With the sample size of 14 sites in lower Marble Canyon, the mean elevation change could be off by as much as about 0.25 m with standard error of about 0.12 m (fig. 42*B*). Uncertainty is expected to increase exponentially with decreasing sample size. This increase is also demonstrated by repeating the analysis for eastern Grand Canyon, where we evaluate subsampling from among 46 deposits in that reach (table 7). This illustrates that the current sample of seven sites results in a standard error of as much as

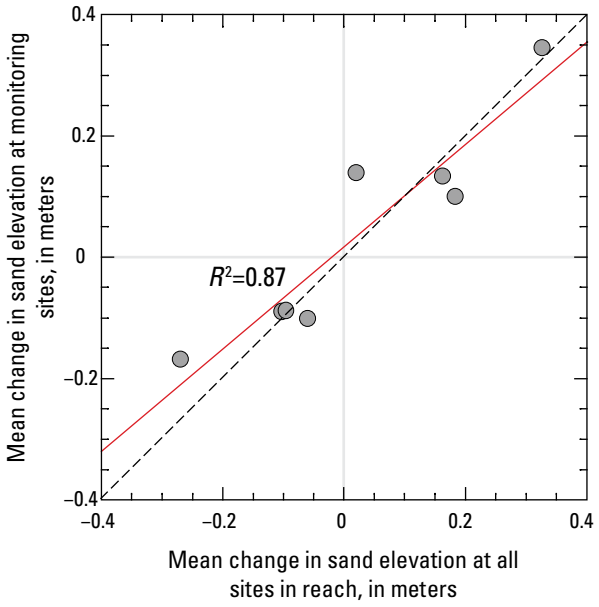

Figure 41. Plot of mean change in sand elevation at monitoring sites as a function of the mean change in sand elevation at a larger sample of deposit types in the same reach, Colorado River corridor, Marble and eastern Grand Canyons. The reaches vary in length from 3 to 52 kilometers (table 6). The black dashed line is the line of perfect match (1:1 correspondence). The solid red line is a linear regression (with coefficient of determination [R^2] shown). Plotted data are from table 7.

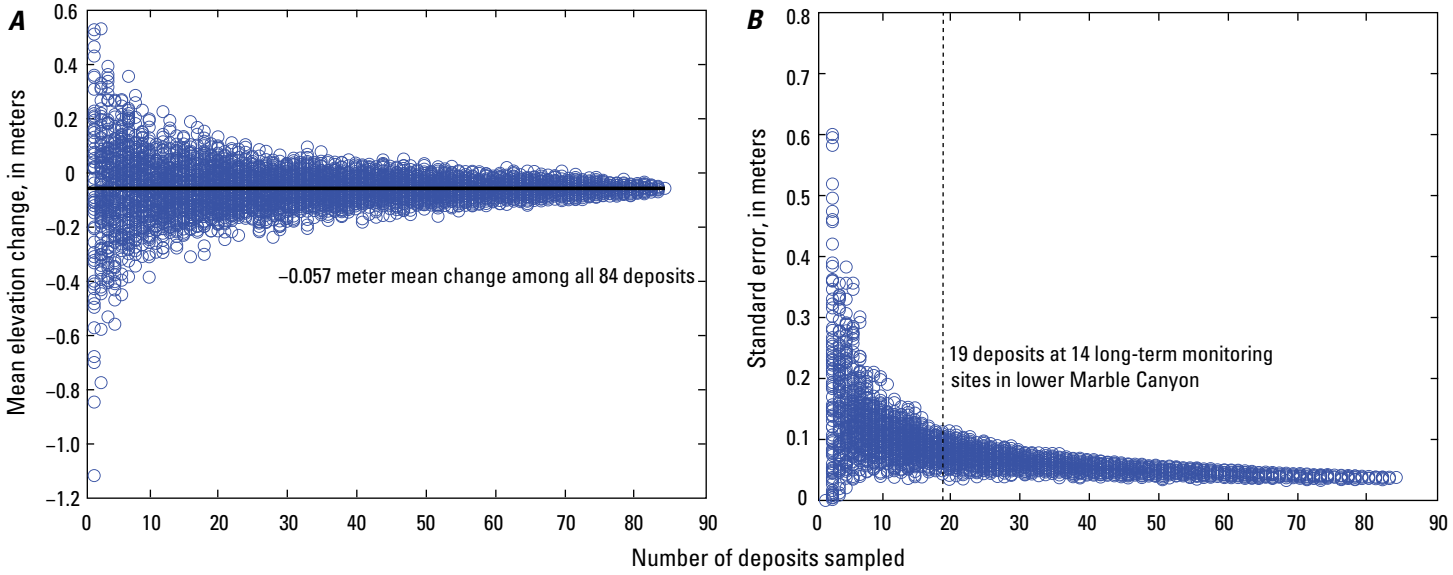

Figure 42. Plots of bootstrap simulation of expected mean (*A*) and standard error (*B*) for estimates of deposit type thickness change for sandbars in lower Marble Canyon, Arizona, as a function of sample size (in *A*) and proportion of sandbar deposits sampled (in *B*). Measurements of thickness change for 84 deposits in lower Marble Canyon were sampled randomly using increasing sample size (1 to 84). For each sample size, 100 random selections of (1 to 84) sites were made from among the 84 deposits (table 7), and the mean and standard error were calculated and plotted. The dashed line in *B* indicates the number of sand deposits that are within the 14 study sites in lower Marble Canyon.

0.24 m (fig. 43). Together, these analyses suggest that samples consisting of 20 percent or more of the sandbar population are required to represent mean changes with standard error on the order of 0.20 m or less. The bootstrap analysis was only carried out for lower Marble Canyon and eastern Grand Canyon because we do not have repeat surveys of large samples of sandbars for other river segments.

In summary, these analyses indicate that (1) the increase in sample size between 1990 and 2008 reduced the uncertainty in our estimate of normalized sandbar volume, (2) mean normalized sandbar volume for the reference series sites in Marble Canyon (n=10) agrees with the mean normalized sandbar volume for the increased sample (n=18) within uncertainty, (3) in segments where we have been able to measure sandbar changes for a much larger set of sites in lower Marble and eastern Grand Canyons, there is a strong positive correlation between the changes at the reference series sites and the larger sample, and (4) our estimates of mean sand elevation change are likely accurate to within 0.12 m in segments with a large number of monitoring sites (lower Marble Canyon), but are likely greater than 0.2 to 0.3 m in segments with fewer monitoring sites.

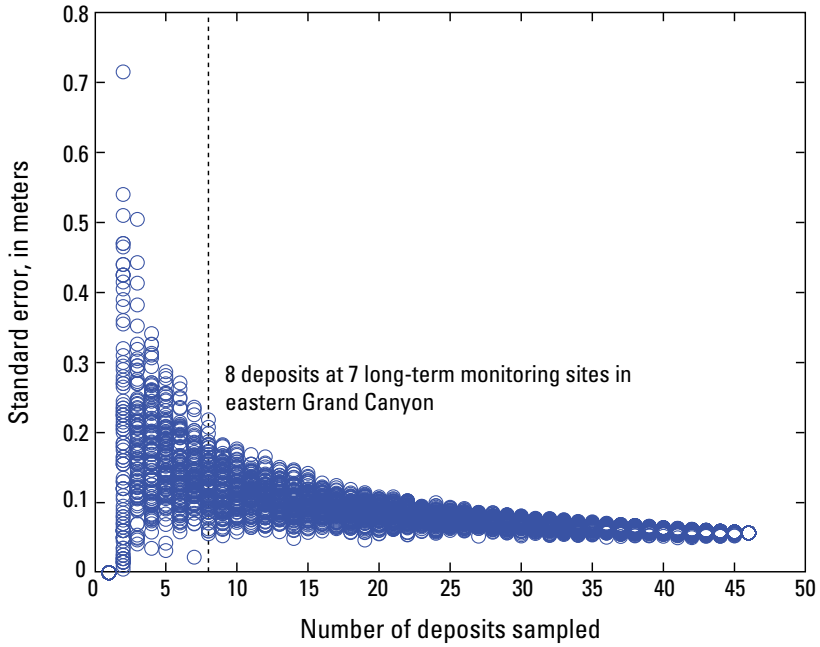

Figure 43. Plot of a bootstrap simulation of expected standard error for estimates of sand deposit thickness change as a function of the proportion of deposit types sampled in eastern Grand Canyon, Arizona. Measurements of thickness change for 46 deposits (table 7) in eastern Grand Canyon were sampled randomly using increasing sample size (1 to 46). For each sample size, 100 random selections of (1 to 46) deposits were made from among the 46 deposits, and the standard error was calculated and plotted. The dashed line indicates the number of sand deposits that are within the 7 study sites in eastern Grand Canyon.

Discussion

There are few rivers in the world where precise annual measurements of fluvial landforms have been made over a multi-decadal period. In this study, we show that tracking sand volumes and areas within three elevation zones at a representative number of sites can reliably and precisely reveal the dominant trends in sandbar change and show how those changes relate to dam operations on one of the Nation's most important regulated rivers (Schmidt and Grams, 2011a). Our measurements of sandbar change show the patterns of sandbar behavior for a river where sediment supplied by intermittent tributary inputs is transported in suspension (Topping and others, 2010) and the depositional sites for sand in the channel, though fixed in location (Grams and others, 2018b), have a complex response to changes in flow or sediment supply (Grams and others, 2013). Because dam operations can change frequently and rapidly, and because tributary sediment inputs are episodic and unpredictable, the primary challenge of sandbar monitoring has always been satisfying the need for both detailed and frequent measurements at each study site, even though these sites span more than 300 km along a remote river corridor. To support the Glen Canyon Dam Adaptive Management Program (GCDAMP), information needs are currently being met by a balance of the systematic annual measurements presented in this report, periodic measurements over long river segments to measure changes in sand mass balance (Grams and others, 2013, 2018b; Kaplinski and others, 2017), occasional high-resolution measurements that bracket specific events (Hazel and others, 2010), and daily measurements with remote cameras to provide low-cost, low-resolution but frequent observations (Grams and others, 2018a).

The response of river channels to sediment deficit or surplus conditions has been extensively described for alluvial rivers (for example, Schumm, 1973; Schumm and Parker, 1973; Baker, 1977; Nanson, 1986; Graf, 1987; Kochel, 1988; Friedman and others, 1996; Dean and Schmidt, 2011), but the transferability of this work to bedrock canyon rivers is unclear. Research on debris-fan-affected canyon reaches of the Green River in Dinosaur National Monument show a similar response of sandbars to controlled floods (Mueller and others, 2014a), although the sand mass-balance is indeterminate for this segment of the Green River (Grams and Schmidt, 2005). Just upstream from Dinosaur National Monument, the river flows through a long, low-gradient and sand-bedded reach, which may offset dam-related reductions in sediment supply (Mueller and others, 2014b). Further, changes in sand transport and storage, and thus sandbar erosion and deposition, are contingent on the degree to which changes in grain size of riverbed sediment control suspended sand concentrations (Rubin and Topping, 2001, 2008). Topping and others (2018, 2020) and Rubin and others (2020) show that in canyon rivers, the degree to which the sources and sinks of sediment in the system are large or small relative to one another depends largely on the grain size of sediment inputs relative to the antecedent grain size. This local grain-size regulation may, at least temporarily, alter the flow and sediment transport field leading to increased dynamism

and variability not controlled by reach-scale geomorphic metrics. In many rivers, vegetation encroachment is an important factor as it traps sediment (Wilcox and Shafroth, 2013), increases bank stability (Pollen-Bankhead and others, 2009; Tal and Paola, 2007), and promotes channel narrowing (Gran and Paola, 2001; Gaeuman and others, 2005; Manners and others, 2014; Dean and others, 2016; Dean and Topping, 2019). Thus, even where there is a comprehensive program of channel measurement, it is difficult to generalize results from individual sites to the system-wide changes in sediment storage. Nonetheless, and despite limitations in sample size and frequency of measurements in this study, it is the long-duration record of those measurements that can provide the ability to quantify temporal and spatial patterns of sandbar response with considerable certainty.

Metrics for Long-term Sandbar Monitoring

In this report, we use two metrics for time-series analysis as key indicators of dominant trends in sandbar change. The first is the sum of high-elevation sandbar volume, computed above a reference surface (the minimum surface), which is used to show changes in the actual volume of sand storage for a given set of sites (requiring constant sample size). The advantage of this metric is that it is a direct measure of sand volume with well-constrained uncertainty that is based on estimated errors in the topographic surfaces and associated volume computations (see appendix 4). The average vertical (elevation) uncertainty is ±0.05 m and, depending on site size, this uncertainty results in less than 5 percent uncertainty in estimates of the summed sandbar volume. The major disadvantage of the summed volume metric is that it is biased toward the largest sites, and those sites may not be representative of a larger number of smaller sites. Currently, the summed volume metric is used to quantify the change in sand storage volume caused by annual dam operations, including HFEs, at the reference series monitoring sites.

The second metric is the time series of mean normalized sand volume. For this metric, the observed sand volume for each survey at each site is normalized by the maximum potential volume at that site and the mean among all monitoring sites is computed. The advantage of this metric is that it accounts for small- or large-scale intra-site variability and allows the inclusion of all surveys at all sites in the 1990–2020. The uncertainty in this metric is standard error of the mean and we ignore measurement uncertainty, which is negligible compared to the observed variance among the sites (see "Automated Sandbar Area and Volume Computation" section).

Our analysis shows that this metric produces the same long-term trend for each site type as the time series that is based on total sand volume, but the trends, though still significant, are smaller relative to the size of the error bars (fig. 27). For much of the analysis period, the trends revealed by the summed sandbar volume show significant changes in sand volume whereas the changes in normalized volume are less than the standard error. This occurs because large changes in volume occur at some sites and small changes occur at other sites. Thus, the error in measured volume change is small and the variance is large because of large variability among the monitoring sites. Together, these metrics indicate the direction and significance of the change in sand volume (summed sand volume) and the variability of this response among the collection of monitoring sites (mean normalized sand volume).

In the framework of our time series approach, maximum sandbar volume is used as a proxy indicator of the maximum potential sand storage at each study site. Because deposition is constrained by both suspended sediment supply (Rubin and Topping, 2001) and flow depth (Wiele and others, 1999), the maximum surface represents the greatest size to which a sandbar can potentially aggrade under the current constraints on HFE peak magnitude (fig. 20). Similarly, the minimum surface represents the most eroded condition that is likely to occur at each site. Although the composition and thickness of the substrate underlying the minimum surface is unknown, it likely consists of "non-erodible" or stable coarse sediment and bedrock in some locations, and inactive and presumably relict pre-dam sand in other locations. Regardless of the composition, for our purposes, we treat the underlying material as non-erodible and inactive storage (Hazel and others, 2006b) because it has been inactive over the range of flows that have been studied since 1990. To test our assumptions that the maximum and minimum surfaces are relatively stable and representative of conditions that have occurred since 1990, we examined the change in maximum volume over the entire monitoring period (fig. 44). For all sandbar types, the maximum volume increased to 80 percent or greater of the final maximum volume within the first 10 years of monitoring. In the second

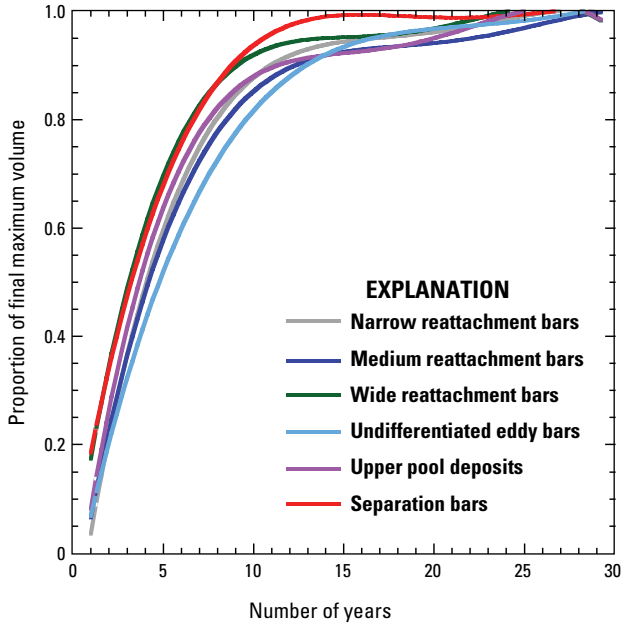

Figure 44. Plot of maximum volume computed incrementally for each of the six sandbar types for the record period for each site in the Colorado River corridor, Marble and Grand Canyons. Maximum volume is defined as the difference between the maximum surface and the minimum surface. The data were normalized by the maximum duration of the respective time span and divided by the ending maximum volume in 2020. All sites are included with a continuous monitoring record except study site 033L (table 1.1 of appendix 1) because of the 12-year gap between the first and second surveys at that site. The curves fit to the data (without the data plotted) are fourth-order polynomials.

10 years of monitoring, the maximum volume was at least 95 percent of the final maximum volume at most site types. Thus, while some changes in the maximum and minimum surfaces continue to occur, these changes are a small percentage of the 30-year maximum volume for all site types, indicating that the maximum volume is stable and consistent among the six sandbar types. This behavior indicates that the normalized sandbar volume metric, which is based on the maximum volume, provides a robust characterization of sandbar volume relative to maximum expected sandbar volume for the range of conditions that have occurred over the 30-year monitoring period.

Because these synthetic surfaces are calculated by computing when (in time) the maximum or minimum elevation values occurred as a function of elevation, they can also be used to generate degradation and aggradation plots that are both a function of time and elevation (fig. 45). These history plots are a palimpsest of the three-dimensional event-history for each individual sandbar. We identified two general response styles that reflect the behavior of the study sites to the sand-depleted and sand-enriched analysis periods. The minimum surface either resulted from (1) a combination of scour during the 1995–1999 high-flow period and near shore erosion in the early 2000s, and the maximum surface was constructed by repeated floods during the HFE protocol with widespread erosion occurring between HFEs, or (2) the sandbar surfaces were lowest in the early 1990s implying the bar surfaces were at or near a minimum elevation at onset of monitoring in 1990 (presumably because of erosion during the 1980s high flow years). These low-lying surfaces were then subject to vertical aggradation during HFEs with little post-flood erosion. The changes at study site 022R in figure 45*A* are typical of the first style of change, where the aggradation map shows large areas of deposition in areas where the sandbar eroded the most in the 1990s. These sites are

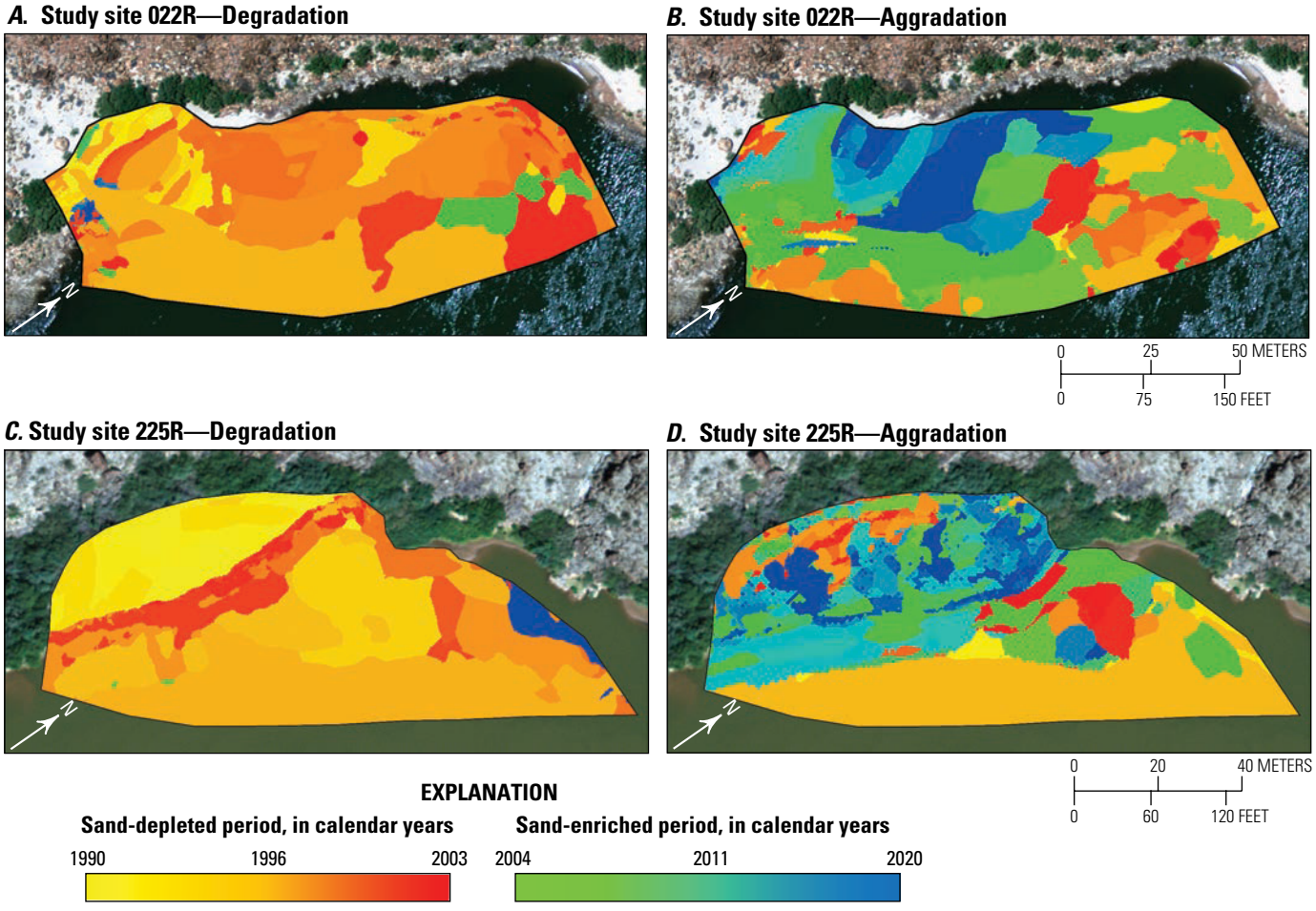

Figure 45. Images showing spatial variability in patterns of deposition and erosion as depicted by the degradation and aggradation maps derived from the mosaicked digital elevation models (DEMs) used in construction of the minimum and maximum surfaces, respectively. Study sites in the Colorado River corridor, Marble and Grand Canyons. *A*, At study site 022R, the degradation map shows that the majority of surveys contributing to the minimum surface were from the sand-depleted period (1990–2003), in particular scour during the 1995–1999 high-flow period. *B*, The aggradation map of study site 022R shows the cumulative effects of repeated floods during the high-flow experiment (HFE) protocol during the sand-enriched period (2004–2020). *C*, At study site 225R, the degradation map is characteristic of a low-elevation, wide reattachment bar or upper pool deposit where the minimum surface is composed of surveys from the sand-depleted period. *D*, The aggradation map of study site 225R illustrates that these bar types are characterized by vertical aggradation during HFEs during the sand-enriched period on top of the original low-elevation surface with relatively little post-flood erosion. Main channel flow in all panels is from right to left and the maps are clipped to the area of the eddy computational boundary. For list of study sites, see table 1. Base images from Durning and others (2016).

generally located in narrow reaches with large stage changes (95 percent of the minimum surface area was contributed by surveys from the sand-depleted period, whereas 57 percent of the maximum surface was contributed by surveys made following HFEs).

The changes at study site 225R are typical of the second style of change (fig. 45*B*). The degradation map is characteristic of sites with low elevation surfaces in the early 1990s, primarily wide reattachment bars and upper pool deposits (41 percent of the minimum surface area was contributed by surveys made between 1990 and 1995). Low-lying bar surfaces were then subject to progressive aggradation during HFEs. However, areas of aggradation are patchy or occur as slivers because the 1996 HFE contributed the most area to the maximum surface (33 percent of the maximum surface area was contributed by the survey made following the 1996 HFE). Surveys made during the sand-enriched period primarily contributed to the maximum surface in locations of minor erosion or wind deflation on mostly stable sandbar surfaces. This pattern of change is different than the widespread areas of aggradation represented by the first style of change (fig. 45*A*) where large areas of bars are cyclically eroded between HFEs and then infilled by subsequent HFEs. These two basic response styles are evident across all bar types but with substantial variability in the pattern of change from site to site. The history plots also indicate the majority of change occurred during the sand-depleted period at most site types and that surveys made during the sand-enriched period contributed a smaller percentage of area to the minimum and maximum surfaces (fig. 45). These simple but interpretively powerful synthetic surfaces are easy to apply using the automated workbench package for large databases developed as part of this study.

Drivers of Sandbar Response

There are two long-held paradigms to explain the controls on sandbar behavior downstream from Glen Canyon Dam. The first paradigm is that local variability in channel and debris fan geometry cause site-to-site variability in sandbar response to individual depositional and erosional events (Schmidt and Graf, 1990; Beus and others, 1992; Schmidt and others, 1999). Recent studies of sandbar behavior (Wright and Kaplinski, 2011) and analyses of reach-scale changes in sand storage have confirmed that nearby sandbars respond differently to the same flow and sediment conditions and that the response of individual bars is commonly inconsistent with the sand mass balance for an encompassing river segment (Grams and others, 2013, 2018b). Our findings confirm this large amount of site-to-site variability. However, variability among sites can be substantially reduced by grouping the sites according to the six types defined by Mueller and others (2018) based on geomorphic criteria (fig. 23). Thus, despite the site-to-site variability, average response among our monitoring sites to large events, such as the HFEs, has been consistent and significant (Hazel and others, 1999, 2010; Grams and others, 2010; Mueller and others, 2014a, 2018).

This variability presents a challenge for a monitoring program that must select a limited number of sites for monitoring with the goal that the average response among those sites reflects the average response among all sandbars in Marble and Grand Canyons (Schmidt and Grams, 2011a). Although the sample size analyses in figures 42 and 43 indicate need for a sample comprising 20 percent or more of the sandbar population, there was a strong positive correlation (R^2=0.87) between the changes at the smaller sample of reference series sites to a much larger sample over the same period (fig. 41). In addition, a time series comparison with two different sample sizes did not significantly change the temporal trends in bar behavior (fig. 40). Thus, we conclude that the current sample (7 to 9 percent in Marble and Grand Canyons, respectively) can characterize annual and decadal system-wide sandbar response, despite local variability in channel and debris fan geometry.

The second paradigm regarding sandbar behavior is that sandbar size, averaged among many sites, is controlled by the segment-scale sand supply to eddies (Howard and Dolan, 1981; Rubin and others, 1994; Schmidt and others, 1995; Webb, 1996; Schmidt, 1999). This view is consistent with theory (Grams and others, 2013) and is supported by studies that showed sandbars were larger in the pre-dam period, when the sand supply was much larger (Webb, 1996; Schmidt and others, 1995) and by studies that show that sandbar response at the short time scale of individual floods has been consistent with relative magnitude of sand supply (Topping and others, 2010, 2019). Sandbar building during HFEs was maximized during periods following tributary floods that resupplied the river with large amounts of very fine sand (Topping and others, 2006; Schmidt and Grams, 2011b; Wright and Kennedy, 2011). In the pre- and post-HFE analyses of Topping and others (2019) for the 1996, 2004, and 2008 HFEs, measured changes in sand mass in three different river segments were strongly correlated with eddy bar deposition at the small sample size of monitoring sites located in those reaches. Modeling studies also indicate widespread aggradation in eddies depends greatly on suspended sediment concentrations (Wiele and others, 1999; Alvarez and Schmeeckle, 2013). Thus, positive correlations between sediment supply and sandbar response have been observed at both short (individual HFEs) and long (pre- to post-dam) time scales and are supported by laboratory observations and numerical modeling.

A corollary to the theory that variations in sandbar response are caused by variations in sediment supply is that progressively more sediment is stored in the channel in the downstream direction, either through progressively less erosion or progressively greater accumulation (Andrews, 1991; Randle and others, 1993; Smillie and others, 1993). This pattern of sediment storage is consistent with field observations and analysis of pre- and post-dam photographs indicating that the magnitude of sandbar erosion decreased in the downstream direction. In a comparison of photographs taken approximately 100 years apart, Schmidt and others (1995) observed that about 80 percent of the sandbars were eroded in the first 50 km downstream from Glen Canyon Dam, whereas only about half of the sandbars were eroded in reaches >200 km downstream from the dam.

Rubin and others (1994) incorporated this perspective of sediment storage in generalized predictions of the long-term trajectory of sandbars at different distances downstream from Glen Canyon Dam. In this conceptual model, the Colorado River downstream from Glen Canyon Dam was divided into (1) an

upstream reach (Marble Canyon) where the deeper parts of the channel and subaerially exposed bars were losing sand, (2) a middle reach (confluence with Little Colorado River to about RM 120) that was transitional between net aggradation in the channel but bars were still eroding, and (3) a downstream reach in which both the exposed sandbars and the subaqueous channel were gaining sediment. Reaches farther downstream in central and western Grand Canyon were believed to have the greatest sediment supply because any sediment outputs from upstream must eventually pass through these downstream reaches. At the time these predictions were made, the proportion of sand stored on the main channel bed and in eddies was unknown and Rubin and others (1994) proposed two alternative scenarios: one where most sand was stored in eddies and the other where the most sand was stored in the main channel. Subsequent studies showed that, in fact, most sand is stored in eddies (Hazel and others, 2006b; Grams and others, 2013), which is the scenario that is the most difficult to manage. Hazel and others (2006b) showed that during periods when there was little or no upstream tributary sand supply, low-elevation eddy deposits were the primary source of sand during HFEs, and eddies in Marble Canyon became depleted of low-elevation storage. Farther downstream, sandbars were maintained but the source of that sand was the progressive erosion of sandbars in Marble Canyon. The annual sandbar monitoring data show this pattern of sandbar response in the 1990 to 1996 period for reattachment bars and upper pool deposits (fig. 38). These observations, together with the studies comparing pre- and post-dam sandbars (Schmidt and others, 1995; Webb, 1996), show that there have been positive downstream trends in sandbar response during periods dominated by sandbar erosion.

However, the high-elevation zones of sandbars reported in this study do not universally reflect this tripartite conceptual model for sediment storage in the canyons. First, our analysis shows that sandbars of similar type in Marble Canyon and Grand Canyon behave similarly more frequently than they behave differently (figs. 38 and 39), with the 1990 to 1996 period as the lone exception. We believe that this reflects differences in sandbar behavior that likely exist between periods of relative sediment depletion compared to periods of relative sediment accumulation. During periods of relative depletion during which most sandbars erode, the evidence is consistent with the model for downstream decreases in the amounts of depletion and erosion. This pattern is likely interrupted during periods of relative sediment enrichment associated with large and (or) frequent floods from the Paria River and Little Colorado River.

Evidence provided by Grams and others (2018b) illustrates how the sand budget and high-elevation sandbar response may be decoupled during the sand-enriched period. Repeat mapping of most of a 52 km river segment showed that, despite sand evacuation as a result of the 2011 equalization flows (see "Flow Regimes and Tributary Sediment Supply" section; fig. 3*B*), the proportion of the bed surface covered by sand changed very little over a 3-year period and was most stable in eddies. Bed grain size in this analysis was also very consistent in a downstream direction in the segment. Changes in areal coverage of sand on the bed can potentially influence suspended-sand concentration (Grams and Wilcock, 2007) and on average, sand in the deepest parts of the channel may be more than twice as coarse as on shallow parts of the bed and sand on the channel bed is 25 percent coarser than sand on the bed in eddies (Rubin and others, 2010, 2020). This antecedent bed grain-size distribution is reversed when the Paria River delivers sand to the Colorado River. Previous work has shown that fine sand introduced by large floods on the Paria River passes through the system within weeks to months and suspended sand concentrations are highest in the few months following these inputs (Topping and others, 2000). This observed variability differs from the geomorphic setting of subaerial sandbars that are not inundated except at the highest discharges. Thus, the decoupling of sandbar response from the sand budget is partly a factor of how bed grain size varies as a function of depth and setting as well as the fact that HFEs are now timed to coincide with years when the Paria River delivers sand to the Colorado River. A similar disconnect between changes in sediment supply and channel change was observed by Dean and others (2020) in the Green and Colorado Rivers in Canyonlands National Park where only a small amount of the annual sediment load was required to achieve the observed channel narrowing. The fact that sandbars in Grand Canyon respond similarly during different HFEs, despite variations in sediment supply, suggests that other factors such as vegetation and geomorphic setting are likely at least as important as downstream variations in sediment mass balance in understanding average sandbar response for a given segment of channel.

An additional explanation for why observed sandbar behavior does not consistently match the conceptual model presented by Rubin and others (1994) is that the sandbars in Marble and Grand Canyons, including the long-term monitoring sites, may be representative of just those sandbars that did not irreversibly erode following closure of Glen Canyon Dam in 1963. Mueller and others (2018) suggested this mechanism to explain the observed similarity in site response between Marble and Grand Canyons. Kearsley and others (1994) showed a 30-year trend of diminishing campsite size and number based on an inventory of pre- and post-dam aerial photographs. The size of campsites, which in the absence of vegetation can be well correlated to sandbar size (see fig. 23 of Hazel and others, 2010), was punctuated by flood-induced increases but generally declined with time at decreasing rates. The 1983 peak discharge caused a short-duration increase in the number of campsites (also see Brian and Thomas, 1984), but the decline continued throughout the system between 1984 and 1991, when direct measurements started to be made as part of this study. We hypothesize that, at the onset of monitoring in 1990, the sandbars in this study were largely adjusted to post-dam flow regulation, especially considering the study sites had survived the sequence of progressively more sediment-starved conditions characteristic of the mid-1980s (see Topping and others, 2003). In fact, the long-term time series in figure 38 suggests that the bars in Grand Canyon may even have been more eroded in the late 1980s than those located farther upstream and closer to the dam (that is, the normalized volumes are less than those in Marble Canyon in 1990). If differences in sand supply associated with tributary inputs migrating through the canyon as distinct waves were the primary driver of sandbar response to floods, we would expect to see deposition and erosion focused in specific reaches and we would expect those reaches

to be somewhat different for each controlled flood. Because the data do not show this pattern, it follows that eddies previously containing subaerial sandbars under pre-dam, sand-enriched conditions may never be restored because, in the post-dam era, these sites require very high suspended sand concentrations for deposition to occur (for example, the response at study site 062R to the 1993 Little Colorado River floods in figs. 13*A* and 25; also see Wiele and others, 1996). The same interpretation might apply to average conditions along a reach. Thus, the sandbars being monitored in this study are likely those that are most efficient at trapping suspended sand in transport and least sensitive to variations in suspended-sand concentration.

To summarize these findings, we present a conceptual model that reflects the sandbar behavior during the three decades of study (at individual sites) in response to flow changes, channel morphology, and vegetation characteristics (fig. 46). This conceptual model identifies channel width as the major first-order controlling variable, and therefore describes the resultant

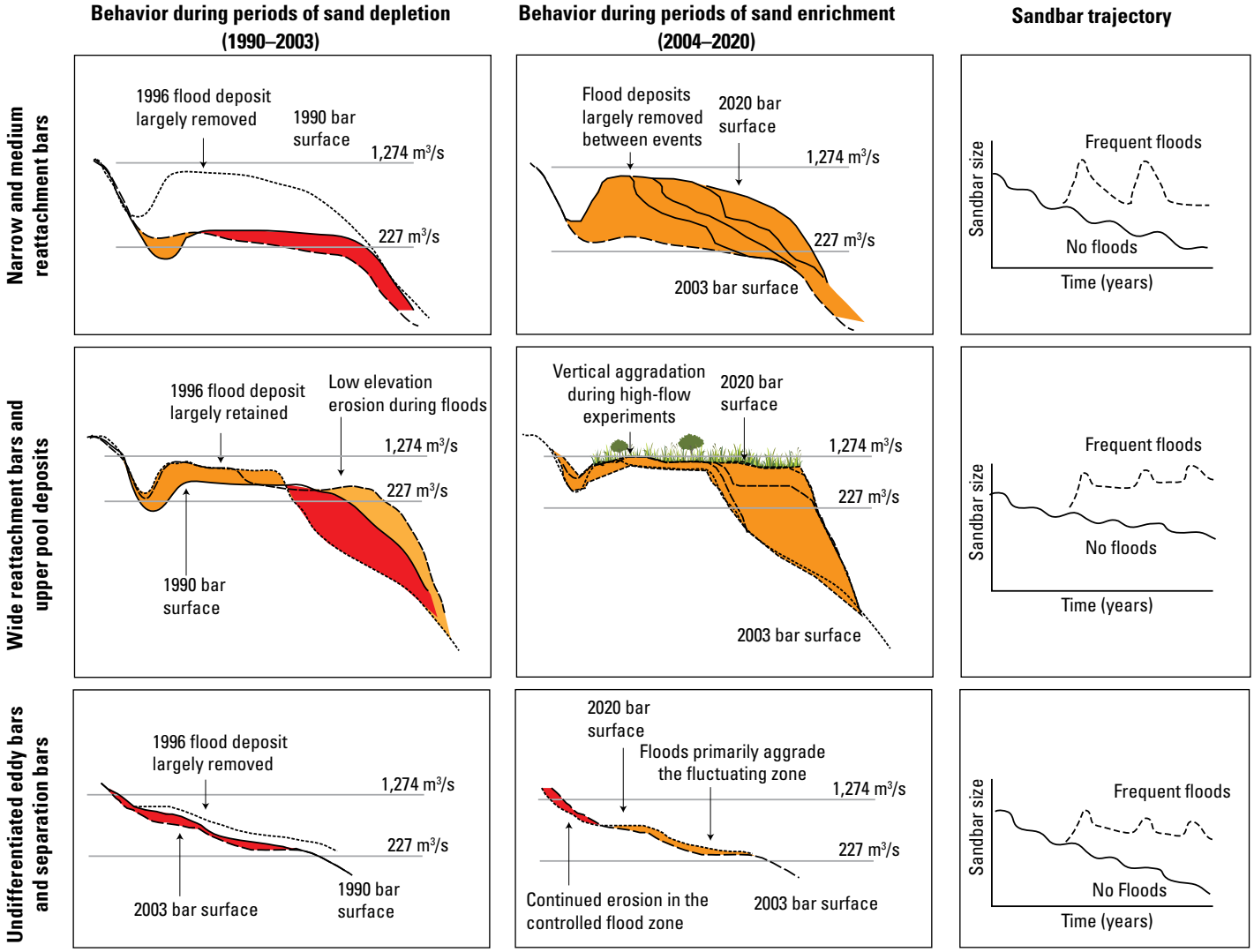

Figure 46. Conceptual model illustration showing temporal changes between sandbar types and corresponding sandbar trajectory during the period of study, Colorado River corridor, Marble and Grand Canyons. The zones are separated by two reference planes that correspond to the elevation reached by flows of 227 and 1,274 cubic meters per second (m^3/s), respectively. Shown are narrow and medium reattachment bars (top row), wide reattachment bars and upper pool deposits (middle row), and separation bars and undifferentiated eddy bars (bottom row)—the six sandbar types identified by Mueller and others (2018) that are used in this study. Orange and red colors represent deposition and erosion events, respectively. The model depicts the response to the 1990–2003 sand-depleted period (left column) and the 2004–2020 sand-enriched period (middle column), respectively. The trajectory (right column) shows the variation in net decreases in sandbar size (solid line) without high-flow experiments (HFEs) and the expected response with frequent HFEs (dashed line). The trajectory shows narrow and medium reattachment bars being maintained in size by occasional HFEs released from Glen Canyon Dam, but not increasing in size owing to substantial erosion following flood events. In contrast, wide reattachment bars and upper pool deposits become increasingly stabilized by vegetation and vertical accretion, and HFEs are expected to decrease in effectiveness through time. Because the allowable magnitude of HFEs at present time is stage limited at separation bars and undifferentiated eddy bars, these bar types are predicted to continue to decline.

sandbar types observed in different hydraulic settings. It shows that reattachment bars located in relatively narrow reaches are less vegetated, the stage changes are greater with increasing discharge than elsewhere, and the temporal trend in sand storage is dynamic as the sites expand and contract in response to floods and normal dam operations. In contrast, reattachment bars and upper pool deposits located in wider reaches, where stage change during floods may be half that of narrow sites, are less dynamic and are more likely to be stabilized by vegetation. These sites are characterized by vertical aggradation of the vegetated sandbar surfaces during HFEs and infilling of return-current channels that are no longer actively inundated (fig. 32). Return channels created by floods during the high flow years of the 1980s became fluvial marshes in the early 1990s (Stevens and others, 1995), and now support dense stands of riparian vegetation (Butterfield and others, 2020). As the elevation of sandbar surfaces increases with successive floods, HFEs have become increasingly stage-limited and are no longer capable of inundating higher elevation bar surfaces, which are now largely inactive floodplain.

Medium reattachment bars show an intermediate response in behavior where a portion of the sandbar near the bank has become stabilized and aggraded to near the maximum flood elevation, and a portion of the sandbar near the channel has remained dynamic (fig. 31). Thus, this bar type lies on a continuum between the narrow and wide spectrum for reattachment bar behavior and only the end members are represented in the conceptual model. Separation bars tend to have a response similar to undifferentiated eddy bars and these bar types are represented together in the conceptual model (fig. 46). This conceptual model, unlike the previous conceptual model of Rubin and others (1994), links the sand-depleted and sand-enriched periods to dam release floods as part of the HFE protocol. In addition, the long term high-elevation sandbar volume trajectory and the continued effectiveness of HFEs is related to the differential vegetation establishment at each bar type.

Sandbar Response to the High-Flow Experiment Protocol

Our assessment of sandbar response has shown that increased HFE frequency as part of the HFE protocol, combined with periods of enhanced sand supply, has maintained sandbars at the majority of monitored sites. The long-term monitoring sites were surveyed annually between late September and mid-October, about 11 months after each HFE carried out between 2012 and 2018. Grams and others (2018a) used comparisons of daily photographs from remote cameras to examine the post-HFE response of sandbars in lieu of direct topographic measurements. The comparisons showed that each of the five HFEs that have been released from Glen Canyon Dam during that period resulted in deposition at more than 50 percent of the sandbars. Erosion of HFE-deposited sand occurred at most sites and the observable size was similar to the pre-HFE sandbar size within 6 to 11 months after each HFE. Most sandbars among the monitoring sites responded consistently. Among the 41 sites with remote cameras, 58 percent increased in size and 21 percent were unchanged. The response was variable at 12 percent of the sites and 9 percent of the sites typically decreased in size. These results are consistent with observations made by a citizen-science campsite monitoring program, consisting of repeat photographs made at 44 sites annually since 1996, which show a similar pattern of deposition and campsite enlargement during controlled floods and erosion between controlled floods, as well as encroachment on campsites by riparian vegetation (Grand Canyon River Guides, Inc., https://www.gcrg.org/adoptabeach).

Measured sandbar responses to the HFE protocol based on annual topographic surveys were generally consistent with the observed sandbar sizes based on repeat photography. The long-term time series indicate there were stable or slight upward trends in sandbar volume between 2012 and 2018 at most sites (fig. 38). These trends were significant for reattachment bars and upper pool deposits, or 70 percent of the monitored sandbars, whereas the trends for undifferentiated eddy bars and separation bars had a weak negative correlation with time (fig. 39; table 8). Overall, the cumulative increases in sandbar volume during this period offset sandbar erosion that characterized the 1990–2003 sand-depleted period for most bar types. The weak negative trend for undifferentiated eddy bars and separation bars during the sand-depleted period continued during the sand-enriched period, indicating that HFE deposition largely eroded during the months between topographic surveys.

Despite overall similarities of net sandbar deposition during the HFE protocol, there was large site-to-site variability in the magnitude of sandbar response between site types. The magnitude of increase was greatest at those sites where the river channel is narrow, stage change during HFEs is greater, and erosion is more rapid after each HFE (that is, narrow and medium reattachment bars). Thus, net deposition was greatest at sites that eroded the most during normal dam operations (fig. 30). At the sites located in reaches where the river is wide and stage change was not as great, less deposition occurred during HFEs and post-flood erosion was less. At wide reattachment bars and upper pool deposits in this geomorphic setting, the combination of vegetation stabilization and vertical aggradation during successive floods effectively narrowed the channel and decreased the space available for deposition (accommodation space) in subsequent floods. This finding implies that, at least at these sites, HFEs can do no better than replace the sediment eroded during normal dam operation between HFEs as HFEs become less effective because of a diminishing amount of accommodation space available for deposition. In addition, the peak discharge of HFEs released during the HFE protocol have been substantially less than those released during previous controlled floods. With the exception of the 2012 HFE, HFEs ranged from 81 to 88 percent of the maximum allowable magnitude when using both the powerplant and the river outlet works (table 4); the result has been less sand deposited at higher elevations in the controlled flood zone than occurred during the 1996 and 2008 HFEs. Thus, wide reattachment bars and upper pool deposits had already built to their maximum size during previous HFEs of higher magnitude, and because they are now largely covered with vegetation, have transitioned to inactive floodplain and are largely stable (figs. 31 and 32).

HFEs have not been effective at changing the long-term trajectory of undifferentiated eddy bars and separation bars and these sites tended to gradually decrease in volume through time (figs. 29 and 38). Although these sites consistently aggrade during HFEs with net deposition in the fluctuating zone and lesser amounts in the controlled flood zone, the subsequent erosion rates are rapid. These sites have not been as stabilized by vegetation, as they are in narrower, higher gradient parts of the river corridor (fig. 24). Separation bars mantle debris fans and may also be more subject to wind deflation at higher elevations. Debris fans project out into the main channel and are less protected than vegetated bars because of local topography relative to prevailing wind direction (East and others, 2016). It may be that this sandbar type will never increase significantly through time without having occasional, very large floods (greater than 1,274 m^3/s) to inundate higher elevation areas on the debris fans. Nevertheless, even in the absence of progressive aggradation, HFEs temporarily improve the condition at some of these sites by filling gullies created by local hillslope runoff and creating larger areas that can be used as campsites (Hadley and others, 2018).

Antecedent sand supply condition, duration, and peak discharge (magnitude) are controlling factors in sandbar volume and deposit thickness during HFEs (Topping and others, 2010). The magnitude of deposition during HFEs and the three HMFs that have occurred was positively correlated with the stage change associated with each event for each of the aggregated sandbar types (fig. 47). Linear regressions fit to the data for the controlled flood zone have R^2 values ranging from 0.71 to 0.80 (significant at the 95 percent confidence level). Thicker deposits were formed at narrow and medium reattachment bars where stage changes were greatest. There was little net deposition during the lower magnitude HMFs for any bar type. The stage change during the HMFs were approximately two-thirds that of the HFEs (table 4), suggesting that powerplant capacity releases were stage-limited.

We use the relations between deposition thickness and stage change to estimate the minimum flood discharge that is required to result in significant deposition for each of the three site type groups. We define significant deposition as a deposit thickness increase that is greater than the 0.05 m uncertainty associated with the topographic surfaces. The discharges required to reach the 0.05 m threshold for significant deposition for the aggregated bar types of narrow and medium reattachment bars as well as wide reattachment bars and upper pool deposits are nearly equal, about 962 m^3/s and 957 m^3/s, respectively (~75 percent of the maximum allowable HFE magnitude; table 4). In contrast, the relation for the undifferentiated eddy bars and separation bars indicates a peak discharge of 1,050 m^3/s would be required to reach the 0.05 m threshold at most sites (~82 percent of the maximum allowable HFE magnitude; table 4). We validated the regressions by adding the one observation of flood deposition that was not used to fit the relations (fig. 47). The observed thickness of deposits following the 1993 Little Colorado River floods (mainstem peak discharge was 966 m^3/s; see "Flow Regimes and Tributary Sediment Supply" section) was close to the predictions of the fitted regression line (the values are

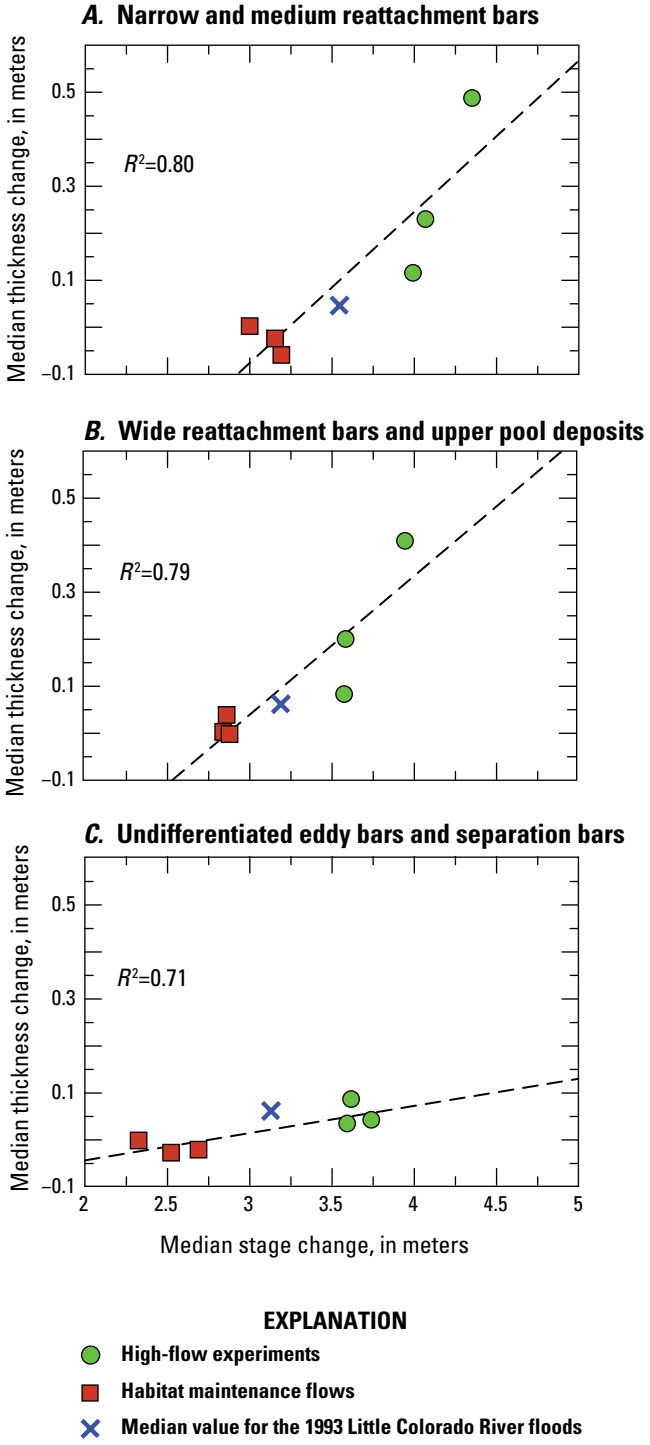

Figure 47. Graphs of the relation between stage change and sandbar thickness change for aggregated sandbar site types in the controlled flood zone, Colorado River corridor, Marble and Grand Canyons. Stage change is based on the elevation difference above 242 cubic meters per second (m^3/s) for habitat maintenance flows (HMFs) released from Glen Canyon Dam in 1997 and 2000, and for high-flow experiments (HFEs) released in 1996, 2004, and 2008. The controlled flood zone is the zone of the sandbar above the elevation inundated by flows of 708 m^3/s. The black dashed linear regression line and coefficient of determination (R^2) are shown on each plot.

within the residual error of the observed values used to fit the model). Thus, the regressions show that the bar building response to HMFs is limited by their lower stage and the requisite HFE magnitude for significant deposition is different for different bar types. Significant deposition is not expected to occur at undifferentiated eddy bars and separation bars unless controlled floods are considerably greater than Glen Canyon Dam powerplant capacity. Furthermore, HFEs will be increasingly less effective at aggrading wide reattachment bars and upper pool deposits because of continued vegetation encroachment and because these two bar types have largely aggraded to the elevation of maximum allowable HFE magnitude at most sites (fig. 46).

Although the results of the regressions in figure 47 can be used to calibrate and test appropriate numerical models for HFE magnitude (as well as confirm the basic process of using HFEs to redistribute tributary sand from the main channel bed to higher elevation sandbars), they cannot be used to evaluate the effect of flood duration on sandbar deposition. Such estimates are relevant to the design of future HFEs but, in part, depend on the suspended sand concentration during the flood and measurements of the capture rate by eddies (Wright and others, 2008; Topping and others, 2010). Wright and Kaplinski (2011) evaluated this dependence on the suspended sand load by computing the percentage of sand passing by two sites (044L and 045L) during the 2008 HFE with daily and more frequent topographic surveys and concluded that capture efficiency was highest at the beginning of peak flow (~4 percent) and then gradually decreased to about 2 percent at the end of the peak. The 2008 HFE was carried out in a relatively sand-enriched condition (Topping and others, 2010), whereas sediment budgets constructed for the 1996 HFE and the 2000 HMF indicate that approximately 90 percent of the sediment discharge from Marble Canyon during each release was derived from low elevation eddy storage, rather than from sandy deposits on the main channel bed (Hazel and others, 2006b). These earlier releases were conducted during relatively sand-depleted conditions; as a result, they exported sediment from the same eddies where bar building was desired (Topping and others, 2010). The result was erosion of upstream sandbars, with an increase in total sandbar volume only occurring in the most downstream reaches (Hazel and others, 1999; Schmidt, 1999). Despite the reduced magnitudes of HFEs, as compared to pre-dam annual snowmelt floods, they are still considered floods (when compared to the historical record) and are high enough to transport large amounts of sand with only a small percentage effectively distributed to sandbars. Thus, even when sand-enriched conditions exist, as during releases carried out as part of the HFE protocol, the results in this study indicate a greater stage increase is required to access high-elevation areas available for deposition. Because of the limited post-dam sand supply, daily or more frequent measurements during an HFE are needed to improve predictive numerical models and for evaluating HFE magnitude and duration, potentially improving the results of future floods.

Relation Between Sandbar Response and Recreational Campsites

Most campsites are located on sandbars and management of the two resources is closely linked (DOI, 2016). HFEs can increase campsite area by building larger bars, filling gullies caused by hillslope runoff, and by burying vegetation (Hazel and others, 2010; Kaplinski and others, 2014). However, deposition during HFEs can also result in a loss of campsite area by steepening the slope of a sandbar (Hadley and others, 2018). Also, vegetation removal by HFEs is minimal and new deposits can be quickly recolonized by buried stems, rhizomes, and seeds (Kearsley and Ayers, 1999; Ralston, 2010). Woody shrubs and clonal species, like arrowweed (*Pluchea sericea*), tend to quickly recover from burial to pre-HFE areal cover in as little as 6 months (Kearsley and Ayers, 1999; Ralston, 2010; figs. 41 and 42). Some vegetated sandbar types, particularly wide reattachment bars and upper pool deposits, may increase in sandbar volume while campsite area remains unchanged or even decreases. Hadley and others (2018) determined that, from 2002 to 2016, useable campsite area declined by 37 percent at the same study sites monitored for sandbar volume in this study and that vegetation encroachment was the primary cause of decreases in campsite area.

Because of increased baseflow and the elimination of large scouring floods, it is likely that vegetation encroachment will continue to reduce exposed sand area (Ralston, 2010; Sankey and others, 2015). On the basis of projected releases as stipulated in the Long-Term Experimental and Management Plan Environmental Impact Statement (DOI, 2016), Kasprak and others (2018) predicted that the areal coverage of bare, open sand deposits will decrease by an additional 12 percent over the next two decades. This estimate is based on the 28 km reach of the Colorado River in lower Marble Canyon and may represent an upper bound on rates of vegetation increase since lower Marble Canyon is wide and there is more exposed sand than elsewhere in the system. Furthermore, vegetation removal has been implemented at selected sites by Grand Canyon National Park along the Colorado River corridor and is being considered as a management tool at additional locations (DOI, 2016; Ralston and Sarr, 2017). Future studies might consider incorporating mechanical vegetation removal from shorelines to better understand the effects of vegetation on deposition and sandbar building and associated campsite area changes.

Narrow reaches of the canyon corridor are associated with more dynamic and less vegetated bars (narrow and medium reattachment bars; fig. 24), and these are the sites that most reliably aggrade during floods. These are also the reaches that overlap with sections of the canyon corridor considered critical for campsite availability. In these critical recreational reaches (Kearsley and Warren, 1993), a greater proportion of both gains and losses of campsite area are affected by HFEs compared to sites in noncritical reaches where vegetation has caused more campsite loss (Kaplinski and others, 2014; Hadley and others, 2018). These narrow and medium reattachment bar populations in narrow reaches

occupy an extensive part of the river corridor and are more likely to be maintained under the prevailing sand supply conditions in the post-dam river system (fig. 46). Collectively, these results provide motivation to perform HFEs often in order to reverse the erosion that will inevitably occur owing to daily flow fluctuations, hillslope runoff and gullying, or the remobilization of sand by wind at sandbars that lack stabilizing vegetation. HFE's have not led to long-term increases in campsite area, but they do maintain bars on a short-term basis and act to slow down the rate of campsite area loss caused by vegetation expansion.

Summary

The data presented in this 31-year synthesis of repeat topographic surveys demonstrate that the eddy sandbars that occur along the banks of the Colorado River downstream from Glen Canyon Dam are persistent and dynamic features of the river corridor in Grand Canyon National Park. Despite widespread erosion of sandbars that followed the onset of flow regulation and the elimination of upstream sediment supply when Glen Canyon Dam was completed in 1963, measurements made since 1990 show an increase in the size of 61 percent of 31 reference series monitoring sites. Increases in sandbar size occurred almost exclusively during controlled floods (high-flow experiment [HFEs] is the term used in this report), and the increase in sandbar thickness was proportional to the magnitude of those depositional events. Sandbars consistently eroded between depositional HFEs, and most sandbars were the smallest ever measured in either March 1996, 10 years after the floods of the mid-1980s, or in 2004, 7 years after the April 1996 HFE and just before the November 2004 HFE.

The study time span included a period dominated by sandbar erosion and a period dominated by deposition. From 1990 through 2003, which we term the sand-depleted period, net erosion occurred at a majority of the reference-series monitoring sites. This period was characterized by a mean discharge of 376 m^3/s and average or greater sand inputs from the Paria River in only 5 out of the 14 years. During the sand-enriched period, which extended from 2004 through 2020, net deposition occurred at 86 percent of the long-term monitoring sites. The sand-enriched period was characterized by a mean discharge of 350 m^3/s and average or greater sand inputs from the Paria River in 9 out of the 17 years. These findings demonstrate that the volume of sand in the high-elevation portions of sandbars is sensitive to long-term trends in the sand mass balance because HFEs during the sand-enriched period were released within months of sand supplied by the Paria River and before that sand was transported through Marble and Grand Canyons.

The magnitude of deposition has varied by site, even over short distances where flow and suspended-sediment properties were similar. Much of this variability results from differences in site geomorphic characteristics and the differences in the amount of vegetation expansion since the 1980s (Mueller and others, 2018). Narrow and medium reattachment bars, which occur in narrow reaches, are more dynamic and less vegetated than other bar types, and the water surface elevation (stage) changes rapidly with discharge. Wide reattachment bars and upper pool deposits, which occur in wider reaches where stage change during floods is smaller, have become stabilized by vegetation and are characterized by vertical aggradation through time, thus decreasing the effectiveness of HFEs at increasing sandbar volume at higher elevations. Separation bars and undifferentiated bars are the two site types that have not aggraded during the period of the HFE protocol.

Substantial deposition (>0.05 m) occurred at all types of reattachment bars and at upper pool deposits at discharges greater than 962 m^3/s. Because of this discharge control on deposition, considerable deposition has not occurred at separation bars and undifferentiated eddy bars, which would require flows greater than 1,050 m^3/s—a discharge that has not occurred during the HFE protocol (only one of the five HFEs released to date has been greater than this discharge). As a result, separation bars and undifferentiated bars have decreased in volume through time in contrast to the other bar types. In addition, the bar building response to HMFs (that is, Glen Canyon Dam powerplant capacity flows of 940 m^3/s) is limited by their lower stage.

Most changes in sandbar volume occurred in the controlled flood zone (the zone of the bar above the elevation inundated by flows of 708 m^3/s), with the exception of upper pool deposits where sand also accumulated in the fluctuation flow zone (the zone between flows of 227 and 708 m^3/s). The response among sites of the same type was similar throughout the 225-mile length of Marble and Grand Canyons, indicating that site characteristics were a stronger control on sandbar deposition and erosion than downstream difference in sand-supply conditions. This result is consistent with observations that sand supplied by tributaries is rapidly transported through the river corridor (in days to months) and that under most conditions, bed sand-grain size is similar throughout the study area (Rubin and others, 2020).

Thus, whereas long-term changes in sand supply drive temporal changes in high-elevation sandbar volume, segment-scale variations in sand supply within Marble and Grand Canyons do not result in measurable differences in high-elevation sandbar volume among similar sites. Similarity in behavior among sites of the same type may also reflect the fact that these bars are representative of the group of surviving bars that did not erode after dam completion in 1963 and the onset of sandbar measurements in this study in 1990. Vegetation has become an increasingly important driver of geomorphic and ecosystem response to controlled floods intended to rebuild eroded sandbars, such as those implemented in the HFE protocol. Although vegetation traps sediment and promotes sand accumulation (Butterfield and others, 2020), vegetation also reduces the area of open sand that is required for recreational campsites on sandbars. The effects of HFEs on sandbars after mechanical removal of plants, or implementation of other types of experimental flows as part of the Glen Canyon Dam Long-Term Experimental Management Plan, will require continued monitoring.

References Cited

Alvarez, L.V, and Schmeeckle, M.W., 2013, Erosion of river sandbars by diurnal stage fluctuations in the Colorado River in the Marble and Grand Canyons—Full-scale laboratory experiments: River Research and Applications, v. 29, no. 7, p. 839–854, https://doi.org/10.1002/rra.2576.

Andrews, E.D., 1991, Sediment transport in the Colorado River basin, *in* Marzolf, G.R., ed., Colorado River Ecology and Dam Management, Proceedings of a Symposium May 24–25, 1990, Santa Fe, New Mexico: National Academies Press, p. 54–74, accessed May 20 14, 2022, at http://www.nap.edu/catalog/1832.html.

Andrews, E.D., Johnson, C.E., Schmidt, J.C., and Gonzales, M., 1999, Topographic evolution of sandbars, *in* Webb, R.H., Schmidt, J.C., Marzolf, G.R., and Valdez, R.A., eds., The controlled flood in Grand Canyon: American Geophysical Union Geophysical Monograph Series 110, p. 117–130, https://doi.org/10.1029/GM110p0117.

Baker, V.R., 1977, Stream-channel response to floods, with examples from central Texas: Geological Society of America Bulletin, v. 88, no. 8, p. 1057–1071, https://doi.org/10.1130/0016-7606(1977)88<1057:SRTFWE>2.0.CO;2.

Bauer, B.O., and Schmidt, J.C., 1993, Waves and sandbar erosion in the Grand Canyon—Applying coastal theory to a fluvial system: Annals of the Association of American Geographers, v. 83, no. 3, p. 475–497, https://doi.org/10.1111/j.1467-8306.1993.tb01946.x.

Belknap, B., and Belknap Evans, L., 2001, Grand Canyon River guide: Evergreen, Colo., Westwater Books, 96 p.

Beus, S.S., Avery, C.C., Stevens, L.E., Cluer, B., Kaplinski, M.A., Anderson, P., Bennett, J., Brod, C., Hazel, J.E, Jr., Gonzales, M., Hayes, H., Protiva, F., and Courson, J., 1992, The influence of variable discharge regimes on Colorado River sand bars below Glen Canyon Dam, Arizona, chap. 6 *of* Beus, S.S., and Avery, C.C., principal investigators, 1992, The influence of variable discharge regimes on Colorado River sand bars below Glen Canyon Dam—Final report: Bureau of Reclamation, Glen Canyon Environmental Studies, National Park Service cooperative agreement no. CA 8006-8-0002 with Northern Arizona University, 62 p., accessed May 20, 2022, at http://www.riversimulator.org/Resources/GCMRC/PhysicalResources/beus1993.pdf.

Beus, S.S., Carothers, S.W., and Avery, C.C., 1985, Topographic changes in fluvial terrace deposits used as campsite beaches along the Colorado River in Grand Canyon: Journal of the Arizona-Nevada Academy of Science, v. 20, no. 2, p. 111–120, accessed May 21, 2022, at http://www.jstor.org/stable/40021335.

Billingsley, G.H., 2000, Geologic map of the Grand Canyon 30' × 60' quadrangle, Coconino and Mohave Counties, northwestern Arizona: U.S. Geological Survey Geologic Investigations Series I–2688, scale 1:100,000, https://doi.org/10.3133/i2688.

Brian, N.J., and Thomas, J.R., 1984, 1983 Colorado River beach campsite inventory—Grand Canyon National Park, Arizona: National Park Service, Division of Resources Management and Planning, Grand Canyon National Park, 56 p.

Budhu, M., and Gobin, R., 1994, Instability of sandbars in Grand Canyon: Journal of Hydraulic Engineering, v. 120, no. 8, p. 919–933, https://doi.org/10.1061/(ASCE)0733-9429(1994)120:8(919).

Butterfield, B.J., Grams, P.E., Durning, L.E., Hazel, J., Palmquist, E.C., Ralston, B.E., and Sankey, J.B., 2020, Associations between riparian plant morphological guilds and fluvial sediment dynamics along the regulated Colorado River in Grand Canyon: River Research and Applications, v. 36, no. 3, p.410–421, https://doi.org/10.1002/rra.3589.

Byrnes, M R, Baker, J.L., and Li, F., 2002, Quantifying potential measurement errors associated with bathymetric change analysis: Vicksburg, Miss., U.S. Army Corps of Engineers Research and Development Center, Engineer Research and Development Center/Coastal Hydraulics Laboratory (ERDC/CHL) CHETN–IV–50, 17 p., accessed May 21, 2022, at https://apps.dtic.mil/dtic/tr/fulltext/u2/a588888.pdf.

Carpenter, M.C., Carruth, R.L., Fink, J.B., Boling, J.K., and Cluer, B.L., 1995, Hydrogeology and deformation of sandbars in response to fluctuations in flow of the Colorado River in the Grand Canyon, Arizona: U.S. Geological Survey Water-Resources Investigations Report 95–4010, 16 p., https://doi.org/10.3133/wri954010.

Chapman, K.A., Best, R.J., Smith, M.E., Mueller, E.R., Grams, P.E., and Parnell, R.A., 2020, Estimating the contribution of tributary sand inputs to controlled flood deposits for sandbar restoration using elemental tracers, Colorado River, Grand Canyon National Park, Arizona: Geological Society of America Bulletin, v. 133, nos. 5–6, p. 1141–1156, https://doi.org/10.1130/B35642.1.

Cluer, B.L., 1992, Daily responses of Colorado River sand bars to releases from Glen Canyon Dam, 1990–1991—Instantaneous erosion and dependent deposition, chap. 5 *of* Beus, S.S., and Avery, C.C., principal investigators, 1992, The influence of variable discharge regimes on Colorado River sand bars below Glen Canyon Dam—Final report: Bureau of Reclamation, Glen Canyon Environmental Studies, National Park Service cooperative agreement no. CA 8006-8-0002 with Northern Arizona University, p. 228–293, accessed May 21, 2022, at http://www.riversimulator.org/Resources/GCMRC/PhysicalResources/beus1993.pdf.

Cluer, B.L., 1995, Cyclic fluvial bias in environmental monitoring, Colorado River in Grand Canyon: Journal of Geology, v. 103, p. 411–421, accessed May 21, 2022, at https://www.jstor.org/stable/30071162.

Collins, B.D., Minasian, D.L., and Kayen, R., 2009, Topographic change detection at select archeological sites in Grand Canyon National Park, Arizona, 2006–2007: U.S. Geological Survey Scientific Investigations Report 2009–5116, 59 p., https://doi.org/10.3133/sir20095116.

Datacom Software Research Limited, 1997, SDR contour Software User Guide, ver. 6.0: Overland Park, Kan., Sokkia Mapping Software, Sokkia Corporation.

Davis, J.C., 2002, Statistics and Data Analysis in Geology (3d ed.): John Wiley and Sons Ltd., 638 p.

Davis, P.A., 2004, Review of results and recommendations for the GCMRC 2000–2003 remote-sensing initiative for monitoring environmental resources within the Colorado River ecosystem: U.S. Geological Survey Open-File Report 2004–1206, 73 p., https://doi.org/10.3133/ofr20041206.

Davis, P.A., 2013, Natural-color and color-infrared image mosaics of the Colorado River corridor in Arizona derived from the May 2009 airborne image collection: U.S. Geological Survey Data Series 780, https://doi.org/10.3133/ds780.

Dean, D.J., and Schmidt, J.C., 2011, The role of feedback mechanisms in historic channel changes of the lower Rio Grande in the Big Bend region: Geomorphology, v. 126, nos. 3–4, p. 333–349, https://doi.org/10.1016/j.geomorph.2010.03.009.

Dean, D.J., and Topping, D.J., 2019, Geomorphic change and biogeomorphic feedbacks in a dryland river—The Little Colorado River, Arizona, USA: Geological Society of America Bulletin, v. 131, nos. 11–12, 23 p., https://doi.org/10.1130/B35047.1.

Dean, D.J., Topping, D.J., Grams, P.E., Walker, A.E., and Schmidt, J.C., 2020, Does channel narrowing by floodplain growth necessarily indicate sediment surplus? Lessons from sediment transport analyses in the Green and Colorado Rivers, Canyonlands, Utah: Journal of Geophysical Research Earth Surface, v. 125, no. 11, 30 p., https://doi.org/10.1029/2019JF005414.

Dean, D.J., Topping, D.J., Schmidt, J.C., Griffiths, R.E., and Sabol, T.A., 2016, Sediment supply versus local hydraulic controls on sediment transport and storage in a river with large sediment loads: Journal of Geophysical Research Earth Surface, v. 121, no. 1, p. 82–110, https://doi.org/10.1002/2015JF003436.

Dexter, L.R., and Cluer, B.L., 1999, Cyclic erosional instability of sandbars along the Colorado River, Grand Canyon, Arizona: Annals of the Association of American Geographers, v. 89, no. 2, p. 238–266, https://org/10.1111/1467-8306.00144.

Dodrill, M.J., Yackulic, C.B., Gerig, B., Pine, W.E., III, Korman, J., and Finch, C., 2015, Do management actions to restore rare habitat benefit native fish conservation? Distribution of juvenile native fish among shoreline habitats of the Colorado River: River Research and Applications, v. 31, no. 10, p. 1203–1217, https://doi.org/10.1002/rra.2842.

Dolan, R., 1981, Analysis of the erosion trends of the sedimentary deposits in Grand Canyon: Durango, Colo., Report submitted to the Bureau of Reclamation, Water and Power Resources Service, Coastal Research Associates, ASIN B0006Y1E1Y, 22 p.

Dolan, R., Howard, A., and Gallenson, A., 1974, Man's impact on the Colorado River in Grand Canyon: American Scientist, v. 62, no. 4, p. 392–401, accessed March 20, 2013, at https://www.jstor.org/stable/27844987.

Doyle, D.R., 1994, Development of the National Spatial Reference System: National Oceanic and Atmospheric Administration, National Geodetic Survey, accessed May 23, 2022, at http://www.ngs.noaa.gov/PUBS_LIB/develop_NSRS.html.

Draut, A.E., 2012, Effects of river regulation on aeolian landscapes, Colorado River, southwestern USA: Journal of Geophysical Research Earth Surface, v. 117, no. F2, https://doi.org/10.1029/2011JF002329.

Draut, A.E., Rubin, D.M., Dierker, J.L., Fairley, H.C., Griffiths, R.E., Hazel, J.E., Jr., Hunter, R.E., Kohl, K., Leap, L.M., Nials, F.L., Topping, D.J., and Yeatts, M., 2008, Application of sedimentary-structure interpretation to geoarchaeological studies in the Colorado River corridor, Grand Canyon, Arizona, USA: Geomorphology, v. 101, no. 3, p. 497–509, https://doi.org/10.1016/j.geomorph.2007.04.032.

Durning, L.E., Sankey, J.B., Davis, P.A., and Sankey, T.T., 2016, Four-band image mosaic of the Colorado River corridor downstream of Glen Canyon Dam in Arizona, derived from the May 2013 airborne image acquisition: U.S. Geological Survey Data Series 1027, https://doi.org/10.3133/ds1027.

East, A.E., Collins, B.D., Sankey, J.B., Corbett, S.C., Fairley, H.C., and Caster, J.J., 2016, Conditions and processes affecting sand resources at archeological sites in the Colorado River corridor below Glen Canyon Dam, Arizona: U.S. Geological Survey Professional Paper 1825, 104 p., https://doi.org/10.3133/pp1825.

Federal Geographic Data Committee (FGDC), 1998, Geospatial positioning accuracy standards, Part 3—National standard for spatial data accuracy: Federal Geographic Data Committee, FGDC–STD–007.3–1998, accessed May 17, 2021, at https://www.fgdc.gov/standards/projects/accuracy/part3/index_html.

Ferrari, R., 1987, Sandy beach area survey along the Colorado River in the Grand Canyon National Park—Glen Canyon Dam environmental study: Durango, Colo., U.S. Geological Survey, Bureau of Reclamation, prepared in cooperation with the Glen Canyon Environmental Studies, no. PB88–183389, GCES/06/87, 15 p.

Friedman, J. M., Osterkamp, W.R., and Lewis, W.M., Jr., 1996, The role of vegetation and bed-level fluctuations in the process of channel narrowing: Geomorphology, v, 14, no. 4, p. 341–351, https://doi.org/10.1016/0169-555X(95)00047-9.

Gaeuman, D.A., Schmidt, J.C., and Wilcock, P.R., 2005, Complex channel responses to changes in stream flow and sediment supply on the lower Duchesne River, Utah: Geomorphology, v. 64, nos. 3–4, p. 185–206, https://doi.org/10.1016/j.geomorph.2004.06.007.

Graf, W.L., 1987, Late Holocene sediment storage in canyons of the Colorado Plateau: Geological Society of America Bulletin, v. 99, no. 2, p. 261–271, https://doi.org/10.1130/0016-7606(1987)99%3C261:LHSSIC%3E2.0.CO;2.

Grams, P.E., Hazel, J.E., Jr., Kaplinski, M., Ross, R.P., Hamill, D., Hensleigh, J., and Gushue, T., 2020, Long-term sandbar monitoring data along the Colorado River in Marble and Grand Canyons, Arizona: U.S. Geological Survey data release, https://doi.org/10.5066/P93F8JJK.

Grams, P.E., and Schmidt, J.C., 1999, Geomorphology of the Green River in the eastern Uinta Mountains, Dinosaur National Monument, Colorado and Utah, *in* Miller, A.J., Gupta, A., eds., Varieties of fluvial form: John Wiley & Sons Ltd., p. 81–111.

Grams, P.E., and Schmidt, J.C., 2005, Equilibrium or indeterminate? Where sediment budgets fail—Sediment mass balance and adjustment of channel form, Green River downstream from Flaming Gorge Dam, Utah and Colorado: Geomorphology, v. 71, nos. 1–2, p. 156–181, https://doi.org/10.1016/j.geomorph.2004.10.012.

Grams, P.E., Schmidt, J.C., and Andersen, M.E., 2010, 2008 high-flow experiment at Glen Canyon Dam—Morphologic response of eddy-deposited sandbars and associated aquatic backwater habitats along the Colorado River in Grand Canyon National Park: U.S. Geological Survey Open-File Report 2010–1032, 73 p., https://doi.org/10.3133/ofr20101032.

Grams, P.E., Schmidt, J.C., and Topping, D.J., 2007, The rate and pattern of bed incision and bank adjustment on the Colorado River in Glen Canyon downstream from Glen Canyon Dam, 1956–2000: Geological Society of America Bulletin, v. 119, nos. 5–6, p. 556–575, https://doi.org/10.1130/B25969.1.

Grams, P.E., Topping, D.J., Schmidt, J.C., Hazel, J.E., Jr., and Kaplinski, M., 2013, Linking morphodynamic response with sediment mass balance on the Colorado River in Marble Canyon—Issues of scale, geomorphic setting, and sampling design: Journal of Geophysical Research Earth Surface, v. 118, no. 2, p. 361–381, https://doi.org/10.1002/jgrf.20050.

Grams, P.E., Tusso, R.B., and Buscombe, D., 2018a, Automated remote cameras for monitoring alluvial sandbars on the Colorado River in Grand Canyon, Arizona: U.S. Geological Survey Open-File Report 2018–1019, 50 p., https://doi.org/10.3133/ofr20181019.

Grams, P.E., Buscombe, D., Topping, D.J., Kaplinski, M.A., and Hazel, J.E., Jr., 2018b, How many measurements are required to construct an accurate sand budget in a large river? Insights from analyses of signal and noise: Earth Surface Processes and Landforms, v. 44, no. 1, p. 160–178, https://doi.org/10.1002/esp.4489.

Grams, P.E., and Wilcock, P.R., 2007, Entrainment of fine sediment into suspension over a coarse immobile bed in equilibrium transport: Water Resources Research, v. 43, no. 10, https://doi.org/10.1029/2006WR005129.

Gran, K., and Paola, C., 2001, Riparian vegetation controls on braided stream dynamics: Water Resources Research, v. 37, no. 12, p. 3275–3283, https://doi.org/10.1029/2000WR000203.

Grant, G.E., Schmidt, J.C., and Lewis, S.L., 2003, A geological framework for interpreting the downstream effects of dams on rivers, *in* O'Connor, J.E., and Grand, G.E., eds., A peculiar river—Geology, geomorphology, and hydrology of the Deschutes River, Oregon: Water Science and Application Series, v. 7, American Geophysical Union, p. 209–225, accessed March 14, 2017, at https://2bh2.pbworks.com/f/DownstreamEffectsDams.pdf.

Griffiths, R.E., Topping, D.J., Anderson, R.S., Hancock, G.S., and Melis, T.S., 2014, Design of a sediment-monitoring gaging network on ephemeral tributaries of the Colorado River in Glen, Marble, and Grand Canyons, Arizona: U.S. Geological Survey Open File Report 2014–1137, 21 p., https://doi.org/10.3133/ofr20141137.

Gushue, T.M., 2019, Colorado River Mile System, Grand Canyon, Arizona: U.S. Geological Survey data release, https://doi.org/10.5066/P9IRL3GV.

Hadley, D.R., Grams, P.E., and Kaplinski, M., 2018, Quantifying geomorphic and vegetation change at sandbar campsites in response to flow regulation and controlled floods, Grand Canyon National Park, Arizona: River Research and Applications, v. 34, no. 9, p. 1208–1218, https://doi.org/10.1002/rra.3349.

Hadley, D.R., Grams, P.E., Kaplinski, M., Hazel, J.E., Jr., and Parnell, R.A., 2017, Geomorphology and vegetation change at Colorado River campsites, Marble and Grand Canyons, Arizona: U.S. Geological Survey Scientific Investigations Report 2018–5096, 64 p., https://doi.org/10.3133/sir20175096.

Hazel, J.E., Jr., Grams, P.E., Schmidt, J.C., and Kaplinski, M., 2010, Sandbar response in Marble and Grand Canyons, Arizona, following the 2008 high-flow experiment on the Colorado River: U.S. Geological Survey Scientific Investigations Report 2010–5015, 52 p., https://doi.org/10.3133/sir20105015.

Hazel J.E., Jr., Kaplinski, M., Parnell, R.A., Kohl, K., and Schmidt, J.C., 2008, Monitoring fine-grained sediment in the Colorado River Ecosystem, Arizona—Control network and conventional survey techniques: U.S. Geological Survey Open-File Report 2008–1276, 15 p., https://doi.org/10.3133/ofr20081276.

Hazel, J.E., Jr., Kaplinski, M., Parnell, R., and Manone M., 2000, Sand deposition in the Colorado River ecosystem from flooding of the Paria River and the effects of the November 1997, Glen Canyon Dam Test Flow—Final Report: Flagstaff, Ariz., Northern Arizona University, Grand Canyon Monitoring and Research Center, 37 p., accessed May 24, 2022, at https://www.library.nps.gov/vufind/Record/npsLibris_204530-01930.

Hazel, J.E., Jr., Kaplinski, M., Parnell, R., Manone, M., and Dale, A., 1999, Topographic and bathymetric changes at thirty-three long-term study sites, *in* Webb, R.H., Schmidt, J.C., Marzolf, G.R., and Valdez, R.A., eds., The controlled flood in Grand Canyon: American Geophysical Union Geophysical Monograph Series, v. 110, p. 161–183, https://doi.org/10.1029/GM110p0161.

Hazel, J.E., Jr., Kaplinski, M., Parnell, R., Kohl, K., and Topping, D.J., 2006a, Stage-discharge relations for the Colorado River in Glen, Marble, and Grand Canyons, Arizona: U.S. Geological Survey Open-File Report 2006–1243, 7 p., https://doi.org/10.3133/ofr20061243.

Hazel, J.E., Jr., Topping, D.J., Schmidt, J.C., and Kaplinski, M., 2006b, Influence of a dam on fine-sediment storage in a canyon river: Journal of Geophysical Research Earth Surface, v. 111, no. F1, p. 1–16, https://doi.org/10.1029/2004JF000193.

Hereford, R., Fairley, H.C., Thompson, K.S., and Balsom, J.R., 1993, Surficial geology, geomorphology, and erosion of archaeologic sites along the Colorado River, eastern Grand Canyon, Grand Canyon National Park: U.S. Geological Survey Open-File Report, 93–517, 46 p., https://doi.org/10.3133/ofr93517.

Howard, A.D., 1975, Establishment of benchmark study sites along the Colorado River in Grand Canyon National Park for monitoring of beach erosion caused by natural forces and human impact: University of Virginia Grand Canyon Study, submitted to the Grand Canyon National Park, National Park Service, technical report no. 1, 182 p. [Available at the Northern Arizona University Cline Library, Special Collections, F788. C6856 1975.]

Howard, A., and Dolan, R., 1979, Changes in the fluvial deposits of the Colorado River in the Grand Canyon caused by Glen Canyon Dam, *in* Linn, R.M., ed., Proceedings of the First Conference on Scientific Research in the National Parks, November 9–12, 1976, New Orleans, La., Volume II: U.S. National Park Service Transactions and Proceedings no. 5, p. 845–851, accessed February 21, 2015, at https://babel.hathitrust.org/cgi/pt?id=uc1.31210024881763&view=1up&seq=1.

Howard, A., and Dolan, R., 1981, Geomorphology of the Colorado River in the Grand Canyon: Journal of Geology, v. 89, no. 3, p. 269–298, http://doi.org/10.1086/628592.

Ingram, H., Tarlock, D.A., and Oggins, C.R., 1991, The law and politics of the operation of Glen Canyon Dam, *in* Marzolf, G.R., ed., Colorado River ecology and dam management, Proceedings of a Symposium, May 24–25, 1990, Santa Fe, New Mex.: Washington, D.C., National Academies Press, p. 10–27, accessed March May 23, 2022, at https://www.nap.edu/catalog/1832.html.

Kaplinski, M., Behan, Hazel, J.E., Jr., Parnell, R.A., and Fairley, H.C., 2005, Recreational values and campsites in the Colorado River ecosystem, *in* Gloss, S.P., Lovich, J.E., and Melis, T.S., eds., The state of the Colorado River ecosystem in Grand Canyon: U.S. Geological Survey Circular 1282, p. 193–205, https://doi.org/10.3133/cir1282.

Kaplinski, M., Hazel, J.E., Jr., and Beus, S.S., 1995, Monitoring the effects of interim flows from Glen Canyon Dam on sand bars in the Colorado River corridor, Grand Canyon National Park, Arizona, Final Report, Volume 2: Flagstaff, Ariz., Northern Arizona University, Glen Canyon Environmental Studies, Bureau of Reclamation, 62 p., accessed May 24, 2022, at https://www.library.nps.gov/vufind/Record/npsLibris_204552-02131.

Kaplinski, M., Hazel, J.E., Jr., Grams, P.E., Kohl, K., Buscombe, D.D., and Tusso, R.B., 2017, Channel mapping river miles 29–62 of the Colorado River in Grand Canyon National Park, Arizona, May 2009: U.S. Geological Survey Open-File Report 2017–1030, 35 p., https://doi.org/10.3133/ofr20171030.

Kaplinski, M., Hazel, J.E., Jr., and Parnell, R.A., 2010, Colorado River campsite monitoring, 1998–2006, Grand Canyon National Park, Arizona, *in* Melis, T.S., Hamill, J.F., Bennet, G.E., Coggins, L.C., Jr., Grams, P.E., Kennedy, T.A., Kubly, D.M., and Ralston, B.E., eds., Proceedings of the Colorado River Basin Science and Resource Management Symposium, November 18–20, 2009, Scottsdale, Arizona: U.S. Geological Survey Scientific Investigations Report 2010–5135, p. 275–284, https://doi.org/10.3133/sir20105135.

Kaplinski, M., Hazel, J.E., Jr., Parnell, R., Breedlove, M., Kohl, K, and Gonzales, M., 2009, Monitoring fine-sediment volume in the Colorado River ecosystem, Arizona: Bathymetric survey techniques: U.S. Geological Survey Open-File Report 2009–1207, 33 p., https://doi.org/10.3133/ofr20091207.

Kaplinski, M., Hazel, J.E., Jr., Parnell, R., Hadley, D.R., and Grams, P.E., 2014, Colorado River campsite monitoring, Grand Canyon National Park, Arizona, 1998–2012: U.S. Geological Survey Open-File Report 2014–1161, 24 p., https://doi.org/10.3133/ofr20141161.

Kasprak, A., Sankey, J.B., Buscombe, D., Caster, J., East, A.E., and Grams, P.E., 2018, Quantifying and forecasting changes in the areal extent of river valley sediment in response to altered hydrology and land cover: Progress in Physical Geography, Earth and Environment, v. 42, no. 6, p. 739–764, https://doi.org/10.1177/0309133318795846.

Kearsley, L.H., and Warren, K.W., 1993, River campsites in Grand Canyon National Park—Inventory and effects of discharge on campsite size and availability: National Park Service Division of Resource Management, Grand Canyon National Park, 65 p., accessed May 24, 2022, at https://www.library.nps.gov/vufind/Record/npsLibris_209980-01442.

Kearsley, L.H., Schmidt, J.C., and Warren, K.D., 1994, Effects of Glen Canyon Dam on Colorado River sand deposits used as campsites in Grand Canyon National Park, USA: Regulated Rivers—Research and Management, v. 9, no. 3, p. 137–149, https://doi.org/10.1002/rrr.3450090302.

Kearsley, M.J.C., and Ayers, T.J., 1996, The effects of interim flows from Glen Canyon Dam on riparian vegetation in the Colorado River corridor, Grand Canyon National Park, Arizona, Final report: Flagstaff, Ariz., Northern Arizona University Grand Canyon National Park, Grand Canyon Science Center, cooperative agreement no. 8041–8–0002, 39 p., accessed May 25, 2022, at http://www.riversimulator.org/Resources/GCMRC/Terrestrial/Kearsley1996b.pdf.

Kearsley, M.J.C., and Ayers, T.J., 1999, Riparian vegetation responses—Snatching defeat from the jaws of victory and vice versa, *in* Webb, R.H., Schmidt, J.C., Marzolf, G.R., and Valdez, R.A., eds., The controlled flood in Grand Canyon: American Geophysical Union Geophysical Monograph Series, v. 110, p. 309–327, https://doi.org/10.1029/GM110p0309.

Kochel, C.R., 1988, Geomorphic impact of large floods—Review and new perspectives on magnitude and frequency, *in* Baker, V.R., Kochel, C.R., and Patton, P.C., eds., Flood Geomorphology: New York, John Wiley, p. 169–187.

Korman, J., Wiele, S.M., and Torizzo, M., 2004, Modeling effects of discharge on habitat quality and dispersal of juvenile humpback chub (*Gila cypha*) in the Colorado River, Grand Canyon: River Research and Applications v. 20, no. 4, p. 379–400, https://doi.org/10.1002/rra.749.

Leopold, L.B., 1969, The rapids and the pools—Grand Canyon, chap. D *of* The Colorado River region and John Wesley Powell: U.S. Geological Survey Professional Paper 669–D, p. 129–145, https://doi.org/10.3133/pp669D.

Magirl, C.S, Breedlove, M.J., Webb, R.H., and Griffiths, P., 2008, Modeling water-surface elevations and virtual shorelines for the Colorado River in Grand Canyon, Arizona: U.S. Geological Survey Scientific Investigations Report 2008–5075, 32 p., https://doi.org/10.3133/sir20085075.

Manners, R.B., Schmidt, J.C., and Scott, M.L., 2014, Mechanisms of vegetation-induced channel narrowing of an unregulated canyon river—Results from a natural field-scale experiment: Geomorphology, v. 211, p. 100–115, https://doi.org/10.1016/j.geomorph.2013.12.033.

Maune, D.F., Kopp, S.M., Crawford, C.A., and Zervas, C.E., 2007, Introduction, *in* Maune, D.F., ed., Digital Elevation Model technologies and applications—The DEM users manual (2d ed.): Bethesda, Md., American Society for Photogrammetry and Remote Sensing, p. 1–35.

Melis, T.S., Webb, R.H., Griffiths, P.G., and Wise, T.J., 1994, Magnitude and frequency data for historic debris flows in Grand Canyon National Park and vicinity, Arizona: U.S. Geological Survey Water-Resources Investigations Report 96–4214, 285 p. https://doi.org/10.3133/wri944214.

Milbert, D.G., and Smith, D.A., 1996, Converting GPS heights into NAVD elevation with the GEOID96 geoid height model: National Geodetic Survey, National Oceanic and Atmospheric Administration, accessed May 24, 2022, at http://www.ngs.noaa.gov/PUBS_LIB/gislis96.html.

Mueller, E.R., Grams, P.E., Hazel, J.E., Jr., and Schmidt, J.C., 2018, Variability in eddy sandbar dynamics during two decades of controlled flooding of the Colorado River in Grand Canyon: Sedimentary Geology, v. 363, p. 181–199, https://doi.org/10.1016/j.sedgeo.2017.11.007.

Mueller, E.R., Grams, P.E., Schmidt, J.C., Hazel, J.E., Jr., Alexander, J.S., and Kaplinski, M., 2014a, The influence of controlled floods on fine sediment storage in debris fan-affected canyons of the Colorado River basin: Geomorphology, v. 226, p. 65–75, https//doi.org/10.1016/j.geomorph.2014.07.029.

Mueller, E.R., Grams, P.E., Schmidt, J.C., Hazel, J.E., Jr., Kaplinski, M.A., Alexander, J.A., and Kohl, K., 2014b, Monitoring and research to describe geomorphic effects of the 2011 controlled flood on the Green River in the Canyon of Lodore, Dinosaur National Monument, Colorado and Utah: U.S. Geological Survey Scientific Investigations Report 2014–5022, 66 p., https://doi.org/10.3133/sir20145022.

Mueller, E.R., Hazel, J.E., Jr., Ross, R.P., and Grams, P.E., 2017, Colorado River eddy sandbar dynamics data: U.S. Geological Survey data release, https://doi.org/10.5066/F7HD7SSW.

Nanson, G.C., 1986, Episodes of vertical accretion and catastrophic stripping—A model of disequilibrium floodplain development: Geological Society of America Bulletin, v. 97, no. 12, p. 1467–1475., https://doi.org/10.1130/0016-7606(1986)97%3C1467:EOVAAC%3E2.0.CO;2.

National Park Service, 2006, Colorado River management plan: National Park Service, Office of Planning and Compliance, Grand Canyon National Park, 35 p., accessed November May 25, 2022, at https://www.nps.gov/grca/learn/management/upload/CRMPIF_s.pdf.

National Research Council, 1996, River resource management in the Grand Canyon: Washington, D.C., National Academies Press, 226 p., https://doi.org/10.17226/5148.

National Research Council, 1999, Downstream—Adaptive management of Glen Canyon Dam and the Colorado River Ecosystem: Washington, D.C., National Academy Press, 230 p., https://doi.org/10.17226/9590.

Palmquist, E.C., Ralston, B.E., Sarr, D.A., and Johnson, T. C., 2018, Monitoring riparian vegetation composition and cover along the Colorado River downstream of Glen Canyon Dam, Arizona: U.S. Geological Survey Techniques and Methods, book 2, chap. 14A, 65 p., https://doi.org/10.3133/tm2A14.

Patten, D.T., 1991, Glen Canyon environmental studies research program—Past, present, and future, *in* Marzolf, G.R., ed., Colorado River ecology and dam management, Proceedings of a Symposium, May 24–25, 1990, Santa Fe, New Mex.: Washington, D.C., National Academies Press, p. 85–104, https://doi.org/10.17226/1832.

Patten, D.T., Harpman, D.A., Voita, M.I., and Randle, T.J., 2001, A managed flood on the Colorado River—Background, objectives, design, and implementation: Ecological Applications, v. 11, no. 3, p. 635–643, https://doi.org/10.1890/1051-0761(2001)011[0635:AMFOTC]2.0.CO;2.

Pederson, J.L., Petersen, P.A. and Dierker, J.L., 2006, Gullying and erosion control at archaeological sites in Grand Canyon, Arizona: Earth Surfaces Processes and Landforms, v. 31, no. 4, p. 507–525, https://doi.org/10.1002/esp.1286.

Pemberton, E.L., 1976, Channel changes in the Colorado River below Glen Canyon Dam, *in* Proceedings of the third Federal Interagency Sedimentation Conference, 1976—March 22–25, 1976, Denver, Colo. Symposium 5—Channel adjustments: Water Resources Council, Sedimentation Committee, p. 5–61—5–73, accessed July 12, 2014, at https://babel.hathitrust.org/cgi/pt?id=mdp.39015027830804&view=1up&seq=5&skin=2021.

Peuker, T.K., Fowler, R.J., Little, J.J., and Mark, D.M., 1978, The triangulated irregular network—Proceedings of the digital terrain models (DTM) Symposium: St. Louis, Mo., American Society of Photogrammetry, p. 516–540, accessed May 25, 2022, at https://www.cartogis.org/docs/proceedings/archive/auto-carto-4-vol-2/pdf/the-triangulated-irregular-network.pdf.

Phillips, B.G., Johnson, R.A., Phillips, A.M., III, and Brian, N.J., 1986, Monitoring the effects of recreational use on Colorado River beaches in Grand Canyon National Park: Flagstaff, Ariz., Museum of Northern Arizona Press, Museum of Northern Arizona Bulletin 55, 131 p., accessed May 26, 2022, at https://shopmusnaz.org/search?type=product&q=bulletin+55.

Pollen-Bankhead, N., Simon, A., Jaeger, K., and Wohl, E., 2009, Destabilization of streambank by removal of invasive species in Canyon de Chelly National Monument, Arizona: Geomorphology, v. 103, no. 3, p. 363–374, https://doi.org/10.1016/j.geomorph.2008.07.004.

Ralston, B.E., 2010, Riparian vegetation response to the March 2008 short-duration, high-flow experiment—Implications of timing and frequency of flood disturbance on nonnative plant establishment along the Colorado River below Glen Canyon Dam: U.S. Geological Survey Open-File Report 2010–1022, 30 p., https://doi.org/10.3133/ofr20101022.

Ralston, B.E., 2011, Summary report of responses of key resources to the 2000 low steady summer flow experiment, along the Colorado River downstream from Glen Canyon Dam, Arizona: U.S. Geological Survey Open-File Report 2011–1220, 129 p., https://doi.org/10.3133/ofr20111220.

Ralston, B.E., and Sarr, D.A., 2017, Case studies of riparian and watershed restoration in the southwestern United States—Principles, challenges, and successes: U.S. Geological Survey Open-File Report 2017–1091, 116 p., https://doi.org/10.3133/ofr20171091.

Randle, T.J., Strand, R.I., and Streifel, A., 1993, Engineering and environmental consideration of Grand Canyon sediment management, *in* Engineering solutions to environmental challenges—13th annual United States Committee on Large Dams (USCOLD) Annual lecture series, Proceedings, Chattanooga, Tennessee, May 1993: U.S. Committee on Large Dams, p. 1–13. [Available at Bureau of Reclamation Library, call no. TC 540 .E56 1993.]

Rossi, R.K., 2018, Evaluation of 'structure-from-motion' from a pole-mounted camera for monitoring geomorphic change: Logan, Utah, Utah State University, M.S. thesis, 211 p., https://doi.org/10.26076/78fc-a4c4.

Rubin, D.M., and Topping, D.J., 2001, Quantifying the relative importance of flow regulation and grain-size regulation of suspended-sediment transport α, and tracking changes in bed-sediment grain size β: Water Resources Research, American Geophysical Union, v. 37, no. 1, p. 133–146, https://doi.org/10.1029/2000WR900250.

Rubin, D.M., and Topping, D.J., 2008, Correction to "Quantifying the relative importance of flow regulation and grain-size regulation of suspended-sediment transport α, and tracking changes in bed-sediment grain size β": Water Resources Research, American Geophysical Union, v. 44, no. 9, 5 p., https://doi.org/10.1029/2008WR006819h.

Rubin, D.M., Anima, R.A., and Sanders, R., 1994, Measurements of sand thickness in Grand Canyon, Arizona, and a conceptual model for characterizing changes in sand bar volume through time and space: U.S. Geological Survey Open-File Report 94–597, 9 p., https://doi.org/10.3133/ofr94597.

Rubin, D.M., Buscombe, D., Wright, S.A., Topping, D.J., Grams, P.E., Schmidt, J.C., Hazel, J.E., Jr., Kaplinski, M.A., and Tusso, R., 2020, Causes of variability in suspended-sand concentration evaluated using measurements in the Colorado River in Grand: Journal of Geophysical Research Earth Surface, v. 125, no. 9, https://doi.org/10.1029/2019JF005226.

Rubin, D.M., Nelson, J.M., and Topping, D.J., 1998, Relation of inversely graded deposits to suspended-sediment grain-size evolution during the 1996 flood experiment in Grand Canyon: Geology, v. 26, no. 2, p. 99–102, https://doi.org/10.1130/0091-7613(1998)026%3C0099:ROIGDT%3E2.3.CO;2.

Rubin, D.M., Schmidt, J.C., and Moore, J.N., 1990, Origin, structure, and evolution of a reattachment bar, Colorado River, Grand Canyon, Arizona: Journal of Sedimentary Research, v. 60, no. 6, p. 982–991, https://doi.org/10.1306/D426765E-2B26-11D7-8648000102C1865D.

Rubin, D.M., Topping, D.J., Chezar, H., Hazel, J.E., Schmidt, J.C., Breedlove, M., Melis, T.S., and Grams, P.E., 2010, 20,000 grain-size observations from the bed of the Colorado River and implications for sediment transport through Grand Canyon, *in* Hydrology and sedimentation for a changing future—Existing and emerging issues, Proceedings of the Joint Federal Interagency Conference 2010, 4th Federal Interagency Hydrologic Modeling Conference, and 9th Federal Interagency Sedimentation Conference, Las Vegas, Nev., June 27–July 1, 2010: Advisory Committee on Water Information, Subcommittee on Sedimentation, accessed January 12, 2014, at https://acwi.gov/sos/pubs/2ndJFIC/Contents/3C_Rubin_03_08_10.pdf.

Rubin, D.M., Topping, D.J., Schmidt, J.C., Hazel, J., Kaplinski, M., and Melis, T.S., 2002, Recent sediment studies refute Glen Canyon Dam hypothesis: EOS, Transactions, American Geophysical Union, v. 83, no. 25, p. 273–278, https://doi.org/10.1029/2002EO000191.

Saleh, R.A., Chayes, D.N., Dasler, J.L., Doyle, D.R., D'Sanchez, R., Renslow, M.S., and Rose, J.J., 2003, Survey protocol evaluation program—Survey PEP report: U.S Geological Survey, Grand Canyon Monitoring Research Center, Final report to the Grand Canyon Monitoring and Research Program. [This report is available from the U.S. Geological Survey Grand Canyon Monitoring Research Center library.]

Sankey, J.B., and Draut, A.E., 2014, Gully annealing by aeolian sediment—Field and remote-sensing investigation of aeolian–hillslope–fluvial interactions, Colorado River corridor, Arizona, USA: Geomorphology, v. 220, pp. 68–80, https://doi.org/10.1016/j.geomorph.2014.05.028.

Sankey, J.B., Ralston, B.E., Grams, P.E., Schmidt, J.C., and Cagney, L.E., 2015, Riparian vegetation, Colorado River, and climate—Five decades of spatiotemporal dynamics in the Grand Canyon with river regulation: Journal of Geophysical Research Biogeosciences, v. 120, no. 8, p. 1532–1547, https://doi.org/10.1002/2015JG002991.

Schmidt, J.C., 1990, Recirculating flow and sedimentation in the Colorado River in Grand Canyon, Arizona: Journal of Geology, v. 98, no. 5, p. 709–724, https://doi.org/10.1086/629435.

Schmidt, J.C., 1999, Summary and synthesis of geomorphic studies conducted during the 1996 controlled flood in Grand Canyon, *in* Webb, R.H., Schmidt, J.C., Marzolf, G.R., and Valdez, R.A., eds., The controlled flood in Grand Canyon: American Geophysical Union Geophysical Monograph Series, v. 110, p. 329–341, https://doi.org/10.1029/GM110p0329.

Schmidt, J.C., and Graf, J.B., 1990, Aggradation and degradation of alluvial sand deposits, 1965 to 1986, Colorado River, Grand Canyon National Park, Arizona: U.S. Geological Survey Professional Paper 1493, 74 p., https://doi.org/10.3133/pp1493.

Schmidt, J.C., and Grams, P.E., 2011a, Understanding physical processes of the Colorado River, chap. 2 *of* Melis, T.S., ed., Effects of three high-flow experiments on the Colorado River ecosystem downstream from Glen Canyon Dam, Arizona: U.S. Geological Survey Circular 1366, p. 17–51, https://doi.org/10.3133/cir1366.

Schmidt, J.C., and Grams, P.E., 2011b, The High flows—Physical science results, chap. 3 *of* Melis, T.S., ed., Effects of three high-flow experiments on the Colorado River ecosystem downstream from Glen Canyon Dam, Arizona: U.S. Geological Survey Circular 1366, p. 53–91, https://doi.org/10.3133/cir1366.

Schmidt, J.C., Grams, P.E., and Leschin, M.F., 1999, Variation and magnitude and style of deposition and erosion in three long (8–12 km) reaches as determined by photographic analyses, *in* Webb, R.H., Schmidt, J.C., Marzolf, G.R., and Valdez, R.A., eds., The controlled flood in Grand Canyon: American Geophysical Union Geophysical Monograph Series, v. 110, p. 185–204, https://doi.org/10.1029/GM110p0185.

Schmidt, J.C., Grams, P.E., and Webb, R.H., 1995, Comparison of the magnitude of erosion along two large regulated rivers: Journal of the American Water Resources Association (JAWRA) v. 31, no. 4, p. 617–630, https://doi.org/10.1111/j.1752-1688.1995.tb03389.x.

Schmidt, J.C., and Rubin, D.M., 1995, Regulated streamflow, fine-grained deposits, and effective discharge in canyons with abundant debris fans, *in* Costa, J.E., Miller, A.J., Potter, K.W., and Wilcock, P.R., eds., Natural and anthropogenic influences in fluvial geomorphology: American Geophysical Union Geophysical Monograph Series, v. 89, p. 177–195, https://doi.org/10.1029/GM089p0177.

Schmidt, J.C., Topping, D.J., Rubin, D.M., Hazel, J.E., Jr., Kaplinski, M., Wiele, S.M., and Goeking, S.A., 2007, Streamflow and sediment data collected to determine the effects of low summer steady flows and habitat maintenance flows in 2000 on the Colorado River between Lees Ferry and Bright Angel Creek, Arizona: U.S. Geological Survey Open-File Report 2007–1268, 79 p., https://doi.org/10.3133/ofr20071268.

Schmidt, J.C., Topping, D.J., Grams, P.E., and Hazel, J.E., 2004, System-wide changes in the distribution of fine sediment in the Colorado River corridor between Glen Canyon Dam and Bright Angel Creek, Arizona—Final report: Logan, Utah, Utah State University, prepared for U.S. Geological Survey Grand Canyon Monitoring and Research Center, cooperative agreement no. 1425–98–FC–22640, 107 p., accessed May 26, 2022, at http://www.riversimulator.org/Resources/GCMRC/PhysicalResources/Schmidt2004.pdf.

Schmidt, J.C., and Wilcock, P.R., 2008, Metrics for assessing the downstream effects of dams: American Geophysical Union, Water Resources Research, v. 44, no. 4, p. 1–19, https://doi.org/10.1029/2006WR005092.

Schumm, S.A., 1973, Geomorphic thresholds and complex response of drainage systems, chap. 13 *of* Morisawa, M., ed., Fluvial Geomorphology—A proceedings volume of the fourth annual geomorphology symposia series held at Binghamton, New York, September 27–28, 1973: George Allen and Unwin, Ltd., p. 299–310.

Schumm, S.A., and Parker, R.S., 1973, Implications of complex response of drainage systems for Quaternary alluvial stratigraphy: Nature Physical Science, v. 243, p. 99–100, https://doi.org/10.1038/physci243099a0.

Smillie, G.M., Jackson, W.L., and Tucker, D., 1993, Colorado River sand budget—Lees Ferry to Little Colorado River: National Park Service technical report NPS/NRWRD/NRTR–92/12, 11 p. [Available at https://www.library.nps.gov/, call no. QE571 .S65 1993 c.1-2 M.]

Stevens, L.E., 1990, The Colorado River in Grand Canyon—A comprehensive guide to its natural and human history (3d ed.): Flagstaff, Ariz., Red Lake Books, 115 p.

Stevens, L.E., Schmidt, J.C., Ayers, T.J., and Brown, B.T., 1995, Flow regulation, geomorphology, and Colorado River marsh development in the Grand Canyon, Arizona: Ecological Applications, v. 5, no. 4, p. 1025–1039, accessed April 21, 2017, at http://doi.org/10.2307/2269352.

Stewart, W., Larkin, K., Orland, B., and Anderson, D., 2003, Boater preferences for beach characteristics downstream from Glen Canyon Dam, Arizona: Journal of Environmental Management, v. 69, no. 2, p. 201–211, https://doi.org/10.1016/j.jenvman.2003.08.001.

Tal, M., and Paola, C., 2007, Dynamic single-thread channels maintained by the interaction of flow and vegetation: Geology, v. 35, no. 4, p. 347–350, https://doi.org/10.1130/G23260A.1.

Topping, D.J., 1997, Physics of flow, sediment transport, hydraulic geometry, and channel geomorphic adjustment during flash floods in an ephemeral river, the Paria River, Utah and Arizona: Seattle, Wash., University of Washington, Ph.D. dissertation, 406 p. [Available at the University of Washington Suzzalo and Allen Libraries, QE 3 Th46044.]

Topping, D.J., Grams, P.E., Griffiths, R.E., Dean, D.J., Wright, S.A., and Unema, J.A., 2020, Self-limitation of sand storage in a bedrock-canyon river arising from the interaction of flow and grain size: Journal of Geophysical Research Earth Surface, v. 126, no. 5, https://doi.org/10.1029/2020JF005565.

Topping, D.J., Grams, P.E., Griffiths, R., Hazel, Jr., J.E., Kaplinski, M., Dean, D.J., Voichick, N., Unema, J., and Sabol, T., 2019, Optimal timing of high-flow experiments for sandbar deposition—High-flow experiments assessment, extended abstracts, March 2019 annual reporting meeting presentations: U.S. Bureau of Reclamation Glen Canyon Dam Adaptive Management Program, p. 3–9, accessed May 26, 2022, at https://pubs.er.usgs.gov/publication/70203738.

Topping, D.J., Mueller, E.R., Schmidt, J.C., Griffiths, R.E., Dean, D.J., and Grams, P.E., 2018, Long-term evolution of sand transport through a river network—Relative influences of a dam versus natural changes in grain size from sand waves: Journal of Geophysical Research Earth Surface, v. 123, no. 8, p. 1879–1909, https://doi.org/10.1029/2017JF004534.

Topping, D.J., Rubin, D.M., Grams, P.E., Griffiths, R.E., Sabol, T.A., Voichick, N., Tusso, R.B., Vanaman, K.M., and McDonald, R.R., 2010, Sediment transport during three controlled-flood experiments on the Colorado River downstream from Glen Canyon Dam, with implications for eddy-sandbar deposition in Grand Canyon National Park: U.S. Geological Survey Open-File Report 2010–1128, 111 p., https://doi.org/10.3133/ofr20101128.

Topping, D.J., Rubin, D.M., Nelson, J.M., Kinzel, P.J., III, and Bennett, J.P., 1999, Linkage between grain-size evolution and sediment depletion during Colorado River floods, *in* Webb, R.H., Schmidt, J.C., Marzolf, G.R., and Valdez, R.A., eds., The controlled flood in Grand Canyon: American Geophysical Union, Geophysical Monograph Series, v. 110, p. 71–98, https://doi.org/10.1029/GM110p0071.

Topping, D.J., Rubin, D.M., Schmidt, J.C., Hazel, J.E., Melis, T.S., Wright, S.A., Kaplinski, M.A., Draut, A.E., and Breedlove, M.J., 2006, Comparison of sediment-transport and bar-response results from the 1996 and 2004 controlled-flood experiments on the Colorado River in Grand Canyon, *in* Proceedings of the Eighth Federal Interagency Sedimentation Conference, April 2–6, 2006, Reno, Nev.: Advisory Committee on Water Information, p. 171–179, accessed May 27, 2022, at https://acwi.gov/sos/pubs/8thFISC/Session%201B-3_Topping.pdf.

Topping, D.J., Rubin, D.M., and Vierra, L.E., Jr., 2000, Colorado River sediment transport—1, Natural sediment limitation and the influence of Glen Canyon Dam: American Geophysical Union, Water Resources Research, v. 36, no. 2, p. 515–542, https://doi.org/10.1029/1999WR900285.

Topping, D.J., Schmidt, J.C., and Vierra, L.E., Jr., 2003, Computation and analysis of the instantaneous-discharge record for the Colorado River at Lees Ferry, Arizona—May 8, 1921, through September 30, 2000: U.S. Geological Survey Professional Paper 1677, 118 p., https://doi.org/10.3133/pp1677.

Turner, R.M., and Karpiscak, M.M., 1980, Recent vegetation changes along the Colorado River between Glen Canyon Dam and Lake Mead, Arizona: U.S. Geological Survey Professional Paper 1132, p. 115, https://doi.org/10.3133/pp1132.

Tusso, R.B., Buscombe, D., and Grams, P.E., 2015, Using oblique digital photography for alluvial sandbar monitoring and low-cost change detection, *in* Beus, S.S., and Avery, C.C, principal investigators, Proceedings of papers of the 5th Federal Interagency Hydraulic Modeling Conference and the 10th Federal Interagency Sedimentation Conference, 2015, April 19–23, 2015, Reno, Nev.: Advisory Committee on Water Information, p. 79–85, accessed May 28, 2022, at https://acwi.gov/sos/pubs/3rdJFIC/index.html.

U.S. Department of the Interior [DOI], 1995, Operation of Glen Canyon Dam—Final Environmental Impact Statement, Colorado River Storage Project, Coconino County, Arizona: Salt Lake City, Utah, Bureau of Reclamation, Upper Colorado Regional Office, 337 p., accessed November 18, 2010, at http://www.usbr.gov/uc/library/envdocs/eis/gc/pdfs/Cov-con/cov-con.pdf.

U.S. Department of the Interior [DOI], 1996, Record of Decision, operation of Glen Canyon Dam—Final Environmental Impact Statement, Appendix G: Washington, D.C., Office of the Secretary of the Interior, Bureau of Reclamation, 15 p., accessed May 26, 2010, at http://www.usbr.gov/uc/rm/amp/pdfs/sp_appndxG_ROD.pdf.

U.S. Department of the Interior [DOI], 2011, Final environmental assessment development and implementation of a protocol for high-flow experimental releases from Glen Canyon Dam, Arizona, 2011 through 2020: Salt Lake City, Utah, Bureau of Reclamation, Upper Colorado Regional Office, 150 p., accessed May 28, 2022, at https://www.usbr.gov/uc/envdocs/ea/gc/HFEProtocol/.

U.S. Department of the Interior [DOI], 2016, Record of Decision for the Glen Canyon Dam long-term experimental and management plan—Final Environmental Impact Statement: Salt Lake City, Utah, Bureau of Reclamation, Upper Colorado Regional Office, National Park Service, Lakewood, Colo., Intermountain Region, 196 p., accessed May 28, 2022, at http://ltempeis.anl.gov/documents/docs/LTEMP_ROD.pdf.

Valdez, R.A., and Ryel, R.J., 1995, Life history and ecology of the humpback chub (*Gila cypha*) in the Colorado River, Grand Canyon, Arizona—Final report: Logan, Utah, BIO/WEST, Inc., submitted to Bureau of Reclamation, Glen Canyon Environmental Studies, contract no. 0–CS–40–09110, technical report no. TR–250–08, 286 p. [Available at https://www.library.nps.gov, call no. M QL638.C94 V353 1995.]

Van Den Berg, J.H., Van Gelder, A., and Mastbergen, D.R., 2002, The importance of breaching as a mechanism of subaqueous slope failure in fine sand: Sedimentology, v. 49, no. 1, p. 81–95, https://doi.org/10.1111/j.1525-139X.2006.00168.x-i1.

Vincent, K.R., and Andrews, E.D., 2008, Depositional settings of sand beaches along whitewater rivers: River Research and Applications, v. 24, no. 6, p. 771–788, https://doi.org/10.1002/rra.1079.

Webb, R.H., 1996, Grand Canyon—A century of change—Rephotography of the 1889–1890

Stanton expedition: Tucson, Ariz., The University of Arizona Press, 290 p.

Webb, R.H., Pringle, P.T., and Rink, G.R., 1989, Debris flows from tributaries of the Colorado River, Grand Canyon National Park: U.S. Geological Survey Professional Paper 1492, 39 p., https://doi.org/10.3133/pp1492.

Webb, R.H., Schmidt, J.C., Marzolf, G.R., and Valdez, R.A., eds., 1999, The controlled flood in Grand Canyon: American Geophysical Union Geophysical Monograph Series, v. 110, 367 p., https://doi.org/10.1029/GM110.

Wiele, S.M., Andrews, E.D., and Griffin, E.R., 1999, The effect of sand concentration on depositional rate, magnitude, and location in the Colorado River Below the Little Colorado River, *in* Webb, R.H., Schmidt, J.C., Marzolf, G.R., and Valdez, R.A., eds., The controlled flood in Grand Canyon: American Geophysical Union Geophysical Monograph Series, v. 110, p. 131–145, https://doi.org/10.1029/GM110p0131.

Wiele, S.M., Graf, J.B., and Smith, J.D., 1996, Sand deposition in the Colorado River in the Grand Canyon from flooding of the Little Colorado River: American Geophysical Union, Water Resources Research, v. 32, no. 12, p. 3579–3596, https://doi.org/10.1029/96WR02842.

Wilcox, A.C., and Shafroth, P.B., 2013, Coupled hydrogeomorphic and woody-seedling responses to controlled flood releases in a dryland river: American Geophysical Union, Water Resources Research, v.49, p. 2843–2860, https://doi.org/10.1002/wrcr.20256.

Williams, G.P., and Wolman, M.G., 1984, Downstream effects of dams on alluvial rivers: U.S. Geological Survey Professional Paper 1286, 83 p., https://doi.org/10.3133/pp1286.

Wright, S.A., and Kaplinski, M., 2011, Flow structures and sandbar dynamics in a canyon river during a controlled flood, Colorado River, Arizona: Journal of Geophysical Research Earth Surface, v. 116, F01019, https://doi.org/10.1029/2009JF001442.

Wright, S.A., and Kennedy, T.A., 2011, Science-based strategies for future high-flow experiments on the Colorado River ecosystem downstream from Glen Canyon Dam, Arizona, chap. 5 *of* Melis, T.S., ed., Effects of three high-flow experiments on the Colorado River ecosystem downstream from Glen Canyon Dam, Arizona: U.S. Geological Survey Circular 1366, p. 127–147, https://doi.org/10.3133/cir1366.

Wright, S.A., Melis, T.S., Topping, D.J., and Rubin, D.M., 2005, Influence of Glen Canyon Dam operations on downstream sand resources of the Colorado River in Grand Canyon, chap. 1 *of* Gloss, S.P., Lovich, J.E., and Melis, T.S., eds., The state of the Colorado River ecosystem in Grand Canyon: U.S. Geological Survey Circular 1282, p. 17–31, https://doi.org/10.3133/cir1282.

Wright, S.A., Schmidt, J.C., Melis, T.S., Topping, D.J., and Rubin, D.M., 2008, Is there enough sand? Evaluating the fate of Grand Canyon sandbars: Geological Society of America Today, v. 18, no. 8, p. 4–10, https://doi.org/10.1130/GSATG12A.1.

Appendixes

Appendix 1. List of Survey River Trips and Geomorphic Characteristics for Selected Study Sites along the Colorado River Corridor, Marble and Grand Canyons, Arizona

Table 1.1. Summary of survey trips and study sites monitored from 1990 to 2020 along the Colorado River corridor, Marble and Grand Canyons, Arizona.

[NAU, Northern Arizona University; GCES, Glen Canyon Environmental Studies; LSSF, low summer steady flow; HFE, high-flow experiment; —, no additional information. For list of study sites, see table 1 of the main text]

Year	River trip dates (yymmdd)	Number of sites surveyed	Source[1]	Notes[2]
1990	900610–901014	33	Beus and others, 1992	Surveys compiled from multiple river trips during the Bureau of Reclamation's 1990–91 experimental flows
1991	910726–910801	33	Beus and others, 1992	Surveys compiled from 4 separate survey trips on the river at the same time
1991	910925–911010	15	Stevens and Ayers, 1995	Surveys collected on NAU/GCES vegetation trip
1991	911025–911110	14	Stevens and Ayers, 1995	Surveys collected on NAU/GCES vegetation trip[3]
1992	921014–921102	31	Kaplinski and others, 1995	First NAU interim flow monitoring trip[4]
1993	930401–930415	27	Kaplinski and others, 1995	Trip made after winter 1993 Little Colorado River floods; site 062R added to monitoring network
1993	931007–931026	32	Kaplinski and others, 1995	—
1994	940407–940425	32	Kaplinski and others, 1995	—
1994	941120–941205	32	Kaplinski and others, 1995	—
1995	950424–950512	32	Kaplinski and others, 1995	—
1996	960214–960304	35	Hazel and others, 1999	Pre-HFE trip[5]; site 055R and reattachment bar at 044L added to monitoring network
1996	960416–960504	35	Hazel and others, 1999	Post-HFE trip[5]
1996	960913–960928	33	Hazel and others, 1999	—
1997	970214–970228	33	Hazel and others, 1999	—
1997	970420–970508	34	Hazel and others, 1999	Site 065R added to monitoring network
1997	970824–970907	34	Hazel and others, 1999	—
1997	971106–971121	34	Hazel and others, 2000	Post-1997 test flow; repeat surveys at site 003L[3]
1998	980415–980429	34	Hazel and others, 2000	—
1999	990506–990522	35	Hazel and others, 2000	Site 035L added to monitoring network
2000	000318–000404	35	Schmidt and others, 2007	2000 LSSF surveys
2000	000602–000618	35	Schmidt and others, 2007	2000 LSSF surveys
2000	000818–000829	20	Schmidt and others, 2007	2000 LSSF surveys; no sites surveyed downstream from site 087L
2000	000909–000917	20	Schmidt and others, 2007	2000 LSSF surveys; no sites surveyed downstream from site 087L
2001	011005–011019	35	Kaplinski and others, 2005	Combined campsite and sandbar survey trip
2002	020427–020514	12	Kaplinski and others, 2014	Surveys collected during reach-based monitoring
2002	020920–021007	42	Schmidt and others, 2004	Sites 033L, 024L, 029L, 041R, 045L[6], 056R, 084R, 167L[7] added to monitoring network
2003	030425–030512	42	Schmidt and others, 2004	—
2003	030920–031006	42	Schmidt and others, 2004	—
2004	040601–040610	7	Kaplinski and others, 2014	Surveys collected during reach-based monitoring
2004	041113–041122	10	Topping and others, 2006	Pre-HFE trip; surveys collected during reach-based monitoring
2004	041202–041215	17	Topping and others, 2006	Post-HFE trip; reach-based monitoring
2004	041230–050108	13	Topping and others, 2006	Post-HFE trip; surveys collected on a streamflow gaging trip
2005	050507–050522	42	Kaplinski and others, 2010	—
2006	061007–061022	42	Kaplinski and others, 2010	—
2007	071013–071029	42	Kaplinski and others, 2010	—
2008	080202–080218	45	Hazel and others, 2010	Pre-HFE trip; sites 009L and 070R added to the monitoring network
2008	080328–080413	45	Hazel and others, 2010	Post-HFE trip

Table 1.1. Summary of survey trips and study sites monitored from 1990 to 2020 along the Colorado River corridor, Marble and Grand Canyons, Arizona.—Continued

Year	River trip dates (yymmdd)	Number of sites surveyed	Source[1]	Notes[2]
2008	080517–080603	27	Grams and others, 2010	Sandbars surveyed as part of backwater habitat monitoring
2008	081011–081026	46	Hazel and others, 2010	Sites 029L, 081L, and 084R surveyed on a backwater habitat monitoring trip in September 2008
2009	091010–091026	45	Grams and others, 2020	—
2011	111005–111021	44	Grams and others, 2020	−006R not surveyed
2012	121003–121019	44	Grams and others, 2020	HFE protocol implemented May 2012
2012	121126–121004	3	Grams and others, 2020	Post-HFE trip; sites 009L, 030R, and 047R surveyed on Grand Canyon National Park resource trip
2013	130921–131007	44	Grams and others, 2020	−006R not surveyed
2014	140924–141010	45	Grams and others, 2020	—
2015	150923–151009	45	Grams and others, 2020	—
2016	161001–161017	45	Grams and others, 2020	—
2017	170930–171016	45	Grams and others, 2020	—
2018	180926–181012	45	Grams and others, 2020	—
2019	191005–191021	45	Grams and others, 2020	—
2020	200930–201016	45	Grams and others, 2020	—

[1]Column lists the researchers who collected the data or publications where the data have previously been reported.

[2]The descriptor "R" denotes the location at the study site on river-right and "L" for river-left, with the observer facing downstream. The number is the approximate location of the river mile marker based on the river mile (RM) centerline upstream or downstream from Lees Ferry (RM 0), Arizona.

[3]Data at sites 003L and 008L collected after the river trip in late November 1991.

[4]Site 081L surveyed on September 23, 1992, on a Glen Canyon Environmental Studies vegetation trip. The interim flow period is described in the text and shown on figure 3.

[5]Pre- and post-1996 HFE surveys at site 065R collected by Andrews and others (1999).

[6]This study site has two deposit types; the separation bar was not surveyed in 2003 and 2005–2007.

[7]Site 167L was partially buried by a debris flow in National Canyon on July 14, 2012, and is therefore not included in analyses of temporal trends (appendix 3).

Table 1.2. Geomorphic characteristics for selected sites and metrics used for sandbar site type along the Colorado River corridor, Marble and Grand Canyons, Arizona.

[Sites are grouped based on the dominant bar type present and by changes in reach-scale metrics defined by a principal component analysis as described by Mueller and others (2018); reach-averaged metrics were calculated at each site for a 1-kilometer reach centered on each monitoring site. Q, discharge; V, volume; m, meter; m^2, square meter; PC1, first principal component; m^3/s, cubic meters per second; >, greater than; —, no data; HFE, high-flow experiment. For list of study sites, see table 1 of the main text]

Site ID[1]	Width (m)[2]	Stage change (m)[3]	Channel slope[4]	Vegetated area (m^2)[5]	PC1	Q-V slope[6]		Q-V slope p-values[7]		High/low elevation standard deviation	Post-flood thickness change (m)[9]	
						Total	Above 227 m^3/s	Total	Above 227 m^3/s		Above 227 m^3/s	Above 708 m^3/s
Group 1a. Narrow reattachment bars												
145L	48.7	5	0.00217	1,044	−1.97	0.85	1.27	0.000	0.001	1.64	0.60	0.69
022R	69.0	5.8	0.00164	1,263	−1.83	−0.45	−0.21	0.574	0.038	1.06	0.42	0.60
213L	57.3	5.8	0.00071	3,994	−1.66	−0.11	0.45	0.146	0.757	0.65	0.63	0.37
084R	58.9	4.9	0.00147	1,161	−1.52	—	0.72	0.357	—	—	0.14	0.22
030R	69.1	5	0.00171	2,180	−1.06	0.63	0.99	0.000	0.000	1.64	0.94	0.54
137L	71.4	4.3	0.00041	2,118	−0.46	0.71	0.87	0.000	0.001	1.44	0.40	0.64
119R	83.4	4.6	0.00177	1,423	−0.44	1.08	1.44	0.000	0.005	0.93	0.85	0.63
122R	85.7	4.2	0.00119	1,269	−0.09	1.06	1.16	0.000	0.002	1.15	0.39	0.39
Group 1b. Medium reattachment bars												
009L	91.6	4.2	0.00118	1,340	0.12	—	1.25	0.358	—	—	0.57	0.49
123L	84.0	4	0.00182	2,124	0.16	−0.54	0.35	0.233	0.118	0.71	0.15	0.42
172L	78.0	3.9	0.00065	4,413	0.50	0.26	0.07	0.876	0.469	1.41	0.36	0.26
044L	86.9	4.1	0.00120	3,819	0.52	−0.24	0.78	0.010	0.306	0.69	0.33	0.24

Table 1.2. Geomorphic characteristics for selected sites and metrics used for sandbar site type along the Colorado River corridor, Marble and Grand Canyons, Arizona.—Continued

Site ID[1]	Width (m)[2]	Stage change (m)[3]	Channel slope[4]	Vegetated area (m^2)[5]	PC1	Q-V slope[6]		Q-V slope p-values[7]		High/low elevation standard deviation	Post-flood thickness change (m)[9]	
						Total	Above 227 m^3/s	Total	Above 227 m^3/s		Above 227 m^3/s	Above 708 m^3/s
045L	95.8	4	0.00088	3,218	0.78	0.17	1.58	0.128	0.881	1.06	0.81	0.23
041R	96.9	4.1	0.00075	4,289	0.96	—	1.56	0.120	—	—	0.43	0.15
003L	99.7	3.4	0.00092	1,950	1.10	−1.03	−0.46	0.12	0.01	0.56	−0.04	0.06
183R	94.6	4.1	0.00127	7,393	1.49	0.26	0.61	0.027	0.437	1.20	0.18	0.41
220R	94.1	3	0.00067	3,385	1.49	0.08	0.50	0.043	0.819	0.89	0.11	0.18
050R	106.5	3.9	0.00096	5,571	1.67	0.10	0.56	0.004	0.684	0.94	0.28	0.17
065R	99.2	2.8	0.00036	2,913	1.72	−0.11	1.12	0.001	0.656	0.56	0.67	0.33
047R	99.5	3.5	0.00070	7,397	2.10	−0.02	0.30	0.044	0.873	0.48	0.44	0.11
Group 1c. Wide reattachment bars												
070R	100.4	2.7	0.00195	6,066	2.43	—	0.44	0.782	—	—	0.48	0.19
194L	100.9	3.8	0.00175	10,258	2.48	−1.08	−0.13	0.698	0.000	0.38	0.16	0.39
068R	108.3	2.4	0.00242	6,803	3.05	−0.64	0.33	0.337	0.123	0.42	0.21	0.21
051L	94.8	3.5	0.00031	16,866	3.82	−0.80	0.06	0.681	0.000	0.46	0.06	0.24
055R	117.9	2.5	0.00010	9,620	3.89	−0.76	−0.13	0.533	0.022	0.28	0.09	0.20
Group 2. Undifferentiated eddy bars												
008L	102.4	3	0.00404	2,233	1.49	—	0.38	—	0.21	—	0.19	0.04
024L	59.5	5	0.00200	929	−1.63	—	2.76	—	0.00	—	0.16	0.01
029L	68.9	4.8	0.00217	732	−1.21	—	1.41	—	0.28	—	0.72	0.17
032R	76.6	2.9	0.00147	1,089	0.52	−0.24	0.66	−0.24	0.00	0.35	0.14	−0.03
056R	84.1	3.1	0.00376	10,036	2.36	—	0.69	—	0.46	—	0.21	0.07
081L	61.7	3.7	0.00118	1,228	−0.53	0.30	1.40	0.000	0.200	0.81	0.41	0.37
167L	68.8	3.6	0.00177	2,539	0.02	—	1.56	—	0.03	—	0.13	0.15
Group 3. Upper pool deposits												
043L	95.4	4.3	0.00007	4,147	0.74	−0.63	0.52	−0.63	0.00	0.01	0.06	0.13
087L	80.3	3.8	0.00019	1,920	0.16	−0.54	−0.17	−0.54	0.32	0.28	−0.02	0.24
093L	74.8	2.9	0.00374	2,306	0.66	−0.94	−0.75	−0.94	0.06	0.01	0.11	0.25
139R	63.7	4.5	0.00265	2,025	−0.92	−0.09	0.55	−0.09	0.15	0.78	0.28	0.23
225R	75.6	2.9	0.00059	3,995	1.07	−1.01	−0.68	−1.01	0.16	0.00	0.18	0.35
104R	55.7	3.9	0.00142	1,858	−0.76	0.82	1.09	0.82	0.00	0.08	0.36	0.45
Group 4. Separation bars												
016L	79.2	3.1	0.00063	1,032	0.46	0.82	1.15	0.82	0.00	0.02	0.26	0.04
033L	77.3	4.7	0.00103	1,108	−0.77	—	−0.14	—	0.86	—	0.12	0.03
035L	89.0	5	0.00097	724	−0.67	−0.42	−0.32	−0.42	0.60	0.72	0.47	0.05
062R	97.8	3.9	0.00118	1,691	0.61	−0.54	−0.17	−0.54	0.60	0.19	0.21	0.07
091R	63.1	4.2	0.00036	1,393	−0.81	0.55	0.02	0.55	0.89	0.04	0.00	0.14
202R	95.3	3.8	0.00096	4,349	1.13	0.63	−0.08	0.63	0.82	0.03	0.05	0.13

[1]The descriptor "R" denotes the location at the study site on river-right and "L" for river-left, with the observer facing downstream. The number is the approximate location of the river mile marker based on the river mile (RM) centerline downstream from Lees Ferry (RM 0), Arizona.

[2]Based on predicted water-surface elevations at 227 m^3/s derived from a one-dimensional flow model of Magirl and others (2008).

[3]Difference in water-surface elevation between the 227 m^3/s and 1,274 m^3/s stage using the site-specific stage-discharge relations of Hazel and others (2006).

[4]Based on a linear relation between an upstream and downstream elevation at 227 m^3/s using the model of Magirl and others (2008).

[5]Averaged vegetated area derived from the remote sensing data of Sankey and others (2015).

[6]Based on linear least-squares relations between the sand volume at each site and the average discharge of the previous 30 days.

[7]The significance of individual Q-V relations based on Student's t-tests (Davis, 2002).

[8]Ratio of the average standard deviation of elevation for all grid points of the emergent sandbar above 227 m^3/s to the average standard deviation values of the submerged eddy and channel below 227m^3/s. Values >1 are sites where scour and fill of the emergent sandbar is greater than scour and fill of the channel bed.

[9]Average sand thickness change based on topographic surveys collected before and after each of the 1996, 2004, and 2008 HFEs.

References Cited

Andrews, E.D., Johnson, C.E., Schmidt, J.C., and Gonzales, M., 1999, Topographic evolution of sandbars, *in* Webb, R.H., Schmidt, J.C., Marzolf, G.R., and Valdez, R.A., eds., The controlled flood in Grand Canyon: American Geophysical Union Geophysical Monograph Series, v. 110, p. 117–130, https://doi.org/10.1029/GM110p0117.

Beus, S.S., Avery, C.C., Stevens, L.E., Cluer, B., Kaplinski, M.A, Anderson, P., Bennett, J., Brod, C., Hazel, J.E., Jr., Gonzales, M., Hayes, H., Protiva, F., and Courson, J., 1992, The influence of variable discharge regimes on Colorado River sand bars below Glen Canyon Dam, Arizona, chap. 6 *of* Beus, S.S., and Avery, C.C., principal investigators, 1992, The influence of variable discharge regimes on Colorado River sand bars below Glen Canyon Dam—Final report: Bureau of Reclamation, Glen Canyon Environmental Studies, National Park Service cooperative agreement no. CA 8006-8-0002 with Northern Arizona University, 62 p., accessed May 20, 2022, at http://www.riversimulator.org/Resources/GCMRC/PhysicalResources/beus1993.pdf.

Davis, J.C., 2002, Statistics and data analysis in geology: John Wiley and Sons Ltd., 3rd edition, 638 p.

Grams, P.E., Hazel, J.E., Jr., Kaplinski, M., Ross, R.P., Hamill, D., Hensleigh, J., and Gushue, T., 2020, Long-term sandbar monitoring data along the Colorado River in Marble and Grand Canyons, Arizona: U.S. Geological Survey data release, https://doi.org/10.5066/P93F8JJK.

Grams, P.E., Schmidt, J.C., and Andersen, M.E., 2010, 2008 high-flow experiment at Glen Canyon Dam—Morphologic response of eddy-deposited sandbars and associated aquatic backwater habitats along the Colorado River in Grand Canyon National Park: U.S. Geological Survey Open-File Report 2010–1032, 73 p., https://doi.org/10.3133/ofr20101032.

Hazel, J.E., Jr., Grams, P.E., Schmidt, J.C., and Kaplinski, M., 2010, Sandbar response in Marble and Grand Canyons, Arizona, following the 2008 high-flow experiment on the Colorado River: U.S. Geological Survey Scientific Investigations Report 2010–5015, 52 p., https://doi.org/10.3133/sir20105015.

Hazel, J.E., Jr., Kaplinski, M., Parnell, R., and Manone M., 2000, Sand deposition in the Colorado River Ecosystem from flooding of the Paria River and the effects of the November 1997, Glen Canyon Dam Test Flow—Final report: Flagstaff, Ariz., Northern Arizona University, submitted to Grand Canyon Monitoring and Research Center, 37 p. [Available at https://www.library.nps.gov, call no. TC557.A62 S36 2000.]

Hazel, J.E., Jr., Kaplinski, M., Parnell, R., Kohl, K., and Topping, D.J., 2006, Stage-discharge relations for the Colorado River in Glen, Marble, and Grand Canyons, Arizona: U.S. Geological Survey Open-File Report 2006–1243, 7 p., https://doi.org/10.3133/ofr20061243.

Hazel, J.E., Jr., Kaplinski, M., Parnell, R., Manone, M., and Dale, A., 1999, Topographic and bathymetric changes at thirty-three long-term study sites, *in* Webb, R.H., Schmidt, J.C., Valdez, R.A., and Marzolf, G.R., eds., The controlled flood in Grand Canyon: American Geophysical Union Geophysical Monograph Series, v. 110, p. 161–183, https://doi.org/10.1029/GM110p0161.

Kaplinski, M., Hazel, J.E., Jr., and Beus, S.S., 1995, Monitoring the effects of interim flows from Glen Canyon Dam on sand bars in the Colorado River Corridor, Grand Canyon National Park, Arizona, Final report to Bureau of Reclamation, Glen Canyon Environmental Studies: Flagstaff, Ariz., Northern Arizona University, 62 p. [Available at https://www.library.nps.gov, call no. M GB1207.K37 M66 1995.]

Kaplinski, M., Behan, J., Hazel, Jr., J.E., Parnell, R.A., and Fairley, H.C., 2005, Recreational values and campsites in the Colorado River ecosystem, chap. 12 *of* Gloss, S.P., Lovich, J.E., and Melis, T.S., eds., The state of the Colorado River ecosystem in Grand Canyon: U.S. Geological Survey Circular 1282, p. 193–205, https://doi.org/10.3133/cir1282.

Kaplinski, M., Hazel, J.E., Jr., Grams, P.E., and Davis, P.A., 2014, Monitoring fine-sediment volume in the Colorado River ecosystem, Arizona—Construction and analysis of digital elevation models: U.S. Geological Survey Open-File Report 2014–1052, 29 p., https://doi.org/10.3133/ofr20141052.

Kaplinski, M., Hazel, J.E., Jr., and Parnell, R., 2010, Colorado River campsite monitoring, 1998–2006, Grand Canyon National Park, Arizona, *in* Melis, T.S., Hamill, J.F., Bennet, G.E., Coggins, L.C., Jr., Grams, P.E., Kennedy, T.A., Kubly, D.M., and Ralston, B.E., eds., Proceedings of the Colorado River Basin Science and Resource Management Symposium, November 18–20, 2009, Scottsdale, Ariz.: U.S. Geological Survey Scientific Investigations Report 2010–5135, p. 275–284, https://doi.org/10.3133/sir20105135.

Magirl, C.S, Webb, R.H., and Griffiths, P., 2008, Modeling water-surface elevations and virtual shorelines for the Colorado River in Grand Canyon, Arizona: U.S. Geological Survey Scientific Investigations Report 2008–5075, 32 p., https://doi.org/10.3133/sir20085075.

Mueller, E.R., Grams, P.E., Hazel, J.E., Jr., and Schmidt, J.C., 2018, Variability in eddy sandbar dynamics during two decades of controlled flooding of the Colorado River in Grand Canyon: Sedimentary Geology, v. 363, p. 181–199, https://doi.org/10.1016/j.sedgeo.2017.11.007.

Sankey, J.B., Ralston, B.E., Grams, P.E., Schmidt, J.C., and Cagney, L.E., 2015, Riparian vegetation, Colorado River, and climate—Five decades of spatiotemporal dynamics in the Grand Canyon with river regulation: Journal of Geophysical Research Biogeosciences, v. 120, no. 8, p. 1532–1547, https://doi.org/10.1002/2015JG002991.

Schmidt, J.C., Topping, D.J., Grams, P.E., and Hazel, J.E., 2004. System-wide changes in the distribution of fine sediment in the Colorado River corridor between Glen Canyon Dam and Bright Angel Creek, Arizona—Final report: Logan, Utah, Utah State University, submitted to U.S. Geological Survey, Grand Canyon Monitoring and Research Center, cooperative agreement no. 1425–98–FC–22640, 107 p., accessed January 20, 2017, at http://www.riversimulator.org/Resources/GCMRC/PhysicalResources/Schmidt2004.pdf.

Schmidt, J.C., Topping, D.J., Rubin, D.M., Hazel, J.E., Jr., Kaplinski, M., Wiele, S.M., and Goeking, S.A., 2007, Streamflow and sediment data collected to determine the effects of low summer steady flows and habitat maintenance flows in 2000 on the Colorado River between Lees Ferry and Bright Angel Creek, Arizona: U.S. Geological Survey Open-File Report 2007–1268, 79 p., https://doi.org/10.3133/ofr20071268.

Stevens, L.E., and Ayers, T.J., 1995, The effects of interim flows from Glen Canyon Dam on riparian vegetation along the Colorado River in Grand Canyon National Park, Arizona—Final 1994 report: Flagstaff, Ariz., Northern Arizona University, submitted to National Park Service (NPS), NPS work order no. CA 8021-8-0002, 137 p. [Available at https://www.library.nps.gov/, call no. M TC557.A62 S74 1995.]

Topping, D.J., Rubin, D.M., Schmidt, J.C., Hazel, J.E., Melis, T.S., Wright, S.A., Kaplinski, M., Draut, A.E., and Breedlove, M.J., 2006, Comparison of sediment-transport and bar-response results from the 1996 and 2004 controlled-flood experiments on the Colorado River in Grand Canyon, *in* Proceedings of the Eighth Federal Interagency Sedimentation Conference (8th FISC), April 2–6, 2006, Reno, Nev.: Advisory Committee on Water Information, p. 171–179, accessed April 20, 2017, at https://acwi.gov/sos/pubs/8thFISC/Session%201B-3_Topping.pdf.

Appendix 2. Description of the Control Point Network Used for Study-Site Monitoring, Colorado River Corridor, Marble and Grand Canyons, Arizona

Control points (also referred to as survey reference marks, monuments, or stations) are intended to be stable, recoverable, and precise positions; they are typically located on bedrock or large boulders (fig. 2.1). The positions are preserved by scribing or chiseling features, or by physical attachment of foreign substances (nails, caps, pins, screws, bolts, rebar, and so on). These stations were placed in a manner that allows for setting tripods over the point so that they can be occupied by total station (TS) or Global Positioning System (GPS) survey equipment using local and geodetic control networks (table 2.1). Within the study area, reference marks have commonly been placed ("monumented") for unrelated studies by surveyors and scientists from multiple government agencies, universities, and private survey firms.

A complete history of these efforts is not available, but researchers in the 1970s affixed carpenter nails and pipe (Howard, 1975; Beus and others, 1985). In the 1980s, Ferrari (1987) chiseled "Y" and "T" features and Schmidt and Graf (1990) drilled holes and cemented carriage bolts. In 1990–1991, Northern Arizona University installed magnetic concrete nails with an indentation in the middle of its head made by Parker Kaelon Company; stamped PK. PK nails are commonly used in land surveying because the dimple in the center of the nail head provides precise and stable positions and because they are recoverable with a metal detector. During the 1990s, contractors for the Bureau of Reclamation (Reclamation) established networks of Global Positioning System (GPS) measurements of aluminum caps mortared into rock or set on rebar, or to small nails or screws set in lead. Glen Canyon Environmental Studies (GCES) connected these GPS-derived positions by conventional traverse by referencing line-of-site measurements to a series of small, cross-cut 'x' symbols. Within the last 15 years, the U.S. Geological Survey's (USGS) Grand Canyon Monitoring and Research Center (GCMRC) has set ⅜″ dimpled pins made of brass or stainless steel (SS) to establish reference positions at new study sites, and to replace previous marks that are in poor condition.

Beginning in 2001, GCMRC used static GPS methods to reference each independent local site to positions published in the National Spatial Reference System (NSRS). Currently all sites listed in this report reference the 2007 realization (NSRS 2007) of the North American Datum of 1983 (NAD 83). A register of the reference marks utilized in this study that contains records of observations and mark maintenance, site descriptions, and photographs is maintained by USGS GCMRC. Records from this database are available upon request.

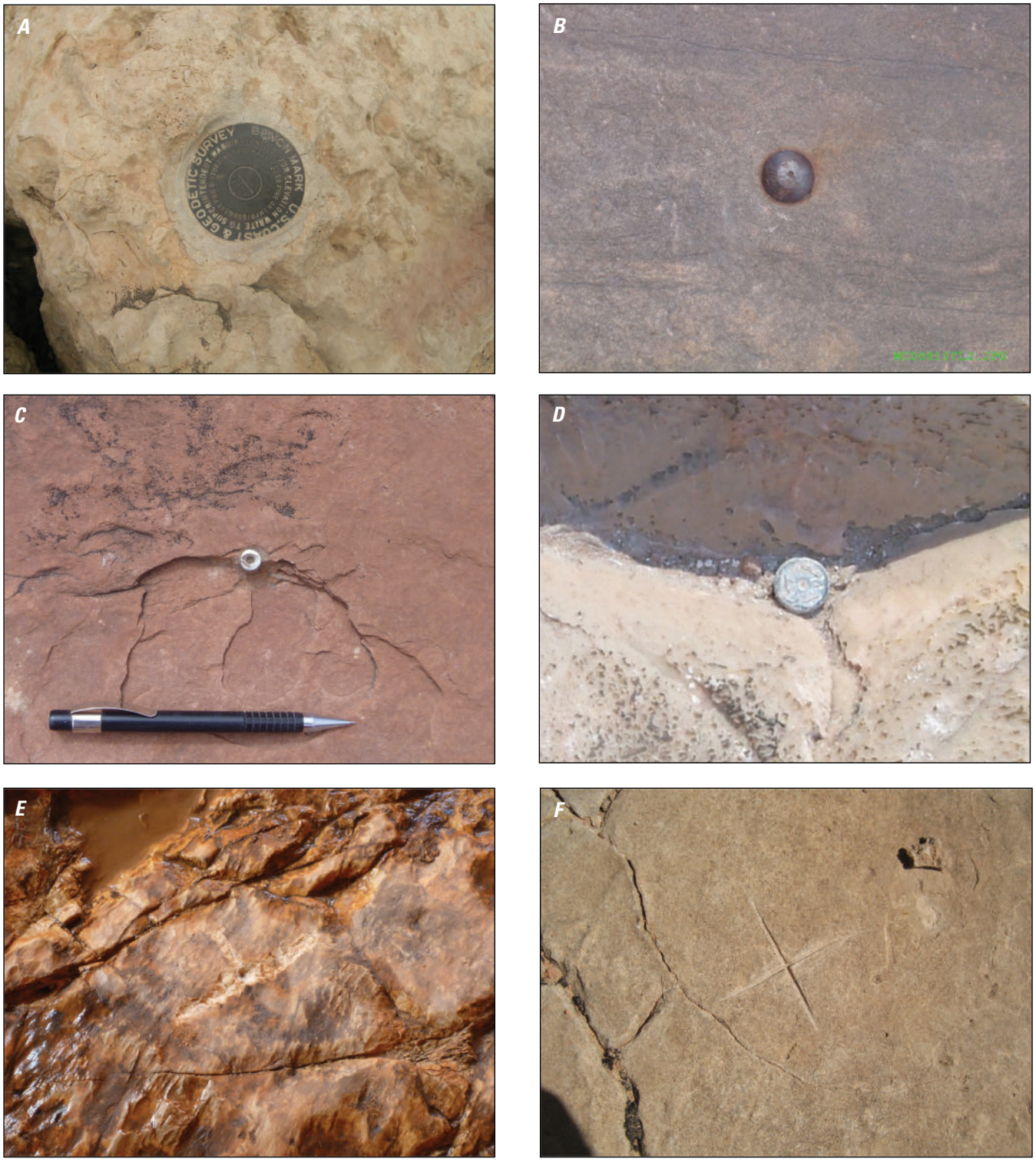

Figure 2.1. Photographs of examples of survey marks in the study area, Colorado River corridor, Marble and Grand Canyons. *A*, Brass cap set in concrete. Cap is 90 millimeters (mm) in diameter. *B*, Carriage bolt. Bolt is 22 mm wide. *C*, Stainless steel pin cemented into a drill hole. Pencil shown for scale. *D*, PK nail driven into a crack. Nail head is 15 mm. *E*, Chiseled T symbol with drill hole. Chiseled T is about 60 × 40 mm. *F*, Scribed cross-cut X. X is about 60 × 60 mm. Photographs by Keith Kohl, U.S. Geological Survey.

Table 2.1. Control points used as benchmarks and backsites at the monitoring sites, Colorado River corridor, Glen, Marble, and Grand Canyons, Arizona.

[Site identification (ID) and control network point ID names are given by location along the river mile centerline (Gushue, 2019). PC, SC, and TC refer to primary, secondary, and tertiary levels of the control network, respectively. Single observation (SO) and total station (TS) indicate control points determined by single-vector Global Positioning System (GPS) and conventional-based observations, respectively. NC, data never collected in the specified datum; ″, inch; SS, stainless steel. For list of study sites, see table 1 of the main text]

Study Site ID[1]	Point ID	Monument type	Local datum			Arizona State Plane central zone		
			Northing (m)	Easting (m)	Elevation (m)	Northing (m)	Easting (m)	Elevation (m)
−006R	TS-06575R	Chiseled X	1057.919	1065.629	89.626	651644.011	245465.329	936.320
−006R	TS-06523L	Scribed X	864.138	1039.634	83.780	651506.363	245326.542	930.547
−006R	TS-06528R	PK nail	1014.452	1000.000	101.655	651649.617	245386.837	948.415
−006R	TS-06525R	Carriage bolt	1000.000	1000.000	100.000	651638.148	245378.025	946.763
−006R	TS-06518R	Chiseled X	1009.526	985.379	104.777	651654.634	245372.243	951.535
−006R	SC-06519R	Brass disc	NC	NC	NC	651618.510	245360.015	939.483
003L	SC002473L	Carriage bolt	1157.244	1151.661	107.327	648023.298	240138.589	934.266
003L	SC002569R	Chiseled X	1000.000	1000.000	100.000	647866.577	239986.463	926.934
003L	SC002585L	Chiseled X	989.759	1109.622	98.022	647855.981	240096.099	924.969
008L	SC008087R	Scribed X	1000.31	1223.958	110.496	640312.509	236463.798	929.624
008L	SO008107L	Carriage bolt	1000.000	1000.000	100.000	640182.408	236646.021	919.123
008L	TC008138R	Hex bolt	1075.227	1165.729	104.204	640217.727	236467.514	923.337
008L	SO008202L	Carriage bolt	1158.422	1000.000	98.614	640053.620	236553.792	917.736
009L	TC008793L	Scribed X	NC	NC	NC	639245.367	236050.906	923.632
009L	SC008800R	Scribed X	NC	NC	NC	639305.958	235933.941	919.680
009L	TS008901R	Scribed X	NC	NC	NC	639022.887	235839.267	914.290
009L	TC009175R	Scribed X	NC	NC	NC	638706.623	235797.747	925.260
016L	PC016638L	Screw in lead	1000.000	1000.000	100.000	630036.971	229239.933	900.088
016L	TC016673L	PK nail	1054.097	1000.000	100.642	629983.211	229245.908	900.729
016L	TS016686R	Scribed X	1052.821	1128.389	101.017	629970.302	229118.196	901.106
022R	PC021601R	⅜″ SS pin	1000.000	1000.000	100.000	622634.195	227418.169	894.902
022R	TC021720R	Chiseled X	1183.994	1000.000	92.104	622467.452	227340.490	886.999
022R	SC022005L	Scribed X	1074.087	879.832	89.103	622516.325	227495.796	883.999
022R	TS022015L	Scribed X	1091.180	886.303	89.398	622503.564	227482.713	884.294
022R	SC022082L	Scribed X	1205.735	909.350	97.082	622409.477	227413.460	891.974
024L	TC023460L	Scribed X	NC	NC	NC	620504.251	226386.753	886.667
024L	TS023557R	Scribed X	NC	NC	NC	620414.238	226237.429	881.488
024L	TC023658L	Scribed X	NC	NC	NC	620256.255	226193.064	883.686
029L	SO029428L	Scribed X	NC	NC	NC	613409.537	220750.037	862.992
029L	TC029616L	Scribed Y	NC	NC	NC	613208.589	220529.36	861.533
029L	SC029854R	Scribed X	NC	NC	NC	612992.090	220210.659	864.409
030R	PC030653R	⅜″ SS pin	1024.391	1136.389	110.186	611922.341	219576.292	870.729
030R	SC030696L	Chiseled X	1000.000	1000.000	100.000	611819.051	219668.575	860.515
030R	TS030794R	Chiseled X	1188.254	1000	100.233	611720.312	219508.367	860.798
032R	SC031851R	Scribed X	1000.000	1000.000	100.000	610286.697	218667.607	856.358
032R	SO031852R	Scribed X	1031.008	995.605	110.291	610295.843	218637.665	866.657
032R	TC031854R	Chiseled X	1032.020	991.867	110.442	610292.885	218635.171	866.804
032R	SO031933R	X with drill hole	1056.405	871.199	100.396	610193.915	218561.990	856.770
032R	TC032010R	Scribed Y	1020.807	718.296	99.987	610040.358	218529.502	856.343
032R	TC032089R	Scribed X	921.371	605.057	99.455	609895.691	218571.619	855.768
033L	TC033269L	Scribed X	991.227	1023.982	97.493	609182.399	220302.351	854.660
033L	TS033270L	Chiseled X	986.068	1010.915	101.473	609180.092	220316.211	858.639
033L	TS033275L	Chiseled T	1000.000	1000.000	100.000	609162.516	220318.404	857.169
033L	TS033308L	Chiseled X	1080.136	1000.000	101.671	609093.795	220277.205	858.856

Table 2.1. Control points used as benchmarks and backsites at the monitoring sites, Colorado River corridor, Glen, Marble, and Grand Canyons, Arizona.—Continued

Study Site ID[1]	Point ID	Monument type	Local datum			Arizona State Plane central zone		
			Northing (m)	Easting (m)	Elevation (m)	Northing (m)	Easting (m)	Elevation (m)
035L	SC034982L	1″ diameter pipe	1195.96	1000.000	100.959	606730.200	220168.786	861.249
035L	TS035047L	Scribed X	1126.234	998.122	94.936	606673.748	220209.768	855.218
035L	SC035121L	Scribed X	1000.000	1000.000	100.000	606574.829	220288.089	860.292
035L	TS035165R	Scribed X	820.013	841.652	91.734	606415.764	220241.216	850.680
041R	TC041114L	PK nail	NC	NC	NC	599387.795	216846.505	852.028
041R	TC041177R	X with drill hole	NC	NC	NC	599350.806	216671.993	848.857
041R	TC041187R	Scribed X	NC	NC	NC	599317.754	216724.775	843.403
041R	TC041358L	Scribed X	NC	NC	NC	599079.656	216587.935	848.747
043L	TC043281L	Scribed X	1010.140	703.306	99.046	598579.497	218556.063	841.891
043L	TC043289R	Scribed X	928.915	752.380	115.991	598489.459	218586.060	858.841
043L	TS043459L	Carriage bolt	1174.817	1000.000	108.734	598674.806	218881.714	851.560
043L	SC043465R	Carriage bolt	1000.000	1000.000	100.000	598504.321	218843.26	842.836
043L	SC043508L	Aluminum disc	1129.138	1079.76	106.592	598612.745	218949.482	849.427
044L	SO044411L	X with drill hole	1058.562	1102.512	76.296	597529.482	219450.549	839.523
044L	SO044452R	PK nail	1000.000	1000.000	100.000	597534.617	219332.625	863.226
044L	PC044480L	Scribed X	922.476	1225.818	107.928	597348.635	219482.244	871.166
044L	TS044580R	Scribed X	801.955	990.853	80.765	597372.000	219219.275	843.984
045L	SC044873R	Scribed X	NC	NC	NC	597242.398	218814.957	840.450
045L	SC044914L	Scribed X	NC	NC	NC	597088.676	218767.833	860.136
047R	TS047560L	Scribed X	NC	NC	NC	595241.835	215986.084	835.366
047R	TC047628L	PK nail	1000.000	1000.000	100.000	595152.168	216059.363	844.815
047R	TS047586R	Chiseled X	959.447	1189.429	90.035	595132.878	215866.671	834.848
047R	TS047657R	Chiseled x	1056.255	1176.328	93.526	595045.687	215908.411	838.335
047R	SC047661R	Chiseled Y	1062.483	1184.511	98.596	595036.302	215902.824	843.405
050R	PC050087R	Screw in lead	883.177	1108.584	100.902	592016.983	218261.300	834.879
050R	TC050111R	Chiseled X	908.157	1112.911	102.152	591996.840	218276.673	836.125
050R	SC050113L	Scribed X	915.283	998.928	106.851	592075.573	218359.356	840.827
050R	SC050160L	PK nail	1000.000	1000.000	100.000	592017.219	218420.753	833.977
051L	TC051284R	Aluminum disc	1285.843	1022.146	103.568	590304.205	218311.184	835.736
051L	SC051370R	PK nail	1136.774	1000.000	101.246	590170.379	218241.965	833.407
051L	SC051458R	PK nail	1000.000	1000.000	100.000	590041.004	218197.672	832.165
055R	SC055751R	Chiseled X	1213.467	1000.000	101.782	584449.760	220688.928	830.160
055R	SC055802L	Scribed X	1075.856	1098.300	101.845	584516.107	220844.445	830.236
055R	PC055874L	Scribed X	1000.000	1000.000	100.000	584403.799	220897.345	828.368
055R	SC055944L	Scribed X	967.385	979.354	109.142	584376.619	220924.746	837.526
055R	TS055915R	Scribed X	1035.71	753.758	108.78	584172.707	220811.646	837.027
056R	TS056442R	Scribed X	NC	NC	NC	583664.318	221374.793	822.404
056R	TS056632L	Scribed X	NC	NC	NC	583483.870	221590.010	823.010
056R	TS056700R	Scribed X	NC	NC	NC	583388.574	221516.641	819.189
062R	TC062823R	Scribed X	748.569	847.728	97.452	574768.102	222619.432	809.143
062R	TC062901L	Carriage bolt	909.124	853.756	93.569	574610.585	222650.944	805.309
062R	PC062978R	Carriage bolt	1000.000	1000.000	100.000	574488.196	222529.887	811.739
062R	TC063044R	Carriage bolt	1053.382	1000.000	98.353	574436.295	222542.308	810.091
065R	SC065131R	Carriage bolt	NC	NC	NC	571224.083	222355.075	812.971
065R	TS065192L	Hex bolt	NC	NC	NC	571092.313	222491.884	801.749
065R	TC065217L	Hex bolt	NC	NC	NC	571050.850	222479.320	801.920
065R	SC065355L	Scribed X	NC	NC	NC	570862.592	222431.219	798.808

Table 2.1. Control points used as benchmarks and backsites at the monitoring sites, Colorado River corridor, Glen, Marble, and Grand Canyons, Arizona.—Continued

Study Site ID[1]	Point ID	Monument type	Local datum			Arizona State Plane central zone		
			Northing (m)	Easting (m)	Elevation (m)	Northing (m)	Easting (m)	Elevation (m)
068R	TS068709L	Scribed X	NC	NC	NC	565874.792	221242.756	791.95
068R	TS068745L	Chiseled X	962.469	1018.603	97.009	565850.876	221170.056	789.325
068R	SC068763L	Carriage bolt	1000.000	1000.000	100.000	565841.827	221129.167	792.316
068R	SC068831R	Scribed X	994.329	1226.771	103.681	566060.558	221189.085	795.993
070R	TC069041L	Scribed X	NC	NC	NC	565738.727	220812.809	826.538
070R	TS070029L	Scribed X	NC	NC	NC	564886.293	220237.787	785.407
070R	SC070170R	Scribed X	NC	NC	NC	565139.306	220023.776	820.038
081L	SC081715L	Carriage bolt	1120.287	1000.000	98.753	560578.968	206204.036	742.356
081L	SC081787L	Chiseled X	1000.000	1000.000	100.000	560630.431	206095.345	743.576
081L	TS081803L	Chiseled X	968.97	1026.488	111.891	560619.779	206055.974	755.447
081L	SC081998L	Scribed X	1000.000	1000.000	100.000	560870.086	205851.548	740.905
084R	TS084555R	Scribed X	NC	NC	NC	563567.893	202843.177	731.131
084R	SC084612R	Scribed X	NC	NC	NC	563561.853	202727.718	730.758
084R	SC084810R	Scribed X	NC	NC	NC	563686.247	202432.799	740.233
087L	TS087626L	Chiseled X	1094.065	1000.000	101.771	565652.706	198433.159	722.052
087L	SC087628R	Scribed X	1022.659	913.034	111.218	565734.093	198510.839	731.524
087L	SC087686R	PK nail	993.885	1008.440	106.940	565751.115	198412.670	727.237
087L	SC087734L	Scribed X	1053.212	1098.116	101.652	565681.386	198330.843	721.926
087L	SC088021R	Brass disc	NC	NC	NC	565805.833	197868.790	734.926
091R	TS091717R	Chiseled X	942.565	1087.296	99.023	566368.308	192655.256	706.063
091R	SC091754L	Chiseled X	1000.000	1000.000	100.000	566287.439	192589.078	707.043
091R	SC091775L	Chiseled X	1033.182	1000.000	100.138	566290.877	192556.076	707.178
093L	TS093774R	Carriage bolt	1038.223	947.901	102.054	565427.081	189601.851	702.042
093L	TS093788L	Chiseled X	1117.759	1000.000	99.695	565336.255	189573.869	699.682
093L	TS093818R	Destroyed	1000.000	1000.000	100.000	565449.346	189541.227	699.986
093L	SC093839R	Scribed X	993.984	1036.043	102.290	565445.129	189504.939	702.277
093L	TS093872L	Scribed X	1029.462	1143.952	102.407	565381.14	189411.145	702.393
093L	SC093878L	Chiseled X	1032.295	1160.579	104.053	565373.810	189395.963	704.039
104R	TS104423R	PK nail	1024.443	1000.000	96.930	574506.059	178111.55	666.480
104R	TS104435R	Chiseled X	1011.733	1026.066	93.458	574517.410	178084.871	663.008
104R	SC104438R	PK nail	1000.000	1000.000	100.000	574530.464	178110.294	669.550
104R	SC104445L	Scribed X	1011.874	1090.566	95.925	574513.954	178020.478	665.475
119R	TC119333R	Scribed X	827.692	1128.548	101.398	579816.635	164871.488	626.485
119R	TC119404R	Chiseled X	941.465	1150.109	97.177	579932.023	164880.988	622.262
119R	SC119450L	Scribed X	1013.041	1011.419	93.997	579988.639	164735.576	619.080
119R	TC119499L	PK nail	1079.725	1000.000	96.673	580053.746	164717.225	621.754
122R	PC122647R	Scribed X	1122.521	1033.74	97.064	581743.464	160332.041	616.520
122R	TC122736L	Scribed X	1009.893	1214.665	97.304	581621.02	160157.663	616.766
122R	SC122741L	Scribed X	1002.689	1205.603	95.241	581632.175	160154.579	614.706
122R	TS122776R	Chiseled X	1017.163	1000.000	99.959	581815.704	160248.286	619.418
122R	TC122784R	PK nail	1000.000	1000.000	100.000	581822.415	160232.493	619.460
122R	TS122797R	4d nail	954.712	1033.754	94.0320	581809.063	160177.623	613.494
123L	SC123161L	Scribed X	941.545	916.810	111.428	581768.788	159557.947	621.850
123L	SC123184R	Chiseled X	1000.000	1000.000	100.000	581867.806	159534.865	610.422
123L	SC123193L	Chiseled X	1003.829	898.700	100.941	581775.295	159493.441	611.363

Table 2.1. Control points used as benchmarks and backsites at the monitoring sites, Colorado River corridor, Glen, Marble, and Grand Canyons, Arizona.—Continued

Study Site ID[1]	Point ID	Monument type	Local datum			Arizona State Plane central zone		
			Northing (m)	Easting (m)	Elevation (m)	Northing (m)	Easting (m)	Elevation (m)
123L	SO123209R	Scribed X	1040.025	1002.255	103.311	581884.862	159498.596	613.733
123L	TS123216R	Chiseled X	1051.135	1000.000	101.529	581886.926	159487.452	611.951
137L	TS137590L	PK nail	1148.971	1000.000	100.753	598027.895	159189.296	568.277
137L	TC137641L	Scribed X	1070.870	1030.289	98.996	598067.351	159115.416	566.384
137L	TS137658L	Chiseled X	1056.29	1061.048	97.842	598058.349	159082.594	565.313
137L	SC137671R	PK nail	1000.000	1000.000	100.000	598140.821	159092.171	567.524
139R	TS139476R	Scribed X	NC	NC	NC	599140.100	156490.325	564.068
139R	SO139588L	Chiseled X	NC	NC	NC	599090.157	156309.963	562.884
139R	TS139615R	Chiseled X	NC	NC	NC	599180.298	156258.896	561.329
139R	SO139623L	Chiseled X	NC	NC	NC	599087.880	156253.398	566.307
145L	SO145864R	PK nail	1000.000	1000.000	100.000	596282.715	147530.196	545.720
145L	SO145867L	Chiseled X	1003.395	916.719	102.013	596277.104	147613.333	547.769
145L	TS145896L	PK nail	1050.924	1000.000	101.654	596231.824	147528.85	547.377
167L	SC167058L	Chiseled X	1228.280	1000.000	100.565	583419.522	125534.440	511.633
167L	TC167072L	Scribed X	NC	NC	NC	583398.548	125524.522	515.049
167L	SC167202L	Scribed X	1000.000	1000.000	100.000	583293.000	125344.458	511.068
172L	SC172531R	Scribed X	1106.237	1012.783	99.559	580912.879	118052.381	504.086
172L	SC172599R	PK nail	1000.000	1000.000	100.000	580872.01	117953.498	504.527
172L	SC172650L	X with drill hole	893.966	1105.025	101.582	580728.528	117912.471	506.115
172L	SC172661L	Brass pin	NC	NC	NC	580727.813	117897.276	506.604
183R	SO183164L	Scribed X	NC	NC	NC	573871.139	104276.148	480.099
183R	SC183185L	Scribed X	1113.947	1174.393	97.493	573884.992	104246.240	474.788
183R	SC183264R	PK nail	1037.011	999.73	109.152	573975.193	104078.045	486.447
183R	SC183360R	PK nail	1000.000	1000.000	100.000	573952.183	104049.056	477.295
194L	SO194520L	Chiseled X	1000.000	1000.000	100.000	565277.304	93033.931	452.900
194L	SC194622R	Scribed X	1146.965	1152.965	110.473	565258.297	92822.654	463.360
194L	PC194634L	Carriage bolt	1270.004	1000.000	120.183	565066.619	92865.064	473.070
194L	TS194666L	Scribed X	NC	NC	NC	565050.838	92857.492	477.511
202R	SC202340R	Scribed X	1044.408	975.551	106.645	561272.828	84158.054	445.162
202R	TS202370R	PK nail	1024.349	1000	97.984	561241.435	84154.23	436.501
202R	TS202384R	Chiseled X	1000.000	1000.000	100.000	561228.380	84133.676	438.517
202R	SO202396L	Scribed X	NC	NC	NC	561100.734	84249.794	436.931
202R	SC202402L	Scribed X	1032.231	1210.807	105.909	561067.711	84273.908	444.434
213L	SO213230R	Scribed X	1026.509	823.030	103.600	546168.612	85265.775	414.243
213L	SC213241L	Carriage bolt	1083.434	1000.000	102.655	546082.668	85430.618	413.315
213L	TS213200L	Destroyed	1000.000	1000.000	100.000	546024.05	85371.244	410.658
213L	TC213305L	Carriage bolt	993.606	1030.224	104.863	545998.049	85387.928	415.523
220R	SC220014R	Scribed X	1105.719	1107.551	94.481	536815.225	85911.716	401.024
220R	TS220038R	Chiseled X	1089.514	1056.045	91.510	536816.174	85965.705	398.056
220R	SC220039L	PK nail	1000.000	1000.000	100.000	536886.146	86044.816	406.552
220R	TS220104R	Chiseled T	1141.456	1000.000	91.028	536750.48	86004.740	397.574
225R	TS225419L	Scribed X	949.078	830.795	98.670	530143.980	82147.959	386.032
225R	TS225487R	Chiseled X	1000.000	1000.000	100.000	530167.463	81972.808	387.367
225R	TS225606R	Chiseled X	1090.963	1000.000	97.816	530084.607	81935.248	385.189
225R	SC225565R	Scribed X	1142.269	1027.831	110.163	530049.365	81888.713	397.539

[1]The descriptor "R" denotes the location at the study site on river-right and "L" for river-left, with the observer facing downstream. The number is the approximate location of the river mile marker based on the river mile (RM) centerline downstream from Lees Ferry (RM 0), Arizona.

References Cited

Beus, S.S., Carothers, S.W., and Avery, C.C., 1985, Topographic changes in fluvial terrace deposits used as campsite beaches along the Colorado River in Grand Canyon: Journal of the Arizona-Nevada Academy of Science, v. 20, no. 2, p. 111–120, accessed January 20, 2017, at http://www.jstor.org/stable/40021335.

Ferrari, R., 1987, Sandy beach area survey along the Colorado River in the Grand Canyon National Park—Glen Canyon Dam environmental study: Durango, Colo., U.S. Geological Survey, U.S. Bureau of Reclamation, prepared in cooperation with the Glen Canyon Environmental Studies, no. PB88–183389, GCES/06/87, 15 p. [This report is available from the U.S. Geological Survey Grand Canyon Monitoring Research library.]

Gushue, T.M., 2019, Colorado River Mile System, Grand Canyon, Arizona: U.S. Geological Survey data release, https://doi.org/10.5066/P9IRL3GV.

Howard, A.D., 1975, Establishment of benchmark study sites along the Colorado River in Grand Canyon National Park for monitoring of beach erosion caused by natural forces and human impact: University of Virginia Grand Canyon Study technical report no. 1, 182 p. [Available at the Northern Arizona University Cline Library, Special Collections, F788. C6856 1975.]

Schmidt, J.C., and Graf, J.B., 1990, Aggradation and degradation of alluvial sand deposits, 1965 to 1986, Colorado River, Grand Canyon National Park, Arizona: U.S. Geological Survey Professional Paper 1493, 74 p., https://doi.org/10.3133/pp1493.

Appendix 3. Empirically Based Stage-Discharge Relations and Debris-Flow Induced Changes to Local Stage-Discharge Relations, Colorado River, Glen Canyon Dam to Diamond Creek, Arizona

Stage-Discharge Relations

The stage-discharge relations developed by Hazel and others (2006) were revised in this study from water-surface elevation data surveyed at known discharges. The study site stage-discharge relations for all 45 study sites (table 1) are shown in figure 3.1. The upstream and downstream extent to which each relation applies, and the statistical fit, are shown in table 3.1. The relations are second-order polynomials empirically developed from surveyed water-surface elevations during periods of steady Glen Canyon Dam discharge, peak flow strand lines from high-flow experiments (HFEs), and the trough and peak discharges from diurnal Glen Canyon Dam operations. The methods by which these relations are calculated are described by Hazel and others (2006). The stage elevation prediction error was estimated by Hazel and others (2006) as ±0.05 meter (m) and have coefficients of determination (R^2) ranging from 0.991 to 0.999 (table 3.1).

Changes Induced by Debris Flows

Over the period of study, 1990–2020, only debris-flow induced changes to debris fans caused significant changes in the local stage-discharge relation. Though most stage discharge relations have been stable during the period of study, there were four tributary flood events that caused substantial changes to either the water surface-elevation or surficial changes to the sandbar surface that directly affected analysis from repeat measurements. These events have implications for the automated volume and area computations included in this report.

The first was a debris flow in Tanner Canyon on August 20, 1993 (fig. 3.2). Aggradation of the debris fan constricted the river by about 30 meters (m) and increased the severity and gradient of the rapid (Melis and others, 1994). The water-surface elevation of the pool upstream from Tanner Canyon Rapids (river mile [RM] 69.0) increased by about 1.2 m at a discharge of 227 cubic meters per second (m^3/s) (fig. 3.3). The riffle that existed at the upstream end of the pool, prior to the event, is no longer present (drowned out) at all observed discharges in the Colorado River (fig. 3.2*A*). Eyewitnesses to the event report that a muddy recessional flow lasting 2 to 3 hours followed the initial pulse of debris as it entered the river (fig. 32*B*, *C*). Reworking of the aggraded debris fan by the 1996 HFE did not entirely remove the changes to the debris fan; large boulders deposited by the debris flow were unchanged by the flood (Webb and others, 1999). Stage data compiled at study site 068R in the years after the 1996 HFE indicate the upper-pool elevation was only reduced by 0.25 to 0.45 m at most flows. Between April 1996 and 2020 the rating curve has remained stable (shown in black in fig. 3.3). Thus, comparison of calculated volume results to previous years will be under- or over-biased because the stage elevations of the zones of interest have changed three times during the period of study. As a result, the data from this monitoring site are not used in time-series analyses that are a function of metrics such as site averaging. The stage-discharge relation shown in figure 3.1 for study site 068R only uses data collected from 1996 to 2020.

The second event to affect a stage-discharge relation utilized in this report occurred in 2002, when the water-surface elevation of the pool upstream from Lava Canyon Rapids (the downstream hydraulic control on the stage-discharge relation just south of study site 065R) increased by 0.3–0.5 m (fig. 3.3). The exact event is uncertain, but we believe that one or more small debris flows may have occurred in Lava Canyon (RM 65.5R) or Palisades Creek (RM 65.5L) that possibly increased the constriction of the river at Lava Canyon Rapids (for location of Lava Canyon and the Palisades debris-fan see fig. 1 of Hazel and others, 2008). This interpretation is based on the fresh appearance of deposits on the debris fan at the mouth of Lava Canyon after the sandbar survey on September 27, 2002, and on gully incision reported by Hazel and others (2008) at the Palisades gully network located downstream from the Palisade Canyon debris fan during this same period. There was active monsoon-thunderstorm precipitation in the region in August and September 2002, but the changes may have occurred during one storm. An unusual frontal system from the Pacific Ocean produced widespread rain and resulted in tributary debris flows to the Colorado River between the mouth of the Little Colorado River and Phantom Ranch on September 7, 2002 (Webb, 2003). The increase in the stage-discharge relation was largely reversed by reworking during the 2004 HFE (fig. 3.3). As a result, the stage-discharge relation for study site 065R used in this report excludes data from the 2002–2004 period.

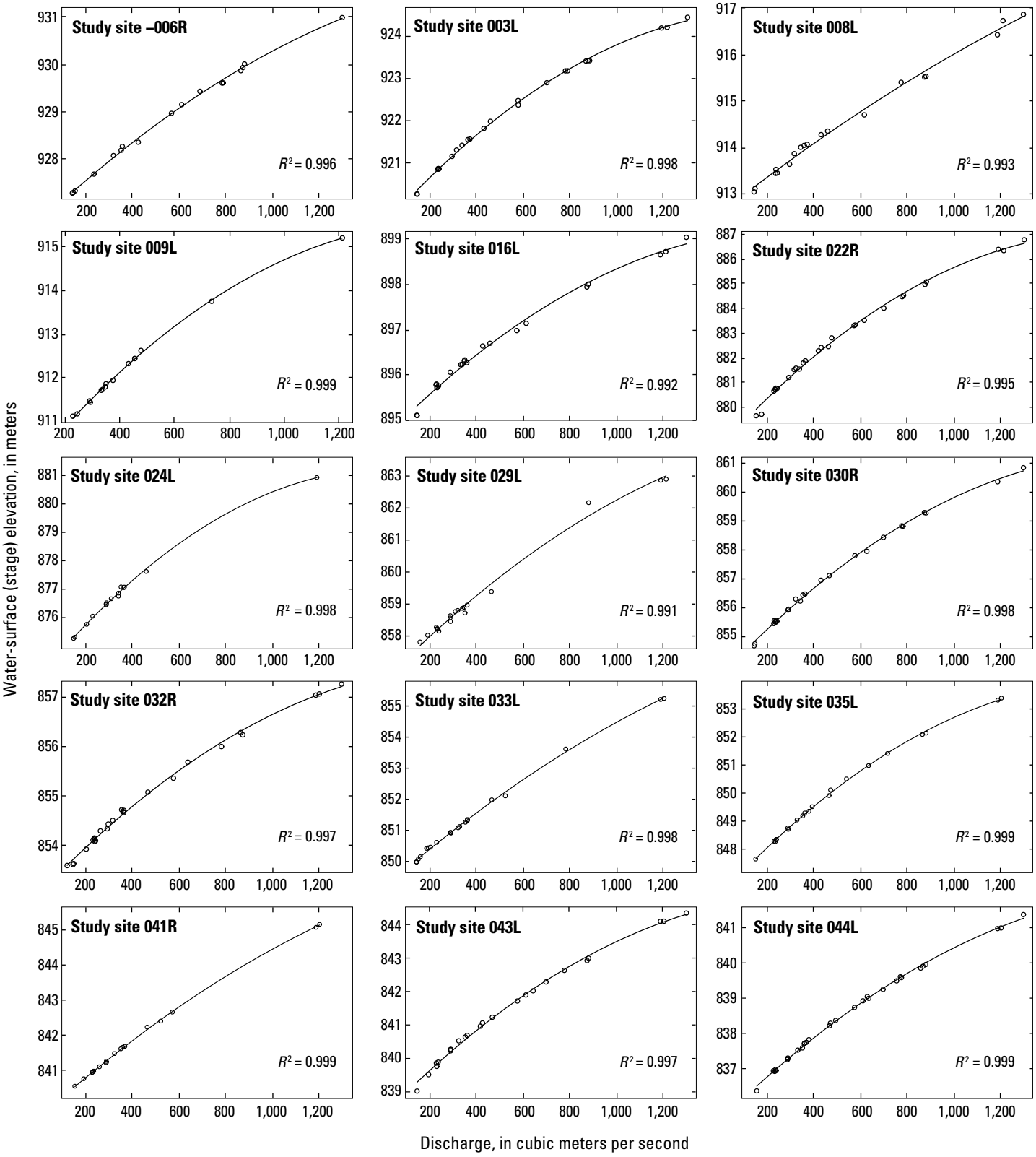

Figure 3.1. Study site stage-discharge relations, Colorado River, Glen Canyon Dam to Diamond Creek, Arizona. The relations are second-order polynomials empirically developed from surveyed water-surface elevations during periods of steady Glen Canyon Dam discharge, peak flow strand lines from high-flow experiments (HFEs) and the trough and peak discharges from diurnal Glen Canyon Dam operations (fig. 3 of the main text). The open circles show the stage elevations and assigned discharges determined from the nearest U.S. Geological Survey (USGS) streamgage stations upstream or downstream from each site. The study site identification is shown in the upper left corner of each plot and map location is shown in figure 1 of the main text. Currently all sites listed in this report reference the 2007 realization (NSRS 2007) of the North American Datum of 1983 (NAD 83). *Z*, elevation in meters (m); *Q*, discharge in cubic meters per second (m^3/s); R^2, coefficient of determination. For list of study sites, see table 1 of the main text.

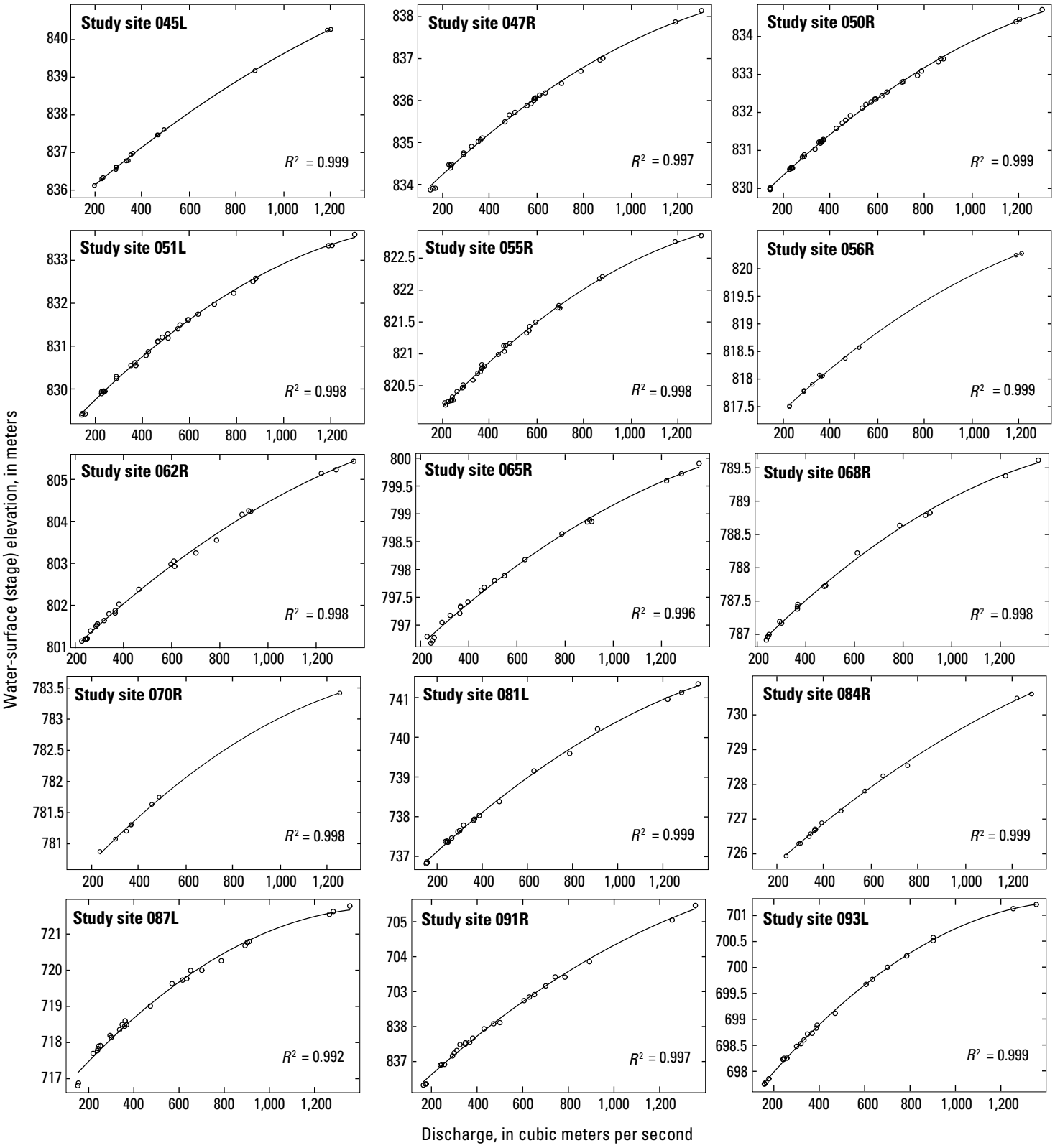

Figure 3.1.—Continued

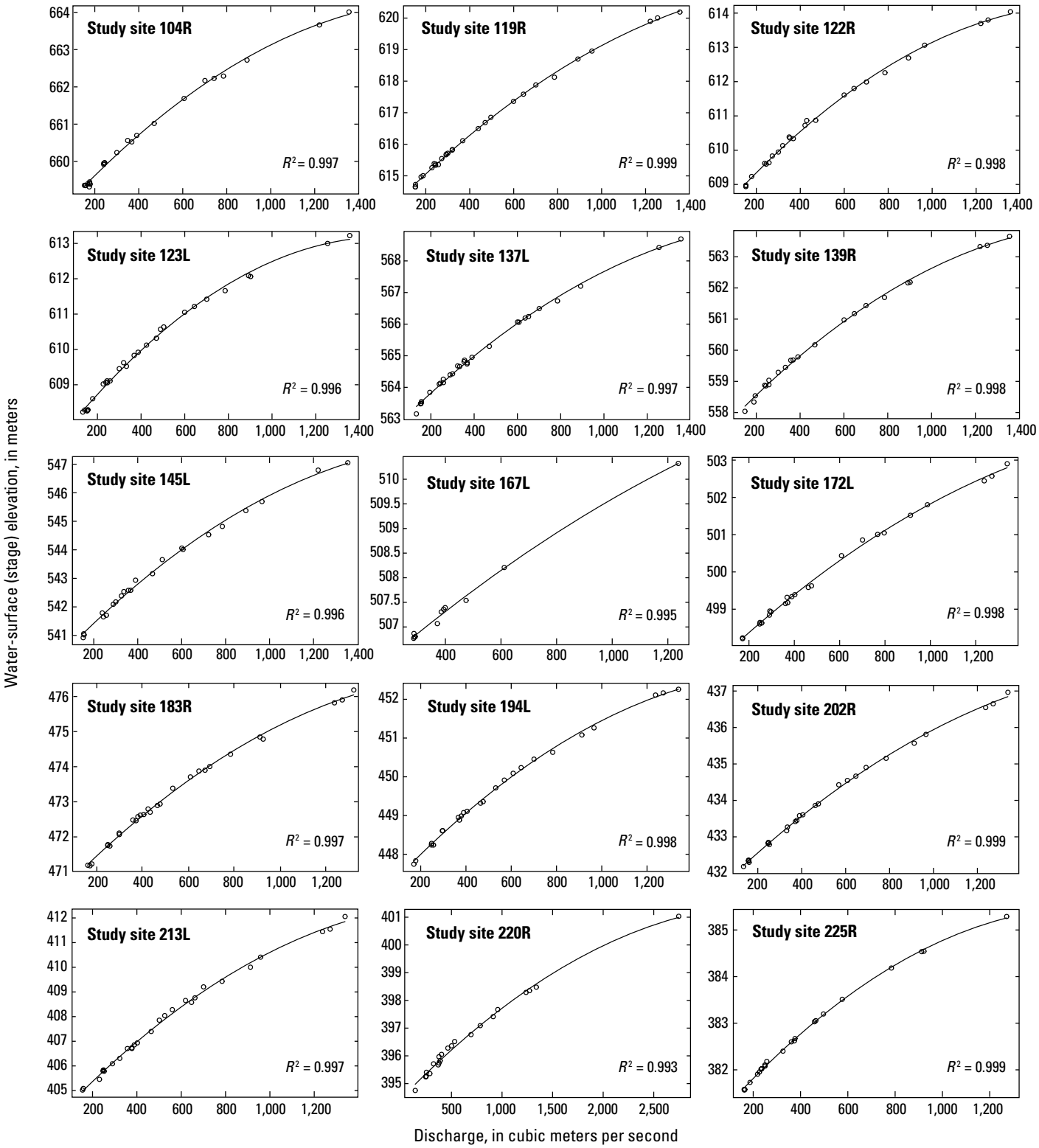

Figure 3.1.—Continued

Table 3.1. Study site names, locations, and stage-discharge relations, Colorado River, Glen Canyon Dam to Diamond Creek, Arizona (fig. 3.1).

[The relations are second-order polynomials empirically developed from surveyed water-surface elevations during periods of steady Glen Canyon Dam discharge, peak flow strand lines from high-flow experiments (HFEs) and the trough and peak discharges from diurnal Glen Canyon Dam operations. Site names are given by location along the river mile (RM) centerline (Gushue, 2019) downstream from Lees Ferry (RM 0), in Grand Canyon National Park except −6.5R (study site −006R), which is in Glen Canyon National Recreation Area (for list of study sites, see table 1 of the main text). Extent is channel reach to which stage-discharge relation applies in river miles; *Z*, elevation in meters (m) above North American Datum of 1983 (NAD 83). Currently all sites listed in this report reference the 2007 realization (NSRS 2007) of the NAD 83 in ellipsoid height. *Q*, discharge; m^3/s, cubic meter per second; R^2, coefficient of determination. Some values use exponential notation (E-notation)]

Study site name (RM)	Upstream extent (RM)	Downstream extent (RM)	Stage-discharge relation	R^2
−006R	−6.7	−6.5	Z=926.68+0.00458Q−9.667E−07Q^2	0.996
003L[a]	2.48	2.68	Z=919.53+0.00611Q−1.845E−06Q^2	0.998
008L	8.1	8.35	Z=912.61+0.00394Q−5.330E−07Q^2	0.993
009L	8.8	9.02	Z=909.45+0.00767Q−2.409E−06Q^2	0.999
016L	16.65	16.8	Z=894.59+0.00522Q−1.466E−06Q^2	0.992
022R	21.05	22.08	Z=878.47+0.0103Q−3.065E−06Q^2	0.995
024L	23.53	23.65	Z=873.92+0.00976Q−3.260E−06Q^2	0.998
029L	29.43	29.55	Z=856.98+0.00557Q−5.457E−07Q^2	0.991
030R	30.68	30.82	Z=853.67+0.00849Q−2.352E−06Q^2	0.998
032R	31.85	32.05	Z=853.04+0.00493Q−1.319E−06Q^2	0.997
033L	33.15	33.3	Z=849.15+0.00655Q−1.217E−06Q^2	0.998
035L	35.03	35.2	Z=846.38+0.00891Q−2.596E−06Q^2	0.999
041R	41.2	41.52	Z=839.64+0.00597Q−1.161E−06Q^2	0.999
043L	43.37	43.47	Z=838.31+0.00709Q−1.901E−06Q^2	0.997
044L	44.4	44.72	Z=835.53+0.00648Q−1.593E−06Q^2	0.999
045L	44.87	45.03	Z=835.06+0.00566Q−1.102E−06Q^2	0.999
047R	47.5	47.75	Z=833.14+0.00581Q−1.537E−06Q^2	0.997
050R	50.1	50.25	Z=829.14+0.00636Q−1.638E−06Q^2	0.999
051L	51.32	51.57	Z=828.6+0.00609Q−1.767E−06Q^2	0.998
055R	55.8	56	Z=819.32+0.00437Q−1.261E−06Q^2	0.998
056R	56.5	56.57	Z=816.58+0.00448Q−1.176E−06Q^2	0.999
062R	62.82	62.98	Z=799.88 +0.00592Q−1.345E−06Q^2	0.998
065R[b]	65.08	65.3	Z=795.79 +0.00445Q−1.075E−06Q^2	0.996
068R[c]	68.65	68.9	Z=786.04+0.00413Q−1.120E−06Q^2	0.998
070R	70.01	70.1	Z=779.87+0.00441Q−1.260E−06Q^2	0.998
081L	81.73	81.78	Z=736.02+0.00575Q−1.374E−06Q^2	0.999
084R	84.5	84.6	Z=724.48+0.00655Q−1.371E−06Q^2	0.999
087L	87.5	87.68	Z=716.09+0.00745Q−2.459E−06Q^2	0.992
091R	91.72	91.8	Z=699.4+0.00639Q−1.473E−06Q^2	0.997
093L	93.75	93.86	Z=696.92+0.00567Q−1.846E−06Q^2	0.999
104R	104.35	104.45	Z=658.38+0.00654Q−1.800E−06Q^2	0.997
119R	119.33	119.45	Z=613.7+0.00717Q−1.736E−06Q^2	0.999
122R	122.7	122.8	Z=607.97+0.00729Q−2.110E−06Q^2	0.998
123L	123.17	123.3	Z=607.28+0.00775Q−2.538E−06Q^2	0.996
137L	137.65	137.72	Z=562.5+0.00692Q−1.765E−06Q^2	0.997
139R	139.5	139.66	Z=557.13+0.00754Q−2.043E−06Q^2	0.998
145L	145.83	145.9	Z=539.88+0.00813Q−2.107E−06Q^2	0.996
167L	167.1	167.25	Z=505.42+0.00511Q−9.275E−07Q^2	0.995
172L	172.5	172.7	Z=497.25+0.00586Q−1.281E−06Q^2	0.998
183R	183.2	183.38	Z=470.18+0.00678Q−1.774E−06Q^2	0.997
194L	194.5	194.7	Z=446.8+0.00635Q−1.692E−06Q^2	0.998
202R	202.3	202.48	Z=431.44+0.00586Q−1.363E−06Q^2	0.999
213L	213.3	213.28	Z=403.55+0.00958Q−2.525E−06Q^2	0.997
220R	220.05	220.12	Z=394.21+0.00469Q−1.145E−06Q^2	0.993
225R	225.4	225.6	Z=380.72+0.00585Q−1.791E−06Q^2	0.999

[a]Excludes data from 2013–2015.

[b]Excludes data from 2002–2004.

[c]Only uses data collected from April 1996 to 2020.

Figure 3.2. Photographs of the Tanner Canyon debris fan eddy-complex and associated pool and eddy sandbar in the Colorado River corridor, Grand Canyon. *A*, Aerial photograph of the area taken on October 12, 1992. Discharge was approximately 227 cubic meters per second (m^3/s). Direction of flow is from top to bottom and study site 068R is located on the right side of the river on the inside bend. The debris fan is located on the left side of the river at the tributary mouth of Tanner Canyon, lower right in the photograph. Note the riffle at the upstream end of the pool at the top of the photograph. *B*, View of Tanner Canyon looking upstream showing muddy, recessional streamflow after the debris-flow event. *C*, The same recessional flow debouching into the Colorado River. View is toward the southwest and the head of Tanner Rapid. Aerial photograph in *A* by the Bureau of Reclamation. Photographs of Tanner Creek on August 20, 1993, in *B* and *C* taken by Suzanne Rhodes. HFE, high-flow experiment; m, meters. For list of study sites, see table 1 of the main text.

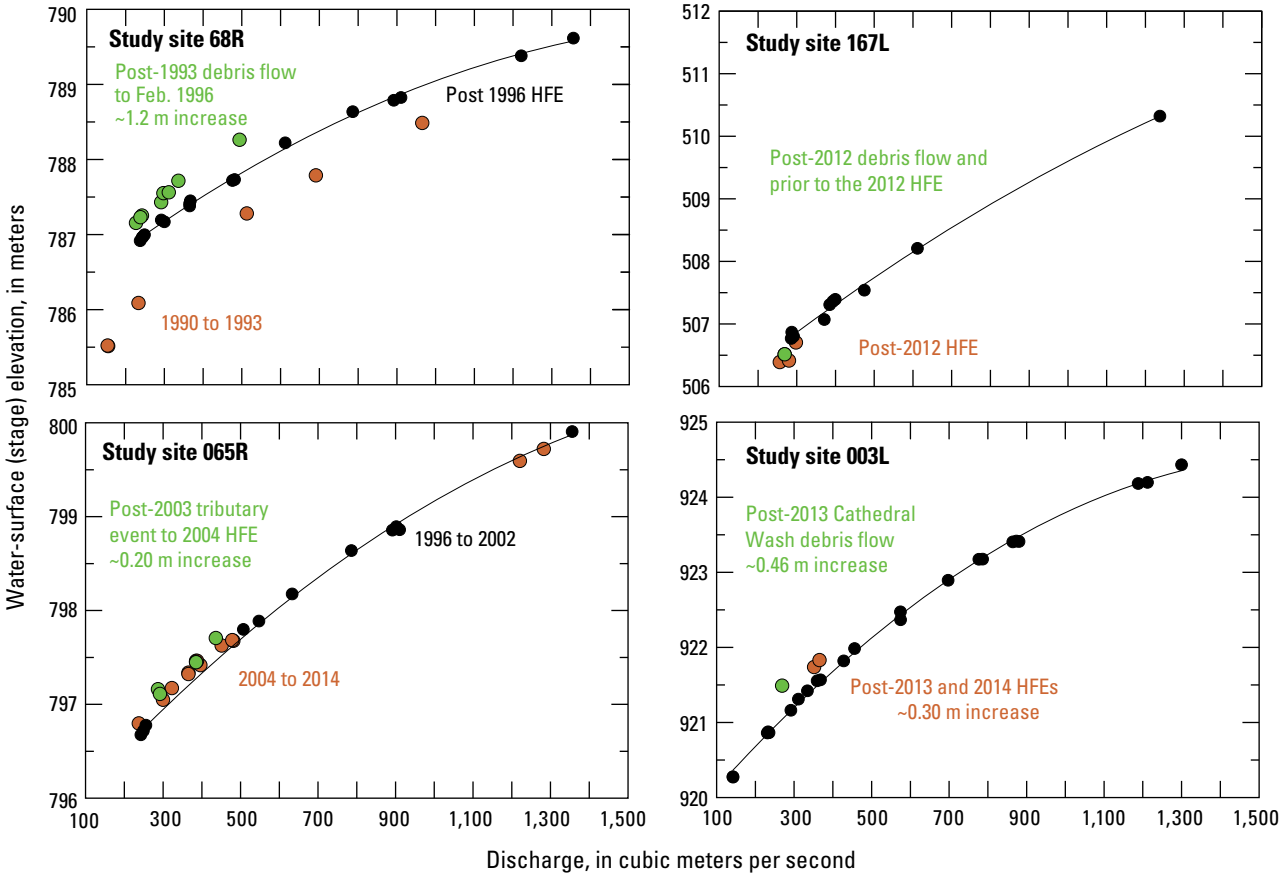

Figure 3.3. Plots of stage-discharge relations for study sites affected by debris flows during the study period, Colorado River corridor, Marble and Grand Canyons. Each plot shows the relation shown in figure 3.1 (black dots) compared to the elevations of stage data measured prior to and after debris-flow events. Debris-flow induced changes to the channel constriction that controls the elevation reached by a particular Glen Canyon Dam discharge can potentially affect the stage-discharge relations utilized in this report. For list of study sites, see table 1 of the main text. HFE, high-flow experiment; m, meter; ~, approximately.

On July 14, 2012, a debris flow in National Canyon completely buried the debris fan, constricted the river thereby enlarging the riffle, and removed portions of long-term monitoring site 167L (fig. 3.4). The debris flow deposited at least 2,060 cubic meters (m^3) of poorly sorted sediment on the downstream margin of the debris fan. The increase in plan area of this part of the debris fan was 2,060 square meters (m^2). The aggradation restricted the river at the downstream part of the riffle by 5 to 10 m and the new aggradation extended 35 m downstream (fig. 3.5). The middle and upstream portion of the debris fan is not surveyed by Northern Arizona University as part of long-term monitoring site 167L. The debris flow transported mostly boulders less than 1 m in diameter, gravel, and coarse sand. A channel was scoured about 2 m and the incision removed the river-side edge of the undifferentiated eddy bar mantling the downstream area of the fan. The changes at National Canyon were not completely removed by subsequent HFEs in 2012, 2013, 2014, 2016, and 2018 and as a result, this study site is not included in time-series analyses. We note, however, that the stage-discharge relation for the site was largely unaffected (fig. 3.3).

On September 11, 2013, a debris flow in Cathedral Wash aggraded the debris fan downstream from study site 003L. As measured on September 21, 2013, the surveyed water surface elevation indicated an approximately 46 centimeter (cm) increase in pool elevation. Reworking of the debris fan by the 2013 HFE and 2014 HFE removed some of this material and the increase in pool elevation was reduced by 15 or 20 cm. The upstream sandbar monitored by Northern Arizona University at study site 003L was largely unaffected. Nonetheless, water-surface stage elevation data collected in 2013–2015 were not used in computation of the stage discharge relation shown in figure 3.1 for study site 003L.

The only other known debris flow to potentially affect a study site (008L) in this study occurred on August 17, 1994, when a debris flow occurred in Jackass Creek. Before the 1994 event, no debris flows had occurred in Jackass Creek between 1890 and 1993 (Melis and others, 1994). Although the debris flow enlarged the fan, no effects to the sandbar mantling the downstream side of the fan were documented and the stage-discharge relation for the site was unaffected.

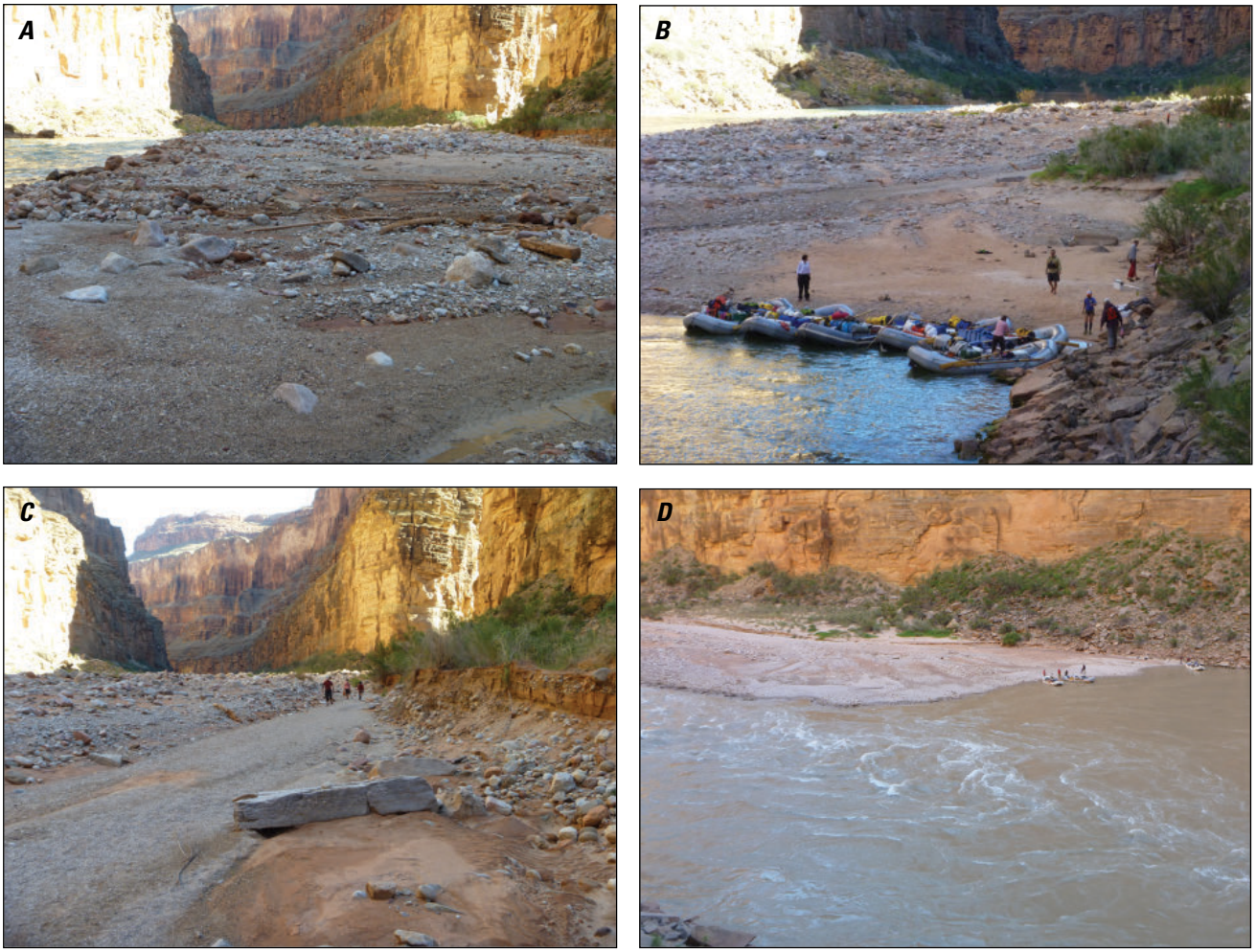

Figure 3.4. Photographs taken on October 16, 2012, following the July 14, 2012, debris flow in National Canyon that removed portions of long-term monitoring site 167L located at lower National Camp, Colorado River corridor, Arizona. *A*, Upstream view of the left side of the new deposit constricting the Colorado River. *B*, Upstream view of the distal, downstream part of the debris fan. The boats are parked at the normal boat mooring for the lower National Camp. The water's edge is 35 meters (m) downstream from the location of the edge of the camp prior to the event. *C*, View upstream of the drainage channel showing incision of the sandbar monitoring site. Photographs by Joseph E. Hazel, Jr., Northern Arizona University. *D*, Photograph taken by remote camera on October 4, 2013, showing reworking and smoothing of the debris fan surface by the 2012 high-flow experiment (HFE). The photographs suggest that few boulders greater than 1 meter (m) in diameter were transported in the debris flow. For list of study sites, see table 1 of the main text.

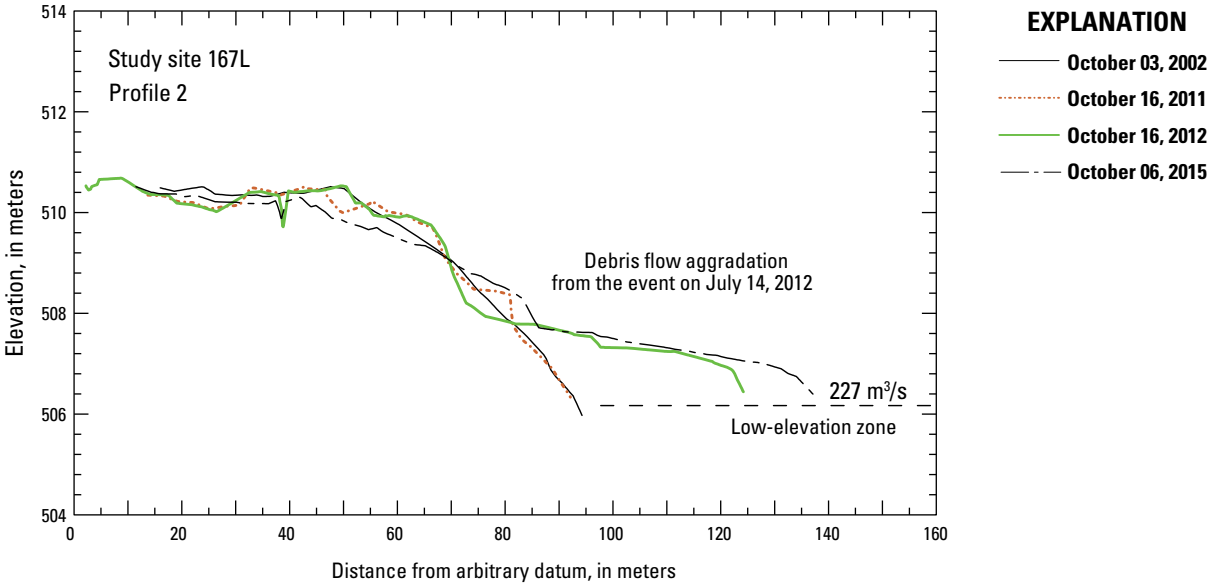

Figure 3.5. Cross-sectional profile across the sandbar and debris fan at study site 167L, Colorado River corridor, Grand Canyon. The profile from the October 2012 survey (3 months after the debris-flow event in National Canyon on July 14, 2012), showing deposition of poorly sorted debris-flow deposits on the downstream side of the existing debris fan. For list of study sites, see table 1 of the main text. The low elevation zone (fig. 21 of the main text) represents the volume of sand between the minimum surface and the elevation reached by a 227 cubic meter per second (m^3/s) flow.

References Cited

Gushue, T.M., 2019, Colorado River Mile System, Grand Canyon, Arizona: U.S. Geological Survey data release, https://doi.org/10.5066/P9IRL3GV.

Hazel, J.E., Jr., Kaplinski, M., Parnell, R., and Fairley, H.C., 2008, Aggradation and degradation of the Palisades gully network, 1996 to 2005, with emphasis on the November 2004 high-flow experiment, Grand Canyon National Park, Arizona: U.S. Geological Survey Open-File Report 2008–1264, 14 p., https://doi.org/10.3133/ofr20081264.

Hazel, J.E., Jr., Kaplinski, M., Parnell, R., Kohl, K.A., and Topping, D.J., 2006, Stage-discharge relations for the Colorado River in Glen, Marble, and Grand Canyons, Arizona, 1990–2005: U.S. Geological Survey Open-File Report 2006–1243, 7 p., https://doi.org/10.3133/ofr20061243.

Melis, T.S., Webb, R.H., Griffiths, P.G., and Wise, T.J., 1994, Magnitude and frequency data for historic debris flows in Grand Canyon National Park and vicinity, Arizona: U.S. Geological Survey Water-Resources Investigations Report 94–4214, 285 p., https://doi.org/10.3133/wri944214.

Webb, R.H., 2003, 2002 debris flows and floods in Grand Canyon: Boatman's Quarterly Review, v. 15, no. 4, p. 14–15, accessed July 28, 2018, at https://static1.squarespace.com/static/61d3bc4beef7c3126df06d78/t/61f722e7009f102334fb4e9d/1643586282035/15-4.pdf.

Webb, R.H, Melis., T.M., Griffiths, P.G., and Elliot, J.G., 1999, Reworking of aggraded debris fans, *in* Webb, R.H., Schmidt, J.C., Marzolf, G.R., and Valdez, R.A., eds., The controlled flood in Grand Canyon: American Geophysical Union Geophysical Monograph Series, v. 110, p. 37–51, https://doi.org/10.1029/GM110p0037.

Appendix 4. Topographic Uncertainty and Computed Digital Elevation Model Volume Error

Elevation uncertainties associated with the digital elevation models (DEMs) were estimated using a number of existing approaches and as a function of data collection method. Uncertainties in elevation and DEM quality arise from (1) the precision and accuracy of the data points used to construct the surface, (2) the distribution and density of point coverage relative to areas of complex topographic morphology, and (3) the techniques used in surface construction and comparison (Lane, 1998; Weschler and Kroll, 2006; Blak, 2007; Weschler, 2007). Three different data collection methods were utilized in this study: (1) total station (TS) surveys, (2) singlebeam (SBES) echosounder sonar surveys, and (3) multibeam echosounder (MBES) sonar surveys. We examined the uncertainty associated with collecting each method to test for systematic errors in the datasets and then test the uncertainty of the surfaces derived from the data for each data collection type.

Our definition of uncertainty is limited to the vertical or elevation component source of error. Because the resolution of the digital elevation models (DEMs) produced in this study are at least an order of magnitude greater than typical values of horizontal positional uncertainty of individual survey points, we consider horizontal uncertainty negligible (Wheaton, 2008). Blunders (see "Data Collection" section) were identified and removed prior to surface construction, and we do not consider these errors in the total error budget. The uncertainty in the absolute position of the control points relative to real-world coordinates is not included in our uncertainty estimates, as we used the same control points for each repeat survey. However, when comparing the measurements in this study to measurements acquired by other methods, such as airborne and terrestrial light detection and ranging (lidar), photogrammetry, or Global Positioning System (GPS), the positional accuracy of the control network should be considered.

DEMs primarily derive uncertainty from two sources: (1) the survey uncertainty associated with acquiring the point data; and (2) the interpolation uncertainty associated with generating a surface from the point datasets (that is, differences in point density and surface construction). If both error components are independent and subject only to random error (Taylor, 1997), estimates of the total uncertainty budget are expressed as:

$$TU_z = \sqrt{(SU_z)^2 + (IU_z)^2}, \quad (4.1)$$

where

TU_Z is the total surface uncertainty for a given survey method,

SU_Z is the survey uncertainty of individual topographic point data, and

IU_Z is the uncertainty associated with interpolating the topographic surface from the point datasets.

Standard methods used to evaluate uncertainty test either the individual components of the uncertainty budget (SU_Z and IU_Z) or directly estimate the total surface uncertainty (TU_Z). In this study, we first examined the survey uncertainty (SU_Z) using quality control checks for each survey method to determine if systematic errors exist in the datasets, then estimated the total uncertainty (TU_Z) of the DEMs. The total uncertainty (TU_Z) associated with the DEMs derived from TS data was estimated directly using checkpoints and repeat surveys. For the bathymetric data, estimates of the survey uncertainty (SU_Z) and interpolation uncertainty (IU_Z) were combined using equation 4.1 to estimate the TU_Z.

Uncertainty estimates are presented using a standard set of statistical parameters. These metrics are the mean error in elevation (ME_Z), mean absolute error in elevation (MAE_Z), root-mean-square error in elevation ($RMSE_Z$) at the 95 percent confidence level, standard deviation (SD), and skewness. These statistics conform to the National Standard for Spatial Data Accuracy (The Federal Geographic Data Committee [FGDC], 1988) and are expressed as:

$$ME_z = \sum_{i=0}^{n} \frac{\Delta EH_i}{n} \quad (4.2)$$

$$MAE_z = \sum_{i=0}^{n} \left(\frac{|\Delta EH_i|}{n} \right) \quad (4.3)$$

$$RMSE_z = 1.96 \sqrt{\sum_{i=0}^{n} \frac{(\Delta EH_i)^2}{n}} \quad (4.4)$$

$$SD = \sqrt{\frac{1}{n} \sum_{i=0}^{n} (\Delta EH_i - ME_z)^2} \quad (4.5)$$

$$Skewness = \frac{n}{(n-1)(n-2)} \sum_{i=0}^{n} \left(\frac{\Delta EH_i - ME_z}{SD} \right)^3, \quad (4.6)$$

where

ΔEH_i is the ellipsoid height difference between corresponding datasets, and

n is the number of sample points.

For this report, we use the MAE_Z statistic for uncertainty estimates. The MAE_Z statistic includes any potential bias associated with repeat measurements (because absolute elevation differences do not cancel out) and provides the best estimate of the average error of the dataset.

Total Station Uncertainty

Total Station Point Data

Total station (TS) measurement quality is a function of instrument precision and the errors associated with the individual points collected. For this study, we chose to analyze three components individually and combine them in quadrature to arrive at an uncertainty for the TS measurements, revising the propagated error associated with these various components determined by Hazel and others (2008). The first component of the assessment is the uncertainty associated with occupying the control points. Second, we assessed the uncertainty associated with external errors that arise during a TS survey. The third component assessed the uncertainty associated with occupying individual ground points with an extendable survey rod.

For the first two components of the assessment, we used backsite observations from a total of 21 surveys selected randomly over five river trips (fig. 4.1*A*; table 4.1) and compared the elevation difference between the observation and published control point. The first component only used the opening backsite observation following the initial leveling, with reciprocal angle measurements and distance averaging. The second component examined backsite observations that occur during surveys of each site (between 300 and 2,000 points per survey). This assessment accounts for errors that arise during the duration of a survey from variations in natural phenomena such as temperature, humidity, and wind. These factors can shift the instrument out of level (referred to as drift), thereby increasing instrument error and variance between measurements. These backsite observations are made frequently during a survey (every 15–30 minutes) and errors are recorded by a single measurement (referred to as a sideshot). For the third component, we targeted the extendable survey rod at all five configurations (base configuration of one rod height, plus four extensions) to examine the random error resulting from the ability of the operator to plumb the rod over a control point (fig. 4.1*B*). Even in calm environmental conditions it is difficult to plumb the rod at the different heights to which the rod can be extended, which can introduce error to the measurement (fig. 4.1*C*). Non-plumb survey rod error was assessed by Wheaton (2008), who found that even a slight tilt angle of 10° can result in as much as 0.06 meter (m) of vertical error when using a 2-m rod.

The results show that there is no systematic error associated with the TS point measurements, with MAE_Z values for all observations (that is, instrument setup, drift, and rod error) less than 0.01 m (table 4.1). The errors associated with backsite checks are of the same order of magnitude as those derived by reciprocal angle measurement, indicating the degradation of measurement precision associated with the data collection method (that is, external and operator error) was minimal. The errors associated with plumbing the extendable rod were observed to be negligible. Despite increasing positional error with each increase in rod length (or height), the vertical uncertainty varied little between different rod heights. Summation of the three components in quadrature shows a combined SU_Z for TS measurements of 0.014 m. This empirical estimate is considerably lower than the accuracy of ±0.05 m identified as the minimum precision of SU_Z by Hazel and others (2008).

Total Station Digital Elevation Model Uncertainty

We estimated the TU_Z of DEMs resampled from triangulated irregular networks (TINs) of the processed TS points using two independent methods. The first test compared checkpoint elevations from independent surveys to DEM elevations (Blak, 2007). The second test compared DEM elevations from repeat surveys.

A checkpoint analysis uses points from an independent survey to compare to the DEM elevations constructed from a different survey and complies with the National Digital Elevation Program (NDEP) standards for vertical accuracy tests (NDEP, 2004). We chose checkpoints from surveys collected on or near the same date at nine study sites with similar TS methods (table 4.2). Point densities of the surveys are typical of the subaerial surveys presented in this report, ranging from 0.03 to 0.13 points per square meter (pts/m^2), with an average density of 0.08 pts/m^2. The maximum interval between surveys was 21 days so the surfaces may have been altered by wind, foot traffic, or rain; however, we verified the analysis by collecting two surveys at the same study site (081L) on April 12, 2011. To ensure that each survey at study site 081L was truly independent, the survey equipment was broken down, a different total station leveled, and the survey conducted with different personnel using the same feature-based point collection method.

Twenty checkpoints were selected (from the surveys listed in table 4.2) in areas located on flat terrain or on uniformly sloping surfaces following the criteria of Blak (2007) and to avoid steep breaks in slope where subsequent interpolation might result in points located on the wrong sides of breaklines (Li, 1991). The checkpoints were confined to areas above the stage elevation reached by the highest discharge between surveys, or erosional cutbank caused by that discharge. The statistical measures of elevation discrepancies between the checkpoints and the elevations interpolated from the DEMs are shown in table 4.3. The ME_Z and MAE_Z differences ranged from −0.018 to 0.038 m and 0.019 to 0.049 m, respectively. The MAE_Z of the combined dataset was 0.032 m, which we use as an estimate of vertical uncertainty for TS surveys.

In addition to using checkpoints, we also examined the same set of surveys by summarizing the elevation difference at concurrent grid points in the 1-m-resolution DEMs (table 4.4). As opposed to the checkpoint comparison, this method includes points in topographically more complex areas. The ME_Z and MAE_Z differences ranged from −0.052 to 0.035 m and 0.035 to 0.109 m, respectively. The combined, or pooled differences from all surveys, have a ME_Z of 0.001 m, showing that when spatially integrated over the surface, elevation differences between surveys balance, or cancel out. However, the combined MAE_Z of 0.063 m is nearly double that of the MAE_Z obtained from the checkpoint analysis. We use the average of these values, 0.048 m, as an estimate of TU_Z rather than using this value in equation 4.1 as an estimate for SU_Z for DEMs constructed solely from TS-acquired data. Averaging these two estimates of interpolation error accounts for the tradeoff between potential bias in the surfaces (because of point density differences) and topographic complexity (slopes and roughness).

Table 4.1. Total station (TS) positional uncertainties at control points used as backsites compared to each extension of the 7.6-meter (m) collapsible survey rod, Colorado River corridor, Marble and Grand Canyons, Arizona.

[*n*, number of observations; m, meter; ME_z, vertical mean error; MAE_z, vertical mean absolute error; $RMSE_z$, vertical root mean square error; SD, standard deviation; BOS, beginning of survey; %, percent]

Observation	*n*	ME_z (m)	MAE_z (m)	95% $RMSE_z$ (m)	SD (m)	Skewness
Backsite BOS[1]	133	−0.001	0.008	0.021	0.006	−0.030
Backsite check[2]	347	0.011	0.008	0.021	0.010	2.218
1 rod height	40	0.006	0.007	0.018	0.007	0.086
One extension	40	0.007	0.007	0.022	0.009	−0.450
Two extensions	40	0.007	0.007	0.023	0.009	0.063
Three extensions	40	0.003	0.003	0.017	0.008	0.285
Four extensions	40	−0.002	0.008	0.023	0.012	−1.367
All extensions[3]	200	0.004	0.008	0.021	0.010	−0.739

[1]Opening survey reciprocal angle measurement in both direct- and reverse-scope and by multiple distance measurement.

[2]Control-point checks and closing shots that record instrument leveling drift during changing environmental conditions.

[3]This row shows an average value for each statistical metric derived by pooling all observations.

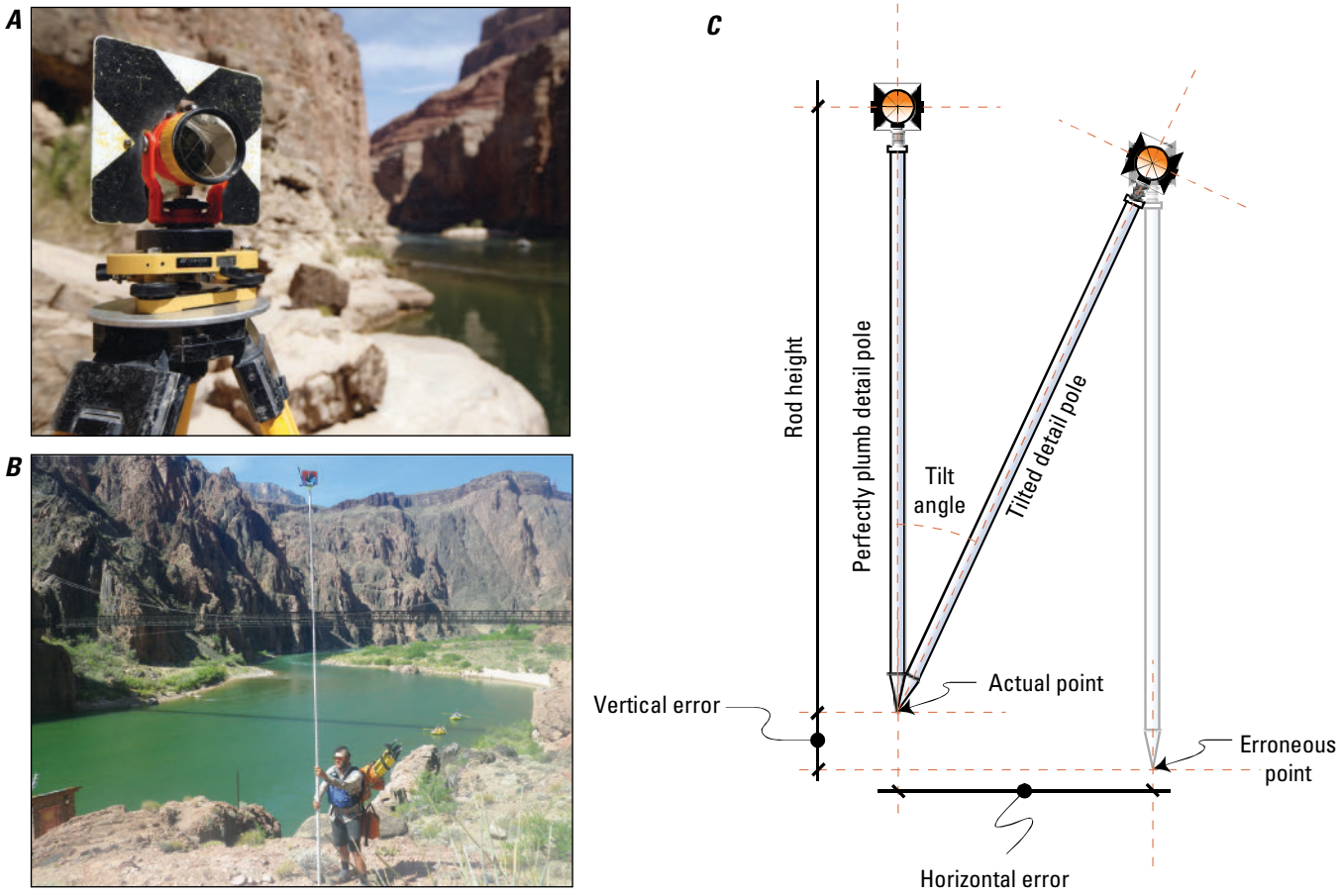

Figure 4.1. Photographs and diagram of an experiment assessing the uncertainty associated with total station point data, Colorado River corridor, Marble and Grand Canyons, Arizona. *A*, Backsite consisting of a reflective prism mounted on an optical plummet-equipped tribrach attached to a slip-leg adjustable tripod. Control point coordinates were independently determined as part of a high-quality geodetic control network. Photograph by M. Kaplinski, Northern Arizona University. *B*, Positioning the 7.6-meter extendable rod with reflective prism approximately plumb over control point SC088021R near study site 087L. Photograph taken on May 14, 2014, by Karen Koestner, Northern Arizona University. *C*, Hypothetical horizontal and vertical position errors that result from tilting of the survey rod. Diagram modified from Wheaton (2008).

Table 4.2. Surveys and point density used in the assessment of total station (TS) surface uncertainty, Colorado River corridor, Marble and Grand Canyons.

[For list of study sites, see table 1 of the main text. For sandbar types, see fig. 23 of the main text. SB, separation bar; RB, reattachment bar; m^3/s, cubic meters per second; *n*, number of observations; m^2; square meter; pts/m^2, points per square meter]

Study site ID[1]	Survey date (mm–dd–yyyy)	Source	Discharge (m^3/s)	*n*	Plan area (m^2)	Point density (pts/m^2)
030R	8–21–2000	Schmidt and others, 2007[2]	227	513	4,334	0.12
030R	9–04–2000	Schmidt and others, 2007	227	414	4,849	0.10
044L, SB	4–05–1996	Andrews and others, 1999[2]	237	618	8,704	0.07
044L, SB	4–19–1996	Hazel and others, 1999	491	578	5,563	0.10
044L, RB	4–05–1996	Andrews and others, 1999[2]	237	685	9,410	0.07
044L, RB	4–19–1996	Hazel and others, 1999	491	597	6,337	0.09
045L	3–10–2008	Wright and Kaplinski, 2011[2]	241	389	6,993	0.06
045L	3–31–2008	Hazel and others, 2010	230	301	4,351	0.07
047R	4–06–1996	Andrews and others, 1999[2]	231	411	11,950	0.03
047R	4–19–1996	Hazel and others, 1999	535	1,216	10,576	0.11
049R[3]	2–05–2008	Grams and others, 2010[2]	277	105	2,756	0.04
049R[3]	2–07–2008	Hazel and others, 2010	241	245	2,535	0.10
049L[3]	2–05–2008	Grams and others, 2010[2]	310	82	1,492	0.05
049L[3]	2–07–2008	Hazel and others, 2010	254	349	3,512	0.10
054R[3]	2–06–2008	Grams and others, 2010[2]	324	149	3,011	0.05
054R[3]	2–08–2008	Hazel and others, 2010	336	408	3,898	0.10
081L	4–12–2011	Grams and others, 2020[2]	467	322	2,398	0.13
081L	4–12–2011	Grams and others, 2020	467	253	2,047	0.12

[1]The descriptor "R" denotes the location at the study site on river-right and "L" for river-left, with the observer facing downstream. The number is the approximate location of the river mile marker based on the river mile (RM) centerline downstream from Lees Ferry (RM 0), Arizona.

[2]Indicates surveys used for manual selection of checkpoints used in the uncertainty analyses shown in table 4.3.

[3]Sites not presented in this report but surveyed by both Grams and others (2010) and Hazel and others (2010).

Table 4.3. Summary statistics of total station (TS) surface uncertainty using checkpoints, Colorado River corridor, Marble and Grand Canyons.

[SB, separation bar; RB, reattachment bar (see fig. 23 of the main text); *n*, number of observations; m, meter; pts/m^2, point per square meter; ME_z, vertical mean error; MAE_z, vertical mean absolute error; %, percent; $RMSE_z$, vertical root mean square error; SD, standard deviation. For list of study sites, see table 1 of the main text]

Study site ID[1]	*n*	Point density (pts/m^2)	ME_z (m)	MAE_z (m)	95% $RMSE_z$ (m)	SD	Skewness
030R	20	0.12	0.007	0.020	0.049	0.024	0.296
044L, SB	20	0.10	0.029	0.049	0.132	0.062	0.625
044L, RB	20	0.09	−0.005	0.026	0.056	0.029	0.232
045L	20	0.07	0.014	0.039	0.091	0.045	−0.328
047R	20	0.11	0.014	0.030	0.068	0.033	−0.317
049R[2]	20	0.10	−0.018	0.031	0.098	0.048	−1.634
049L[2]	20	0.10	0.038	0.043	0.095	0.032	−0.777
054R[2]	20	0.10	0.008	0.032	0.079	0.040	−1.642
081L	20	0.12	0.002	0.019	0.050	0.026	−0.117
Combined[3]	**180**	**0.10**	**0.010**	**0.032**	**0.084**	**0.042**	**−0.132**

[1]The descriptor "R" denotes the location at the study site on river-right and "L" for river-left, with the observer facing downstream. The number is the approximate location of the river mile marker based on the river mile (RM) centerline downstream from Lees Ferry (RM 0), Arizona.

[2]Sites not presented in this report but surveyed by both Grams and others (2010) and Hazel and others (2010).

[3]This row shows an average value for each statistical metric derived by pooling all observations.

Table 4.4. Summary statistics of total station (TS) surface uncertainty using repeat surveys, Colorado River corridor, Marble and Grand Canyons.

[SB, separation bar; RB, reattachment bar (see fig. 23 of the main text). *n*, number of observations; m, meter; ME_Z, mean error; MAE_Z, mean absolute error; %, percent; $RMSE_Z$, vertical root mean square error; SD, standard deviation. For list of study sites, see table 1 of the main text]

Study site ID[1]	*n*	ME_Z (m)	MAE_Z (m)	95% $RMSE_Z$ (m)	SD (m)	Skewness
030R	3043	0.008	0.036	0.101	0.051	0.804
044L, SB	2,270	0.034	0.073	0.189	0.090	−0.433
044L, RB	2,178	−0.006	0.045	0.121	0.062	−0.599
045L	438	0.035	0.079	0.215	0.104	−1.067
047R	4,392	0.006	0.071	0.078	0.094	0.378
049R[2]	2,086	0.013	0.051	0.150	0.076	−0.693
049L[2]	902	−0.025	0.089	0.236	0.118	−0.261
054R[2]	2,498	−0.052	0.109	0.307	0.148	−0.726
081L	1,838	0.009	0.035	0.112	0.057	0.969
Combined[3]	**19,644**	**0.001**	**0.063**	**0.185**	**0.094**	**−0.798**

[1]The descriptor "R" denotes the location at the study site on river-right and "L" for river-left, with the observer facing downstream. The number is the approximate location of the river mile marker based on the river mile (RM) centerline downstream from Lees Ferry (RM 0), Arizona.

[2]Sites not presented in this report but surveyed by both Grams and others (2010), and Hazel and others (2010).

[3]This row shows an average value for each statistical metric derived by pooling all observations.

Bathymetric Uncertainty

Bathymetric Point Data

In comparison to TS point data, the position and depth values of bathymetric data have additional sources of error to consider. Bathymetric surveys are affected by the type and quality of the depth measurement system, system calibration and alignment, vessel motion, stability, and velocity, and echosounder sensitivity to sediment surface material density (Wilson and Richards, 2006). The effects of these various sources of error are difficult to measure independently in the field and we use a technique that assesses bathymetric point quality by examining the elevation difference between overlapping points.

Crossline checks were conducted to evaluate the uncertainty of bathymetric point data (Blak, 2007). This check is an elevation comparison of the elevation of soundings from intersection points of crossing survey lines or transects. For SBES soundings collected in August and September 2000, we evaluated 1,403 points located within 0.05 m of each other and calculated an ME_Z less than 0.01 m (table 4.5; Kaplinski and others 2009, 2014). A similar crossline check for MBES data collected between 2000 and 2004 indicated a mean error ranging from −0.047 to 0.014 m, with an average ME_Z of −0.011 m (table 4.6; Kaplinski and others 2009, 2014). These data show that there were minimal biases or systematic errors in both the SBES and MBES data. For each bathymetric survey method, the combined, or pooled, elevation differences show an MAE_Z of 0.075 m for SBES data and 0.063 m for MBES data, respectively (tables 4.5 and 4.6).

Table 4.5. Summary statistics of singlebeam echosounder (SBES) bathymetry measurement uncertainty determined by crossline check analysis (modified from Kaplinski and others, 2014), Colorado River corridor, Marble and Grand Canyons.

[Crossline checks were carried out on eight individual SBES transects on each river trip (survey date) by selecting pairs of points that were within a 1-meter (m) radius. *n*, number of observations; ME_Z, mean error; MAE_Z, mean absolute error; %, percent; $RMSE_Z$, vertical root mean square error; SD, standard deviation]

Survey date	*n*	ME_Z (m)	MAE_Z (m)	95% $RMSE_Z$ (m)	SD (m)	Skewness
Aug. 2000	545	0.000	0.075	0.194	0.099	0.328
Sept. 2000	858	−0.006	0.075	0.188	0.096	0.099
Combined[1]	**1,403**	**−0.003**	**0.075**	**0.191**	**0.097**	**0.207**

[1]This row shows an average value for each statistical metric derived by pooling all observations.

Table 4.6. Summary statistics of multibeam echosounder (MBES) bathymetry measurement uncertainty determined by crossline check analysis (modified from Kaplinski and others, 2009), Colorado River Corridor, Marble and Grand Canyons.

[Crossline checks were carried out on separate surveys on each river trip (survey date) by comparing sounding elevations from an individual sweep to the elevation of a reference surface. *n*, number of observations; m, meter; ME_Z, mean error; MAE_Z, mean absolute error; %, percent; $RMSE_Z$, vertical root mean square error; SD, standard deviation].

Survey date	*n*	ME_Z (m)	MAE_Z (m)	95% $RMSE_Z$ (m)	SD (m)	Skewness
Aug. 2000	12,101	0.014	0.071	0.174	0.088	−0.121
Sept. 2000	21,743	−0.047	0.082	0.200	0.091	0.525
May 2002	19,514	0.008	0.056	0.146	0.074	0.779
June 2004	21,585	−0.030	0.056	0.137	0.063	0.166
Nov. 2004	28,996	−0.001	0.038	0.094	0.048	0.250
Dec. 2004	33,844	−0.025	0.078	0.191	0.094	0.256
Combined[1]	**137,783**	**−0.016**	**0.063**	**0.161**	**0.080**	**0.191**

[1]This row shows an average value for each statistical metric derived by pooling all observations.

Bathymetric Digital Elevation Model Uncertainty

Because of the lack of independent verification of depth observations (Byrnes and others, 2002; Wilson and Richards, 2006; Bennion, 2009), direct estimates of bathymetric surface uncertainty constructed from the point data are not possible. Sand on the bed is continually in motion during most flows (Rubin and others, 2001) and we did not utilize SBES or MBES repeat surveys (as in the assessment of TS uncertainty). Therefore, we estimated IU_Z using a point resampling analysis and examine the effects of differing point densities on surface elevation uncertainty to assess the veracity of the findings. These results are then combined with the estimate of SU_Z (see "Bathymetric Point Data" section) in equation 4.1 to arrive at an estimate of TU_Z for each bathymetric survey method.

Point Resampling Analysis

A comparison of IU_Z errors between the two bathymetry methods was obtained by resampling the highest density MBES dataset available (0.25-m mean point spacing and a point density of 15 points per square meter [pts/m^2]). Surveys collected between 2000 and 2008 at 10 sites were chosen for the analysis (table 4.7). To ensure consistent results, the chosen sites represent a wide range of both size and topographic complexity. The high-density dataset from each site was resampled to a spatial distribution and point density similar to the MBES and SBES data utilized in this study (that is, 2×2 m grids of uniformly spaced points, and points spaced 2 m apart along 10×10 m transects, respectively). TIN models were created from the resampled point datasets. Then, a 1-m-spaced grid of points was generated over the survey area with elevations assigned from the TIN model. Finally, an estimate of IU_Z was derived by comparing interpolated elevations from the 1-m grid to a random sub-sample of 5 percent of the points from the original, higher density (0.25 m) MBES dataset.

Summary statistics of the elevation differences between the subsample points and the resampled surrogate SBES and MBES surfaces are shown in table 4.7. The ME_Z for the MBES surfaces were near zero or slightly negative, whereas the SBES surfaces were offset from zero, ranging from −0.061 to −0.005 with a combined ME_Z of −0.022 m. The combined MAE_Z was 0.145 m and 0.083 m for the SBES and MBES grid types, respectively. The comparisons show positive or negative skew and unimodal distributions; however, the combined ME_Z of −0.022 m indicate a systematic bias is present in the resampled SBES simulations. Histograms of the resampling elevation differences indicate the distributions are left-skewed with a greater percentage of negative values, whereas the MBES surfaces have mostly symmetric distributions, as shown in figure 4.2.

Theoretically, the comparison of a repeat dataset should result in a difference value of zero and any other differences arising from the uncertainties introduced during data collection, processing, and analysis. Since this is not possible given the data being resampled are the same, the differences can be attributed to the effects of differing point density and distribution. We explored this relation further by progressively filtering the highest density MBES survey dataset at study site 003L to coarser, gridded distributions with different point spacing at 0.25 m intervals, using an approach similar to that of Brasington and others (2000). Considering the higher density dataset as the best representation of true surface morphology available, new surfaces were created from each filtered dataset and then differenced from the original surface. A simulated 10×10 m SBES surface was also included in the comparison.

Two tests were conducted on the filtered datasets (fig. 4.3). First, topographic complexity was characterized by dividing the three-dimensional surface area (SA) by two-dimensional plan area (PA) of each grid. Differences in SA/PA ratios decreased with each removal of points until the overall point density was reduced from 15 to 0.16 pts/m^2 (fig. 4.3*A*). This point density corresponded to a point separation distance of 2.75 m. Below this threshold, the SA/PA ratios indicate a rapid loss in surface resolution before tapering off at the resolution represented by the 4×4 m data (0.08 pts/m^2) and the 10×10 m transect data (0.10 pts/m^2).

Table 4.7. Interpolation errors calculated from the multibeam echosounder (MBES) validation surface in the assessment of bathymetry surface uncertainty, Colorado River corridor, Marble and Grand Canyons.

[*n*, number of observations; SBES, singlebeam echosounder; m, meter; ME_z, vertical mean error; MAE_z, vertical mean absolute error; $RMSE_z$, vertical root mean square error; SD, standard deviation; —, not applicable. For list of study sites, see table 1 of the main text]

Study site ID[1]	Survey (mm–dd–yyyy)	*n*	Grid surface type[2]	ME_z (m)	MAE_z (m)	95% $RMSE_z$ (m)	SD	Skewness
003L	11–13–2004	12,436	SBES	−0.061	0.111	0.470	0.232	−1.943
003L	11–13–2004	12,436	MBES	−0.007	0.043	0.203	0.103	−0.666
009L	3–29–2008	11,954	SBES	−0.024	0.145	0.610	0.310	0.894
009L	3–29–2008	11,954	MBES	−0.001	0.087	0.399	0.203	2.287
022R	11–14–2004	16,908	SBES	−0.024	0.233	0.795	0.405	0.152
022R	11–14–2004	16,908	MBES	0.002	0.142	0.555	0.283	0.632
032R	12–08–2004	8,259	SBES	−0.023	0.168	0.673	0.342	0.929
032R	12–08–2004	8,259	MBES	−0.001	0.094	0.397	0.202	−0.004
043L	8–23–2000	18,755	SBES	−0.029	0.235	0.818	0.416	0.203
043L	8–23–2000	18,755	MBES	−0.007	0.165	0.614	0.313	0.732
047R	4–08–2008	26,227	SBES	−0.014	0.113	0.348	0.177	−0.655
047R	4–08–2008	26,227	MBES	−0.002	0.051	0.183	0.093	−0.158
055R	12–08–2004	24,410	SBES	−0.005	0.114	0.524	0.268	1.044
055R	12–08–2004	24,410	MBES	0.001	0.055	0.297	0.151	1.405
063L[3]	9–15–2000	26,933	SBES	−0.019	0.144	0.498	0.253	−1.57
063L[3]	9–15–2000	26,933	MBES	−0.001	0.089	0.322	0.164	1.159
123L	2–06–2008	10,719	SBES	−0.034	0.179	0.610	0.309	−0.158
123L	2–06–2008	10,719	MBES	−0.007	0.106	0.420	0.214	0.030
225R	2–18–2008	13,653	SBES	−0.015	0.077	0.258	0.131	−1.388
225R	2–18–2008	13,653	MBES	−0.003	0.044	0.148	0.076	0.683
Combined[4]	**—**	**161,895**	**SBES**	**−0.022**	**0.145**	**0.470**	**0.284**	**0.059**
Combined[4]	**—**	**161,895**	**MBES**	**−0.002**	**0.083**	**0.220**	**0.186**	**0.981**

[1]The descriptor "R" denotes the location at the study site on river-right and "L" for river-left, with the observer facing downstream. The number is the approximate location of the river mile marker based on the river mile (RM) centerline downstream from Lees Ferry (RM 0), Arizona.

[2]Indicates a 1 m gridded surface linearly interpolated from resampled, synthetic 10×10 m SBES and 2×2 m MBES data, respectively.

[3]Sites not presented in this report but surveyed by Hazel and others (2010).

[4]This row shows an average value for each statistical metric derived by pooling all observations.

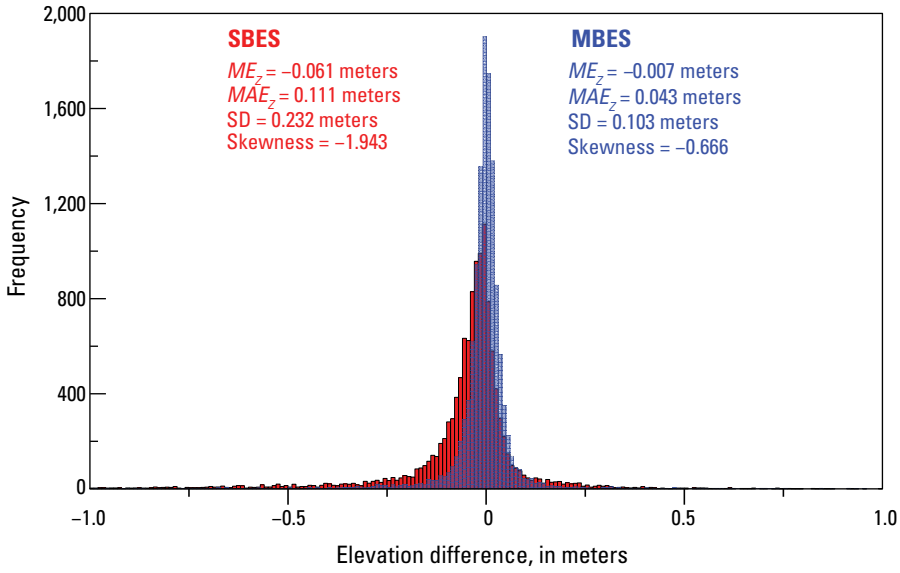

Figure 4.2. Histogram of elevation difference showing bias and variability between two surfaces constructed by resampling points from a high-density, 0.25-meter (m) multibeam echosounder (MBES) dataset, Colorado River corridor, Marble Canyon. A 2×2 m uniform grid in blue (simulating the MBES surveys in this report) and 10×10 m transects with 2 m point spacing in red (simulating the SBES surveys in this report). This example is from study site 003L. For list of study sites, see table 1 of the main text. ME_z, vertical mean error; MAE_z, vertical mean absolute error; SD, standard deviation.

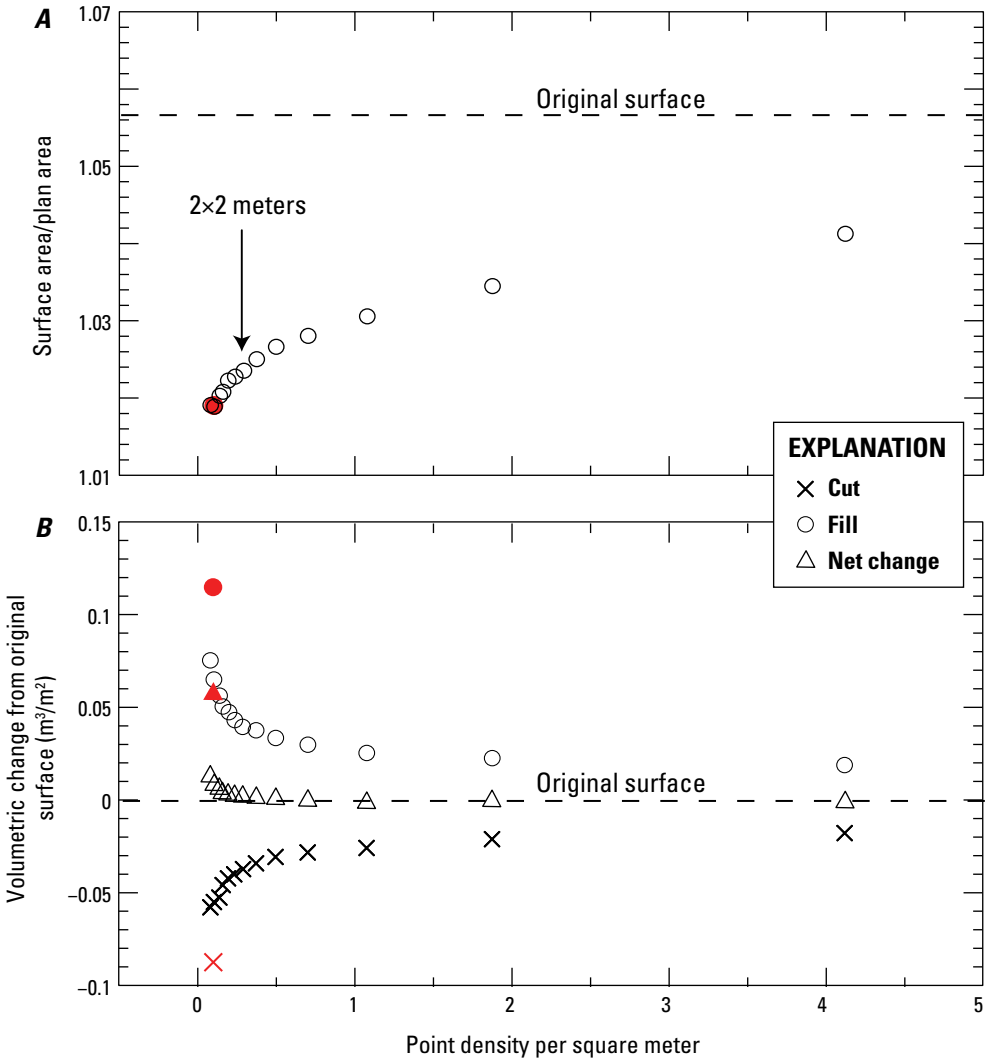

Figure 4.3. Plots showing the effect of differing point distribution and density on surface representation based on resampling a high density 0.25-meter (m) multibeam echo sounder (MBES) point dataset from study site 003L, Colorado River corridor, Marble Canyon. *A*, Topographic complexity was characterized by the ratio of three-dimensional surface area to two-dimensional plan area. *B*, Volumetric change based on subtraction from the original surface. The points were systematically filtered to coarser gridded distributions at 0.25 m point spacing. A singlebeam echo sounder (SBES) 10×10 m grid with 2 m point spacing resampled from the original surface is indicated by red symbols. m^2, square meter; m^3, cubic meter.

The second test compared volumetric change against point density and distribution (fig. 4.3*B*). The results indicate negligible information loss until a threshold similar to that demonstrated by the SA/PA test. The volume of cut and fill approximately balances, resulting in little volumetric change. For point densities below ~0.10 pts/m^2, the rate of information loss increases, and the volume of fill exceeds cut, giving an overall net positive balance. These results indicate that the differences of the lower density, gridded point resolutions effectively balance out, but once point spacing exceeds 3 to 4 m, the loss of slope break information results in the smoothing of surface slope. The net increase in elevation for the 10×10 m SBES surrogate surface was 0.059 m (table 4.7) when spatially distributed across the surface, suggesting that closer spaced transects are required to resolve areas of the bed characterized by rocks and steep slopes.

The procedure described above accounts for the fact that the effects of decreasing point density may, to some degree, cancel each other out over a large area. Even though surface representation was degraded when the original surface was progressively filtered, the net elevation change was negligible (less than [<] 0.010 m) until reaching a point density of 0.14 pts/m^2 (3 m spacing). The SBES data, however, have a higher demonstrable elevation uncertainty because of the large gaps in points that are interpolated between transects. The degradation effects suggest that, depending on the shape of the surface, decreased point spacing on a concave surface (for example, a channel) will result in an increase in elevation, or raising of the surface. The effect on a convex surface (for example, a sandbar) will lead to a decrease in elevation, or a lowering of the surface. We note that the resampling analysis was primarily conducted over large areas of the channel and reflects the topographic complexity of a channel feature. We take these collective observations of surface interpolation error into consideration and believe the combined MAE_Z of 0.145 m and 0.083 m for SBES and MBES, respectively, reasonably represents the surface interpolation uncertainty for both bathymetric methods (table 4.7).

Total Bathymetric Digital Elevation Model Uncertainty

For DEMs, the TU_Z derived from bathymetric survey data uses equation 4.1 to combine the survey uncertainty (SU_Z) estimated from crossline checks with the interpolation uncertainty (IU_Z) estimated using a resampling analysis. SBES and MBES TU_Z values are 0.163 m and 0.104 m, respectively (table 4.8). These uncertainty estimates agree favorably with an alternative estimate for MBES uncertainty made by Kaplinski and others (2014) using a fiducial surface technique and differentiating two areas of the channel bed as either smooth or rough. These areas presumably correspond to sand and relatively flat and immobile gravel or boulders, respectively. As described by Brock and others (2001), a fiducial surface represents baseline morphology that has not changed between surveys. Using this technique with a large statistical sample (1,000,000 or more observations), Kaplinski and others (2014) observed higher elevation differences in rough areas and reported the MAE_Z average as 0.27 m, whereas the average for smooth areas was 0.07 m. The difference between the smooth and rough classifications highlights the importance of some knowledge of surface roughness and topographic complexity of the surveyed areas.

Table 4.8. Summary of topographic surface uncertainty assessment for each data collection method in the study area in the Colorado River corridor, Marble and Grand Canyons.

[n/a, not applicable; TS, total station; MBES, multibeam echosounder; SBES, singlebeam echosounder]

Survey methodology	Point uncertainty (SU_Z)	Interpolation uncertainty (IU_Z)	Total surface uncertainty (TU_Z)
TS	0.014[1]	n/a	0.048[2]
MBES	0.063[3]	0.083[4]	0.104[5]
SBES	0.075[3]	0.145[4]	0.163[5]

[1]Determined by repeat control point measurements.

[2]Average of two different estimates of interpolation error.

[3]Determined by crossline checks for bathymetric data (Kaplinski and others, 2009).

[4]Determined by point resampling analysis of a higher density (0.25 meter) MBES dataset.

[5]Calculated using equation 4.1 with SU_Z estimated from crossline checks and IU_Z determined by point resampling analysis.

Merging of Datasets and Applying Surface Uncertainty

Surveys with both TS and bathymetric data were merged to create a continuous elevation map of the eddy and adjacent main channel at each study site. The previous section makes the distinction between a different uncertainty associated with each survey method and these are applied to the volumes reported in this study. While this study only reports survey-specific volumes, these results are also important for comparative analyses that utilize DEM differencing to examine volume of erosion and deposition in the study area (for example, Grams and others, 2010; Hazel and others, 2010; Wright and Kaplinski, 2011). An important consideration in DEM generation and differencing is the grid size and representation of the topographic surfaces under study. In this section, we assess the most appropriate grid cell size for the datasets and assign uncertainty to the surfaces from the analyses.

Digital Elevation Model Grid Size

The density of the original dataset dictates DEM resolution in most studies. For an ideal resolution, the number of grid cells should equal the number of measured points (McCullagh, 1988). However, the TS and SBES data do not have the needed point density to be reliably interpolated to a 1-m cell size using either this criterion, or the DEM grid-size estimator proposed by Hu (2003). This rationale for DEM grid size is more applicable to remote sensing applications (for example, lidar, multi-beam, or digital photogrammetry) where more uniform point sampling patterns are generated. In this report, we utilize a feature-based surveying methodology for subaerial topography, which allows accurate surface representation (because of breaklines) with much lower point densities than those generated by remote sensing. We acknowledge that a 1-m grid constructed from 2 m MBES data or 10×10 m transect SBES data may not be necessarily appropriate. However, the 1-m grid represents the best compromise between computation efficiency and information loss. A coarser grid may lead to the loss of potentially important breaks in slope, whereas a finer grid may be appropriate for subaerial topography collected with feature-based TS survey methods. The tradeoff, however, is the grid size may not be representative of the real elevation surface determined by bathymetric surveys or provide significant improvement on calculated volumes. The 1-m grid is sufficient for computing sand volumes and locations of erosion and deposition but still captures smaller scale detail, such as backwater channels or lateral bank migration.

Assigning Spatially Uniform Elevation Uncertainty

We employ these uncertainty estimates by multiplying the assigned value of TU_Z for each survey method by the area over which the method was used. This yields a spatially uniform estimate of volume uncertainty for each elevation bin (that is, low-elevation, fluctuating flow, and high-elevation zones) enclosed by a computational boundary. The surveys were collected during a range of flow conditions, but the elevation reached by a discharge of 227 m^3/s can be used for segregation of volume uncertainty because generally sand above this elevation is either within the fluctuating zone of dam releases or always subaerial. We acknowledge there is generally overlap between survey methods when combining datasets to create comprehensive maps

of the study sites but using the same stage elevation separating the volume bins is computationally more efficient. The uncertainty estimated for the TS surveys is applied to the two elevation zones above the 227 m^3/s stage elevation (fluctuating zones and high-elevation zones; see fig. 21 of the main text) in this report by multiplying ±0.05 m by the area of each zone rounded to the nearest one (1) digit. The uncertainty estimated for bathymetric surveys is applied to the low-elevation eddy and channel zones (below the 227 m^3/s stage elevation) by multiplying ±0.163 m and ±0.104 m by the area of each zone, depending on which bathymetry method was used. These are the error estimates for the data that can be visualized online at the U.S. Geological Survey (USGS) Grand Canyon sandbar monitoring website at https://www.usgs.gov/apps/sandbar and are also available from Grams and others (2020; https://doi.org/10.5066/P93F8JJK).

References Cited

Andrews, E.D., Johnson, C.E., Schmidt, J.C., and Gonzales, M., 1999, Topographic evolution of sandbars, *in* Webb, R.H., Schmidt, J.C., Marzolf, G.R., and Valdez, R.A., eds., The controlled flood in Grand Canyon: American Geophysical Union Geophysical Monograph Series, v. 110, p. 117–130, https://doi.org/10.1029/GM110p0117.

Bennion, D., 2009, Statistical and spatial analysis of bathymetric data for the St. Clair River, 1971–2007: U.S. Geological Survey Scientific Investigations Report 2009–5044, 58 p., https://doi.org/10.3133/sir20095044.

Blak, T.A., 2007, DEM quality assessment, *in* Maune, D.F., ed., Digital elevation model technologies and applications—the DEM users manual (2d ed.): Bethesda, Md., American Society for Photogrammetry and Remote Sensing, p. 425–448.

Brasington, J., Rumsby, B.T., and Mcvey, R.A., 2000, Monitoring and modelling morphological change in a braided gravel-bed river using high resolution GPS-based survey: Earth Surface Processes and Landforms, v. 25, no. 9, p. 973–990, https://doi.org/10.1002/1096-9837(200008)25:9%3C973::AID-ESP111%3E3.0.CO;2-Y.

Brock, J.C., Sallenger, A.H., Krabill, W.B., Swift, R.N., and Wright, C.W., 2001, Recognition of fiducial surfaces in lidar surveys of coastal topography: Photogrammetric Engineering and Remote Sensing, v. 67, no. 11, p. 1245–1258, accessed May 31, 2022, at https://www.researchgate.net/publication/287562794_Recognition_of_Fiducial_Surfaces_in_Lidar_Surveys_of_Coastal_Topography.

Byrnes, M R, Baker, J.L., and Li, F., 2002, Quantifying potential measurement errors associated with bathymetric change analysis: Vicksburg, Miss., U.S. Army Corps of Engineers Research and Development Center, Engineer Research and Development Center/Coastal Hydraulics Laboratory (ERDC/CHL) CHETN–IV–50, 17 p., https://apps.dtic.mil/dtic/tr/fulltext/u2/a588888.pdf.

Federal Geographic Data Committee [FGDC], 1998, Geospatial positioning accuracy standards, part 3—National standard for spatial data accuracy: Federal Geographic Data Committee FGDC–STD–007.3–1998, accessed May 17, 2021, at https://www.fgdc.gov/standards/projects/accuracy/part3/index_html.

Grams, P.E., Hazel, J.E., Jr., Kaplinski, M., Ross, R.P., Hamill, D., Hensleigh, J., and Gushue, T., 2020, Long-term sandbar monitoring data along the Colorado River in Marble and Grand Canyons, Arizona: U.S. Geological Survey data release, https://doi.org/10.5066/P93F8JJK.

Grams, P.E., Schmidt, J.C., and Andersen, M.E., 2010, 2008 high-flow experiment at Glen Canyon Dam—Morphologic response of eddy-deposited sandbars and associated aquatic backwater habitats along the Colorado River in Grand Canyon National Park: U.S. Geological Survey Open-File Report 2010–1032, 73 p., https://doi.org/10.3133/ofr20101032.

Hazel J.E., Jr., Kaplinski, M., Parnell, R., Kohl, K., and Schmidt, J.C., 2008, Monitoring fine-grained sediment in the Colorado River ecosystem, Arizona—Control network and conventional survey techniques: U.S. Geological Survey Open-File Report 2008–1276, 15 p., https://doi.org/10.3133/ofr20081276.

Hazel, J.E., Jr., Kaplinski, M., Parnell, R., Manone, M., and Dale, A., 1999, Topographic and bathymetric changes at thirty-three long-term study sites, *in* Webb, R.H., Schmidt, J.C., Marzolf, G.R., and Valdez, R.A., eds., The controlled flood in Grand Canyon: American Geophysical Union Geophysical Monograph Series, v. 110, p. 161–183, https://doi.org/10.1029/GM110p0161.

Hazel, J.E., Jr., Grams, P.E., Schmidt, J.C., and Kaplinski, M., 2010, Sandbar response in Marble and Grand Canyons, Arizona, following the 2008 high-flow experiment on the Colorado River: U.S. Geological Survey Scientific Investigations Report 2010–5015, 52 p., https://doi.org/10.3133/sir20105015.

Hu, Y., 2003, Automated extraction of digital terrain models, roads and buildings using airborne lidar data: Calgary, University of Calgary, Department of Geomatics Engineering, UCGE report 20187, Ph.D. dissertation, 206 p., accessed May 17, 2021, at https://www.ucalgary.ca/engo_webdocs/CVT/03.20187.YongHu.pdf. [Also available at http://dx.doi.org/10.11575/PRISM/16691.]

Kaplinski, M., Hazel, J.E., Jr., Grams, P.E., Davis, P.A., 2014, Monitoring fine-sediment volume in the Colorado River ecosystem, Arizona—Construction and analysis of digital elevation models: U.S. Geological Survey Open-File Report 2014–1052, 29 p., https://doi.org/10.3133/ofr20141052.

Kaplinski, M., Hazel, J.E., Jr., Parnell, R., Breedlove, M., Kohl, K, and Gonzales, M., 2009, Monitoring fine-sediment volume in the Colorado River ecosystem, Arizona: bathymetric survey techniques: U.S. Geological Survey Open-File Report 2009–1207, 33 p., https://doi.org/10.3133/ofr20141052.

Lane, S.N., 1998, The use of digital terrain modeling the understanding of dynamic river channel systems, *in* Lane, S.N., Richards, K.S., and Chandler, J.H., eds., Landform monitoring, modeling, and analysis: John Wiley & Sons, p. 311–342.

Li, Z., 1991, Effects of checkpoints on the reliability of DTM accuracy estimates obtained from experimental tests: Photogrammetric Engineering and Remote Sensing, v. 57, no. 10, p. 1333–1340, accessed May 31, 2022, at https://www.asprs.org/wp-content/uploads/pers/1991journal/oct/1991_oct_1333-1340.pdf.

McCullagh, M.J., 1988, Terrain and surface modeling systems—Theory and practice: Photogrammetric Record, v. 12, no. 72, p. 747–779, https://doi.org/10.1111/j.1477-9730.1988.tb00627.x.

National Digital Elevation Program [NDEP], 2004, Guidelines for digital elevation data, ver. 1.0: National Digital Elevation Program, accessed May 10, 2004, at http://giscenter.isu.edu/pdf/NDEPElevationGuidelinesVer1.pdf.

Rubin, D.M., Tate, G.B., Topping, D.J., and Anima, R.A., 2001, Use of rotating side-scan sonar to measure bedload, *in* Seventh Federal Interagency Sedimentation Conference, Reno, Nev., March 25–29, 2001, Proceedings: Subcommittee on Sedimentation, v. 1, p. III–139 to III–143, accessed May 28, 2022, at https://acwi.gov/sos/pubs/7thFISC/7Fisc-V1/7FISC1-3.PDF-.

Schmidt, J.C., Topping, D.J., Rubin, D.M., Hazel, J.E., Jr., Kaplinski, M., Wiele, S.M., and Goeking, S.A., 2007, Streamflow and sediment data collected to determine the effects of low summer steady flows and habitat maintenance flows in 2000 on the Colorado River between Lees Ferry and Bright Angel Creek, Arizona: U.S. Geological Survey Open-File Report 2007–1268, 79 p., https://doi.org/10.3133/ofr20071268.

Taylor, J.R., 1997, An Introduction to Error Analysis—The study of uncertainties in physical measurements (2d ed.): Sausalito, Calif., University Science Books, 327 p.

Wechsler, S.P., 2007, Uncertainties associated with digital elevation models for hydrologic applications—A review: Hydrology and Earth System Sciences, v. 11, no. 4, p. 1481–1500, https://doi.org/10.5194/hess-11-1481-2007.

Wechsler, S.P., and Kroll, C.N., 2006, Quantifying DEM uncertainty and its effect on topographic parameters: Photogrammetric Engineering and Remote Sensing, v. 72, no. 9, p. 1081–1090, https://doi.org/10.14358/PERS.72.9.1081.

Wheaton, J.M., 2008, Uncertainty in morphological sediment budgeting of rivers: Southampton, U.K., University of Southampton, Ph.D. dissertation, , 412 p. [Also available at http://www.joewheaton.org/Home/research/projects-1/phdthesis.]

Wilson, G.L., and Richards, J.M., 2006, Procedural documentation and accuracy assessment of bathymetric maps and area/capacity tables for small reservoirs: U.S. Geological Survey Scientific Investigations Report 2006–5208, 24 p., 11 plates, https://doi.org/10.3133/sir20065208.

Wright, S.A., and Kaplinski, M., 2011, Flow structures and sandbar dynamics in a canyon river during a controlled flood, Colorado River, Arizona: Journal of Geophysical Research Earth Surface, v. 116, no. F1, https://doi.org/10.1029/2009JF001442.

Moffett Field Publishing Service Center
Manuscript approved July 19, 2022
Edited by Lisa Binder and Monica Erdman
Illustration support by Kimber Petersen
Layout by Cory Hurd

ISSN 2330-7102 (online)
https://doi.org/10.3133/pp1873